AN ABSTRACT OF THE THESIS OF

Timothy R. Baumgartner for the degree of Doctor of Philosophy

in Oceanography presented on June 10, 1987

Title: High Resolution Paleoclimatology from the Varved Sediments of the Gulf of California

Redacted for privacy

Abstract Approved: ___

Year-to-year variability in the siliceous phytoplankton preserved in a twenty-year sequence of varved sediments from the central Gulf of California, shows a significant coherence with large-scale interannual change in climate over the Pacific. The microfossil record suggests that phytoplankton productivity in the central Gulf increased during periods of greater tropical influence associated with the El Niño/Southern Oscillation phenomenon (ENSO).

The source of interannual change in the ocean climate of the Gulf of California is investigated by comparing monthly sea level and coastal temperature anomalies in the Gulf to the large-scale circulation in the ocean and atmosphere. It is shown here that the interannual variability in the Gulf is strongly coupled to the intensity of the north equatorial circulation and is thus dependent upon Pacific-wide climatic change associated with the ENSO phenomenon. This does not mean that the Gulf is not subject to influence from the California Current, but rather that influence is regulated by the ENSO cycle.

A varve chronology which encompasses the period from 1908 through 1978 has been reconstructed from five closely spaced box cores along the Guaymas slope in the central Gulf of California. Correlation of the lamina stratigraphies among core sites indicates that seasonal deposition is sufficiently uniform to produce millimeter-scale laminae that can be traced for nearly 20 km. The varve chronology is applied here to

critically examine an established model of the origin of the varves. The model assigns a principal role to a summer pulse of river-borne terrigenous sediments which is inferred from the annual runoff cycle of major mainland rivers. This notion is tested by comparison of mass fluxes from the dark "summer" laminae, against available discharge data before and after construction of dams on the rivers. The test contradicts the model for fluvial transfer of terrigenous material to the central Gulf, but not necessarily for the southern Gulf. A modified hypothesis is proposed whereby terrigenous sediment is delivered to the central Gulf through predominantly eolian processes by the pick up and transport of desert dust associated with convective summer thunderstorms over Sonora.

The unusually strong El Niño event which occurred during 1982 and 1983, provided an opportunity to investigate the corresponding response of the Gulf of California. This was undertaken for peak spring conditions during March 1983. Rates of primary productivity measured during this period reached very high values in the central Gulf. These observations coupled with measurements of high phytoplankton biomass and the indication of high biogenic flux over the shelf and slope off Guaymas appear to confirm that phytoplankton production is enhanced in the central Gulf during El Niño events as inferred from analysis of the varve record. Synthesis of the hydrographic and biological data from March, 1983 has lead to a conceptual model for increased fertilization of the central Gulf during El Niño years by the nutrient enrichment of the subsurface source water which is entrained by coastal upwelling along the eastern margin during winter and spring.

HIGH RESOLUTION PALEOCLIMATOLOGY FROM THE VARVED SEDIMENTS OF THE GULF OF CALIFORNIA

by

TIMOTHY R. BAUMGARTNER

A THESIS

submitted to

Oregon State University

in partial fulfillment of
the requirements for
the degree of

Doctor of Philosophy

Completed June 10, 1987

Commencement June 1988

APPROVED:

Redacted for privacy

Professor of Oceanography in charge of Major

Redacted for privacy

Dean of College of Oceanography

Redacted for privacy

Dean of Graduate School

Date thesis is presented June 10, 1987

Typed by Jackie Poppleton for Timothy Baumgartner

DEDICATION

To the memory of my parents

and

to my daughter Jessica,

who I hope will agree

someday that this was

worth it

ACKNOWLEDGEMENTS

I would first like to thank Hans Schrader for his continued encouragement, advice and patience as major professor during my long and somewhat jerky career as a graduate student at Oregon State. Throughout the agreements and disagreements, it has been a very rewarding association. I am also deeply indebted to Nick Pisias who agreed to assume the role of major professor upon Hans' departure from Corvallis. His support has been invaluable during the final and critical phase of assembling this work into a coherent dissertation. I thank Vern Kulm, Bill Quinn, Roger Peterson, and Jeffrey Barnes as my committee members for their constructive suggestions during various stages in the development of the thesis. Bill Quinn was especially helpful for introducing me to the complexities of El Niño and the Southern Oscillation. Although not members of the committee, David Enfield provided critical reviews of the chapters dealing with the physical aspects of El Niño, while Dave Nelson helped with review and discussion of the biological consequences. Mitch Lyle helped with constructive comments on Chapters III and IV. Ron Zaneveld and Bob Bartz provided the encouragement and technical support to measure suspended particulates.

I am particularly grateful to Andy Soutar as the person who introduced me to the pleasures of marine varves and who has been an unofficial mentor over these years. This work would not have been possible without his sharing his talents, sampling equipment, and laboratory facilities at Scripps. Sue Rau provided the cheerful supervision needed to get us started cutting up the box cores. Jim Cowen contributed a crucial element to Chapter III with the ^{210}Pb analyses. Terry Hendricks sacrificed valuable time in order to finish building the data logger which was necessary for a pivotal cruise.

I am especially fortunate to have been associated during this time with an outstanding group of colleagues and students at the Centro de Investigación Científica y

de Educacion Superior de Ensenada. In addition to his cherished friendship and role as in-house critic, Vicente Ferreira has provided vital assistance with nearly all phases of the field and laboratory work, including computational and programming support. Pedro Moreno contributed able technical assistance with the X-radiography, photography and sediment analyses of the box cores. My close encounters with physical oceanography would probably not have occurred without Niels Christensen's encouragement and his attempts to reeducate me. The final chapter of this thesis would certainly not have been possible without the shared enthusiasm of Chema Robles and Rubén Lara to find out just what does happen in the Gulf of California during El Niño. Along with the discussions of what they might mean, Chema's organization of the collection and processing of the hydrographic data provided much of the raw material for Chapter IV. Eduardo Valdez, along with Rubén Lara, is responsible for the collection and analysis of the primary productivity and chlorophyll data used in Chapter IV. Saúl Alvarez, as director of C.I.C.E.S.E., provided encouragement and the freedom for me to pursue the thesis and course work for Oregon State while working at C.I.C.E.S.E. The Conséjo Nacional de Ciencia y Tecnología of Mexico supplied much of the financial support for this research, including the use of the Research Vessel EL PUMA. The Secretaría de Marina of Mexico, through the Dirección de Oceanografía also provided for the use of the Research Vessel MATAMOROS.

Without Jackie Poppleton I would not be able to write these acknowledgements. Besides her normal working hours, she devoted many evenings and several weekends in front of the MacWord processor so that I could be at the graduate school office on time with this thesis. Her skill and good nature plainly rescued me from the horrible and inexorable fate of missing the final deadline. Thank you Jackie.

I would like to also thank Paul and LuWanda Dauphin for their amazing hospitality during my later trips to Corvallis. Without them, living arrangements in Corvallis

would have been too gruesome to contemplate. Likewise the hospitality of George and Jean Hemingway and that of Andy and Sue has made my many necessary trips to San Diego much more enjoyable.

Thanks also to Ana and Catalina for the caring and moral support-- albeit not in the same years.

And finally, I acknowledge the dubious distinction awarded me by Paul and Gordon.

TABLE OF CONTENTS

LIST OF FIGURES

CHAPTER I

CHAPTER II

CHAPTER IV

LIST OF TABLES

CHAPTER I

CHAPTER II

CHAPTER III

HIGH RESOLUTION PALEOCLIMATOLOGY FROM THE VARVED SEDIMENTS OF THE GULF OF CALIFORNIA

GENERAL INTRODUCTION

Variation in the annual accumulation of the organic and inorganic remains preserved in the modern varved sediments of the Gulf of California comprises a history of Pacific-wide climatic forcing which can be clearly resolved into year-to-year changes. These sediments provide a bridge across the gap which separates time scales normally contemplated by marine geologists and those which are important to physical and biological oceanographers. The course of this investigation has been guided by the desire to merge these disparate time scales and often different approaches to viewing the natural world. The results presented here are intended to show the fidelity with which climatic information may be recorded by the geological record and to demonstrate that this information can provide valuable insight into the ways in which the present pelagic ecosystem, including the processes and paths of sediment transport, responds to short-term climatic forcing.

Examination of the varved sediments is limited to the upper tens of centimeters corresponding to deposition during the twentieth century. This study is focused on material obtained by box coring along the eastern margin of the central Gulf of California off Guaymas, Sonora. This area was chosen for its presumed sensitivity to intense winter-spring coastal upwelling and summer-fall fluvial discharge which were considered the principal elements of climatic forcing to produce the seasonal alteration in the composition of particles forming the individual laminae. The box cores were recovered from depths close to 650 m which is near the center of the mid-water oxygen minimum responsible for preservation of the laminae by inhibiting the activity of burrowing animals which otherwise would mix and destroy the primary laminated structure.

Compilation and analysis of the appropriate historical instrumental records of interannual climate variability was undertaken in order to provide adequate interpretations of the results obtained from the sediments. The somewhat unsettling revelation from the varve record that productivity of the siliceous phytoplankton appears to increase during El Niño events was the primary motivation for the undertaking of an urgent and comprehensive campaign to monitor the physical, biological and sedimentological consequences of the 1982-1983 El Niño in the Gulf of California.

The format followed in the organization of this dissertation is to present the principal pieces in manuscript form. Two of these have already been published. The analysis of the twenty-year varve record of siliceous phytoplankton variability which comprises Chapter I, was published in 1985 in Marine Geology (Baumgartner, Ferreira-Bartrina, Schrader and Soutar as co-authors). Chapter II, which describes the coupling of the Gulf of California to large-scale interannual climatic variability was published in the Journal of Marine Research in 1985 (Baumgartner and Christensen, co-authors). The reconstruction of a master varve chronology for the Guaymas slope and its application to test the fluvial hypothesis for the origin of summer laminae which are presented as Chapter III, has been submitted for publication in an American Association of Petroleum Geologists Memoir volume being edited by P. Dauphin and G. Ness and to be entitled "The Gulf and Peninsular Province of the Californias" (the co-authors are Baumgartner, Ferreira-Bartrina, Cowen, Soutar, Schrader and Moreno). Chapter IV which describes the physical processes controlling primary productivity in the Gulf during March 1983, and which proposes the model for nutrient enrichment during El Niño years, has not yet been submitted for publication. In whatever form it is ultimately submitted, the co-authors will include Robles-Pacheco, Valdez-Holguin, Ferreira-Bartrina and Lara-Lara to recognize their substantial contributions made in the collection and processing of the samples and data from the March 1983 cruise on which this chapter is based.

CHAPTER I

A 20-YEAR VARVE RECORD OF SILICEOUS PHYTOPLANKTON VARIABILITY IN THE CENTRAL GULF OF CALIFORNIA

ABSTRACT

Year-to-year variability in the structure of the preserved siliceous phytoplankton assemblage is reconstructed from a box core retrieved from the varved sediments along the Guaymas slope of the Gulf of California. A 20-year record from 1953 through 1972 is obtained from interpretation of the varve stratigraphy supported by ^{210}Pb and ^{228}Th dating. Ecological time series derived from microfossil analysis show a strong coherence with interannual sea level anomalies indicating a response to large-scale climatic variability associated with the El Niño/Southern Oscillation phenomenon. El Niño periods are generally marked by increases in preserved abundances of the total siliceous assemblage and in particular by greater numbers of individuals within species whose distribution is limited to tropical and subtropical waters.

INTRODUCTION

Anoxic depositional environments underlying highly productive coastal seas characterized by high sedimentation rates (silled basins and fjords or open continental slopes) provide a rich potential for high-resolution paleoclimatic histories. Such environments favor the preservation of sequences of millimeter-scale laminae whose origin lies in the seasonal variation in composition of particles supplied to the bottom (Soutar and Crill, 1977; Soutar et al., 1981). Seasonally deposited laminae are valuable not only for their record of environmental information but also for their temporal significance. If the sediment surface is not lost during sampling and a zero age can be assigned to the surface, then an absolute chronology may be reconstructed with a precision approaching ± one year (Soutar and Crill, 1977).

The Gulf of California is a long and narrow sea divided into two major physiographic regions, the upper and the lower Gulf. The lower Gulf, south of the midriff islands around 29°N, is comprised of a series of basins which progressively deepen to oceanic depth towards the mouth, and is in open communication with the Pacific. The accumulation and preservation of rhythmically laminated sediments is maintained by an oxygen minimum layer within the water column between 300 and 1000 m depth and by the annual cycle of regional climate which controls the composition of sediments arriving at the sea floor (Soutar et al., 1981). The oxygen-depleted mid-water layer of the Gulf is an extension of the widespread oxygen minimum within the intermediate waters in the Eastern Tropical Pacific Ocean (Calvert, 1964). The strength and position of this feature depends upon the balance between the oxygen consumption by oxidation of settling organic particles and the oxygen replenishment to this layer by physical mixing, advection, and diffusion (Wyrtki, 1962). The high biological productivity and restricted circulation within the Gulf of California produces a strong oxygen minimum

centered near 600 m depth which bathes the bottom sediments of the continental slopes, prohibiting significant sediment disturbance by the macrobenthos.

The seasonal deposition of laminae along the slopes of the Gulf was inferred by Calvert (1966). This interpretation is now supported by comparison of laminae sequences with depositional rates derived from radiometric dating of the sediments with ^{210}Pb (DeMaster, 1979). Thus the rhytmically laminated sediments are considered sequences of annual "varves" conforming to the general definition originally proposed by De Geer (1921); i.e., each marine varve consists of a pair of light and dark laminae. Soutar et al. (1981) and Donegan and Schrader (1982) provide recent reviews and details of the sedimentation response to the annual climatic cycle and resulting formation of the seasonal laminae.

The value of these sediments as records of environmental change are limited by the quality of their preserved paleoecological signals. This study is an assessment of the usefulness of the varved sediments in the Gulf to provide a year-to-year resolution of the behaviour of the physical climate, employing the microfossil contents within the annual sediment layers.

The approach taken here is to compare a continuous, instrumentally recorded index of climatic variation to the naturally recorded annual average of ecologic information carried by the siliceous phytoplankton. The instrumental record used here is the non-seasonal anomaly of sea level which indicates the deviation of sea level from the normal long-term average of the annual cycle. Sea level is recognized as an important index of year-to-year variation in ocean climate (Enfield and Allen, 1980). Comparison of the Gulf of California sea level index to the varve record provides a test of whether large-scale, interannual climatic variability produces an ecological signal which is preserved in the microfossil assemblage. The record examined is a twenty-year interval

from 1952 to 1972 determined by the surface age of the core and the initiation of sea level data collection in the Gulf of California during 1952.

The sample material used in this study was taken from a single box core retrieved from the Guaymas slope in the central Gulf of California during May of 1973. The core, 7305-2208, is located at lat. 27° 53'N, long. 111° 36'W in 670 meters water depth (Fig. I-1). Core 7305-2208 was chosen because prior work by Bruland (1974) provided a ^{210}Pb radioisotope chronology indicating continuous varve sedimentation over the last 150 years. Examination of the siliceous phytoplankters is based upon the determination of microfossil densities, species richness, and the behaviour of biogeographic groups of taxa. We also selected four individual species for comparison with aspects of the variation exhibited by the total assemblage.

Figure I-1

Location of core site 7305-2208. Isobaths in meters, taken from Bischoff and Niemitz (1980).

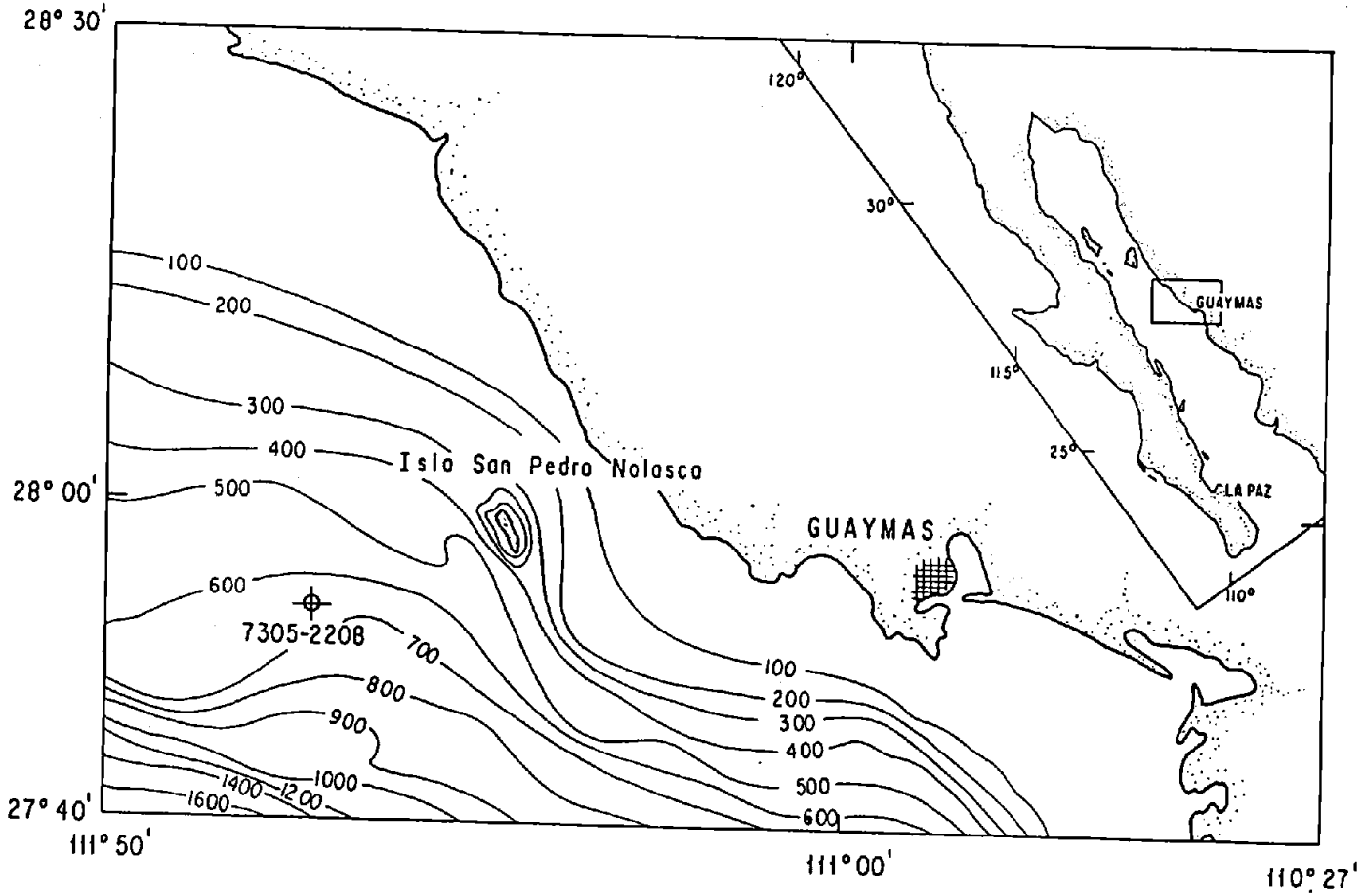
28° 30'
28° 00'
27° 40'
111° 50'
111° 00'
110° 27'
120°
30°
115°
25°
110°
GUAYMAS
LA PAZ
Isla San Pedro Nolasco
GUAYMAS
7305-2208
100
200
300
400
500
600
700
800
900
1000
1200
1400
1600

Figure I-1

METHODS

The core material was obtained with a 30 x 30 x 100 cm Soutar box corer (see Bruland, 1974, Fig. I-3). The sediment was left undisturbed in the coring box during transit. On shore the core was frozen, extruded, and cut into longitudinal 1-cm thick slabs with a high-speed band saw. The left side of Figure I-2 is a positive print of the X-radiograph of the slab used in this study. The slope of the core surface and the laminae reflect distortion due to freeze thrusting. The freshly sawed and cleaned face of the frozen slab displayed a well-laminated structure of regularly alternating light and dark layers which were readily apparent with the unaided eye along its entire length.

Based upon the reconstruction of the chronology described below, each of the upper 20 varves was sampled from the 1-cm thick slab shown in Figure I-2, cutting across the width of the frozen slab with a scalpel. The subsamples were cleaned of organic matter by heating them in a beaker with hydrogen peroxide for eight hours. The subsamples were then size-fractionated into greater than 62 μm, and 24 to 62 μm size fractions. This was done initially with the idea that other microfossil groups, in addition to diatoms and silicoflagellates, would be analyzed. However, planktonic foraminifera and radiolaria were too rare in the large size fraction to warrant extensive analysis.

Microscope mounts were made from 1/160 aliquots of the >62 μm size fraction and 1/80 aliquots of the 24-62 μm fraction. These aliquots were taken by automatic pipette from suspensions which were homogenized by an air bubbler. Two ml of suspension were randomly strewn over a 22 x 30 mm cover slip, dried, and mounted Pleurax.

Analysis of the total assemblage was carried out on only the 24-62 μm size fraction. Comparison of the > 62 μm fraction to the smaller size fraction indicated that, with exception of a few very large centric forms (e.g., Coscinodiscus asteromphalus),

Figure I-2

X-radiograph and interpretative line drawing of varve stratigraphy in the upper 9 cm of 1-cm thick slab from core 7305-2208. Lower boundaries of first 20 varves are labeled along left side of line drawing; cm depth scale oriented normal to varves in line drawing.

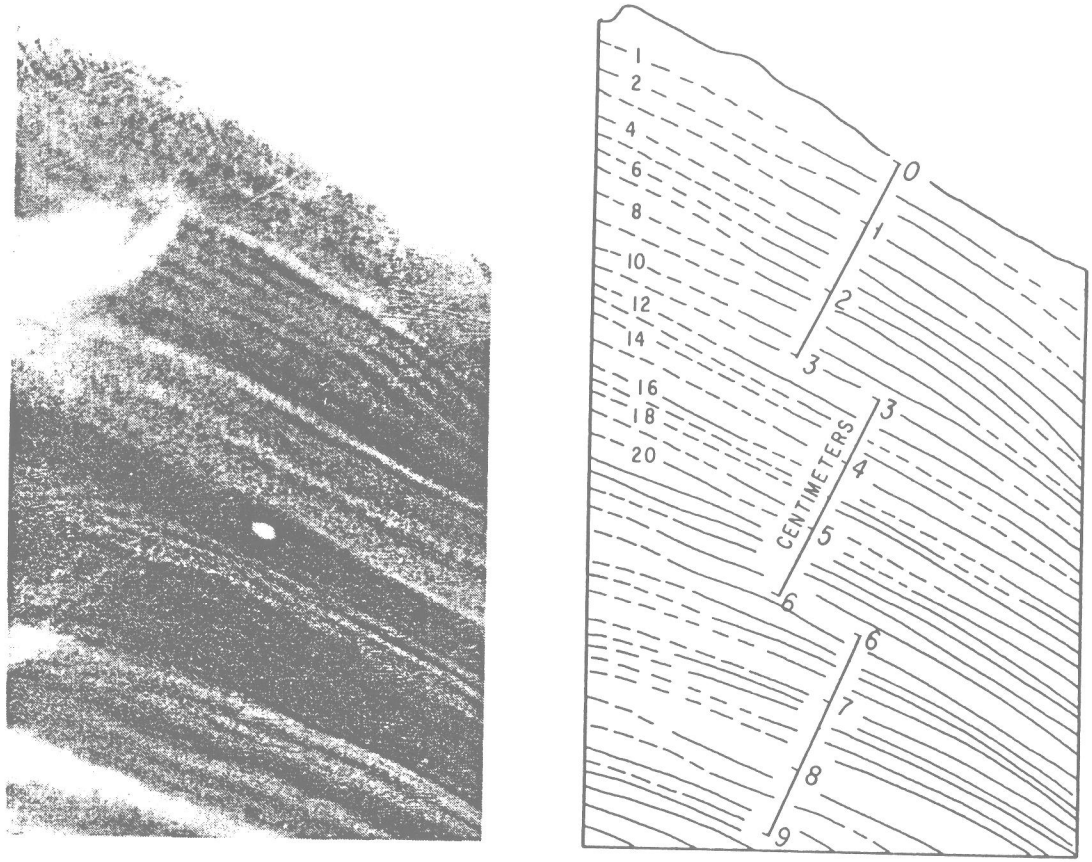

Figure I-2

all species were better represented within the 24-62 μm fraction. For analysis of the total assemblage, more than 300 diatom valves and silicoflagellate skeletons were counted, except for varve sample number 18 where the diatom density was excessively low. The conventions proposed by Schrader and Gersonde (1978) for counting valves and valve fragments were adopted for this study. A total of 67 species and species groups were used for estimation of the density of individuals and species-richness (Table I-1). Form species were used to retain, in the analysis, those taxa which could not be properly identified due to their poor state or preservation of where taxonomic ambiguities were present. Our category of Dictyocha calida also includes forms which Murray and Schrader (1983) have separated into Dictyocha sp. A, sp. 2 and sp. B.

Analysis of four individual species was performed on both the >62 μm and the 24-62 μm fractions for the first 18 varves. For these species, a minimum of 5% of the area of the 24-62 μm cover slip and 10% of the area of the >62 μm cover slip was scanned counting only whole specimens. Very rarely do these individual counts fall below ten specimens for the rarer species in a varve sample.

RECONSTRUCTION OF CHRONOLOGY

Radioisotope Chronology

The stratigraphic variation of "excess" ^{210}Pb in core 7305-2208 was measured by Bruland (1974). We have plotted the observed activities of excess ^{210}Pb throughout the upper 7 cm of the core in Figure I-3. The ^{210}Pb subsamples were taken parallel to the laminae boundaries from a slab adjacent to that used for determining the laminar stratigraphy (Fig. I-2). Details of the analytical procedures are given by Bruland (1974).

The stratigraphic position of the upper 20 varves examined in this study (measured normal to the laminae structure) is shown schematically along the depth axis in Figure I-3. The average sedimentation rate determined by varve counts versus depth

Figure I-3

Semi-log plot of excess ^{210}Pb in upper 7 cm of core 7305-2208 (adapted from Bruland, 1974). Horizontal bars represent stratigraphic thicknesses of the ^{210}Pb subsamples in relation to depth scale of Figure I-2. Vertical bars indicate range of uncertainty from counting error. Stratigraphic position of first 20 varves with respect to depth scale of Figure I-2 shown beneath the ^{210}Pb plot. Line fitted through ^{210}Pb measurements corresponds to an average sedimentation rate of 2.4 mm/year.

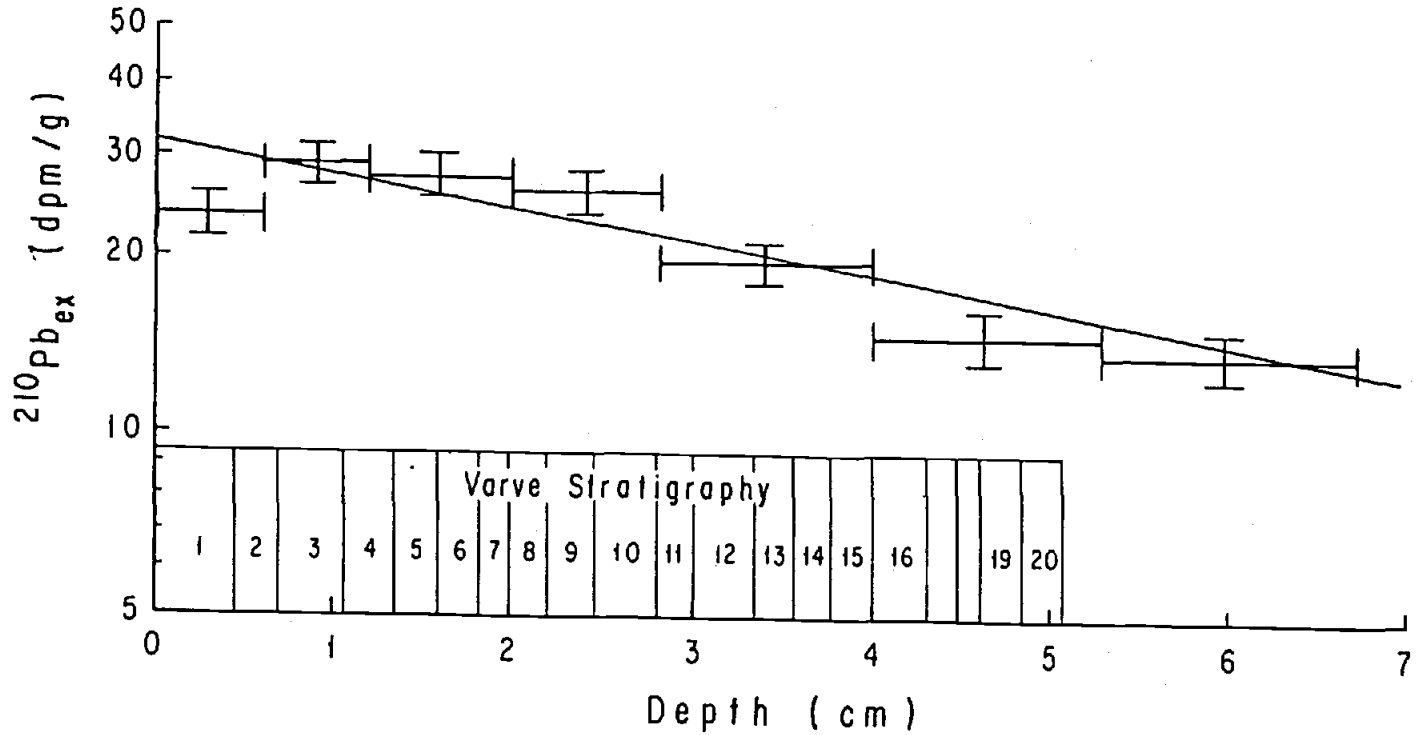
50
40
30
20
10
5
$^{210}Pb_{ex}$ (dpm/g)
Varve Stratigraphy
1
2
3
4
5
6
7
8
9
10
11
12
13
14
15
16
19
20
0
1
2
3
4
5
6
7
Depth (cm)

Figure I-3

in the upper 7 cm is 2.4 mm/year. The line with this slope is plotted through the ^{210}Pb activities on Figure I-3 to illustrate the agreement with the ^{210}Pb decay. The anomalously low ^{210}Pb activity of the surface subsample is probably due to a salt dilution effect.

Very high $^{228}Th/^{232}Th$ activity ratios near the surface, shown by Bruland (1974), indicate that the actual depositional interface was recovered. The sedimentation rate in the upper 4 cm of the core estimated by decay of ^{228}Th is 3 mm/yr. This agrees well with our independent interpretation of the varve stratigraphy in Figure I-3 which indicates the upper 4 cm represent 15 years, yielding a sedimentation rate of 2.7 mm/yr. The surface activity of ^{210}Pb (32 dpm/g) extrapolated from the 2.4 mm/yr. sedimentation rate of the upper 7 cm also agrees closely with the average value determined recently from five box cores on the Guaymas slope (33 dpm/g).

We must point out, however, a discrepancy between the sedimentation rates stated by Bruland (1974) and ourselves for this core which are based on the same data. Review of the original interpretation of the varve stratigraphy used by Bruland found a substantial error where almost 15 varves were apparently counted twice; our revised varve counts show an average sedimentation rate of 2.1 mm/yr through the upper 30 cm of the core. Thus the apparent discrepancy between the ^{228}Th and ^{210}Pb decay rates noted by Bruland (1974) does not exist.

Varve Chronology

Analysis of the ^{210}Pb decay demonstrates that there are no major stratigraphic discontinuities present in the upper 7 cm of the material used in this study. However, the more recent work on Guaymas slope cores shows that the combination of analytical error and the apparent natural variation of ^{210}Pb limits the resolution of a ^{210}Pb derived chronology to a minimum of approximately $\pm$ five years. Therefore, determination of

chronology accurate to within ± one year must ultimately depend upon correct interpretation of the laminar structure for reconstruction of a varve chronostratigraphy.

We assumed that each light-dark laminae couplet visible on the radiograph is a varve and represents deposition during one climatic year. Due to the distortion during freezing, none of the boundaries are resolved across the entire width of the radiograph; therefore, continuity on the radiograph was not used as a criterion for acceptance of a boundary. Where clearly resolved in the X-radiograph the varve boundaries are marked by solid lines on the line drawing of Figure I-2. The broken lines mark the extrapolated segments of the poorly resolved varve boundaries.

Resolution of the X-radiograph is very good for the sequence of varves numbered 5 through 12. It is disminished, but adequate for determination of boundaries from varve number 1 through 4. Resolution of the sequence of varves 13 through 18 is relatively poor. Boundaries at the bases of varves 14, 15, 17 and 18 are, however, distinct enough for definite recognition. Boundaries at the bases of varves 13 and 16 are more questionable, but included so that any error would favor over-sampling of the phytoplankton variability. Resolution of the boundaries of varves 19 and 20 is, again, adequate for definite recognition.

Assuming that the varve stratigraphy presented in Figure I-2 accurately represents the annual deposition over a continous twenty-year period, it cannot be applied as an absolute chronology until we are sure of the surface age. Based upon the thoruim isotope analysis by Bruland (1974), the depositional surface was recovered, indicating an age of spring, 1973 for the upper laminae in the core. However, the cutting, curation, and handling of the slab used in this study eroded off some of the upper material. This loss appears to have included most of the upper light lamina which would represent deposition during the Spring of 1973. Thus, our best estimate for the date at the base

of the first varve is the beginning of 1972 coinciding with the initiation of the light laminae.

VARIATION IN PRESERVED SILICEOUS PHYTOPLANKTON ASSEMBLAGE

Variation of the total assemblage is characterized by three ecological criteria consisting of (1) the density of individuals, (2) species richness, and (3) distribution within the major biogeographic categories of the diatom and silicoflagellate species.

The parameter referred to as density of individuals is the total number of individuals within all taxonomic groups preserved in a given varve sample. The density of individuals in each varve was obtained by estimating the number on the cover slip from the total counted and the area traversed during the count. The total number of diatom and silicoflagellates per cm^2 of sediment surface was then computed by dividing the total number in the sample by the depositional surface area of the varve measured from the slab. This value provides a relative estimate of the diatom and silicoflagellate cell flux preserved each year in the sediments based upon the 24-62 μm size fraction. These values range from approximately 5800 (varve 18) to 115,000 cells/cm^2-yr (varve 8). The 67 species groups adopted for estimation of the density of individuals as well as species richness are listed in Table I-1. The upper plot in Figure I-4 shows the series of cell densities (or fluxes) in standard units of $\log_{10}$(cells/cm^2 -yr). Standardization removes the mean of the series and normalizes all values to the standard deviation of the series.

Species richness in the varve samples was obtained by summing the number of taxa encountered. Because no more than 350 individuals were counted per sample, this is a conservative estimate. However, the values are presented to show the general pattern of year-to-year variation in the number of phytoplankton species preserved,

Table I-1

Raw counts of diatom and silicoflagellate taxa. Biogeographic category of each taxa indicated by number before name: 1 = warm-water group; 2 = cool-water group; 3 = cosmopolitan group; 0 = no biogeographic significance.

Note: Biogeographic distributions based upon Cupp, 1943; Fenner et al., 1976; Fryxell and Hasle, 1972; Hasle, 1960 & 1976; Hendey, 1964; Hustedt, 1930 & 1959; Jouse et al., 1971; Kanaya and Koizumi, 1966; Karohji, 1972; Kozlova and Mukhina, 1967; Poelchau, 1976; Simonsen, 1974; Smayda, 1958; Venrick, 1971.

Table I-1

	Varve Number									
	1	2	3	4	5	6	7	8	9	10
3 *Actinocyclus curvatulus*	5	4	4	1	2	2	1	6	4	2
3 *A. ehrenbergii*	5	5	5	1	2	1	5	7	12	8
3 *Actinoptychus splendens*	2	1	7	6	2	4	2	8	6	5
3 *A. undulatus*	21	28	33	37	35	40	46	53	34	62
1 *Asteromphalus arachne*	0	0	0	0	2	0	0	0	1	0
1 *A. elegans*	1	0	0	0	1	1	0	3	1	0
1 *A. flabellatus*	1	1	0	4	0	1	1	1	1	0
3 *A. heptactis*	5	2	3	2	1	2	3	2	1	0
2 *A. robustus*	0	0	0	0	1	0	0	0	0	0
0 *Bacteriastrum spp.*	27	16	19	9	8	11	11	8	11	0
0 *Chaetoceros spp (veg cells)*	8	6	12	12	8	8	5	9	3	6
0 *C. spp (resting spores)*	3	5	29	16	14	8	12	8	5	7
1 *Coscinodiscus africanus*	0	1	0	1	0	0	1	0	0	0
2 *C. centralis*	2	5	2	0	0	0	0	0	1	1
2 *C. curvatulus*	1	3	0	5	10	0	4	1	2	1
2 *C. granii*	3	3	4	0	4	2	2	1	2	1
2 *C. marginatus*	1	0	0	1	0	1	0	1	1	1
1 *C. nodulifer*	37	66	32	35	27	42	44	48	52	41
2 *C. perforatus-fimbriatus*	26	37	26	25	31	39	30	29	26	20
3 *C. radiatus*	0	0	0	4	0	2	4	0	0	0
3 *C. stellaris*	4	7	0	2	6	8	7	4	9	8
3 *Cyclotella striata*	0	0	1	0	2	0	0	1	0	0
1 *C. stylorum*	0	0	5	4	3	2	2	0	0	2
2 *Ditylum brightwellii*	9	5	4	2	3	1	2	5	3	0
1 *Hemiaulus sinensis*	0	0	0	0	0	0	0	0	0	0
1 *Hemidiscus cuneiformis*	12	7	5	5	8	16	18	12	8	4
2 *Lithodesmium undulatum*	12	7	2	5	3	4	5	7	3	1
3 *Nitzschia bicapitata-braarudii*	0	1	0	0	1	1	0	0	0	0
1 *N. marina*	0	0	0	0	1	0	0	0	1	0
3 *N. pungens*	0	0	0	0	1	0	0	1	0	0
2 *Odontella aurita*	2	0	0	2	1	0	2	3	1	0
2 *O. mobiliensis*	1	1	0	0	0	0	0	0	0	0
3 *Paralia sulcata*	0	0	0	1	1	1	1	0	1	1
1 *Planktoniella sol*	1	0	0	1	0	0	1	0	0	0
1 *Pseudoeunotia doliolus*	8	7	11	14	10	12	13	11	8	5
3 *Rhizosolenia alata*	4	2	0	1	1	2	1	0	2	1
1 *R. bergonii*	0	0	1	0	0	0	0	2	0	0
3 *R. calcar-avis*	0	1	0	1	0	0	0	0	0	0
3 *R. hebetata*	0	1	0	0	0	0	0	0	0	0
1 *R. robusta*	1	0	0	0	0	0	0	0	0	1
3 *R. setigera*	1	0	1	3	2	4	0	0	1	2
3 *R. styliformis*	2	0	0	1	0	1	0	0	1	0
1 *Roperia tesselata*	9	4	13	13	13	12	21	12	16	15
1 *Stephanopyxis palmeriana*	2	10	1	2	4	4	2	2	0	5
3 *S. turris*	9	17	6	16	8	1	2	3	15	14
1 *Thalassionema bacillaris*	5	3	10	12	10	11	5	14	1	7
3 *T. nitzschioides*	11	11	24	28	24	23	27	32	11	12
2 *Thalassiosira anguste-lineata*	0	1	0	0	0	0	1	1	0	0
2 *T. decipiens*	0	0	0	0	0	1	0	0	0	2
3 *T. eccentrica*	0	1	5	2	2	6	3	5	3	2
1 *T. endoseriata*	9	1	0	0	2	2	5	5	2	2
1 *T. lineata*	0	0	1	3	0	0	0	0	0	0
3 *T. oestrupii*	0	1	2	1	4	1	0	2	0	1
1 *T. punctifera*	5	8	6	4	5	7	6	8	8	4
0 *T. simonsenii*	0	0	0	0	3	0	1	2	0	2
3 *T. subtillis*	1	0	0	0	0	0	0	0	0	0
3 *T. symmetrica*	0	0	0	0	0	0	0	2	0	0
0 *Thalassiothrix sp indet*	0	0	0	1	0	2	0	2	1	1
1 *T. frauenfeldii*	2	1	0	1	0	0	2	1	0	0
3 *T. longissima*	9	8	9	6	9	12	15	9	11	15
1 *T. mediterranea-delicata*	1	1	4	7	2	2	3	1	10	6
1 *T. vanhoeffenii*	0	0	0	0	0	0	1	0	0	0
3 *Trigonium alterans*	0	0	0	1	0	0	0	0	0	0
1 *Dictyocha calida*	5	4	4	8	6	3	5	1	3	3
2 *D. epiodon*	0	0	0	1	2	0	0	0	0	1
3 *D. messanensis*	21	20	18	10	17	16	23	23	27	37
1 *Octactis pulchra*	16	5	14	6	6	4	2	8	10	8

Table I-1.....continued

	Varve Number									
	11	12	13	14	15	16	17	18	19	20
3 *Actinocyclus curvatulus*	5	6	0	2	5	5	3	0	4	0
3 *A. enhenbergii*	8	2	4	1	3	6	3	2	8	3
3 *Actinoptychus splendens*	1	8	3	7	8	2	3	1	6	3
3 *A. undulatus*	58	41	40	42	34	38	35	28	47	33
1 *Asteromphalus arachne*	0	0	0	1	1	1	0	0	0	0
1 *A. elegans*	0	0	0	0	0	0	0	0	0	1
1 *A. flabellatus*	1	0	1	1	1	1	2	0	0	0
3 *A. heptactis*	3	3	2	1	0	1	4	0	1	1
2 *A. robustus*	0	0	0	0	0	0	1	0	0	0
0 *Bacteriastrum spp.*	10	18	29	13	21	22	20	1	7	5
0 *Chaetoceros spp (veg cells)*	8	9	8	18	17	20	21	4	9	8
0 *C. spp (resting spores)*	14	9	9	10	17	12	4	2	7	4
1 *Coscinodiscus africanus*	0	0	0	0	0	2	0	0	0	0
2 *C. centralis*	1	4	7	2	2	0	0	0	1	0
2 *C. curvatulus*	1	0	1	4	0	0	1	0	0	6
2 *C. granii*	2	0	2	2	0	4	1	0	1	2
2 *C. marginatus*	2	0	1	0	0	2	1	0	2	1
1 *C. nodulifer*	44	33	41	35	42	24	24	14	39	41
2 *C. perforatus-fimbriatus*	27	17	17	26	24	23	15	15	30	25
3 *C. radiatus*	0	0	0	2	0	0	0	0	0	3
3 *C. stellaris*	6	2	5	9	9	10	5	5	6	4
3 *Cyclotella striata*	0	0	0	0	0	0	0	0	0	1
1 *C. stylorum*	2	0	1	1	0	0	0	0	0	1
2 *Ditylum brightwellii*	0	2	0	3	3	0	2	0	0	1
1 *Hemiaulus sinensis*	0	0	0	0	1	0	0	0	0	0
1 *Hemidiscus cuneiformis*	6	7	5	6	1	13	9	2	8	4
2 *Lithodesmium undulatum*	2	1	2	1	0	5	8	0	2	1
3 *Nitzschia bicapitata-braarudii*	2	0	0	0	0	0	0	0	0	0
1 *N. marina*	0	1	0	1	0	0	0	0	0	0
3 *N. pungens*	0	0	0	1	0	2	1	0	0	0
2 *Odontella aurita*	0	4	0	3	0	1	4	0	1	0
2 *O. mobiliensis*	0	0	0	0	0	0	1	0	0	0
3 *Paralia sulcata*	1	0	0	0	1	0	0	1	1	2
1 *Planktoniella sol*	0	0	0	0	1	0	0	0	0	0
1 *Pseudoeunotia doliolus*	8	7	4	10	7	3	2	3	0	6
3 *Rhizosolenia alata*	0	0	3	5	6	4	1	0	0	0
1 *R. bergonii*	1	0	0	0	1	1	2	0	0	0
3 *R. calcar-avis*	0	0	0	1	0	1	0	0	0	0
3 *R. hebetata*	0	0	0	0	1	0	0	0	0	1
1 *R. robusta*	0	0	0	2	1	0	1	0	0	0
3 *R. setigera*	0	1	0	1	2	0	0	0	1	3
3 *R. styliformis*	0	0	0	1	1	0	0	0	2	0
1 *Roperia tesselata*	11	22	15	30	23	29	19	13	20	4
1 *Stephanopyxis palmeriana*	2	2	9	5	11	4	19	13	20	1
3 *S. turris*	23	28	37	16	17	9	27	22	28	48
1 *Thalassionema bacillaris*	6	10	3	18	15	18	8	3	5	7
3 *T. nitzschioides*	22	12	5	24	20	15	17	7	17	19
2 *Thalassiosira anguste-lineata*	0	0	1	0	0	0	1	0	2	2
2 *T. decipiens*	0	0	0	0	0	0	0	0	1	0
3 *T. eccentrica*	1	0	2	3	1	0	0	1	1	2
1 *T. endoseriata*	2	2	1	5	0	4	5	2	0	0
1 *T. lineata*	0	0	0	0	0	0	1	0	0	0
3 *T. oestrupii*	3	2	1	1	0	0	0	2	2	0
1 *T. punctifera*	3	3	6	1	7	9	10	5	7	9
0 *T. simonsenii*	2	2	1	1	0	0	0	2	2	0
3 *T. subtillis*	0	0	0	0	0	0	0	0	0	0
3 *T. symmetrica*	0	0	1	1	3	0	1	0	0	0
0 *Thalassiothrix sp indet*	0	2	0	1	2	0	1	0	0	0
1 *T. frauenfeldii*	0	0	0	0	0	0	1	0	1	2
3 *T. longissima*	11	14	6	9	8	15	7	5	14	16
1 *T. mediterranea-delicata*	8	4	2	3	3	3	3	1	2	2
1 *T. vanhoeffenii*	0	0	0	0	1	0	0	0	0	0
3 *Trigonium alterans*	0	0	0	0	1	1	0	0	0	1
1 *Dictyocha calida*	4	5	7	7	3	4	3	4	3	4
2 *D. epiodon*	0	1	1	1	0	0	0	0	0	12
3 *D. messanensis*	23	17	18	19	12	21	15	10	21	11
1 *Octactis pulchra*	8	13	5	12	7	8	2	3	4	4

Figure I-4

Plots of the five total assemblage parameters obtained from the 24-62 μm size fraction. Each series presented in units of its standard deviation. Original units for the upper two series correspond to $\log_{10}$ cells/cm^2-year for density of individuals and total number of taxa per year for species richness. Bottom three plots are indices of relative importance of each biogeographic subassemblage. A biogeographic index is computed as:

$$G_k = \sum_{i=1}^{n} (10 + \log p_i)$$

where G_k is the annual value for the kth group; p_i is the proportion of the ith species in the kth biogeographic group computed as a proportion of the total assemblage and n is the number of species in the biogeographic group.

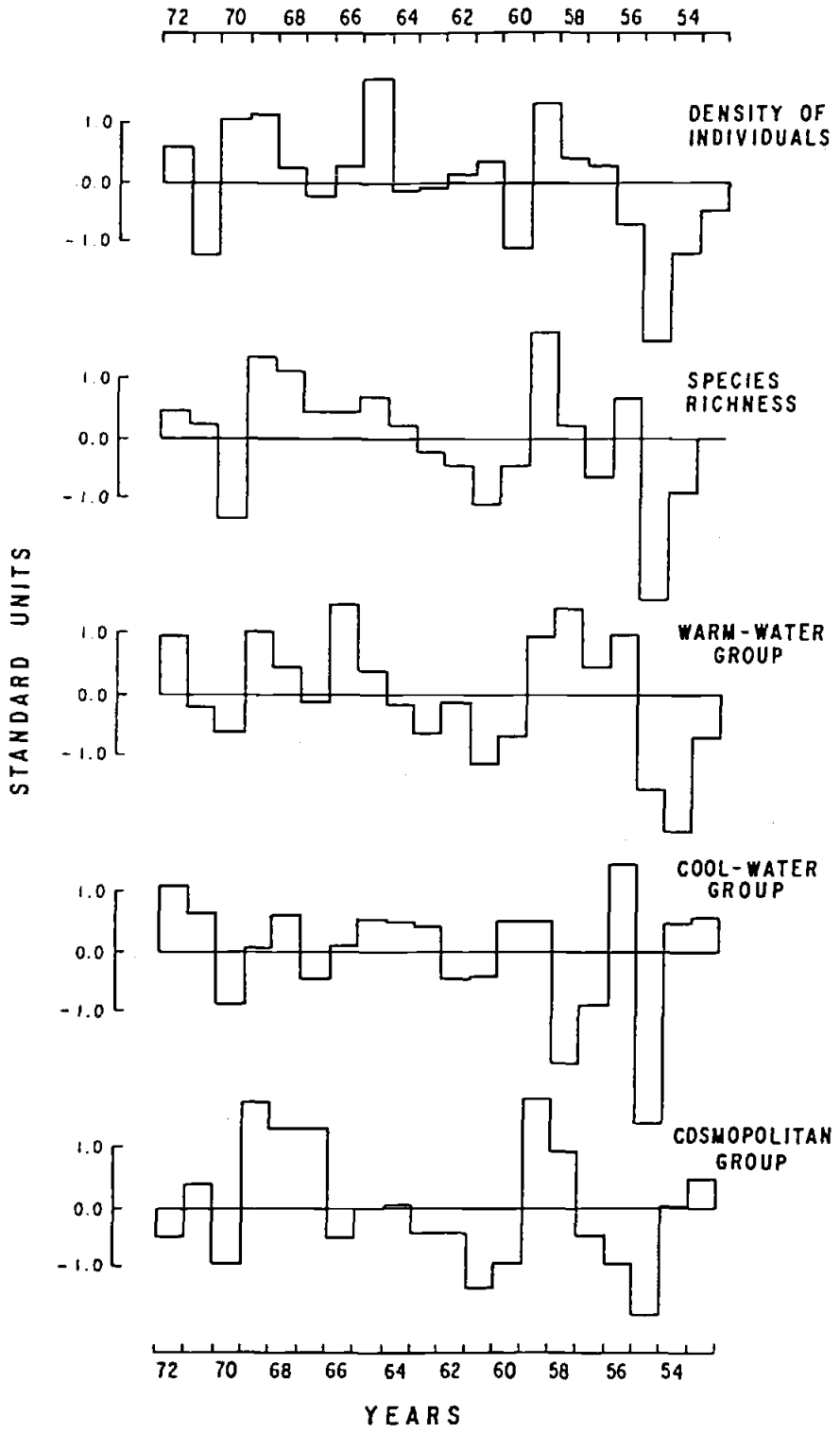
72 70 68 66 64 62 60 58 56 54
DENSITY OF INDIVIDUALS
SPECIES RICHNESS
WARM-WATER GROUP
COOL-WATER GROUP
COSMOPOLITAN GROUP
1.0
0.0
-1.0
STANDARD UNITS
YEARS

Figure I-4

which suggests the history of structural changes which occurred in the living planktic diatom community. The varve series of species-richness is shown in the second plot of Figure I-4. The richness values are plotted as standard units. The original values vary from 25 (varve 18) to 48 (varve 14) taxa.

Three broad biogeographic categories (see Table I-1) were adopted to examine the behaviour of the total species assemblage in terms of the biogeographic distributions of component taxa. These categories are warm-water, cool-water, and cosmopolitan subassemblages. The warm-water subassemblage consists of those species with reported ranges from equatorial/tropical through subtropical latitudes within the eastern Pacific. This group corresponds to the major ecosystems denoted by McGowan (1974) as Equatorial, Eastern Tropical Pacific and Central Pacific. The cool-water sub-assemblage is composed of species which occur from subtropical through subartic latitudes. This group corresponds to the Transitional and Subartic ecosystems associated with the California Current and also includes forms present in the Central Pacific. All species which range from the tropics through at least northern temperate (south boreal) latitudes are placed in the cosmopolitan category. Five species groups could not be assigned to a biogeographic category and are so indicated in Table I-1.

The relative abundances of species approaches a logarithmic distribution with the majority of individuals belonging to only a few taxa. In order to preserve the information from the rarer taxa, we have transformed the relative species abundances into a logarithmic index. The annual value associated with a biogeographic group relative to all other years is thus defined by:

$$G_{jk} = \sum_{i=1}^{n} (10 + \log p_i)$$

where j = 1-20 varves, k = 1-3 of the biogeographic groups, and p_i is the proportion of the ith species in a given biogeographic group which is computed as a proportion of the total assemblage. The serial variation of each biogeographic category throughout the twenty varves is presented in the lower three plots of Figure I-4. Values of the index G_j for each of the three biogeographic groups are plotted in standard units.

Linear correlations among all pairs of the total assemblage parameters are shown in Table I-2. Of the three biogeographic groups, the warm-water forms are most closely associated with the density of individuals. Species richness is strongly controlled by variation in the warm-water and cosmopolitan groups, but is also clearly associated with the density of individuals as well as the cool-water group. The warm-water and cool-water groups are poorly correlated as expected, and the warm-water and cosmopolitan groups are only moderately correlated. These observations suggest that the production and subsequent preservation of skeletal material, reflected in the density of individuals, is most closely related to variation in the warm-water subassemblage.

Four species were selected from the warm-water group for independent counts to compare the behaviour of individual component taxa to the warm-water subassemblage. Three of these species exhibit rare to low abundances: Octactis pulchra (relative abundance of 1-5%), Hemidiscus cuneiformis (1-5%) and Roperia tesselata (1-8%). The fourth species, Coscinodiscus nodulifer, ranges from moderate to high abundances (7-20%) throughout the varve series. Figure I-5 shows the standardized values of total valves per varve and illustrates a generally similar pattern of variability for all four species. The correlation coefficients of Table I-3 indicate reasonable coherence among the species and that individual species within the warm-water group do tend to behave in similar fashion. However, correlation of the warm-water index to individual species shows that none of the species is a close duplicate of the index. Despite these low to moderate correlations, the four species provide sufficient redundancy of information to

Table I-2

Correlation matrix for total assemblage parameters. Values ≥0.52 associated with probability ≥0.98 that the correlation is real; n = 20

	species richness	density of individuals	cosmopolitan group	cool-water group
warm-water group	0.74	0.59	0.43	0.21
cool-water group	0.64	0.23	0.24	
cosmopolitan group	0.78	0.43		
density of individuals	0.58			

Figure I-5

Patterns of annual abundances of four species from the warm-water sub-assemblage presented as standard units. Original units are estimated total number of valves per year. Data obtained from analysis of both size fractions: 24-62 μm and >62 μm.

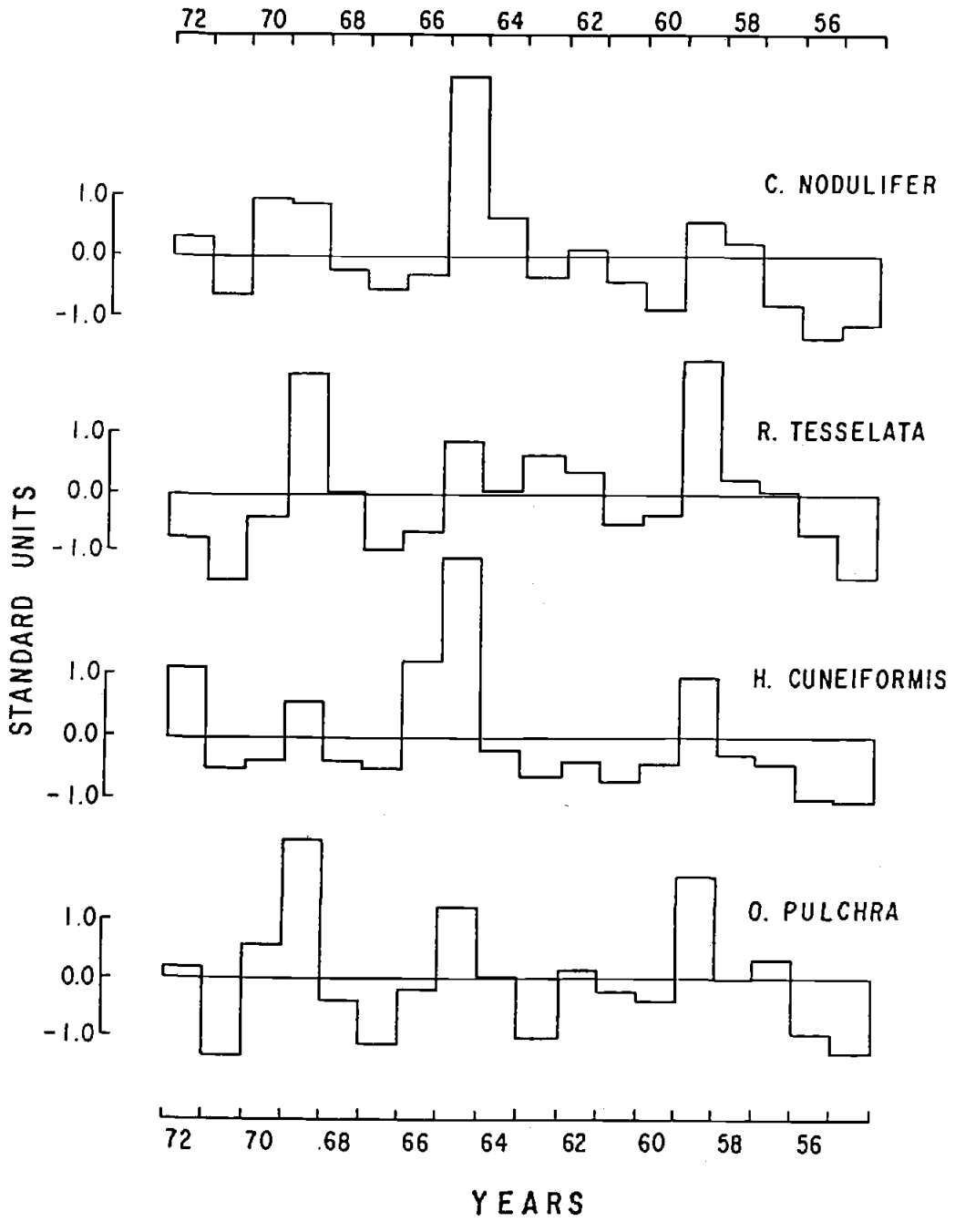
72 70 68 66 64 62 60 58 56
C. NODULIFER
R. TESSELATA
H. CUNEIFORMIS
O. PULCHRA
1.0
0.0
-1.0
STANDARD UNITS
72 70 68 66 64 62 60 58 56
YEARS

Figure I-5

Table I-3

Correlation matrix for abundances of four warm-water species and the index of warm-water group. Values ≥0.47 associated with probability ≥0.95 that correlation is real; n = 18

	warm-water group	*Coscinodiscus nodulifer*	*Roperia tesselata*	*Hemidiscus cuneiformis*
Octactis pulchra	0.44	0.71	0.83	0.62
Hemisdiscus cuneiformis	0.49	0.80	0.44	
Roperia tesselata	0.40	0.55		
Coscinodiscus nodulifer	0.24			

verify the pattern of the warm-water index while pointing out that the cumulative tendency in behaviour of the sum of warm-water species shown by the index may vary somewhat differently from each of its component taxa.

ECOLOGIC RESPONSE TO CLIMATIC CHANGE

Short-term variation in the ocean-atmosphere climatic system exhibits characteristic periods ranging from three to seven years, encompassing large areas of the globe, but most clearly evident in the tropical and subtropical regions of the Pacific. Such large-scale climatic variability is now clearly associated with the interrelated phenomena of the El Niño and the Southern Oscillation (Philander, 1983).

Year-to-year sea level fluctuation in the Gulf of California is strongly associated with the El Niño/Southern Oscillation phenomenon (Fig. I-6). The sea level anomalies shown in Figure I-6 are deviations of a given monthly value from the long-term mean of that month, so that seasonal variability is removed, and year-to-year changes are emphasized. The raw sea level data used are a regional average from stations at Guaymas, Topolobampo, La Paz and Mazatlán taken from Grivel-Piña (1977). The Southern Oscillation index consists of the differences in non-seasonal monthly anomalies in atmospheric pressure at sea level between Easter Island and at Darwin, Australia (Quinn et al., 1978). Both series were low-pass filtered to remove all frequencies higher than one cycle per year.

Interannual variation of sea level in the Gulf is therefore a sensitive index of large-scale ocean climate. Baumgartner and Christensen (in preparation), as well as McLain and Thomas (1983), suggest that this variability is related to the strength of meridional transport of water along the west coast of North America. Bernal (1981) has successfully related sea level anomalies with zooplankton variability in the California Current. Positive sea level anomalies in our Figure I-6 are interpreted as indicating

Figure I-6

Comparison of monthly sea level anomalies in the Gulf of California with an index of the Southern Oscillation for 1953-1974 interval. Note that Southern Oscillation index is inverted. Both series are low-pass filtered to remove frequencies higher than 1 yr^{-1}. El Niño events noted by Quinn et al. (1978) are indicated above the sea level curve.

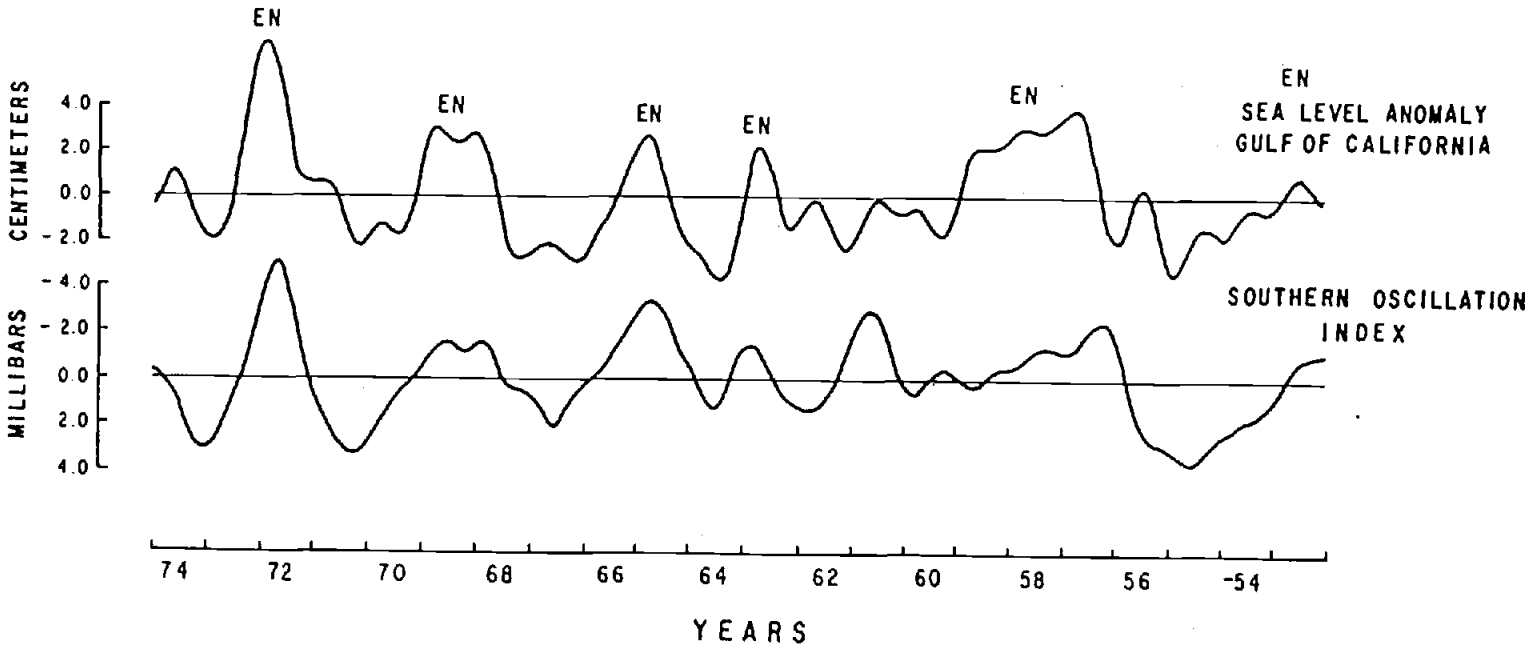
EN
EN
EN
EN
EN
EN
SEA LEVEL ANOMALY
GULF OF CALIFORNIA
CENTIMETERS
4.0
2.0
0.0
-2.0
MILLIBARS
-4.0
-2.0
0.0
2.0
4.0
SOUTHERN OSCILLATION
INDEX
74
72
70
68
66
64
62
60
58
56
-54
YEARS

Figure I-6

greater relative tropical influence within the Gulf, associated with weakened southward transport along the eastern limb of the North Pacific gyre and increased northward transport of tropical water along the coast of Central America.

The existence of a signal in the siliceous phytoplankton assemblage, which occurs as a response to climatic change, is evaluated by comparison of the sea level anomalies to the ecological data. In order to make this comparison we have computed average annual sea level anomalies over a calendar year from the monthly anomalies. This permits the calculation of correlation coefficients from compatible series of data. The upper plot in Figure I-7 shows the 12-month averages of the sea level anomaly for comparison with the relative importance of the warm-water group and the density of individuals. Table I-4 presents the correlations between the sea level anomaly and the parameters used to characterize the total assemblage as well as the abundances of the four individual species.

Of the five total assemblage parameters, the warm-water index and density of individuals are most highly correlated to sea level, reaching very high levels of significance while species richness is moderately correlated to sea level. The cool-water index is uncorrelated and the cosmopolitan index is poorly correlated to sea level. Comparison of the plots on Figure I-7 also indicates that the pattern of year-to-year climatic change is indeed reflected in the fossil plankton assemblage. The principal El Niño events occurring through the periods 1957-1959, 1965, 1968-1969 and 1972 are accompanied by increases in the index of warm-water forms and density of individuals occurring around these periods. Three of the individual species from the warm-water group also show significant correlations to sea level; only C. nodulifer is poorly correlated.

Figure I-7

Comparison of Gulf of California sea level anomalies plotted as 12-month averages to the warm-water biogeographic index and the density of individuals from Figure I-4.

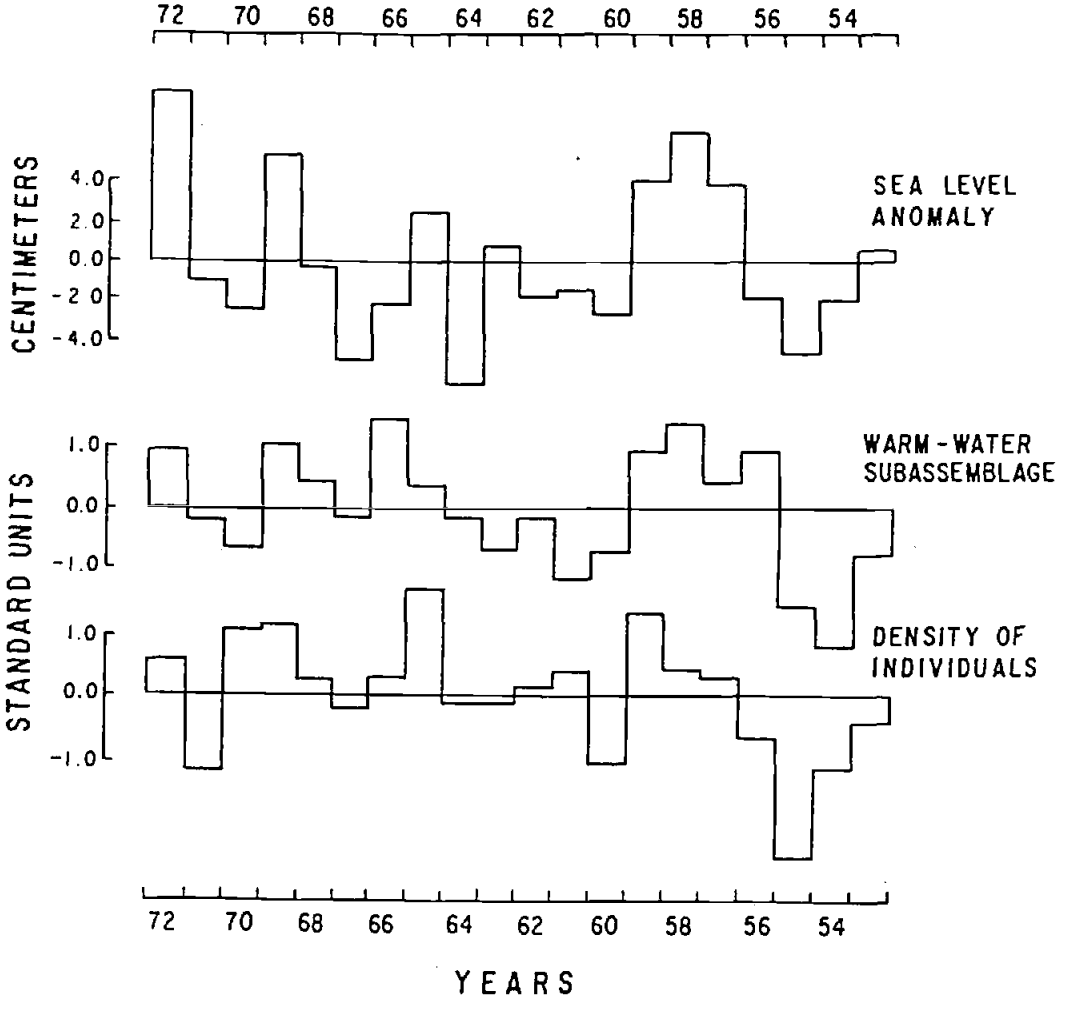
72 70 68 66 64 62 60 58 56 54
CENTIMETERS
4.0
2.0
0.0
-2.0
-4.0
SEA LEVEL ANOMALY
STANDARD UNITS
1.0
0.0
-1.0
WARM-WATER SUBASSEMBLAGE
1.0
0.0
-1.0
DENSITY OF INDIVIDUALS
72 70 68 66 64 62 60 58 56 54
YEARS

Figure I-7

Table I-4

Correlations (r) between the non-seasonal sea level anomaly series and the total assemblage parameters plus the abundances of four individual species. P indicates probability of $r \neq 0$. For assemblage parameters n = 20; for individual species n = 18

	Sea level anomaly	
	r	P
Density of individuals	0.54	>0.98
Species richness	0.43	>0.90
Warm-water group	0.55	>0.98
Cool-water group	0.11	<0.50
Cosmopolitan group	0.37	>0.80
Coscinodiscus nodulifer	0.33	>0.80
Roperia tesselata	0.49	>0.95
Hemidiscus cuneiformis	0.45	>0.90
Octactis pulchra	0.55	>0.98

CONCLUSIONS

The results of this study leave little doubt that a signal of year-to-year ecological response to climate is recorded by the siliceous phytoplankton assemblage within the varved sediments of the Gulf of California. This signal appears to consist in the increase or decrease of the abundances and subsequent preservation of tropical to sub-tropical warm-water species which might be relatively easily monitored from the sediments by following the behaviour of several well-selected indictor taxa. The association of the indices estimating variation for the warm-water group and for density of individuals indicates that productivity of the siliceous assemblage in the central Gulf is strongly dependent upon the warm-water subassemblage which increases during El Niño periods.

Investigation of the mechanism of this ecologic response to interannual climatic change is beyond the scope of this paper. However, we may note that other major ecosystems in the eastern Pacific also experience significant interannual variability in biological productivity associated with the El Niño phenomenon. This has been well-documented for the California Current System (Bernal, 1981) and the Peru Current System (Cowles, et al., 1977; Cushing, 1981). The variation of productivity in the Gulf of California inferred from this study is, however, inversely related to productivity patterns in the California and Peru Current Systems. Our data suggests that in the Gulf of California, El Niño conditions are associated with increased diatom productivity, while the California and Peru Currents suffer significant decreases in overall biological productivity during El Niño periods.

ACKNOWLEDGMENTS

This work was supported by CoNaCyT Grant PCMABNA-005321 from the Mexican Government and through Grants ATM 81-21775-01 and OCE-18001 from the U.S. National Science Foundation. We wish to thank Sergio Ramos who drafted the figures and Gilda Elorriaga and Carmen de Jesús who typed several versions of the manuscript. Mark Whiting and Laurel Muelhausen reviewed early versions of the paper. William Quinn provided data for calculation of the Southern Oscillation index.

REFERENCES

Bernal, P.A., 1981. A review of the low frequency response of the pelagic ecosystem in the California Current. Calif. Coop. Oceanic Fish. Invest. Rpts., 22:49-62.

Bischoff, J.L. and J.W. Niemitz, 1980. Bathymetric maps of the Gulf of California. U.S. Geological Survey, Miscellaneous Investigation Series, Map 1-1244.

Bruland, K.W., 1974. ^{210}Pb geochronology in the coastal marine environment. Ph.D. Dissertation, University of California, San Diego, 106 pp.

Calvert, S.E., 1964. Factors affecting the formation of laminated diatomaceous sediments in the Gulf of California. In: Tj.H. van Andel and G.G. Shor (eds), Marine Geology of the Gulf of California. Mem. Amer. Assoc. Petrol. Geol., 3:311-330.

Calvert, S.E., 1966. Origin of diatom-rich varved sediments from the Gulf of California. J. Geol., 76:546-565.

Cowles, T.J., R.T. Barber and O. Guillen, 1977. Biological consequences of the 1975 El Niño. Science, 195:285-287.

Cupp, E.E., 1943. Marine plankton diatoms of the west coast of North America. Bull. Scripps Instit. Ocean., 5:1-238.

Cushing, D.H., 1981. The effect of El Niño upon the Peruvian anchoveta stock. In: F.A. Richards (ed), Coastal Upwelling. Amer. Geophys. Union, pp. 449-457.

De Geer, G., 1912. A geochronology of the last 12,000 years. Cong. Geol., Internat. 11th, Stockholm, 1910, Comptes Rendus., pp. 241-253.

DeMaster, D.J., 1979. The marine budgets of silica and ^{32}Si. Ph.D. Dissertation, Yale Univ., 308 pp.

Donegan D. and H. Schrader, 1982. Biogenic and abiogenic components of laminated hemipelagic sediments in the central Gulf of California. Mar. Geol., 48:215-237.

Enfield, D.B. and J.S. Allen, 1980. On the structure and dynamics of monthly mean sea level anomalies along the Pacific coast of North and South America. J. Phys. Oceanogr., 10:557-578.

Fenner, J., H.J. Schrader and H. Wienigk, 1976. Diatom phytoplankton studies in the southern Pacific Ocean, composition and correlation to the Antarctic convergence and its paleoecological significance. In: C.D. Hollister, C. Craddock et al. (eds), Initial Reports of the Deep Sea Drilling Project, Vol. 35, U.S. Government Printing Office, Washington, DC, pp. 757-813.

Fryxell, G.A. and G.R. Hasle, 1972. Thalassiosira eccentrica (Ehrenb.) Cleve, T. symmetrica sp. nov., and some related centric diatoms. J. Phycol., 8:297-317.

Grivel-Piña, F., 1977. Datos Geofísicos, Serie A, Oceanografía 3. Instituto Geofísica. Univ. Nac. Auton. de México, 197 pp.

Hasle, G.R., 1960. Phytoplankton and ciliate species from the tropical Pacific. Skr. Norske Vidensk., Akad. Oslo, Mat. Nat. Kl., 2:1-50.

Hasle, G.R., 1976. The biogeography of some marine planktonic diatoms. Deep-Sea Res., 23:319-338.

Hendey, N.I., 1964. An introductory account of the smaller algae of British coastal waters. Part V. Bacillariophyceae (Diatoms). Her majesty's Stationary Office, London, 317 pp.

Hustedt, F., 1930. Die Kieselalgen Deutschlands, Österreichs und der Schweiz mit Berücksichtigung der übrigen Länder Europas sowie der agrenzenden Meeresgebiete. In: L. Rabenhorst (ed), Kryptogamenflora von Deutschland, Österreich und der Schweiz, 7: Part 1. Akad. Verlag., Leipzig, 920 pp.

Hustedt, F., 1959. Die Kieselalgen Deutschlands, Österreichs und der Schweiz mit Berücksichtigung der übrigen Länder Europas sowie der agrenzenden Meeresgebiete. In: L. Rabenhorst (ed), Kryptogamenflora von Deutschland, Österreich und der Schweiz, 7: Part 2. Acad. Verlag., Leipzig, 845 pp.

Jousé, A.P., O.G. Kozlova and V.V. Mukhina, 1971. Distribution of diatoms in the surface layer of sediment from the Pacific Ocean. In: B.M. Funnel and W.R. Riedel (eds), Micropaleontology of the Oceans. Cambridge University Press, pp. 263-269.

Kanaya, T. and I. Koizumi, 1966. Interpretation of diatom thanatocoenoses from the North Pacific applied to a study of core V20-130. The Science Report of the Tohoku University, Sendai, Japan, 2nd Series (Geology), 37:89-130.

Karohji, K., 1972. Regional distribution of phytoplankton in the Bering Sea and eastern and northern subarctic regins of the North Pacific Ocean in summer. In: A.Y. Takenonti (ed), Biological Oceanography of the northern North Pacific. Idemitsu Shoten, Japan, pp. 99-115.

Kozlova, O.G. and V.V. Mukhina, 1967. Diatoms and silicoflagellates in suspension and floor sediments of the Pacific Ocean. Int. Geol. Rev., 9:1322-1342.

McLain, D.R. and D. Thomas, 1983. Year-to-year fluctuations of the California Countercurrent and effects on marine organisms. Calif. Coop. Oceanic Fish. Invest. Rpts., 24:165-181.

McGowan, J.A., 1974. The nature of oceanic ecosystems. In: C.B. Miller (ed), The Biology of the Oceanic Pacific. Oregon State University Press, pp. 9-28.

Murray, D. and H. Schrader, 1983. Distribution of silicoflagellates in plankton and core top samples from the Gulf of California. Mar. Micropaleo., 7:517-539.

Philander, S.G.H., 1983. El Niño Southern Oscillation phenomena. Nature, 302:295-301.

Poelchau, H.S., 1976. Distribution of Holocene silicoflagellates in North Pacific sediments. Micropaleo., 22:164-193.

Quinn, W.H., D.O. Zopf, K.S. Short and R.T.W. Kuo Yang, 1978. Historical trends and statistics of the Southern Oscillation, El Niño and Indonesian droughts. Fish. Bull., 76:663-678.

Schrader, H-J. and R. Gersonde, 1978. Diatoms and silicoflagellates. Utrecht Micropaleont. Bull., 17:129-176.

Simonsen, R., 1974. The diatom plankton of the Indian Ocean Expedition of RV "Meteor" 1964-1965. In: "Meteor" Forschung., Deutschen Forschungsgem., Reihe D., No. 19. Biologie, pp. 1-65.

Smayda, T.J., 1958. Biogeographical studies of marine phytoplankton. Oikos, 9:158-191.

Soutar, A. and P.A. Crill, 1977. Sedimentation and climatic patterns in the Santa Barbara Basin during the 19th and 20th centuries. Geol. Soc. Amer. Bull., 88:1161-1172.

Soutar, A., S.R. Johnson and T.R. Baumgartner, 1981. In search of modern depositional analogs to the Monterey Formation. In: R.E. Garrison and K. Pisciotto (eds), The Monterey Formation and Related Siliceous Rocks of California. Spec. Publ., soc. Econ. Paleontol. and Mineral. Pac. Sect., pp. 123-147.

Venrick, E.L., 1971. Recurrent groups of diatom species in the North Pacific. Ecology, 52:614-625.

Wyrtki, K., 1962. The oxygen minimum in relation to ocean circulation. Deep-Sea Res., 9:11-23.

CHAPTER II

COUPLING OF THE GULF OF CALIFORNIA TO LARGE-SCALE INTERANNUAL CLIMATIC VARIABILITY

ABSTRACT

The source of interannual changes in the ocean climate of the Gulf of California, indicated by sea level and shore temperature anomalies, is determined by comparison with large-scale circulation in the Pacific Ocean and atmosphere. Independent modes of variability in the large-scale circulation are defined by empirical orthogonal function analysis of eight time series representing the principal ocean currents and surface wind systems. Interannual ocean climate in the Gulf of California is related only to the equatorial mode of variability commonly known as the El Niño/Southern Oscillation. There is no discernible relationship between the Gulf and independent modes of variability in the North Pacific gyre. Interannual variability in the Gulf is associated with the cyclonic north equatorial circulation composed of the North Equatorial Countercurrent, the North Equatorial Current and the Costa Rica Current.

INTRODUCTION

The Gulf of California is a marginal sea approximately 1000 km long and 200 km wide separated from the Pacific by the narrow peninsula of Baja California. South of the large midriff islands near 29°N, the Gulf is formed into a series of basins whose si depths shoal from approximately 300 m at the entrance to 1600 m in the north (Rusnak et al., 1964). South of 28°N, the water column is in open communication with the Pacific. The mouth of the Gulf is located in a hydrographically complex region of oceanic transition (Roden, 1971).

Two major wind-driven current systems may influence the ocean climate of the Gulf of California. These are the equatorial system and the North Pacific anticyclonic gyre system. The surface currents vary significantly throughout an annual cycle as a response to changing strengths and positions of major wind systems. Two principal circulation patterns are described by Wyrtki (1966) which dominate around March-April and September-October (Fig. II-1). The spring pattern consists of a strong North Pacific gyre with California Current water spread across the entrance to the Gulf of California and a relatively weakened equatorial system withdrawn to the south. The autumn pattern shows a weakened North Pacific gyre and a strong North Equatorial Countercurrent and the development of the Costa Rica Current extending northward to the entrance of the Gulf.

Our examination of the coupling of the Gulf of California to interannual variability of large-scale circulation in the ocean and atmosphere is guided by formulating a simple hypothesis suggested by the seasonal variation in the current patterns seen in Figure II-1. We postulate the existence of two principal sources for interannual variability in the Gulf. These are independent fluctuations in the strength of: (a) the North Pacific gyre, and (b) the equatorial circulation, either of which may result in non-seasonal predominance or enhancement of one seasonal circulation pattern over the other.

Figure II-1

Principal seasonal circulation patterns of wind driven surface currents in the Eastern Tropical Pacific and California Current regions (adapted from Wyrtki, 1965a, 1965b). Current systems are indicated by abbreviations over areas of generalized flow shown by arrows (California Current: CC; North Equatorial Current: NEC; North Equatorial Countercurrent: NECC; South Equatorial Current: SEC; Costa Rica Current: CRC). Dashed boundaries distinguish seasonal extensions of the NECC and the southern limit of the CC; Intertropical Convergence is marked by dotted line.

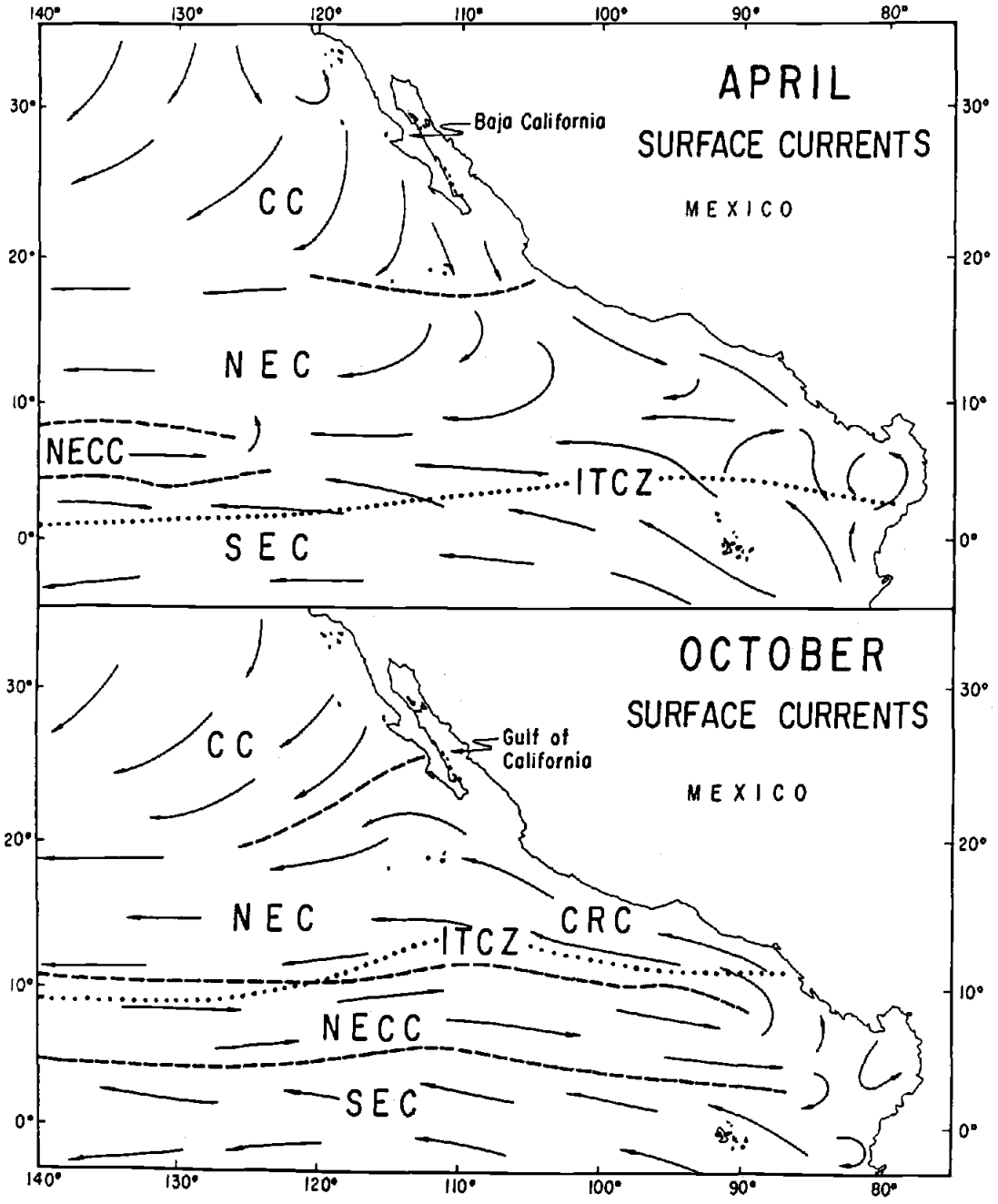
APRIL
SURFACE CURRENTS
MEXICO
Baja California
CC
NEC
NECC
ITCZ
SEC
OCTOBER
SURFACE CURRENTS
MEXICO
Gulf of California
CC
NEC
CRC
ITCZ
NECC
SEC
140°
130°
120°
110°
100°
90°
80°
30°
20°
10°
0°

Figure II-1

Interannual climatic variability in the tropical Pacific and much of global interannual change, linked to the tropical Pacific through large-scale teleconnections (Bjerknes, 1969; Horel and Wallace, 1981), is now known to be associated with the interrelated phenomena of El Niño and the Southern Oscillation (Philander, 1983). Interannual variability in the southward transport of the North Pacific gyre is not expected to be totally independent of the equatorial current circulation which is strongly influenced by the occurrence of El Niño (Wyrtki, 1979a). Numerical models presented by McCreary (1976, 1978) indicate that the effects of El Niño originating along the equator, propagate poleward along the eastern boundary of the Pacific. Both Enfield and Allen (1980) and Chelton and Davis (1982) have demonstrated the poleward propagation of the El Niño signal in sea level along the western coasts of the Americas. Over interannual time scales, the coastal sea level anomalies are strongly coherent over thousands of kilometers. Thus the edge of the North Pacific gyre is clearly affected by the El Niño, and Chelton (1980, 1981) has demonstrated that the southward transport of the California Current is related to the occurrence of El Niño.

Evidence for independent sources of variability and statistical decoupling of the North Pacific gyre from the equatorial circulation is found, however, in the annual values of transport across the gyre computed by White (1975). Comparison of this index to the current index of the North Equatorial Current (White, 1977), shows features which are uncorrelated although the scale of variability is similar. White and Barnett (1972) have postulated a feedback system operating at mid-latitude between the ocean and atmosphere which should tend to decouple the subtropical gyre from the variability in the equatorial Pacific. Chelton and Davis (1982) have also demonstrated that a significant portion of the dominant pattern of variability in coastal sea level from Mexico to Alaska is associated with basin-wide atmospheric forcing in the mid-latitude North Pacific.

Our hypothesis for interannual change of ocean climate in the Gulf of California is tested by correlation of Gulf sea level and temperature anomalies to statistically independent modes representing variability in the ocean and atmosphere from the equatorial through the central and eastern North Pacific. Time series of eight variables are chosen to economically represent the remote forcing upon the Gulf by the equatorial circulation and the eastern limb of the subtropical North Pacific gyre. The variance of these remote processes is decomposed into uncorrelated modes as empirical orthogonal functions (EOF's).

LARGE-SCALE INTERANNUAL VARIABILITY IN THE OCEAN AND ATMOSPHERE

Remote Climatic Variables

The time series selected to summarize the large-scale ocean circulation are indices of transport for the North Equatorial Current (NEC), the North Equatorial Countercurrent (NECC), the South Equatorial Current (SEC) and the eastern limb of the North Pacific gyre (ENPG). These indices are sea level differences across the currents, indicating relative changes in surface current strengths. Proxy indices of the atmospheric circulation associated with these currents are obtained from atmospheric pressure differences at sea level between appropriate high and low pressure centers. Distribution of the pressure centers in relation to the currents is shown in Figure II-2.

Wyrtki (1974a) has described the method for computing the indices of the equatorial currents which is based on the mean meridional structure of dynamic heights and the use of sea level measured at islands in the central and western Pacific. The NEC index is obtained from sea level at Honolulu, Hawaii and Kwajalein Island, and represents the difference in dynamic height between the north equatorial ridge and the Countercurrent trough. The NECC index is the sea level difference between Christmas Island on the equatorial ridge and Kwajalein Island in the Countercurrent trough. The

Figure II-2

Locations of atmospheric pressure centers and the ocean surface current systems referred to in the text. Locations of coastal (San Francisco) and mid-Pacific island sea level stations are also indicated (H: Honolulu; K: Kwajalein; Ch: Christmas; Ca: Canton; T: Tahiti). Monthly atmospheric pressure at sea level averaged from 13 grid points within the boundary shown for Aleutian Low, from 12 points within the boundary of North Pacific High and from four points within the boundary of the Mexican Low. Monthly pressure values of South Pacific High and Indonesian Low represented by Easter Island (E) and Darwin, Australia (D), respectively.

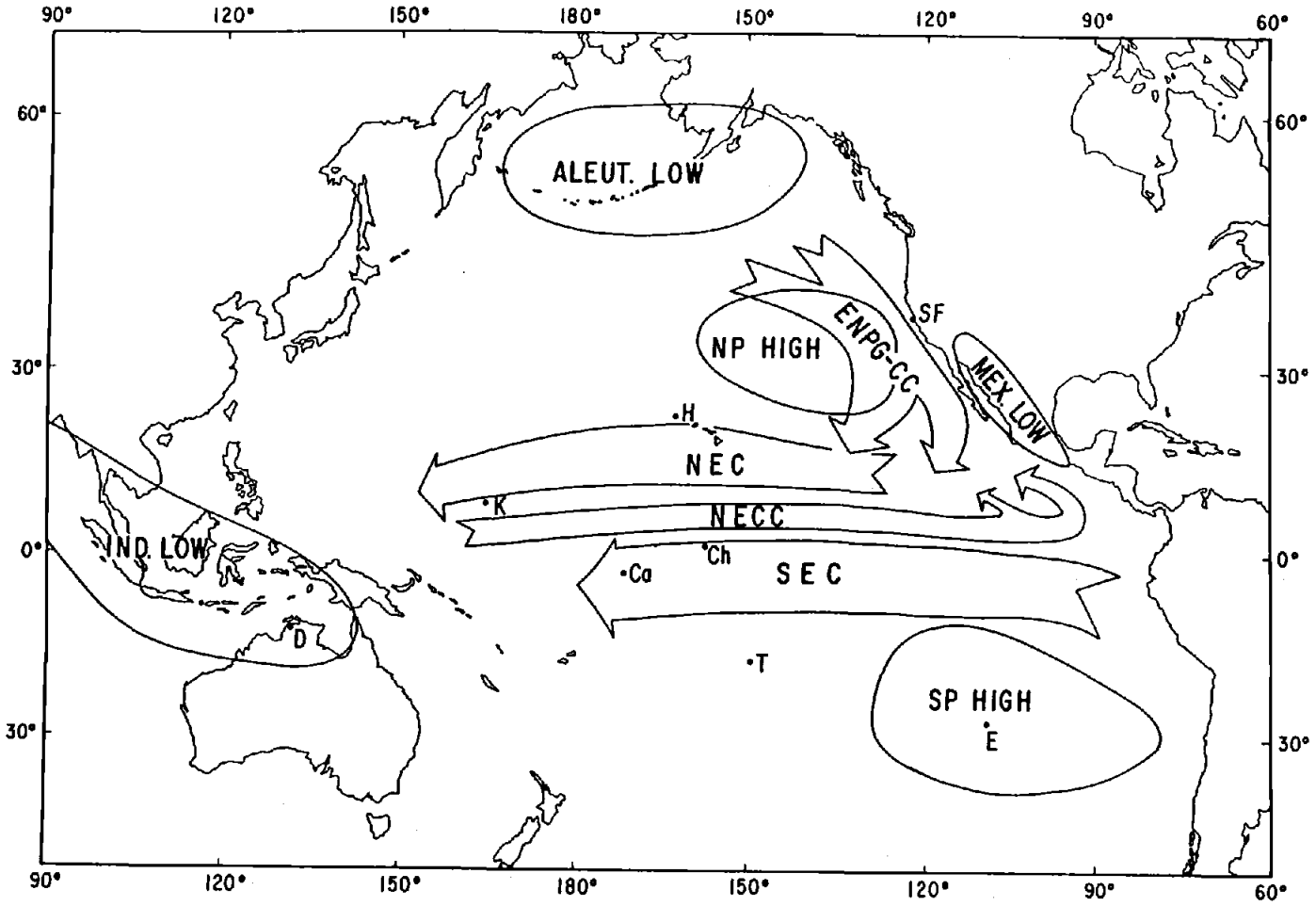
90°
120°
150°
180°
150°
120°
90°
60°
60°
30°
0°
30°
ALEUT. LOW
NP HIGH
ENPC-CC
SF
MEX. LOW
H
NEC
K
NECC
IND. LOW
Ca
Ch
SEC
D
T
SP HIGH
E

Figure II-2

SEC index is the sea level difference between Tahiti (with some time intervals patched by data from Pago Pago, American Samoa) and Canton Island which lie on the south equatorial ridge and in the equatorial trough, respectively. Positions of the island stations are shown in Figure II-2.

Flow within the eastern limb of the anticyclonic North Pacific gyre (ENPG) which encompasses the California Current is represented by the sea level difference between Honolulu and San Francisco (see also Fig. II-2). This was proposed by Saur (1972) as a current index to evaluate large scale variability in transport. Because it covers a substantially greater (>3000 km) distance than the width of the eastern boundary current, it is not an index of advection in just the California Current which has a width of between 300 and 1000 km. Rather, the ENPG index is linearly proportional to the average of the transport incorporating all surface currents flowing between San Francisco and Honolulu (assuming the Coriolis parameter to be constant; see Christensen and Rodriguez, 1979). For example, an increase in the northward flowing inshore California Countercurrent would have the same effect on coastal sea level and the difference index, as a decrease in the strength of the California Current.

Price (1981) has identified four current regimes between Honolulu and San Francisco. The broadest portion is a southward interior flow, which is bounded on the east by the higher velocity, California Current. These two central southward flows are bordered by two narrow northward flows: the Davidson Countercurrent along the California coast and a countercurrent adjacent to the Hawaiian Islands. Price (1981) has shown that a good correlation ($r = -.63$) exists between the sea level difference from Honolulu to San Francisco and the total average surface transport. He also shows that San Francisco alone is poorly correlated to the total transport ($r = -.18$) while Honolulu itself is better correlated ($r = -.71$) than the Honolulu-San Francisco difference. We have retained the difference index here rather than employ the Honolulu sea level values alone (in spite of the slightly lower correlation to transport) because of its physical

relationship to geostrophic flow as well as because Price (1981) shows that the sea level difference is a better predictor of the flow in the California Current (r = -.56) than is the Honolulu sea level (r = -.41). Our ENPG difference index is thus preferred to individual station values even though each station may respond to different modes of forcing (San Francisco affected by poleward propagation of equatorial processes versus the influence of changes in the basin-wide wind field on Hawaii). Different physical modes which may occur together in a single series should be separated into independent statistical modes by the EOF analysis.

Raw data for the current indices consist of the monthly averages of the difference in sea level across the currents between 1952 and 1974. After removing linear trends and the long-term means, the annual cycle was removed by subtracting the 23-year average from each month leaving monthly anomalies. These series were then low-pass filtered employing a Lanczos taper (Blackman and Tukey, 1959) with a filter-length of 24 points to remove frequencies higher than 1 yr^{-1}. The length of the data series after filtering is reduced to 21 years ranging from 1953 through 1973. The filtered series of the current indices are presented in the lower section of Figure II-3.

Four atmospheric series are constructed from pressure differences between the high and low centers shown on Figure II-2. These are proxy indices intended to summarize the variability of the wind fields acting over the currents. Two of these indices represent regional geostrophic pressure gradients and two represent Pacific-wide sea level pressure (SLP) fluctuations associated with the Southern Oscillation.

The surface winds acting on the eastern limb of the subtropical gyre are characterized by the two atmospheric pressure gradients. The index used for the surface westerlies blowing over the northern margin of the subtropical gyre is called the Aleutian Gradient (AG). This is constructed from the difference between the monthly anomalies of the spatially averaged pressure within the mean annual position of the North Pacific high pressure cell and the monthly anomalies of the spatially averaged

Figure II-3

Eight time series of atmospheric and oceanic indices representing the remote climatic variables. Atmospheric indices constructed from differences between the high- and low-pressure centers (AG = NP High-Aleut. Low; MG = NP High-Mex. Low; NPO = NP High-Darwin; SO = Easter-Darwin). The ocean current indices are differences between sea level stations (ENPG = Honolulu-San Francisco; NEC = Honolulu-Kwajalein; NECC = Christmas-Kwajalein; SEC = Tahiti-Canton).

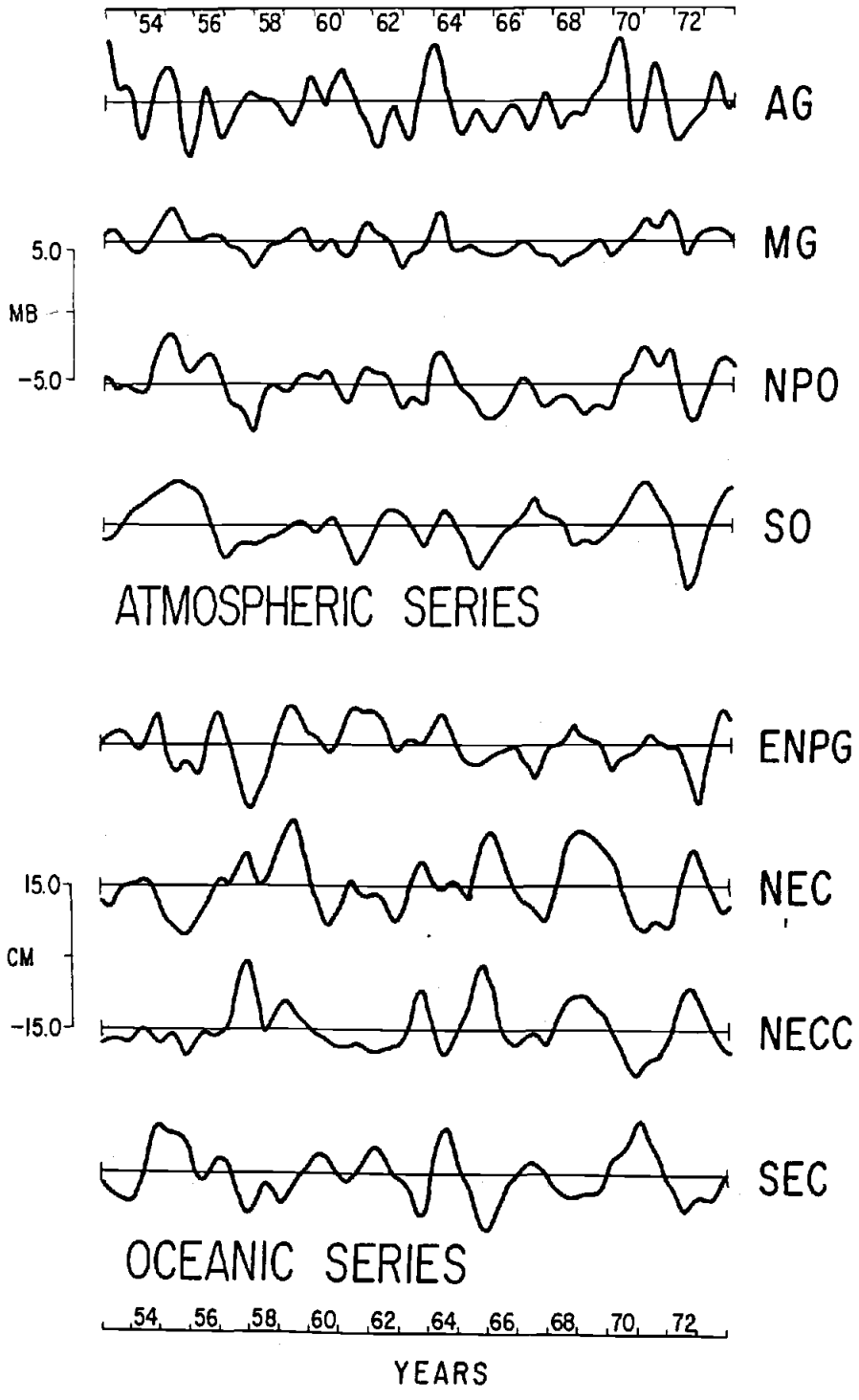
54 56 58 60 62 64 66 68 70 72
AG
5.0
MB
-5.0
MG
NPO
SO
ATMOSPHERIC SERIES
ENPG
15.0
CM
-15.0
NEC
NECC
SEC
OCEANIC SERIES
54 56 58 60 62 64 66 68 70 72
YEARS

Figure II-3

pressure within the mean annual position of the Aleutian low pressure cell. The northwesterly surface winds paralleling the coast are represented by the gradient between the low pressure over Mexico and the North Pacific high. The index is denoted as the Mexican Gradient (MG) and is the difference between the monthly anomalies of the spatially averaged pressure of the mean position of the North Pacific high and the monthly anomalies of pressure within the mean annual position of the low pressure cell over northwestern Mexico.

The remaining two atmospheric indices represent large-scale zonal atmospheric circulation associated with the Southern Oscillation. The original statistical definition of the Southern Oscillation phenomenon (Walker and Bliss, 1932; Berlage, 1957) indicated an interannual redistribution of mass between the eastern and western hemispheres, focused over southeastern Pacific and Indonesian "centers of action". Improved SLP data coverage in the North Pacific shows that the eastern Pacific surface high pressure region is partitioned into NE and SE centers of action, separated by a latitudinal trough along the ITCZ (Wright, 1977; his Figs. 8 through 11). Krishnamurti (1971) and Krishnamurti et al. (1973) also document a thermally direct east-west circulation regime connecting the Indonesian low pressure region of ascent with both the South and North Pacific subtropical high pressure regions of subsidence.

The two indices are therefore constructed from the differences in SLP over the two subtropical high pressure regions and the single equatorial low pressure center over Indonesia. The South Pacific index is obtained from the differences in monthly averages of SLP anomalies at Easter Island within the southeast Pacific high pressure center, and Darwin, Australia, lying within the equatorial low pressure center (Fig. II-2). This series is one of several used to describe the Southern Oscillation (Quinn, et al., 1978) and is so denoted here as the Southern Oscillation index (SO). The index of east-west circulation over the North Pacific is obtained from the difference in the monthly anomalies of spatially averaged SLP values within the mean annual position of

the subtropical North Pacific high pressure cell and SLP at Darwin, Australia. This series is designated as the North Pacific Oscillation index (NPO) to distinguish it from the SO index. It should be understood, however, that our NPO index describes the North Pacific manifestation of the Southern Oscillation phenomenon rather than any distinct process.

The relationship between anomalous behaviour of the Pacific tradewinds and the Southern Oscillation phenomenon has been described by various authors. Rasmusson and Carpenter (1982) have graphically demonstrated this association by showing the evolution of composited wind anomalies averaged through six El Niño events. Their data show substantial weakening, reversal or deviation of normal easterly flow in both the northeast and southeast tradewinds associated with weakening of the subtropical high-pressure centers, and movement of the center of maximum equatorial convergence from over Indonesia to the western Pacific concurrent with the development of the positive SST anomaly along the equator.

A similar index to our SO (i.e., incorporating the difference between Easter and Darwin and highly correlated to our SO series) is correlated ($r > .50$) to the zonal component of the southeast tradewinds in the core region of the central equatorial Pacific (Egger et al., 1981). Correlation of the meridional component of the northeast trades to the Southern Oscillation index of Egger et al. (1981) also yields $r < .50$. This association reflects the anomalous equatorial convergence of the northeast trades during warm episodes demonstrated by Reiter (1978) and by Rasmusson and Carpenter (1982; their Figs. 19-20). Rasmusson and Carpenter (1982; their Figs. 18-19) also show the development of westerly anomalies in the core region of the northeast trades during the initial phases of a composite El Niño event. We include the NPO index in our analysis because it incorporates the behaviour of the North Pacific high and should therefore be more related to the northeast surface wind field than is the SO index.

The data used to calculate the spatially averaged monthly anomalies within the boundaries of the high and low pressure cells in the North Pacific, shown in Figure II-2, were provided by the Climate Analysis Group of the Scripps Institution of Oceanography on a 5° diamond grid. This grid was compiled from twice-daily analys of weather maps from the National Weather Service, NOAA. Treatment of the four pressure gradient indices was the same as for the current indices described above.

Examination of Figure II-3 shows the association and dissimilarities in the eight filtered time series of the remote variables. The correlations given in Table II-1 allow for more quantitative comparison among the series. The degree of association among all series has been enhanced by filtering out a great deal of incoherent variability. Significance of the correlations is therefore derived from the statistic r/σ where σ is the large lag standard error of the correlation, and r is the correlation coefficient. σ is determined from the integral time scales of the series by comparison of the length of record to autocorrelations of the series such that:

$$\sigma^2 = \frac{1}{N}\left[1 + 2\sum_{\tau=1}^{M} C_x(\tau)\, C_y(\tau)\right]. \qquad (1)$$

C_x and C_y are the autocorrelation functions of series x and y, τ is the lag, M is a large number of lags at which σ reaches a stable value (M = 36), and N is the length of record. σ^2 is equivalent to the artificial skill of prediction constructed by Davis (1976).

Table II-1 shows the interdependence between the NPO and the SO indices (r = .68) which are linked by the contribution of Darwin to both series. The correlation between the NPO and the SO is subdued because the NP high and Easter (which are not strongly correlated, r = .33) dominate the Darwin series in their respective indices; their variances are roughly twice (NP high) to three times (SP high) greater than that of Darwin. As a result, the NPO and the SO indices are more significantly correlated to

Table II-1

Correlation matrix of the remote climatic variables.

	AG	MG	NPO	SO	ENPG	NEC	NECC	SEC
AG		.24	.15	.12	.00	-.16	-.08	.07
MG	90.0		.85	.39	-.36	.40	-.48	.53
NPO		>99.9		.68	-.43	-.62	-.71	.73
SO		>95.0	>99.9		-.13	-.62	-.67	.66
ENPG		>90.0	>95.0			-.03	.38	-.23
NEC		>95.0	>99.0	>99.0			.77	-.63
NECC		>99.0	>99.9	>99.9	>95.0	>99.9		-.77
SEC		>99.0	>99.9	>99.0		>99.0	>99.9	

Correlation coefficients (r) shown above diagonal; levels of significance ≥90% are tabulated below the diagonal. AG = Aleutian Gradient, MG = Mexican Gradient, NPO = North Pacific Oscillation, SO = Southern Oscillation, ENPG = Eastern North Pacific Gyre, NEC = North Equatorial Current, NECC = North Equatorial Countercurrent, SEC = South Equatorial Current.

their contributing high pressure series (NPO vs NP high: r = .90; SO vs Easter: r = .94) than to Darwin (r = .78; r = .80). The interdependence between the NPO and the SO also reflects the real spatial structure of the Southern Oscillation mentioned above as described by Wright (1977).

The very high correlation of the MG and NPO is due to the dominance of the NP high-pressure center in both indices. Both the NPO and the SO are strongly correlated with the equatorial currents. The NPO and MG show a significant, although not a high correlation, with the ENPG. The ENPG is surprisingly uncorrelated with the AG. The lack of correlation between the ENPG and the NEC is interesting since the NEC supposedly receives 45% of its water from the subtropical gyre (Wyrtki, 1966), and less than 40% from the NECC with which a significant though low correlation to the ENPG is obtained.

EOF Analysis of Large-Scale Variability

Although Table II-1 reveals the association of variance among large-scale climatic processes, the correlation structure does not define any clear pattern of variability associated with the North Pacific gyre which is independent from the equatorial circulation. Calculation of empirical orthogonal functions (EOF's) eliminates the redundancy in these data by partitioning the variance of the original eight series into a set of eight orthogonal (uncorrelated) eigenvectors (the empirical functions) whose mean squared amplitudes are given by the eigenvalues (Kundu et al., 1975). EOF's were determined from the correlation matrix so that each original series is normalized to unit variance prior to the analysis. Thus the sum of the eigenvalues, which is equivalent to the sum of the total normalized variance of the original series, is equal to the number of series (in this case, 8). The time varying amplitudes (expansion coefficients) of the eigenfunctions represent the independent modes of variability composed of the shared variance in the original series.

The eigenvalues are plotted in Figure II-4 as percentages of the total normalized variance. There is a large decrease in variance from the first to second eigenvalue, and a smaller but pronounced drop between the third and fourth. The first three eigenfunctions comprise 82% of the total normalized variance of the original time series and lend themselves to consistent physical interpretations. The remaining five eigenfunctions are ignored as uninterpretable noise for our purpose here.

The series of expansion coefficients of the first three eigenfunctions are plotted at the head of Figures II-5 through II-7. The climatic significance of each eigenfunction is ascertained by the contribution of variance received from each of the original series. The portion of variance (R_{ij}^2) contributed to the ith eigenfunction by the jth original series is

$$R_{ij}^2 = \frac{(X_{ij})^2 \lambda_i}{\sum_{i=1}^{n=8} (X_{ij})^2 \lambda_i} \qquad (2)$$

where X_{ij} is the jth element in the ith eigenvector and λ_i is the ith eigenvalue.

The composition of each eigenfunction and its corresponding climatic significance is shown by plotting the original time series, contributing more than 10% of its variance, below the eigenfunction in Figures II-5 through II-7. The percentage contribution of variance to each EOF by the original series ($100R_{ij}^2$) along with the individual eigenvector elements (X_{ij}) are shown to the right of the series. Note that series yielding negative elements in the eigenvector are inverted so that they are positively correlated with their expansion coefficient.

The first eigenfunction (Fig. II-5) represents the variability in the major atmospheric cells of zonal circulation north and south of the equator (NPO and SO) and their association with the zonal equatorial currents. The first eigenfunction is therefore denoted as the equatorial mode of variability. It is a clear reflection of the El Niño/

Figure II-4

Plot of the percentage of total normalized variance from the eight original remote variables which is partitioned into each of the eigenfunctions.

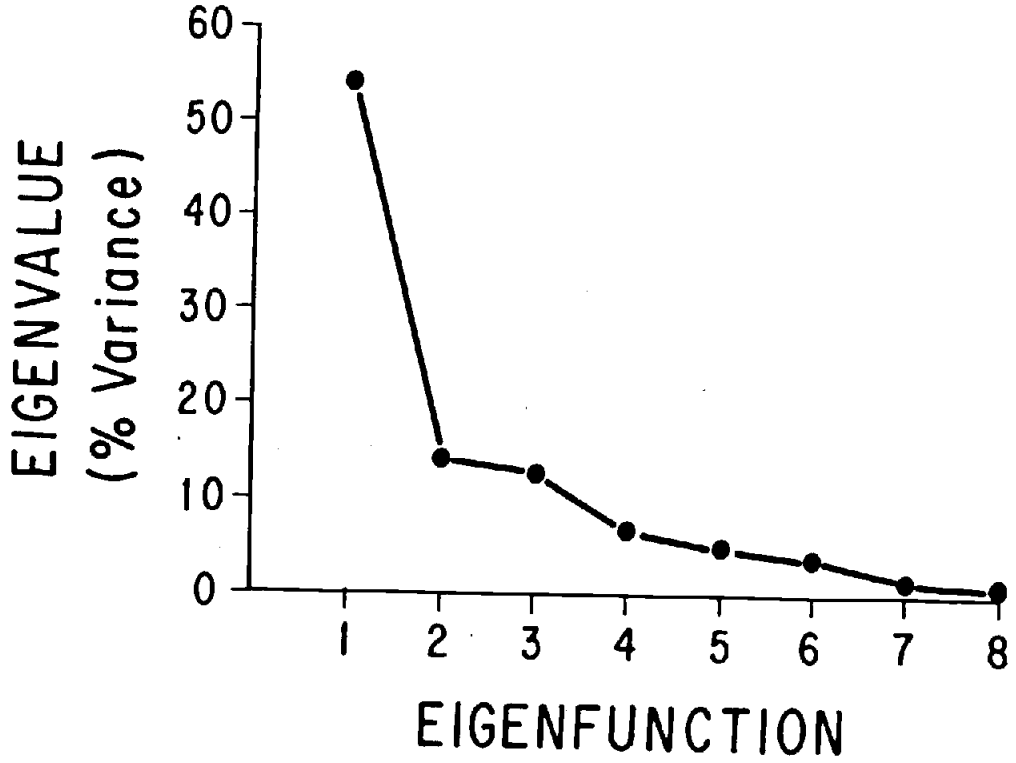
EIGENVALUE
(% Variance)
60
50
40
30
20
10
0
1
2
3
4
5
6
7
8
EIGENFUNCTION

Figure II-4

Figure II-5

Time series of first eigenfunction of remote variables plotted at top of figure. Vertical scale for eigenfunction in units of the total normalized variance. Original series arranged below according to their percent contribution ($100R_{ij}^2$) to this EOF. Series with negative eigenvector elements (X_{ij}) are inverted to agree with sense of variance in the EOF. Variances of original series plotted here are not normalized; units given in cm and mb. Only those series contributing more than 10% of their variance to this EOF are shown.

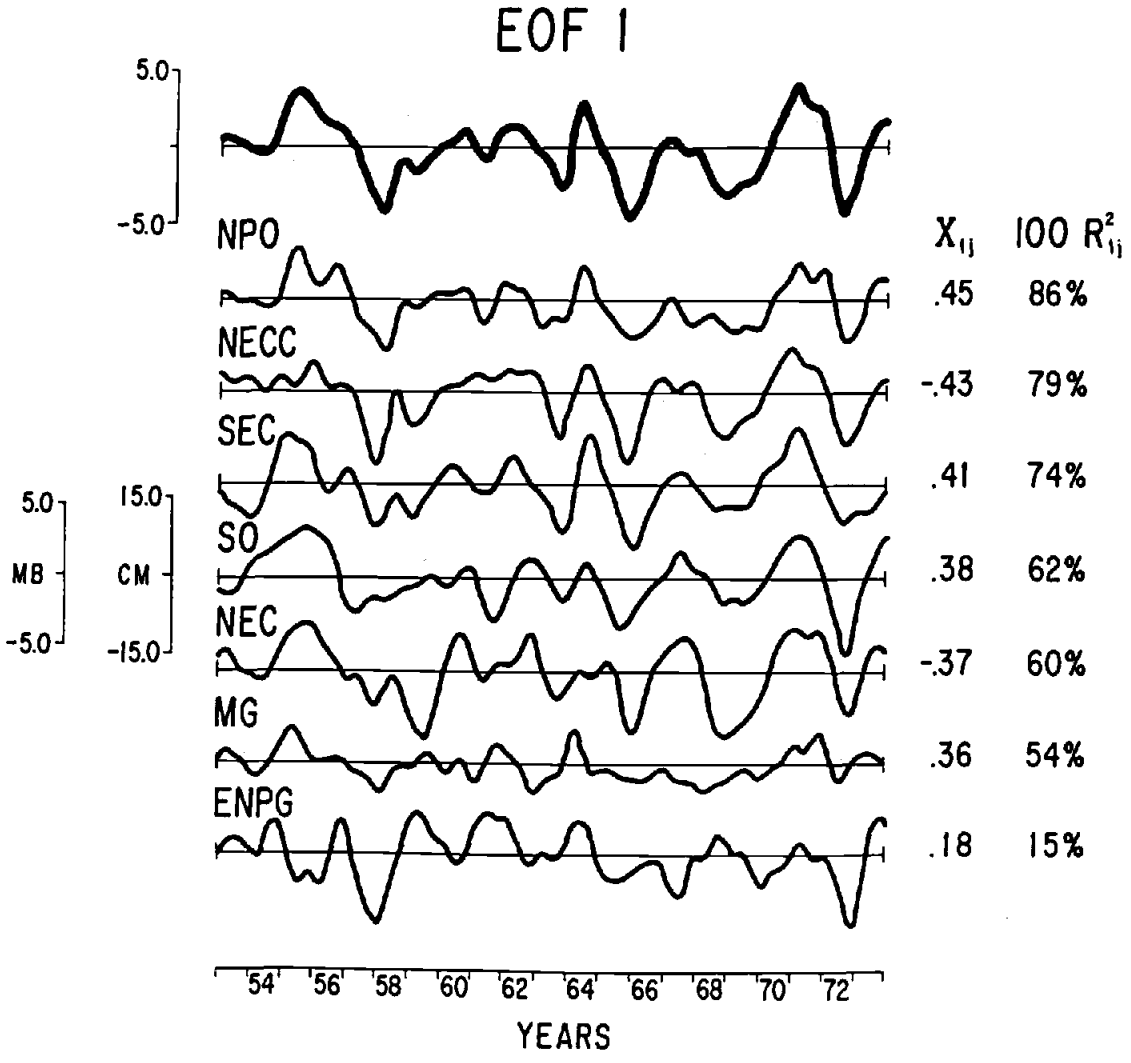
EOF 1
5.0
-5.0
NPO
NECC
SEC
SO
NEC
MG
ENPG
X_{1j}
$100\ R^2_{1j}$
.45 86%
-.43 79%
.41 74%
.38 62%
-.37 60%
.36 54%
.18 15%
5.0
MB
-5.0
15.0
CM
-15.0
54 56 58 60 62 64 66 68 70 72
YEARS

Figure II-5

Southern Oscillation phenomenon and possesses a high proportion (54%) of the total normalized variance of the original series.

The small contribution of the ENPG to the first EOF suggests that there is no systematic spin-up or spin-down of the gyre with the variability of the basin-wide wind field associated with El Niño. This is consistent with numerical solutions found by McCreary (1976) which shows the effect of El Niño confined to equatorial and coastal regions. However, we can visually identify on Figure II-5, definite decreases in the strength of the gyre during strong El Niños. It is also interesting to note that the strength of the ENPG varies inversely with respect to the sign of the NEC in this eigenfunction.

The dominant source of variability in the second eigenfunction (Fig. II-6) is the strength of the ENPG. In this EOF, 50% of the variability of the ENPG is positively associated with a considerable share of the transport in the NEC (22%). Thus an increase of the ENPG variance contributing to this mode coincides with an increase in the amplitude of the portion of variance shared with the NEC. The association of the MG and AG in this EOF is compatible with positive forcing of the surface winds over the gyre. Because the second eigenfunction is orthogonal to the first, it represents a source of variability which is independent of the El Niño/Southern Oscillation phenomenon. The high positive loading on the ENPG and the NEC indicates that this EOF represents independent variation of the subtropical gyre.

The portion of the total normalized variance contained in the third EOF (13%) is comparable to that of the second EOF (15%) and thus cannot be ignored in our climatic interpretation (Fig. II-7). Only two of the original series contribute significantly to the third eigenfuction. The Aleutian Gradient contributes 76% while the North Pacific gyre contributes 22%. The inverse relationship between these two series in this EOF is incompatible with the interpretation of wind forcing of the surface westerlies over the northern margin of the gyre. However, it may be that during a period of a strong, deep

Figure II-6

Time series of second eigenfunction of remote climatic variables plotted at top of figure. Original series arranged as in Figure II-5.

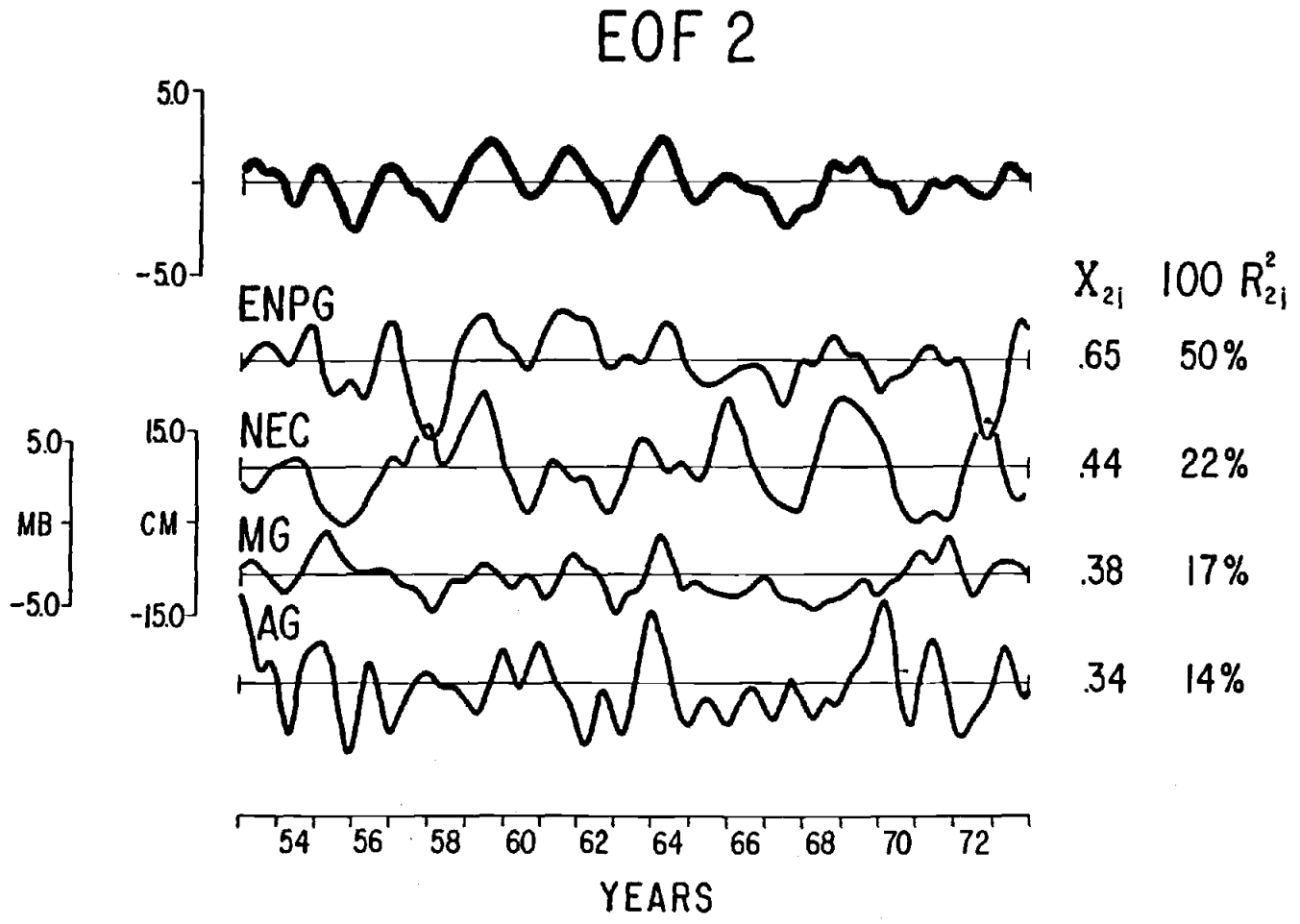
EOF 2
5.0
-5.0
ENPG
NEC
MG
AG
X_{2i}
$100\ R^2_{2i}$
.65
50%
.44
22%
.38
17%
.34
14%
5.0
MB
-5.0
15.0
CM
-15.0
54
56
58
60
62
64
66
68
70
72
YEARS

Figure II-6

Figure II-7

Time series of third eigenfunction of remote climatic variables plotted at top of figure. Original series arranged as in Figure II-5.

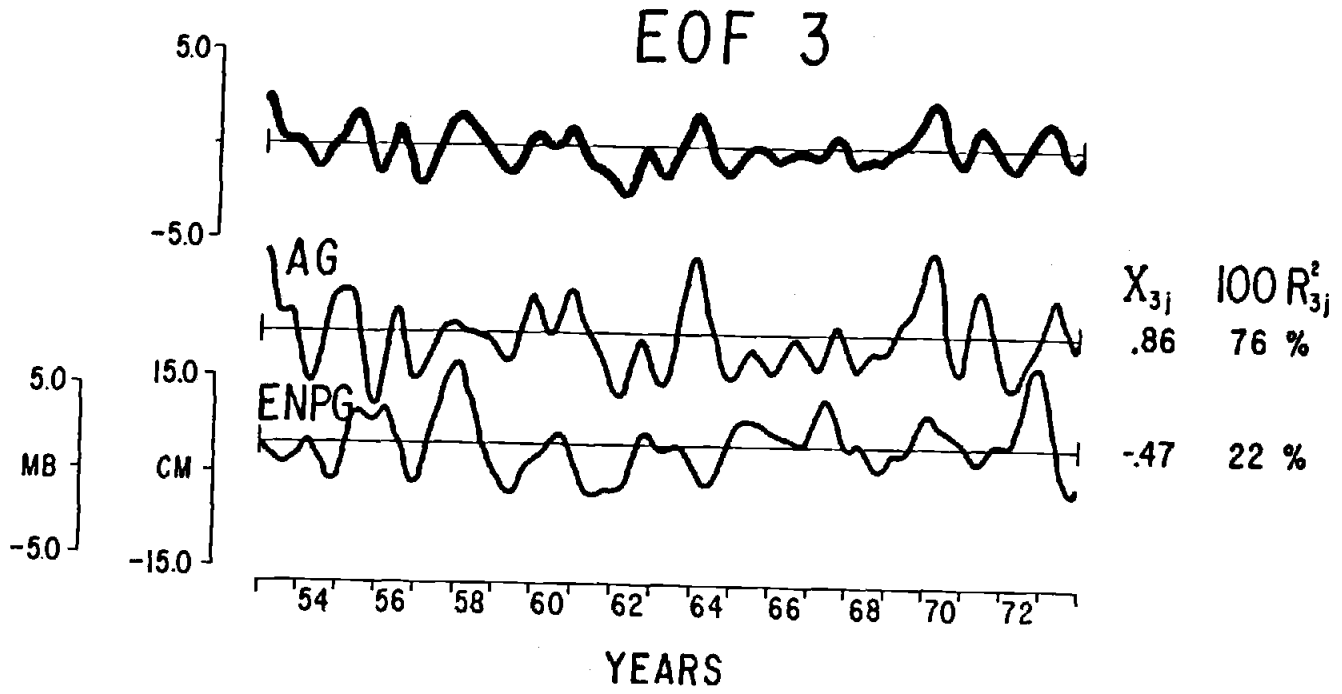
EOF 3
5.0
-5.0
AG
ENPG
5.0
MB
-5.0
15.0
CM
-15.0
X_{3j}
$100\,R^2_{3j}$
.86
76 %
-.47
22 %
54
56
58
60
62
64
66
68
70
72
YEARS

Figure II-7

Aleutian low and weakened North Pacific high, more water is diverted northward along the North American coast within the subarctic gyre following increased cyclonic flow about the low-pressure system. This would tend to reduce flow within the California Current and the eastern limb of the North Pacific gyre. Flow of the subtropical gyre in this EOF is slightly less than half of that obtained in the second EOF.

INTERANNUAL VARIABILITY IN THE GULF OF CALIFORNIA

Observations

Two variables are available to provide a history of interannual ocean climate in the Gulf of California. These are sea level and surface temperature measured at the tide stations in Mazatlán, Topolobampo, Guaymas and La Paz. Raw data for the sea level series consist of monthly means of hourly observations; monthly means of the temperature series were made from daily observations. Sea level and temperature anomalies were computed for each station in the same manner as for the remote variables. Regional sea level and temperature series were then obtained by averaging the monthly anomalies from the four stations. Missing data for individual stations range from several months to a maximum of four years for Topolobampo, so that some of the intervals averaged are from only two stations. The regional sea level and temperature anomalies were low-pass filtered with the same filter as used for the remote variables.

The regional averages of sea level and temperature anomalies in the Gulf of California from 1952 through 1974 are plotted in Figure II-8. Both series exhibit periods of two to four years with maximum amplitudes of over 15 cm and 2°C. These values represent approximately 60% of the mean annual cycle of sea level change and almost 20% of the mean annual cycle in temperature.

Correlation between the sea level and temperature anomalies in the Gulf is relatively low: $r = 0.40$ ($P > 95\%$). As shown below, the sea level anomalies in the Gulf are more closely associated with variability of sea level in coastal regions on the open

Figure II-8

Low-pass filtered monthly sea level and shore temperature anomalies from the Gulf of California. These series are regional averages computed from stations at Mazatlán, Topolobampo, Guaymas and La Paz.

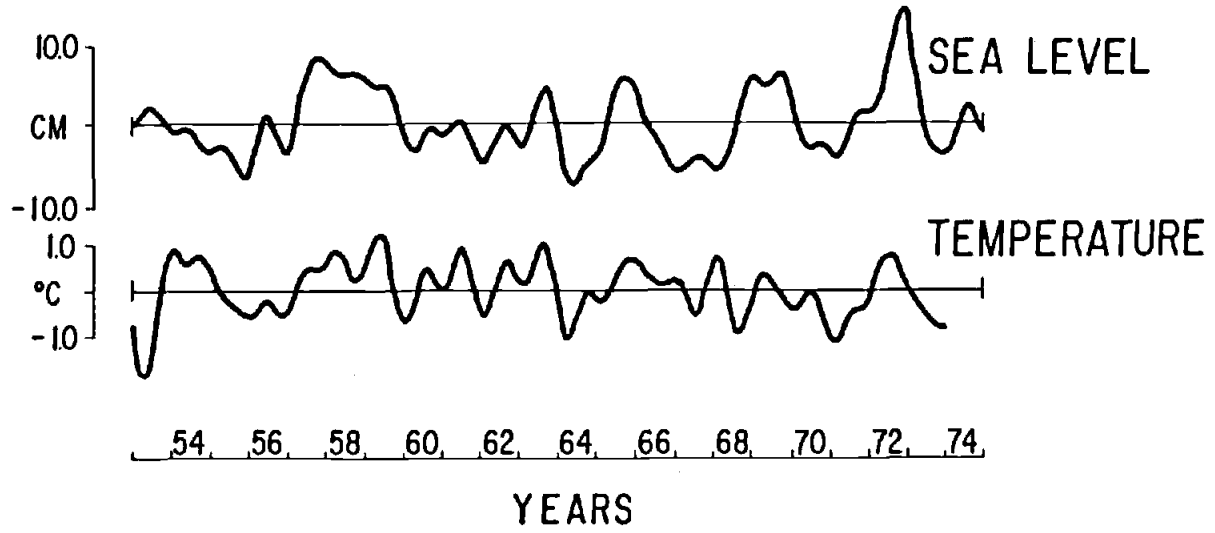
10.0
CM
-10.0
SEA LEVEL
1.0
°C
-1.0
TEMPERATURE
54
56
58
60
62
64
66
68
70
72
74
YEARS

Figure II-8

ocean than with the shore temperatures inside the Gulf. We interpret this to indicate that shore temperatures in the Gulf respond more to local forcing than does sea level. This is consistent with results from Enfield and Allen (1980) showing that large-scale geographic coherence is considerably greater in sea level than for shore temperatures in the northern hemisphere.

Coupling of the Gulf of California to Large-Scale Variability

Comparison of sea level anomalies in the Gulf to regional sea level anomalies off southern Mexico and from the coast of northern Baja California and Southern California in the U.S. (denoted here as the coast of lower California) reveals the geographic coherence of interannual variation in sea level documented by Enfield and Allen (1980) and Chelton and Davis (1982). The three sea level series are presented in Figure II-9, with the locations of the sea level regions and individual stations shown in the inset map. The regional sea level anomalies from southern Mexico and lower California were constructed from the individual stations in the same way as that of the Gulf of California and were low-pass filtered with the same filter.

Sea level anomalies from the Gulf are highly correlated with those off southern Mexico ($r = 0.92$; $P > 99.9\%$). Visual examination of Figure II-9 indicates that all the large amplitude events and many of the smaller ones in the Gulf series are present in the southern region. Lowered correlations between the Gulf sea level and the lower California series ($r = 0.80$; $P > 99.9\%$) suggest a diminishing coherence in the variability of sea level to the north. Cross-correlation of the series shows that the Gulf series lags southern Mexico by one month, but the difference in the correlation coefficient at this lag is insignificant ($r = 0.93$). There is no lag between the Gulf and lower California series.

In order to examine the association of the Gulf of California with the large-scale ocean-atmosphere climate, we have computed the correlation between the regional sea

Figure II-9

Filtered monthly sea level anomalies from the Gulf of California compared to regional averages of coastal sea level off Southern México and lower California. Location of stations used to compute regional averages are shown on inset map. (LA: Los Angeles; SD: San Diego; E: Ensenada; G: Guaymas; T: Topolobampo; LP: La Paz; Mz: Mazatlán; Mn: Manzanillo; A: Acapulco; Sc: Salinacruz).

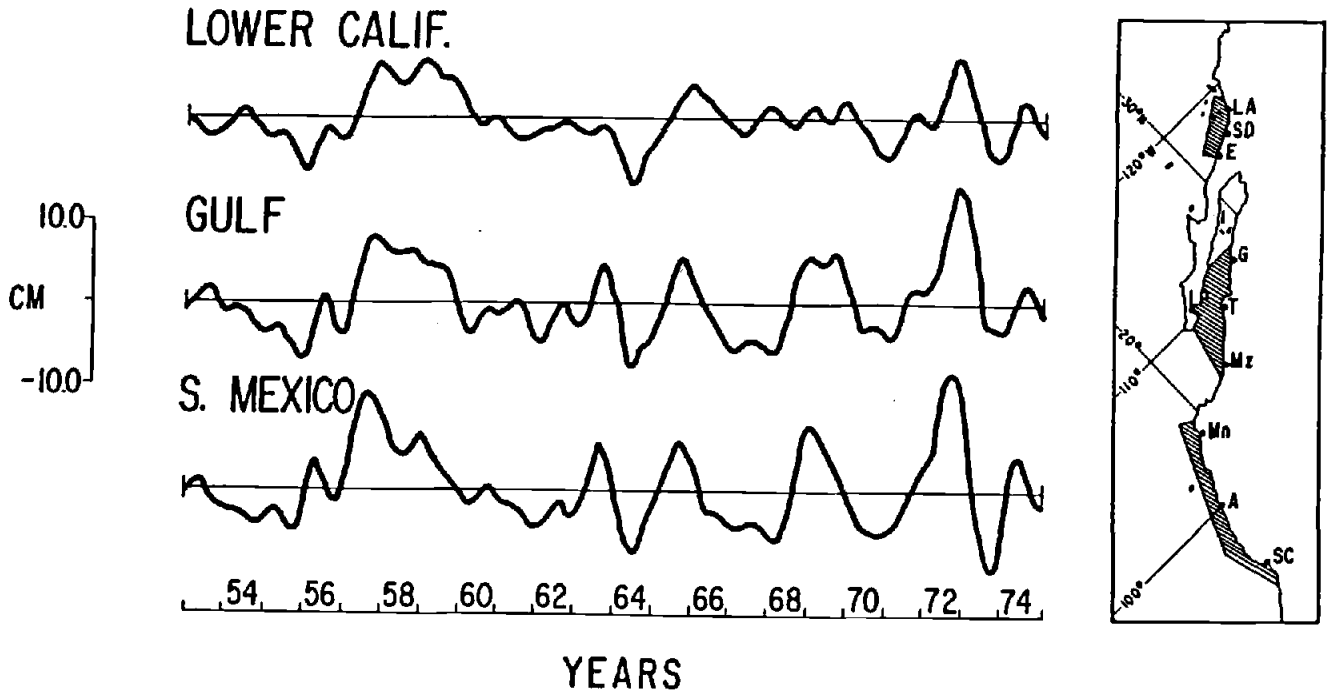
LOWER CALIF.
GULF
S. MEXICO
10.0
CM
-10.0
54
56
58
60
62
64
66
68
70
72
74
YEARS
LA
SD
E
G
T
Mz
Mn
A
SC
-120°
-110°
-100°

Figure II-9

Table II-2

Correlations (r) between first three EOF's of the remote variables and regional sea level and shore temperature in the Gulf of California and with regional sea levels off the coast of southern México and lower California. Significances ≥90% are shown in parenthesis below the correlation coefficients.

	EOF 1	EOF 2	EOF 3
Gulf of California Sea level	-.72	.15	.24
	(>99.9)		
Gulf of California Temperature	-.49	-.04	-.15
	(>99.0)		
Southern México Sea Level	-.74	.06	.19
	(>99.9)		
Lower California Sea Level	-.71	-.02	.13
	(>99.9)		

level anomalies and each of the first three climate modes from the EOF analysis (Table II-2). We also include in Table II-2, the correlation of the EOF's to the Gulf temperature anomalies, as well as the regional sea level anomalies off southern Mexico and lower California, for comparison. Linear correlation is an appropriate measure of correspondence since the covariance of the two variables compared is normalized by the product of the standard deviations of the two series. Differences among variances of the EOF defined climatic modes, therefore, do not bias the correlation test. Because the EOF's are independent from one another, there is also no ambiguity in the results of the test.

Correlation of regional sea level anomalies in the Gulf to the first EOF is highly significant ($r = -0.72$; $P > 99.9\%$). The coefficient of determination (r^2) indicates that 52% of the interannual variability in the Gulf sea level can be explained by the equatorial circulation which is in turn an expression of the El Niño/Southern Oscillation phenomenon. The regional sea level anomaly series of southern Mexico and lower California are similarly correlated to the first climatic mode, with southern Mexico exhibiting a slightly higher correlation ($r^2 = 0.55$) and lower California a somewhat decreased correlation ($r^2 = 0.50$).

The corelation between regional shore temperature in the Gulf and the first climatic mode is considerably lower ($r = -0.49$; $r^2 = 0.24$) than those of the sea level series, but is still highly significant. This ephasizes the reduced importance of the shore temperatures in representing variability in ocean climate.

Correlation of Gulf sea level and shore temperatures with the second climatic mode yields a negative result. Virtually none of the variance in Gulf sea level or temperature corresponds to variability in the strength of the North Pacific gyre as defined by the second EOF. This result answers the question posed by our original hypothesis to guide this study. The second EOF with its high loading on the ENPG and the NEC with lesser contribution from the MG (alongshore wind) and AG (westerlies) is the

principal index of variation of the North Pacific gyre independent from the El Niño/ Southern Oscillation phenomenon. It is clear that our hypothesis is not supported at this stage: interannual ocean climate in the Gulf does not respond to fluctuations in the strength of the subtropical gyre which are independent from El Niño. This conclusion can be extended to the regions of open coast north and south of the Gulf which also behave with a total lack of correspondence to the second climatic mode.

The third climatic mode carries a sufficient share of variance of the North Pacific gyre so that its possible relationship to the Gulf is also examined in Table II-2. The correlation between the Gulf and third EOF does not reach a significant value although it is slightly higher than that of the second EOF. Comparison of the Gulf and the regional sea levels north and south of the Gulf to the third EOF reinforces our conclusion that there is no source of variability within the North Pacific gyre independent of the equatorial circulation which plays a significant role in determining interannual variability in the Gulf.

DISCUSSION

Our examination of coupling of the Gulf of California to large-scale variability is based upon low frequency changes in the intensity of major current systems and their association with the atmospheric circulation. Since the foregoing analysis clearly shows that the Gulf does not respond to variations in the intensity of the North Pacific gyre which are independent from the equatorial circulation, we shall concentrate our discussion on the role of the equatorial currents and their relationship to El Niño.

Within the second EOF, a considerable share of the variance of the NEC is positively correlated to that contributed by the ENPG (Fig. II-6). This suggests a sense of coupling between the ENPG and the NEC which agrees with continuity through the eastern and the southern limbs of the subtropical ocean gyre. Moreover, existence of this mode indicates that a significant portion of the flow around the eastern limb of the North Pacific gyre into the NEC is independent of the El Niño phenomenon. This agrees with evidence presented recently by Wright (1983) that SST anomaly differences between the north central and northeastern Pacific behave with significant independence from the Southern Oscillation. The lack of correlation of the second EOF with the regional sea level anomalies observed along the coast and in the Gulf of California (Table II-2) further indicates that it represents a flow separated from the coastal boundary and limited to the offshore region. This mode probably reflects the variability in the broad southerly interior flow described by Price (1981). It is important to note, however, that although the ENPG is composed principally of variance which is independent of El Niño, the intense El Niño events of 1957-1958 and 1972 are associated with marked decreases in this index. This association and resulting contribution of the ENPG to the first EOF suggests a retardation or spin-down across the entire eastern limb of the gyre during major El Niño events.

The relationships seen in the first EOF (Fig. II-5) show that a decrease in values of the NPO and SO indices during an El Niño event coincides with an anomalous

weakening of the westward flowing SEC and strengthening of the eastward flowing NECC (positive direction downwards in Fig. II-5). Figure II-5 also demonstrates that for the portion of the variance contributed to the first mode by the NEC, the westward flow of the NEC is intensified rather than weakened during El Niño.

A strong positive coupling between the NEC and NECC was observed by Wyrtki (1974a,b) over an averaged annual cycle; i.e., zonal transports of these two currents vary in phase, both strong in the fall and weak in spring. He also found that the strength of the SEC varies out of phase with the northern hemisphere currents over the annual cycle. Wyrtki (1974a) noted that the NEC and NECC currents should be strongly coupled because their geostrophic transports are governed by fluctuations in the depth of the trough in the meridional profile of the dynamic topography across the two currents. At the same time, he noted that seasonal fluctuations of the SEC is also coupled to that of the NEC and NECC through the linkage of the dynamic topography.

Figure II-10a illustrates the generalized meridional profile of dynamic topography in the central Pacific (Wyrtki, 1974a,b). The NEC and the NECC can be viewed as a compressed, elongated cyclonic gyre with a central zone of divergence running along the axis forming the Countercurrent trough between the NEC and NECC. The configuration of this cyclonic gyre is seen in early estimates of mass transport from mean wind stresses in the eastern Pacific (Reid, 1948; his Fig. 14).

Deepening of the Countercurrent trough at 10°N results in steepening of the pres sure gradients across both the NEC and the NECC, increasing their geostrophic transports. Meyers (1975) has shown that the vertical displacement, or ridging of the thermocline at 10°N (and concommitant deepening of the Countercurrent trough abo the thermocline ridge), varies over the annual cycle by Ekman pumping as a response to variation in the pattern of wind stress curl. He shows that the ridge in the thermocline at 10°N rises to a miximum in fall when seasonal wind stress curl along 10°N (betwe

Figure II-10

(a) Schematic section of dynamic topography from 20°N to 10°S in the central Pacific showing location of convergences (ridges) and divergences (troughs) in relation to the current systems and the direction of flow (E/W). The solid line indicates topographic configuration during weakened eastward flow in the NECC and strong west-ward flow in the SEC (anti-El Niño conditions). The dashed line shows change in topography associated with strengthened eastward flow in the NECC and weakened westward flow in the SEC (El Niño conditions). (b) Schematic diagram of expanded and intensified north equatorial cyclonic gyre circulation in relation to contracted anticyclonic North Pacific and South Pacific gyres inferred to exist during El Niño episodes.

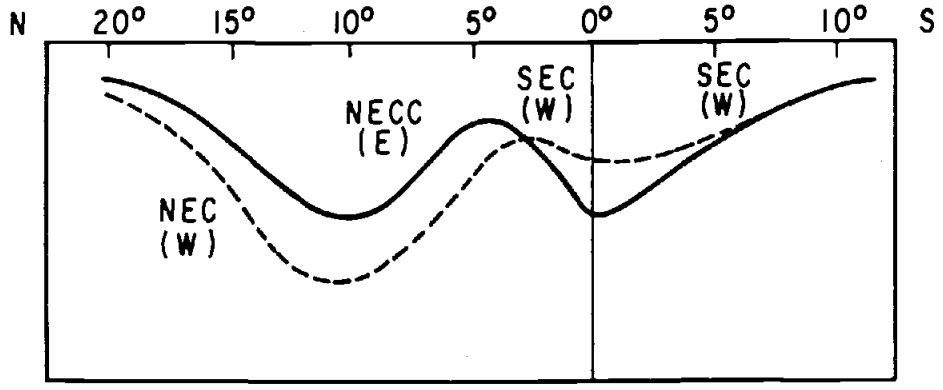

a

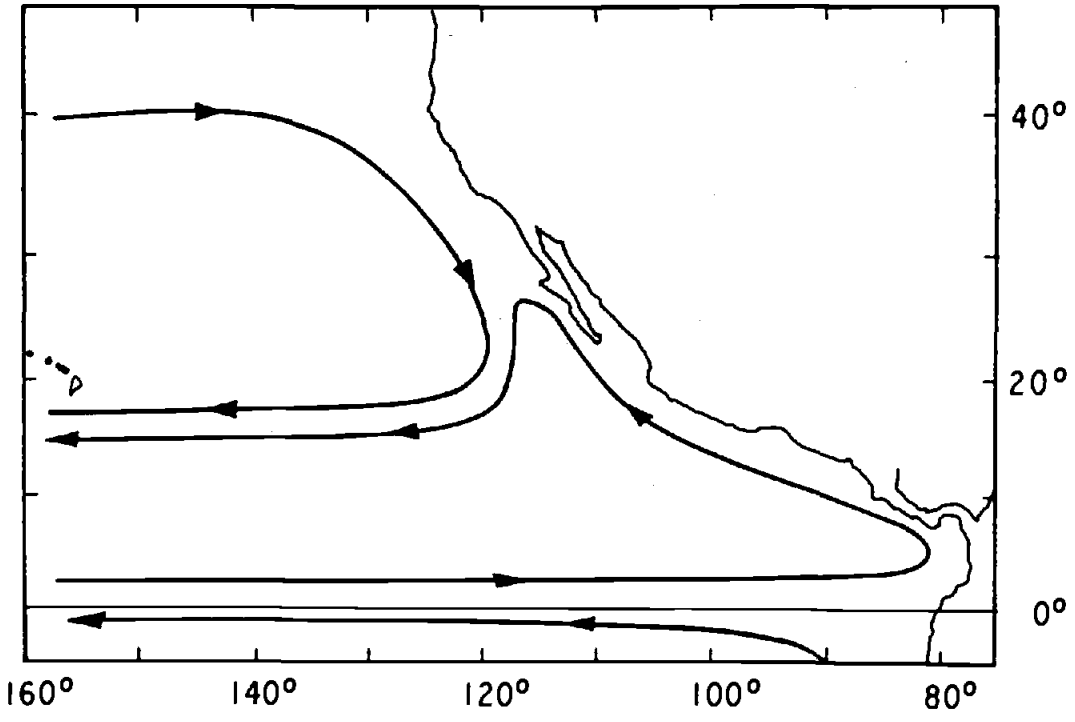

b

Figure II-10

150°-160°W) is positive. Likewise, the elevation of the ridge is lowest (shallow trou in spring when the seasonal wind stress curl is negative.

Pazen and Meyers (1982) examined variation in the spatial pattern of wind stress curl over interannual time scales in relation to the El Niño/Southern Oscillation phenomenon. Distribution of annual mean wind stress curl were calculated for El Niño and anti-El Niño conditions. Annual mean curl calculated from the El Niño years shows a strong intensification of cyclonic wind stress curl extending across the entire North Pacific near 10°N over the Countercurrent trough. The interannual variation in wind stress curl is thus entirely consistent with a deepening of Countercurrent trough during El Niño conditions and the resulting strengthening of the NEC and NECC. The broken line in Figure II-10a indicates a generalized profile of dynamic topography during El Niño conditions, associated with intensification of the gyre formed by the NEC and NECC and the resulting weakening of the SEC.

The model solutions found by McCreary (1976) succinctly describe the intensification of this "north equatorial gyre" as a baroclinic response to the relaxation of the equatorial tradewind field. The excitation of equatorially trapped Kelvin waves rapidly adjust the meridional pressure gradients to the change in wind-stress. An asymmetric change in zonal wind stress, with greatest weakening north of the equator near 5°N, results in the development of a strong ridging of the thermocline beneath the band of maximum wind stress curl just south of 10°N (McCreary, 1976, his Fig. 6). This ridge (indicating a deepening of the Countercurrent trough) is well developed and extends all the way to the eastern boundary within approximately 70 days after initializing the model. Zonal flow asociated with the thermocline ridge near 10°N, and the deepening of the thermocline along the equator, produces a strong eastward flowing jet aproximately 200 km north of the equator simulating intensification of the NECC. Intensification of westward flow also is shown along the thermocline ridge roughly 700 km north of the equator, simulating increased transport in the NEC (McCreary, 1976; his

Fig. 8). The east-west jets weaken near the eastern boundary, where they are linked by a south to north coastal jet (McCreary, 1976; his Fig. 7). Arrival of the equatorial Kelvin waves at the eastern boundary generates a polewardly propagating Kelvin wave front producing an equivalent downwelling of the thermocline along the eastern boundary and the subsequent poleward coastal jet to drain off the equatorial flow.

Figure II-10b is an idealized sketch of the postulated configuration of the cyclonic equatorial gyre and the anticyclonic subtropical gyre systems during an El Niño event. This pattern reflects the principal relationships in our first EOF and is consistent with the numerical solutions presented by McCreary (1976, 1978) and the intensification of cyclonic curl along 10°N which occurs with El Niño (Pazen and Meyers, 1982). Inter sification of the north equatorial cyclonic gyre results in expansion and increased divergence away from the center. Along the eastern boundary, convergence is directed toward the coast with commensurate rise in sea level (and downwelling) there. Dynamic adjustments necessary for geostrophic balance along the coastal boundary require increased poleward advection within the Costa Rica Current (CRC; see Fig. II-1, Oct. pattern). McCreary (1976) notes that the poleward coastal countercurrent along North America (Davidson Current) should also be strengthened during El Niño.

The stream pattern shown in Figure II-10b is similar to that seen in the lower half of Figure II-1, representing the mean circulation between August and December as described by Wyrtki (1966). During this period of the year, the NECC is fully developed with most of its water feeding into the CRC. The California Current separates from the coast near 25°N and supposedly supplies water to the NEC only above 20°N. Below 20°N all the water of the NEC is derived from the CRC. This suggests that the occur rence of the El Niño in the eastern North Pacific is an enhancement of the normal seasonal circulation obtained in autumn.

Figure II-11 presents the monthly averages of the filtered NECC index and the regional sea level anomalies for the Gulf and Southern Mexico over all El Niño

Figure II-11

Composites of the filtered NECC index and regional sea level anomalies in the Gulf of California and along the coast of southern México during the 1957-1958, 1963, 1965, 1968-1969 and 1972 El Niño episodes. The year centered on the El Niño event is indicated by 0 under the abscissa, the year preceding and the year following are indicated by -1 and +1, respectively. The phases of El Niño development described by Rasmusson and Carpenter (1982) are shown above the abscissa (Antecedent through Mature). Ordinate scale refers to sea level height for the regional anomalies (Gulf of California, southern México) and to sea level difference for the NECC index.

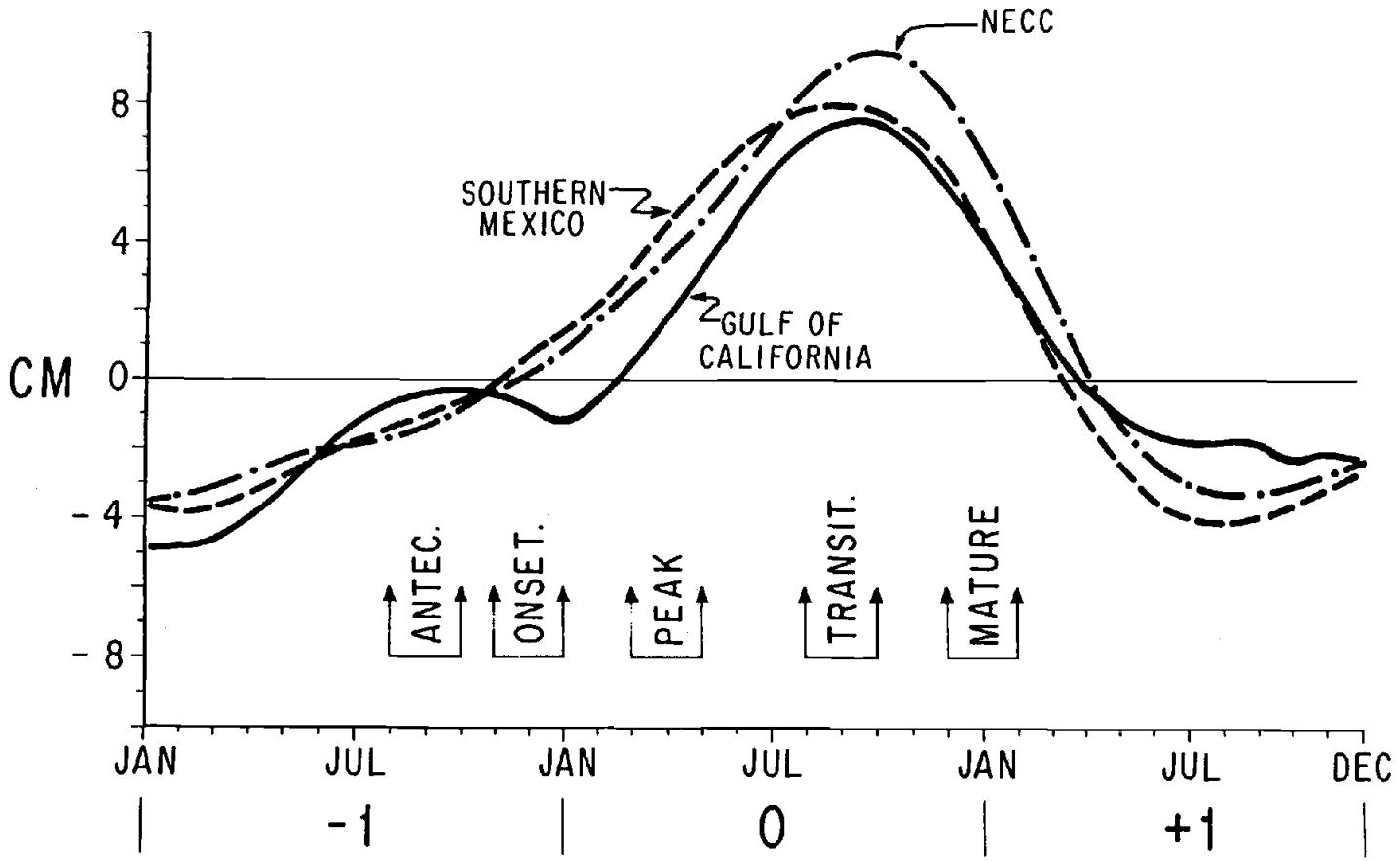
NECC
SOUTHERN MEXICO
GULF OF CALIFORNIA
CM
8
4
0
- 4
- 8
ANTEC.
ONSET.
PEAK
TRANSIT.
MATURE
JAN
JUL
JAN
JUL
JAN
JUL
DEC
-1
0
+1

Figure II-11

occurrences in our data set to show a composite of the year preceding El Niño (-1), the El Niño year (0), and the year following (+1). This illustrates the principal tendencies in timing of the development of the events. This technique was employed by Rasmusson and Carpenter (1982) to describe the evolution of a "normal" El Niño occurrence. Stages in the development of El Niño defined by Rasmusson and Carpenter (1982), placed along the horizontal axis (Antecedent, Onset, Peak, Transitional, Mature), are based upon the history of the SST anomaly off the Peru coast just south of the equator.

Figure II-11 shows that the maximum height of the sea level anomalies and the NECC flow lag significantly from the peak phase in the development of the SST anomaly off Peru and Ecuador (March and April) during a composite El Niño episode. Rather, the peak in sea level development off southern Mexico and in the Gulf of California occurs between August and October. This coincides closely with the annual cycle of sea level variation in both regions which has already been removed from the series. It also coincides with the normal seasonal period of strengthened flow in the NECC and the NEC and the anomalous strengthening of the NECC shown in Figure II-11.

Wyrtki (1979b) has also pointed out that the El Niño events of 1972 and 1976 occurred over two time scales. The evolution of the eastern equatorial warming occurred between 50 and 100 days from the weakening of the tradewinds. This timing roughly corresponds to the period between the "Onset" and "Peak" phases resulting in a first peak in SST along the Peruvian coast from April through July (Rasmusson and Carpenter, 1982; their Figs. 8 and 10), also seen in sea level at the Galápagos Islands (Wyrtki, 1977; his Figs. 4 and 6). Wyrtki (1979b) argues that the 50 to 100-day time scale is determined by the time an equatorial Kelvin wave requires to reach the eastern boundary from the region of generation in the western Pacific. A second El Niño time scale is of the order of one year and is associated with the period of anomalous strengthening of the NECC (Fig. II-11). Wyrtki (1977; his Figs. 4 and 6) shows that

this period culminated in a second peak in the Galápagos sea level in December, 1972. A subdued second peak occurring between October and January is also found in the SST along Peru (Rasmusson and Carpenter, 1982; their Figs. 8 and 10).

These observations recall Philander's (1979) proposal that although the initial, rapid changes in the equatorial wind stress result in adjustments of the current systems to equilibrium by the propogation of waves, subsequent changes in the wind field which occur over time scales long compared to that of waves, will result in a continuous adjustment in which the excitation of waves is not required to maintain equilibrium. The time scale associated with the composites of the low-frequency anomalous flow in the NECC and elevation of sea levels off southern Mexico and in the Gulf of California, illustrated in Figure II-11, may thus represent continuous adjustment of the current systems to low-frequency variation in the structure of the wind field. This suggests that the principal timing and effect of El Niño upon the Gulf of California and along the Mexican coast is associated with an increasing eastward transport of water through the NECC reaching a maximum in the second half of an El Niño year.

Because the mouth of the Gulf of California is located within a region of water mass transition, the ocean climate of the Gulf should be particularly sensitive to interannual variability in large-scale circulation. The changes of poleward advection in the CRC versus the equatorward advection of the California Current resulting from interannual expansion of the cyclonic north equatorial gyre should result in a significant change in the distribution of tropical and California Current water masses relative to the mouth of the Gulf of California.

Figure II-12 (Roden, 1971) shows the surface distribution of water masses during November 1969. This configuration coincides with the decay of the positive Gulf sea level anomaly at the close of the 1968-1969 El Niño event and represents a transition between El Niño and anti-El Niño conditions. The salient feature is the northward penetration of Tropical Surface Water still remaining across the entrance of

Figure II-12

Distribution of salinity at the sea surface during November 1969, showing the boundaries of the Pacific surface water masses in the region of the Gulf of California (adapted from Roden, 1971).

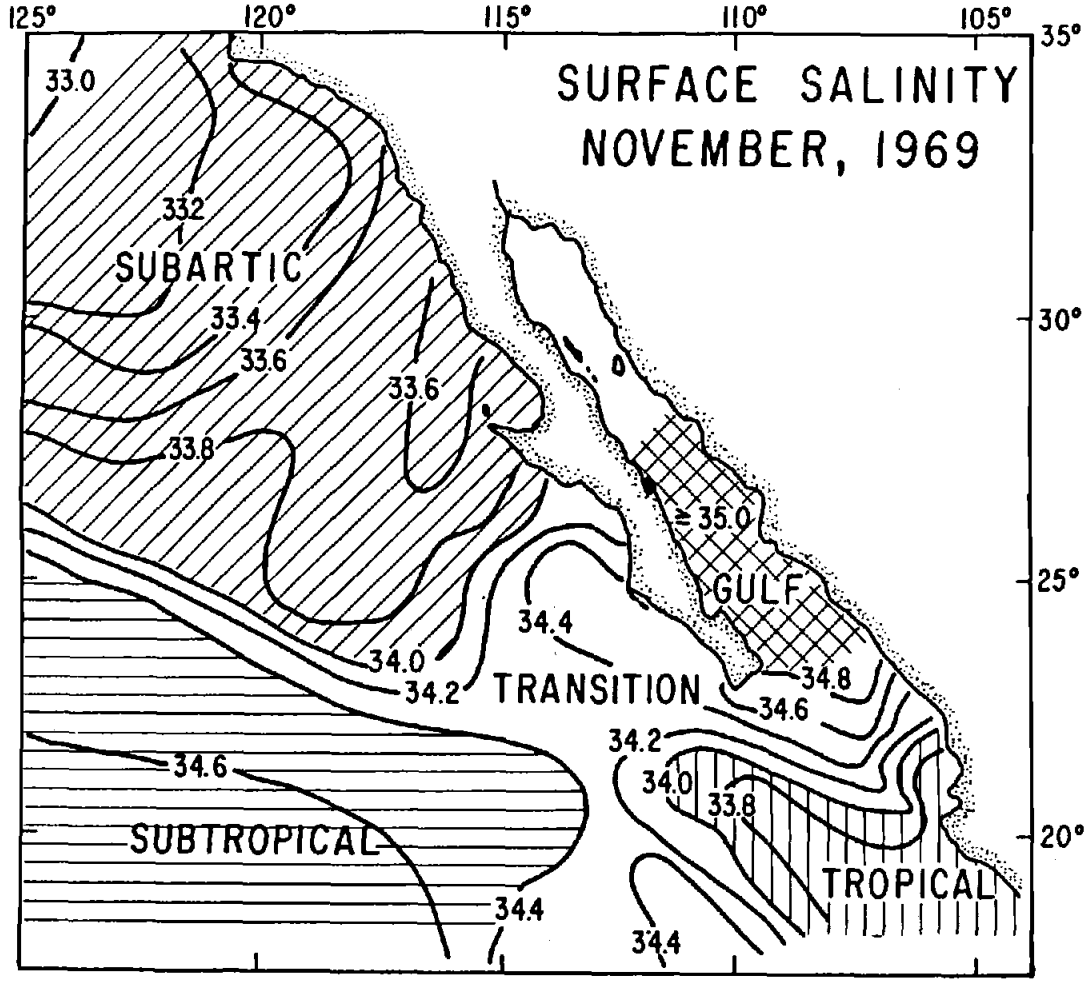
125°
120°
115°
110°
105°
35°
30°
25°
20°
SURFACE SALINITY
NOVEMBER, 1969
33.0
33.2
SUBARTIC
33.4
33.6
33.6
33.8
≥35.0
GULF
34.4
34.0
34.2
TRANSITION
34.8
34.6
34.2
34.0
33.8
34.6
SUBTROPICAL
TROPICAL
34.4
34.4

Figure II-12

the Gulf which reflects the pattern of flow drawn in Figure II-10b. During the peak phase of El Niño, we would expect to see the complete blanketing of the mouth with water from the Costa Rica Current limiting the source of exchange with the Gulf to Tropical Surface Water above roughly 50 m with Subtropical Subsurface Water below 50 m. During anti-El Niño periods, exchange with the Gulf above 150 m should be limited to the Transition and Subarctic Water of the California Current.

CONCLUSIONS

The principal source of interannual variability in the sea level climate of the Gulf of California is the changing intensity of the equatorial circulation associated with the El Niño/Southern Oscillation phenomenon. There is no significant share of interannual variability in the Gulf which can be related to an independent mode of variability originating in the North Pacific and statistically uncoupled from the occurrence of El Niño. None-the-less, EOF analysis of the large-scale processes indicates that a significant portion of the interannual variation in the flow within the eastern limb of the North Pacific gyre into the North Equatorial Current is independent of the El Niño/ Southern Oscillation phenomenon. This result does not mean that the Gulf is not subject to influence from the California Current, but rather such influence is regulated by the occurrence of El Niño.

The relationship among remote variables comprising the first climatic mode indicates that during an El Niño episode the cyclonic north equatorial gyre in the eastern Pacific intensifies. The cyclonic circulation consists of the North Equatorial Countercurrent and North Equatorial Current which are linked along the coast of Central America and Mexico by the northward flowing Costa Rica Current. The intensification leads to increased poleward advection within the Costa Rica Current and its northward penetration across the mouth of the Gulf of California as the California Current withdraws away from the entrance of the Gulf (Figs. II-10 and II-12) or separates from the coastal boundary. Evolution of the positive sea level anomalies within the Gulf and along southern Mexico indicate that north of the equator the occurrence of El Niño is an enhancement of the mean seasonal climatic pattern obtained during Autumn.

Interannual variability in the intensity and sense of advection across the mouth has important implications for the fluctuations in water mass structure within the Gulf of California. The transition between anti-El Niño and El Niño periods may be marked

by a change from the California Current to the Costa Rica Current as the source of surface and near surface waters available for exchange with the Gulf.

ACKNOWLEDGEMENTS

This investigation was supported by CoNaCyT Grant PCMABNA-005321 from the Mexican Government. Coastal sea level data from Mexican stations was furnished by the Universidad Autónoma de México through Ing. Francisco Grivel. Jerome Namias and Robert Born of Scripps Institution of Oceanography provided the atmospheric pressure data from the North Pacific. Klaus Wyrtki of the University of Hawaii supplied the sea level differences between the island stations in the Pacific. William Quinn of Oregon State University provided the atmospheric pressure data for Easter Island and Darwin, Australia, and sea level data for San Diego and Los Angeles. David Enfield, also of Oregon State University, provided sea level data for the San Francisco-Honolulu index. We thank William Quinn for the time spent in discussing El Niño and the Southern Oscillation, and David Enfield and Roger Lucas for critical reading and helpful comments to improve early versions of this paper. Detailed comments from an anonymous reviewer have lead to substantial improvement in the later version whch was read by Pedro Ripa for a final critique. We thank Sergio Ramos for drafting the figures, Carmen de Jesús and Guadalupe Pérez for typing, and especially Luis Fok-Pun for programming and data processing.

REFERENCES

Berlage, H.P., 1957. Fluctuations of the general atmospheric circulation of more than one year, their nature and prognostic value. Mededel. Verhandel., Koninkl. Nederlands Meteor. Inst., No. 69, 152 pp.

Bjerknes, J., 1969. Atmospheric teleconnections from the equatorial Pacific. Month. Weather Rev., 97:163-172.

Blackman, R.B. and J.W. Tukey, 1959. The Measurement of Power Spectra. Dover Publishing Inc., New York, 190 pp.

Chelton, D.B., 1980. Low frequency sea level variability along the west coast of North America. Ph.D. Dissertation, Scripps Institution of Oceanography, University of California, San Diego, 212 pp.

Chelton, D.B., 1981. Interannual variability of the California Current—physical factors. Calif. Coop. Fish. Investig. Rept., 22:34-48.

Chelton, D.B. and R.E. Davis, 1982. Monthly mean sea level variability along the west coast of North America. J. Phys. Oceanogr., 9:757-784.

Christensen, N. Jr., and N. Rodriguez S., 1979. A study of sea level variations and currents off Baja California. J. Phys. Oceanogr., 9:631-638.

Davis, R.E., 1976. Predictability of the sea surface temperature and sea level pressure anomalies over the North Pacific ocean. J. Phys. Oceanogr., 6:249-266.

Egger, J., G. Meyers and P.B. Wright, 1981. Pressure, wind and cloudiness in the tropical Pacific related to the Southern Oscillation. Month. Weather. Rev., 109:1139-1149.

Enfield, D.B. and J.S. Allen, 1980. On the structure and dynamics of monthly mean sea level anomalies along the Pacific Coast of North and South America. J. Phys. Oceanogr., 10:557-578.

Horel, J.D. and J. M. Wallace, 1981. Planetary-scale atmospheric phenomena associated with the Southern Oscillation. Month. Weather Rev., 109:813-829.

Krishnamurti, T.N., 1971. Tropical east-west circulation during the northern summer. J. Atmos. Sci., 28:1342-1347.

Krishnamurti, T.N., M. Kanamitsu, W.J. Koss and J.D. Lee, 1973. Tropical east-west circulations during the northern winter. J. Atmos. Sci., 30:780-787.

Kundu, P.K., J.S. Allen and R.L. Smith, 1975. Modal decomposition of the velocity field near the Oregon coast. J. Phys. Oceanogr., 5:683-704.

McCreary, J., 1976. Eastern tropical ocean response to changing wind systems with application to El Niño. J. Phys. Oceanogr., 6:632-645.

McCreary, J.P., 1978. Eastern tropical ocean response to changing wind systems. In: Review Papers of Equatorial Oceanography—Proc. FINE Workshop. Nova University Press, Ft. Lauderdale, FL., Chap. 7.

Meyers, G., 1975. Seasonal variations in transport of the Pacific North Equatorial Current relative to the wind field. J. Phys. Oceanogr., 5:442-449.

Pazen, S.E. and G. Meyers, 1982. Interannual fluctuations of the tropical Pacific wind field and the Southern Oscillation. Month. Weather Rev., 110:587-600.

Philander, S.G.H., 1983. El Niño Southern Oscillation phenomena. Nature, 302:295-301.

Price, J.M., 1981. Monthly mean sea level fluctuations at Honolulu and San Francisco and the intervening geostrophic currents. J. Phys. Oceanogr., 11:1375-1382.

Quinn, W.H., D.O. Zoph, K.S. Short and R.T.W. Kuo Yang, 1978. Historical trends and statistics of the Southern Oscillation, El Niño, and Indonesian droughts. Fish. Bull., 76:663-678.

Rasmusson, E.M. and T.H. Carpenter, 1982. Variations in tropical sea surface temperature and surface wind fields associated with the Southern Oscillation/El Niño. Month. Weather Rev., 110:354-384.

Reid, R.O., 1948. The equatorial currents of the eastern pacific as maintained by the stress of the wind. J. Mar. Res., 7, 74-99.

Reiter, E.R., 1978. Long-term wind variability in the tropical Pacific, its possible causes and effects. Month. Weather Rev., 106:324-330.

Roden, G.I., 1971. Aspects of the transition zone in the northeastern Pacific. J. Geophys. Res., 76:3462-3475.

Rusnak, G.A., R.L. Fisher and F.P. Shepard, 1964. Bathymetry and faults of the Gulf of California. In: Tj.H. van Andel and G.G. Shor, Jr. (eds), Marine Geology of the Gulf of California. Amer. Assoc. Petrol. Geol. Mem. 3, Tulsa, OK, p. 59-75.

Saur, J.F.T., 1972. Monthly sea level differences between the Hawaiian Islands and the California coast. Fish. Bull., 70:619-636.

Walker, G.T. and E.W. Bliss, 1932. World Weather V, Mem. Roy. Met. Soc., London, 4:53-84.

White, W.B. and T.P. Barnett, 1972. A servomechansm in the ocean/atmosphere system of the mid-latitude North Pacific. J. Phys. Oceanogr., 2:372-381.

White, W.B., 1975. Secular variability in the large-scale baroclinic transport of the North Pacific from 1950-1970. J. Mar. Res., 33:144-155.

White, W.B., 1977. Secular variability in the baroclinic structure of the interior North Pacific from 1950-1970. J. Mar. Res., 35:587-607.

Wright, P.B., 1977. The Southern Oscillation —patterns and mechanisms of the teleconnections and thepersistence. Hawaii Institute of Geophysics Rept. HIG-77-13.

Wright, P.B.;, 1983. Sea surface temperature fluctuations in the Pacific, 0-50°N. Tropical Ocean-Atmospheric Newsletter, No. 19, pp. 14-15.

Wyrtki, K., 1965a. Summary of the physical oceanography of the eastern Pacific Ocean. University of California, IMR Ref. 65-10, 78 pp.

Wyrtki, K., 1965b. Surface currents of the Eastern Tropical Pacific. Inter. Amer. Trop. Tuna Comm. Bull., 9:271-304.

Wyrtki, K., 1966. Oceanography of the eastern equatorial Pacific Ocean. Oceanogr. Mar. Biol. Ann. Rev., 4:33-68.

Wyrtki, K., 1974a. Equatorial currents in the Pacific 1950 to 1970 and their relations to the trade winds. J. Phys. Oceanogr., 4:372-380.

Wyrtki, K., 1974b. Sea level and the seasonal fluctuations of the equatorial currents in the western Pacific Ocean. J. Phys. Oceanogr., 4:91-103.

Wyrtki, K., 1977. Sea level during the 1972 El Niño. J. Phys. Oceanogr., 7:779-787.

Wyrtki, K., 1979a. Sea level variations: monitoring the breath of the Pacific. EOS, 60:25-27.

Wyrtki, K., 1979b. The response of sea surface topography to the 1976 El Niño. J. Phys. Oceanogr., 9:1223-1231.

CHAPTER III

VARVE FORMATION IN THE CENTRAL GULF OF CALIFORNIA: A RECONSIDERATION OF THE ORIGIN OF THE DARK LAMINAE FROM THE TWENTIETH CENTURY VARVE RECORD

ABSTRACT

Formation of the dark "summer" laminae of the varved sediments from the anaerobic slopes of the central Gulf of California has previously been considered a response to the summer-fall runoff maxima from the major rivers of Sonora. Reconstruction of a twentieth century varve chronology allows a direct comparison of river discharge data to the mass flux of material to the dark laminae. Although small-scale mass movement has resulted in numerous local unconformities in the varve stratigraphy, a continuous record of seasonal deposition is obtained from a set of five closely spaced box cores taken along the slope off Guaymas, Sonora. The varve chronostratigraphy is supported by ^{210}Pb dating of the five cores. Individual laminae can be traced over the entire set of box cores indicating that varve deposition occurs uniformly along the slope over a minimum distance of nearly 20 kilometers.

The varve record shows no indication that construction of dams across the major Sonoran rivers, begun during the 1940's, has had any effect on deposition of the dark laminae. Mass flux to the dark laminae measured from one core does show an apparent relationship to the "free" undammed summer-fall river discharge of the Sonora, Yaqui and Mayo Rivers compiled from stations above the dams or for periods prior to dam construction. However, no relationship exists between the mass flux values and the "controlled" discharge of the rivers below the dams. We propose that the transfer of terrigenous material from the mainland to the central Gulf, occurs principally through eolian processes by removal and transport of desert dust associated with convective summer thunderstorms.

INTRODUCTION

Alternating light- and dark-colored millimeter-scale laminae were first described from the Gulf of California by Revelle (1939) who later suggested that the laminated structure is produced by seasonality in plankton production (Revelle, 1950). Byrne (1957) further proposed that the laminae formation is a response to a seasonal pulse of elevated diatom production and sedimentation, superimposed on a continuous flux of terrigenous clays over the year. Calvert (1964) demonstrated that the laminated sediments are confined to the basin slopes, and that their occurrence is determined by a mid-water oxygen minimum intersecting the slopes between roughly 300 and 1200 m depth. Although laminated sediments occur along the slopes of the central and southern Gulf, the richly diatomaceous laminae are confined to the region of the more biologically productive central Gulf (Calvert, 1966a,b).

Byrne's (1957) hypothesis considered the light-dark laminae couplets to be annual varves. To verify this, Calvert (1966b) compared deposition rates derived from radiocarbon dating and lamina counts from three cores of the central Gulf. Only one of these cores actually yielded an unequivocal result, but later work with ^{210}Pb (Bruland, 1974; DeMaster, 1979; Baumgartner et al., 1985) confirmed the annual nature of the lamina couplets.

Calvert (1966b) incorporated Byrne's proposal into a conceptual framework of two alternative hypotheses to guide his examination of the process of varve formation in the central Gulf. These two hypotheses are contrasting models based upon the inferred annual variation in supply of the two principal sediment components: opal phytoplankton remains and detrital mineral grains of terrigenous origin. One model (reflecting that of Byrne, 1957) would produce a laminae couplet by varying the supply of organic remains by means of a spring pulse of phytoplankton production superimposed on a steady supply of terrigenous material. The second model would control laminae

formation by superimposing a summer pulse of terrigenous silts and clays on a steady supply of organic detritus. Calvert (1966b) developed a cogent argument in favor of the second model based upon (1) an assumed pattern of steady phytoplankton production throughout the year, (2) the observed annual cycle in discharge of the principal river systems flowing into the Gulf, and (3) his determination of the composition and inferred rates of accumulation of biogenous and terrigenous material in the light and dark laminae.

Twenty years after its publication, this paper by Calvert (1966b) remains a landmark for its thoughtful analysis. Recent work, however, indicates that his argument for steady production of phytoplankton is an over-simplification. Microfossil analysis of light- and dark-laminae in the central Gulf (Donegan and Schrader, 1981, 1982) suggests that seasonality in phytoplankton production is an important factor in the timing for the deposition of the light laminae as well as for their diatom-rich composition. Although Donogan and Schrader (1982) argue that light laminae deposition is a response to elevated levels of winter-spring primary production, no one has questioned Calvert's conclusion that discharge to the central Gulf from the principal Sonoran rivers is responsible for the formation of dark laminae.

One principal objective of this paper is to examine the origin of the dark laminae by testing their response to river runoff. Calvert (1966b) inferred an annually variable supply of terrigenous sediment over the slopes of the Guaymas basin as a function of discharge of the suspended load from major mainland rivers. These river systems exhibit a well-defined annual cycle in monthly mean flow which is dominated by a summer peak occurring in August. However, construction of dams across the rivers flowing to the central Gulf, begun in the 1940's, has eliminated the seasonal runoff peak below the dams. This provides us with a completed large-scale experiment with which to determine whether or not a seasonal injection of material has played a

significant role in the modern process of varve formation along the adjacent continental slope. The continental drainage systems and the effect of damming upon the principal rivers flowing to the central Gulf are described in a section preceeding our analysis of the relationship between river runoff and dark laminae deposition.

Our study is based upon a suite of five box cores collected from a small area of the continental slope off Guaymas, Sonora (Fig. III-1) during the summer of 1978. The cores were taken from between 600 to 650 m depth where the mid-water oxygen minimum is most intense and the laminar structure is least disturbed by burrowing and deposit feeding macrofauna (Calvert, 1964). Location of the study area was chosen for its joint proximity to the principal center of coastal upwelling in the central Gulf (see Badan et al., 1985) and to the mouth of the Yaqui River (Fig. III-1) which drains the largest area of any of the rivers emptying into the central Gulf. The cores were not placed closer to the mouth of the Yaqui because of steepened slopes and the presence of large submarine channels within the bathymetric reentrant off Guaymas.

A major part of this investigation consists of the reconstruction of a modern varve chronology which encompasses most of the twentieth century. This is a crucial first step for comparison of the varve record to any instrumentally recorded parameter of climatic variation. Development of the chronology to obtain an accurately dated record of laminae deposition from the five box cores has therefore been carefully documented here.

We have also made a considerable effort to determine the lateral continuity of individual laminae. Box core sites were spaced roughly 5 km apart in the along-slope direction for this purpose. This is an important question since the extent of lateral continuity must reflect the degree of homogeneity of deposition along the slope related to the spatial scales of regional climatic and oceanographic forcing. The problem of lateral continuity is therefore closely linked to any consideration of the processes of

Figure III-1

Distribution of box core sites along the Guaymas slope. Bathymetry is based upon surveys undertaken during collection of cores in July 1978. Location of study area shown on inset map of the Gulf of California (adapted from Bischoff and Niemetz, 1980); all depths are given in meters.

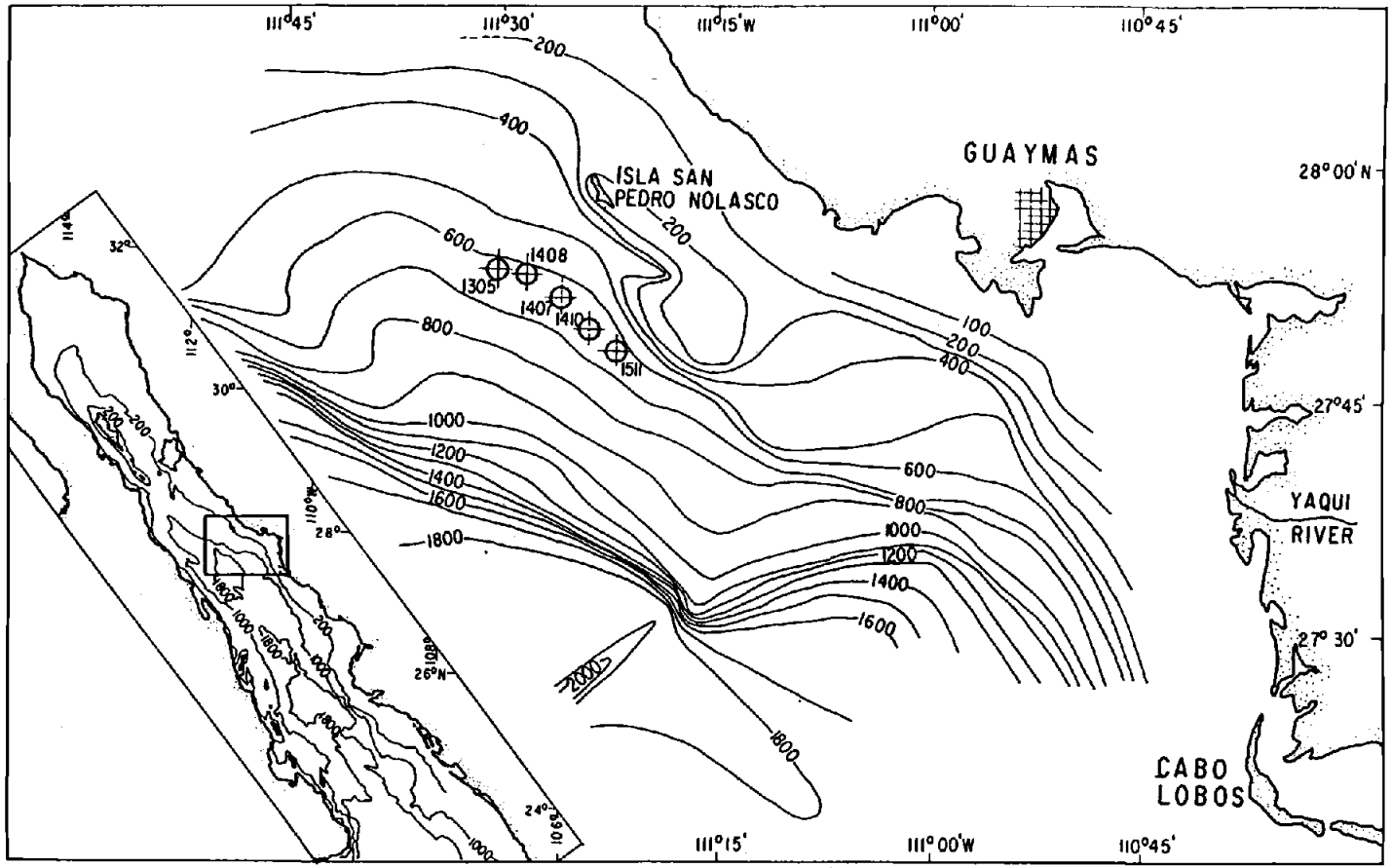
111°45'
111°30'
111°15'W
111°00'
110°45'
GUAYMAS
28°00'N
ISLA SAN
PEDRO NOLASCO
1408
1305
1407
1410
1511
27°45'
YAQUI
RIVER
27° 30'
CABO
LOBOS
111°15'
111°00'W
110°45'

Figure III-1

varve formation. The replicate sampling provided for by the multiple box cores also turned out to be essential for the complete assembly of an area-wide varve stratigraphy as the initial stage in reconstruction of the twentieth century chronology.

METHODS

Sampling Procedures

Samples were recovered with an open-vented box corer with interchangeable coring boxes measuring 30 x 30 x 100 cm (Soutar, 1978). Coring was carried out from the Research Vessel MATAMOROS, provided by the Mexican Navy. Immediately after bringing the corer aboard ship, the box with sediment sample and approximately 20 cm of overlying water was lowered into a bath of dry ice and isopropyl alcohol. This resulted in rapid freezing of the outer several cm of sediment with the formation of a microcrystalline network of frozen pore water throughout the exterior region of the core. Cores were left in the cold bath for approximately 24 hours to insure complete freezing. All cores were extruded from the boxes onboard ship and sealed in heavy polyethylene sheeting and placed in frozen storage.

While the outer several cm are frozen almost immediately, and suffer no initial deformation, the interior of the core freezes slowly with the accompanying formation of large crystals and brine pockets towards the center of the core. Expansion and deformation of the core is therefore greatest near the last-frozen center of the core, causing vertical doming of laminae which increases toward the surface of the core. The structure and stratigraphy of the box cores are documented by X-radiography of 1-cm thick vertical slabs down the cores. Because of the internal deformation due to freezing, these slabs were taken only from the outer faces of the cores where this deformation is minimal. The cores were sectioned with a high-speed band saw.

X-Radiography and Photography of Box Cores

In order to resolve the fine-scale laminar structure of the slabs by X-radiography, the X-ray beam must pass through the slab parallel to the internal planes. Because the lamina surfaces dip toward the outside faces of the core (due to freezing deformation), a

minimum of two radiographs taken with different slab orientations, was necessary to adequately reveal the fine lamina structure over the entire length of a slab. For some slabs, it was necessary to make five or more radiographs. All exposures were made at 40 kV with a film-to-source distance of 117 cm to obtain maximum contrast (Bouma, 1969). The film used was Kodak XTL-2 in 8 x 10-inch "Ready-Paks".

From each set of radiographs taken for a given slab, a slab mosaic was constructed from positive prints to present the optimum resolution of the laminae throughout the slab. The individual slab mosaics were in turn, assembled into radiograph composites of the complete working halves of the five cores. Figures III-2 through III-6 represent each half box core folded out onto a single plane for display of its three-dimensional structure. The heavy broken lines between the front and side faces indicate the fold lines at the two corners of the half-cores in Figures III-2 through III-6. The relationship between the geometry of the folded-out radiography composite and the working half-core is indicated by the sketch in Figure III-2. Note that only the upper 40 cm of each core is presented here although the original core composites range from 70 to 85 cm in length.

Photographs of the exterior slab surfaces (Fig. III-8) were shot with fluorescent lighting using a macro-lens and a high-contrast 35 mm Kodak TP 2415 film. The subject-to-film distance was 123 cm. Distortion in the photographs was minimized by alignment of the camera with a mirror on the subject plane before each exposure.

^{210}Pb Dating

Subsamples were taken at regular stratigraphic intervals from radiographed slabs of all five box cores for radiometric dating by excess ^{210}Pb (Bruland, 1974). Individual subsamples cover stratigraphic thicknesses of between 1 and 2 cm corresponding to between 1 and 4 lamina couplets (Fig. III-9). ^{210}Pb activities were measured indirectly

by counting the alpha activity of its granddaughter ^{210}Po. ^{210}Po has a half-life of about 138 days and the intermediate ^{210}Pb daughter, ^{210}Bi, has a half-life of only five days. Sufficient time (two years) elapsed between core collection and chemical separation to allow ^{210}Po ingrowth to reach equilibrium with ^{210}Pb in the youngest material.

The frozen subsamples were thawed and centrifuged to remove the pore water and minimize dry weight bias introduced by residual sea salt. After drying, aliquots of sediment were spiked with ^{208}Po as a yield tracer and digested in a mixture of warm, concentrated HCl and HNO_3 acids. The acid slurry was diluted with distilled deionized water and centrifuged. The resulting supernatant, containing the ^{210}Po and ^{210}Pb, was then dried, rinsed with concentrated HCL, and dried again. Finally, the residual salts were dissolved in 0.5 N HCl and heated to 75°C on a heat/stir plate with the addition o small amounts of ascorbic acid until the solution cleared. The polonium was plated onto polished silver planchets after the method of Flynn (1968). The planchets were inserted into teflon holders with magnetic stir bars which were placed in the warm solution and spun for two and one-half to three hours.

The plated subsamples were counted for 24 hours using low background lithium-drifted silicon surface barrier detectors. The resulting ^{210}Po activity was corrected for decay since the time of chemical separation of ^{210}Po from ^{210}Pb (i.e., plating). This corrected ^{210}Po activity was then equivalent to the total ^{210}Pb activity (excess and supported) in the sediments at the time of plating. This ^{210}Pb activity was further corrected for decay from the time of collection to plating.

The total ^{210}Pb activities at time of collection converge to a near constant value for the deepest two subsamples in all five cores. This low value of ^{210}Pb activity was assumed to be that supported from the in situ decay of the parent ^{226}Ra. The value used for this background ^{226}Ra was thus obtained by averaging values from the two deepest subsamples in each core (3.81 ± 0.53 dpm/g). The associated limits of uncertainty

correspond to the standard deviation of the deep sample activities which includes the analytical error from counting (considerably lower). The unsupported (excess) ^{210}Pb values were then found by subtracting this standard background of supported ^{210}Pb from each measured total ^{210}Pb activity.

LATERAL CONTINUITY OF LAMINAE

The structure of each of the five box cores (Figs. III-2 to III-6) is dominated by sequences of millimeter-scale laminae. Where well represented, the laminae are defined as alternating light and dark tones on the radiographs. However, there is a great deal of variation in the relative absorption (tonal) characteristics among both the individual light and among the dark laminae so that non-repetitive stratigraphic patterns of optical density occur throughout the lamina sequences. Although many of the distinctive lamina sequences can be readily traced horizontally around the faces of the individual box cores, none of the five cores contains a complete, stratigraphically continuous lamina sequence.

Van Andel (1964) attempted to trace the laminae over several kilometers in the Gulf using small diameter (approximately 5 cm) gravity cores. The results were not encouraging: "The horizontal extent of individual layers or group of layers is not known, but it is probably small, inasmuch as correlation between a group of closely spaced cores (approximately 1-mile spacings) proves impossible." A cursory examination of Figures III-2 through III-6 illustrates why van Andel's initial attempt was defeated. Each of the cores shows obvious secondary structures reflecting a complex history of small-scale, natural physical disturbance. For some of the cores it would indeed be difficult to correlate the lamina stratigraphy from one side to the other based only upon two 5-cm wide vertical strips. The secondary structures commonly

Figure III-2

Radiograph composite of the upper 40 cm of box core 1305. The composite was assembled from mosaics of individual slabs cut from the exterior faces of the working half-core. The side faces are folded out onto the plane of the front face as shown in the diagram. The corners between the sides and front of the core are indicated by the heavy broken lines at top of the composite. Borders between individual slabs, appearing as blank strips on composite, are shown on diagram as light dotted lines. Arrow marks the presence of discontinuity in lamina stratigraphy which occurs in all five cores and which places a lower limit on our present reconstruction of the varve chronostratigraphy. Scale to right is in centimeters.

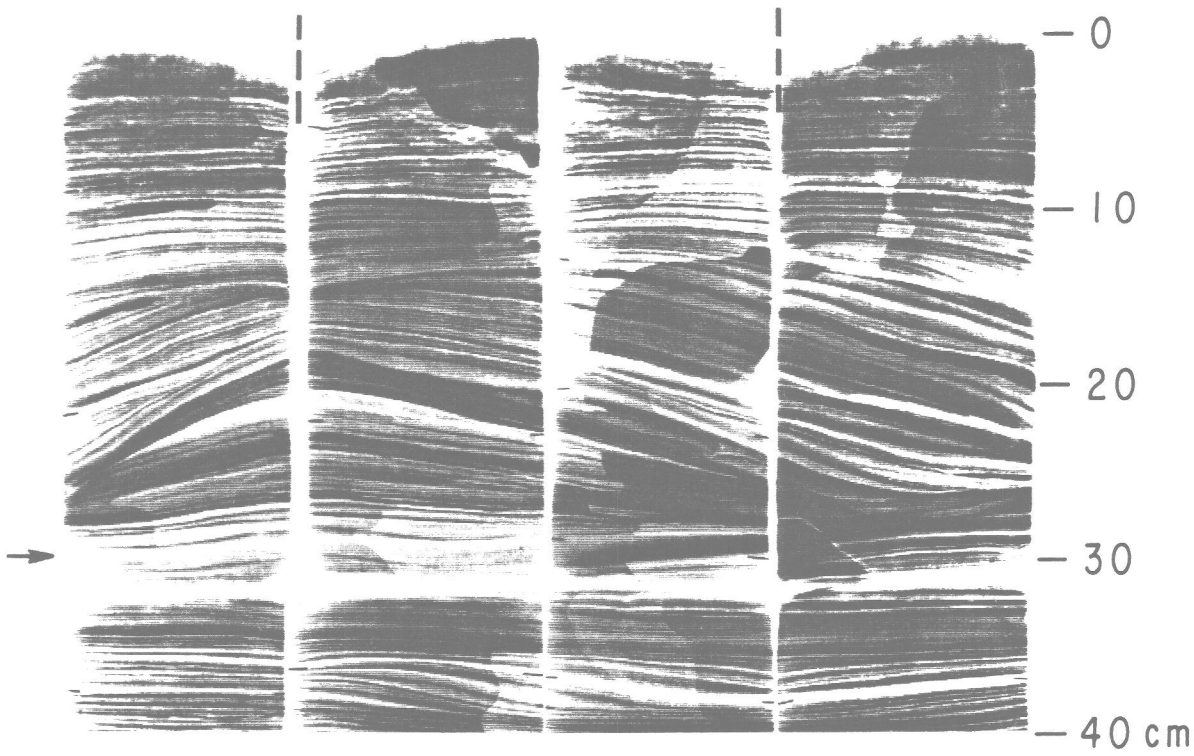

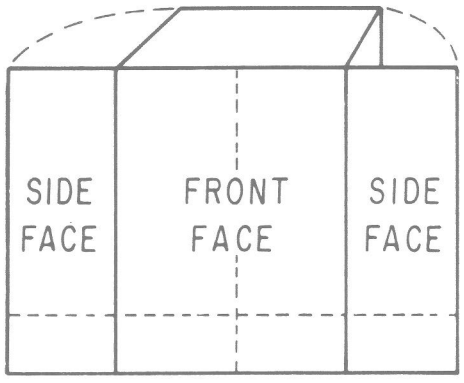

DISPLAY OF HALF-CORE RADIOGRAPH COMPOSITES

Figure III-2

Figure III-3

Radiograph composite of upper 40 cm of core 1407 assembled as shown in Figure III-2. Arrow points to area-wide discontinuity in lamina stratigraphy.

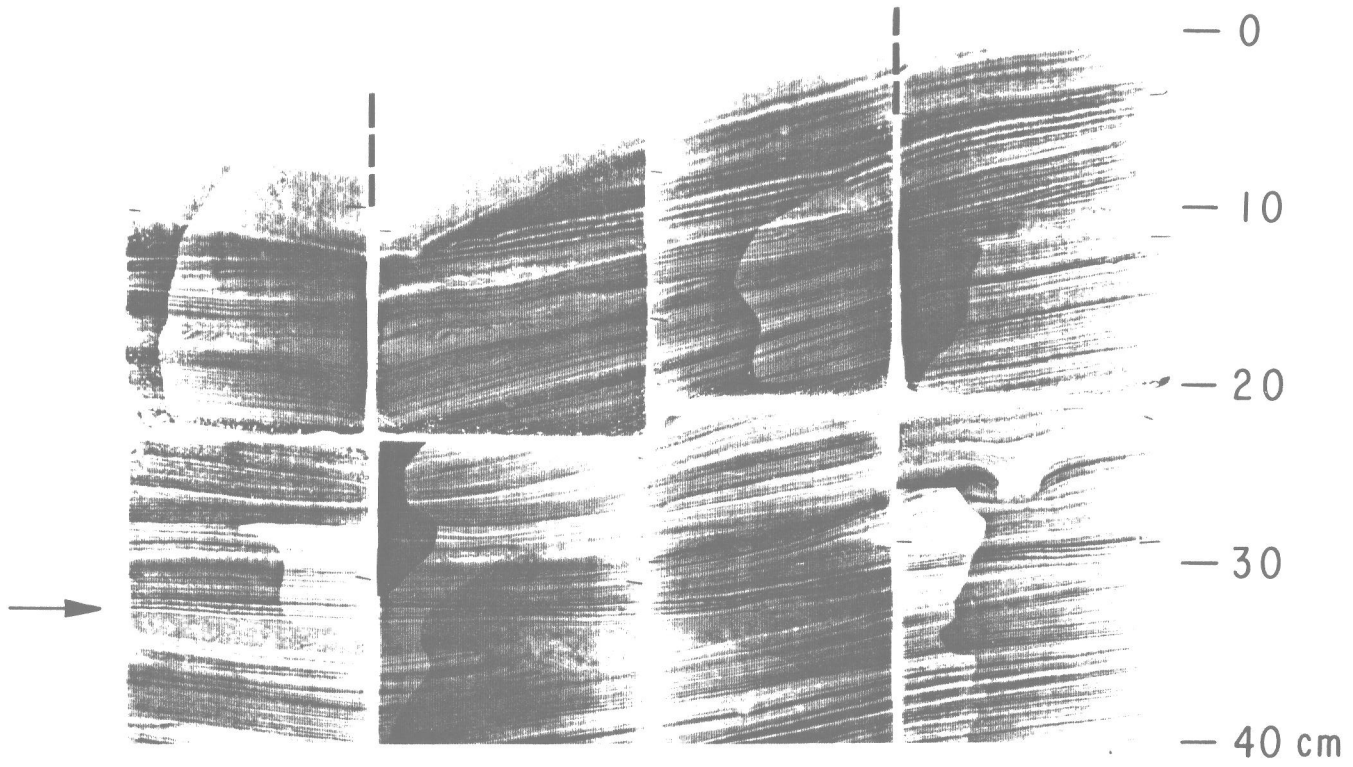

Figure III-3

Figure III-4

Radiograph composite of upper 40 cm of core 1408 assembled as shown in Figure III-2. Arrow points to area-wide discontinuity in lamina stratigraphy.

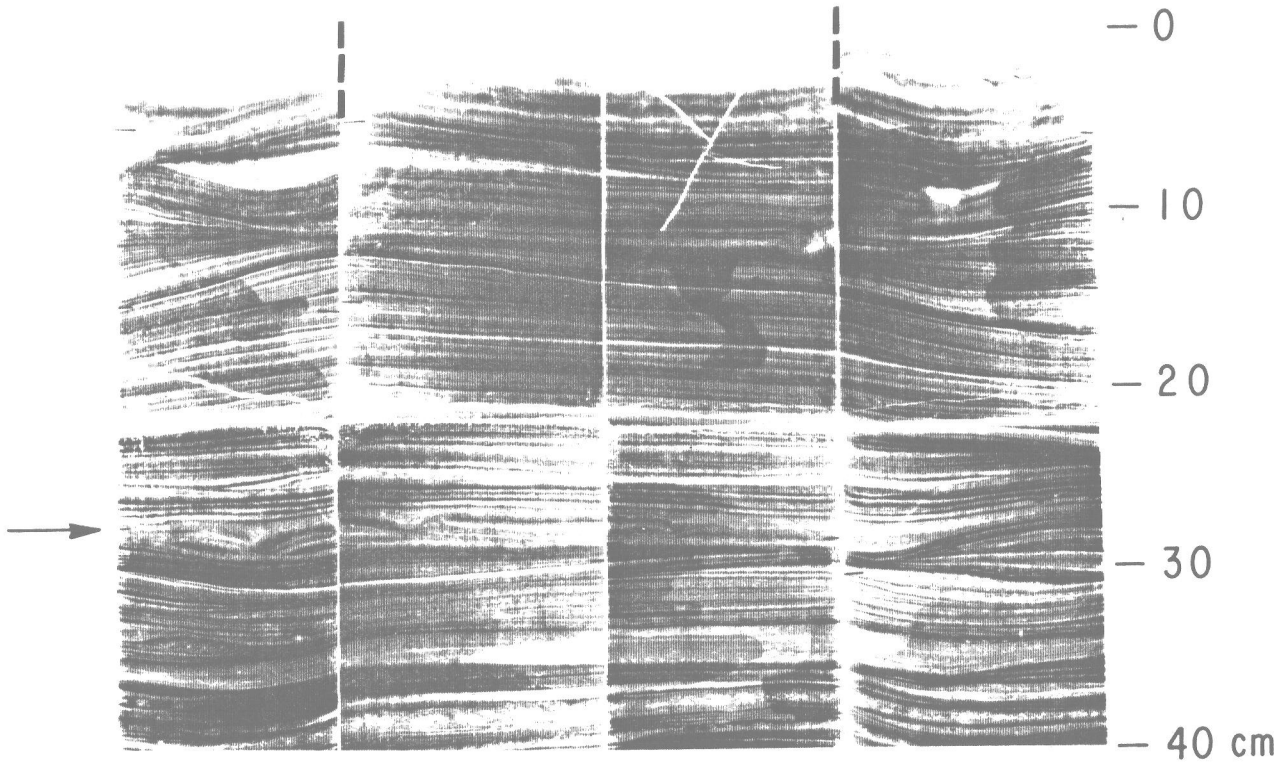

Figure III-4

Figure III-5

Radiograph composite of upper 40 cm of core 1410 assembled as shown in Figure III-2. Arrow points to area-side discontinuity in lamina stratigraphy.

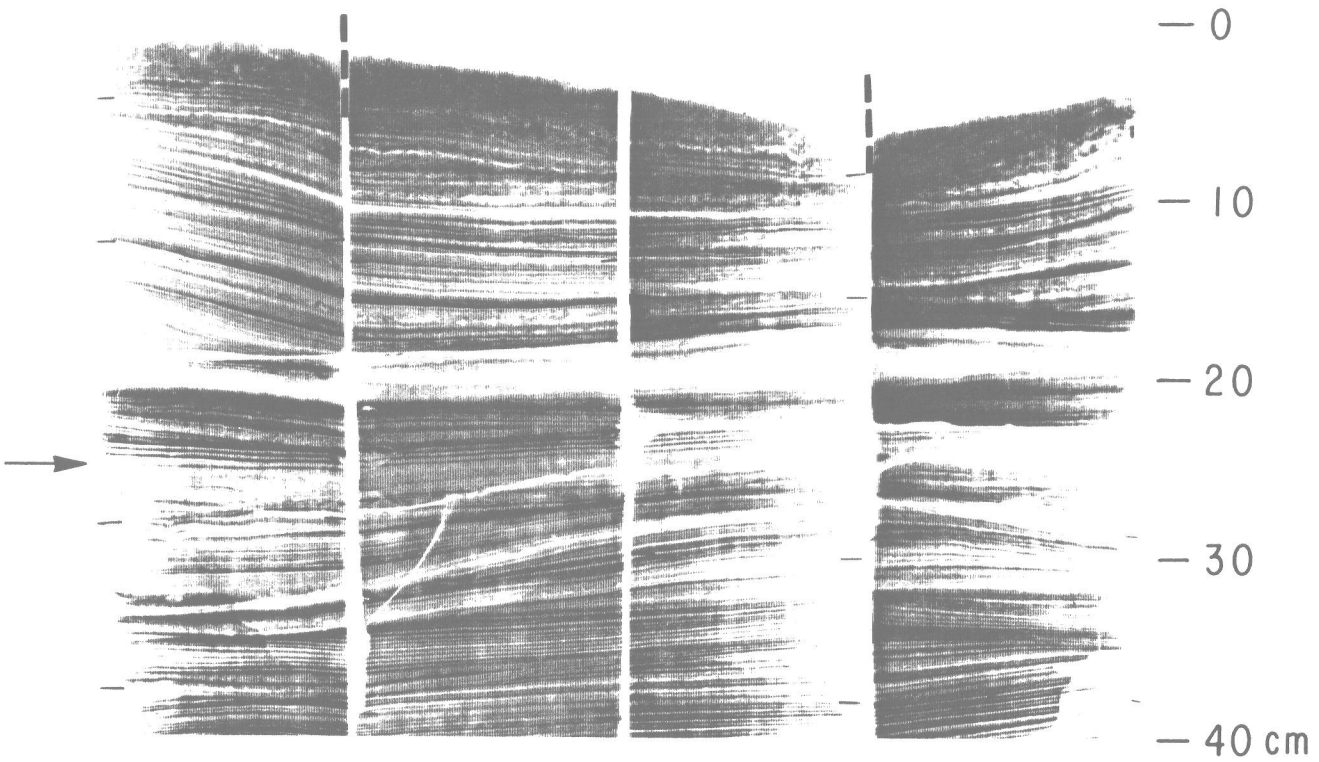

Figure III-5

Figure III-6

Radiograph composite of upper 40 cm of core 1511 assembled as shown in Figure III-2. Arrow points to area-wide discontinuity in lamina stratigraphy.

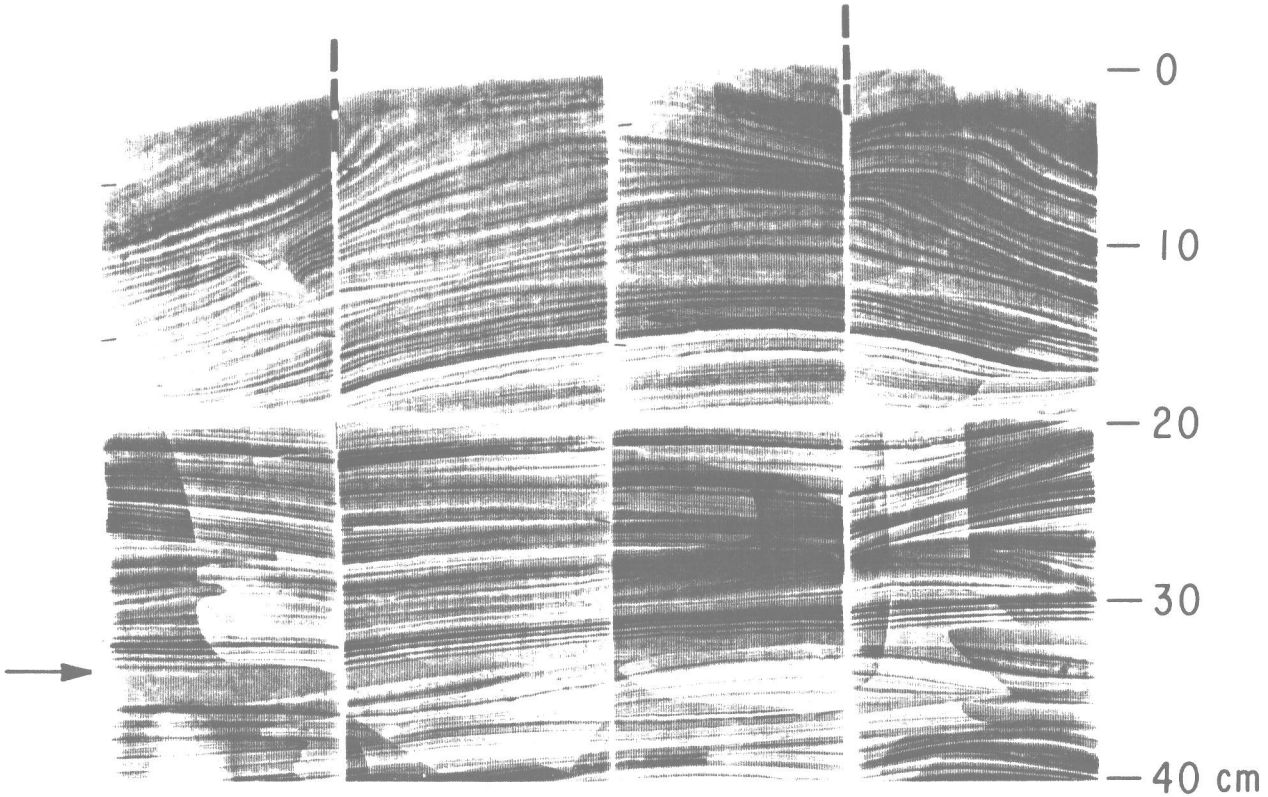

Figure III-6

interrupt or distort the lamina stratigraphy, often at different depths within the same core.

The secondary structures generally occur as planar discontinuities separating lamina sequences, and as lenticular channels and tabular bodies characterized by internally homogeneous material. These are occasionally associated with some plastic deformation of the laminae sequences. The secondary structures appear to be the result of small-scale, gravity-induced mass movement of the sediment. The planar discontinuities are interpreted as low-angle surfaces of shear failure accompanied by gliding or slumping. A good example of such a structure is found in core 1305 near 15 cm depth on the left-hand side of the core (Fig. III-2). The result is a clearly marked angular unconformity which diminishes and dies out toward the right side of the core. These features are common throughout all of the five cores.

The thin lenticular and roughly tabular bodies are probably the result of sediment gravity flows. A distinct channel with homogeneous fill is exposed in core 1408 between 5 and 10 cm on the left-hand side of the core (Fig. III-4). The surface sediment of core 1407 (Fig. III-3) has been eroded on the left side, and the cut is filled with homogenized material. The lamina sequence which is laterally adjacent, continues upward undisturbed to the sediment-water interface. Between roughly 30 and 35 cm in core 1407 is another channel, or tabular flow, which contains rip-up clasts and shows evidence of gouging underlying material near the center of the core (Fig. III-3). This structure thins toward the right and forms a low angle unconformity on the right side of the core. The sediment gravity flow structures are less common than the shear planes, but are present in all cores.

In addition to the physical disturbances, some of the cores show evidence of biological disturbance which has degraded the original laminar structure. The most serious of these are the thin horizontal burrowing complexes which are spread laterally through

tens of centimeters and appear as layers of white mottles disrupting the stratigraphic continuity of the lamina sequence. These are best observed in core 1407 near 29 cm on the left-hand side (Fig. III-3), and in a nearly continuous layer between 38 and 40 cm in core 1408 (Fig. III-4). Rare occurrences of vertical burrowing also exist, such as in core 1407 (right side, near 25 cm; Fig. III-3) and in core 15ll near 11 cm on the left side (Fig. III-6), but these are not extensive enough to seriously perturb the continuity of surrounding laminae.

In order to determine the among-core lateral continuity of the laminae, the stratigraphically continuous intervals of the laminae were first identified and reconstructed for each core (Fig. III-7). The clearest segments from each radiograph composite were spliced together to provide as continuous a record of laminae deposition as possible for each core site. The blank areas between unbroken lamina sequences within individual cores in Figure III-7 indicate the presence of discontinuities which occur across an entire core. These stratigraphic reconstructions extend to approximately one-third of the full length of the cores, to the point where all five cores are interrupted by a single discontinuity. This is the ony area-wide discontinuity discovered within the upper 40 cm of the five cores. The upper surface of the tabular structure associated with this area-wide discontinuity is marked by an arrow in Figures III-2 through III-6. Until a core is recovered from the study area which bridges this stratigraphic gap, there appears to be no control with which to assess the possible loss of material (and the corresponding hiatus) associated with the discontinuity.

Arrangement of cores in Figure III-7 corresponds to the location of the core sites along the slope shown in Figure III-1. After identification of the local discontinuities in each core, the laminae sequences were correlated based upon visual inspection of the radiograph prints. Lamina sequences were correlated by comparison of the patterns of laminae thicknesses and X-ray intensities much as tree-ring series are correlated. Each

Figure III-7

Reconstructed lamina sequences from the five box cores from the Guaymas slope. Vertical continuity within each core is maximized by fitting selected sections from different regions of the cores. Correlation lines mark prominent laminae which are clearly identifiable among the five cores. Blank areas within the lamina sequences indicate discontinuities which occur across an entire core. Distances between core sites are shown at the bottom of the figure. The sediment gravity flow forming the base of each reconstruction is included here in the core stratigraphies.

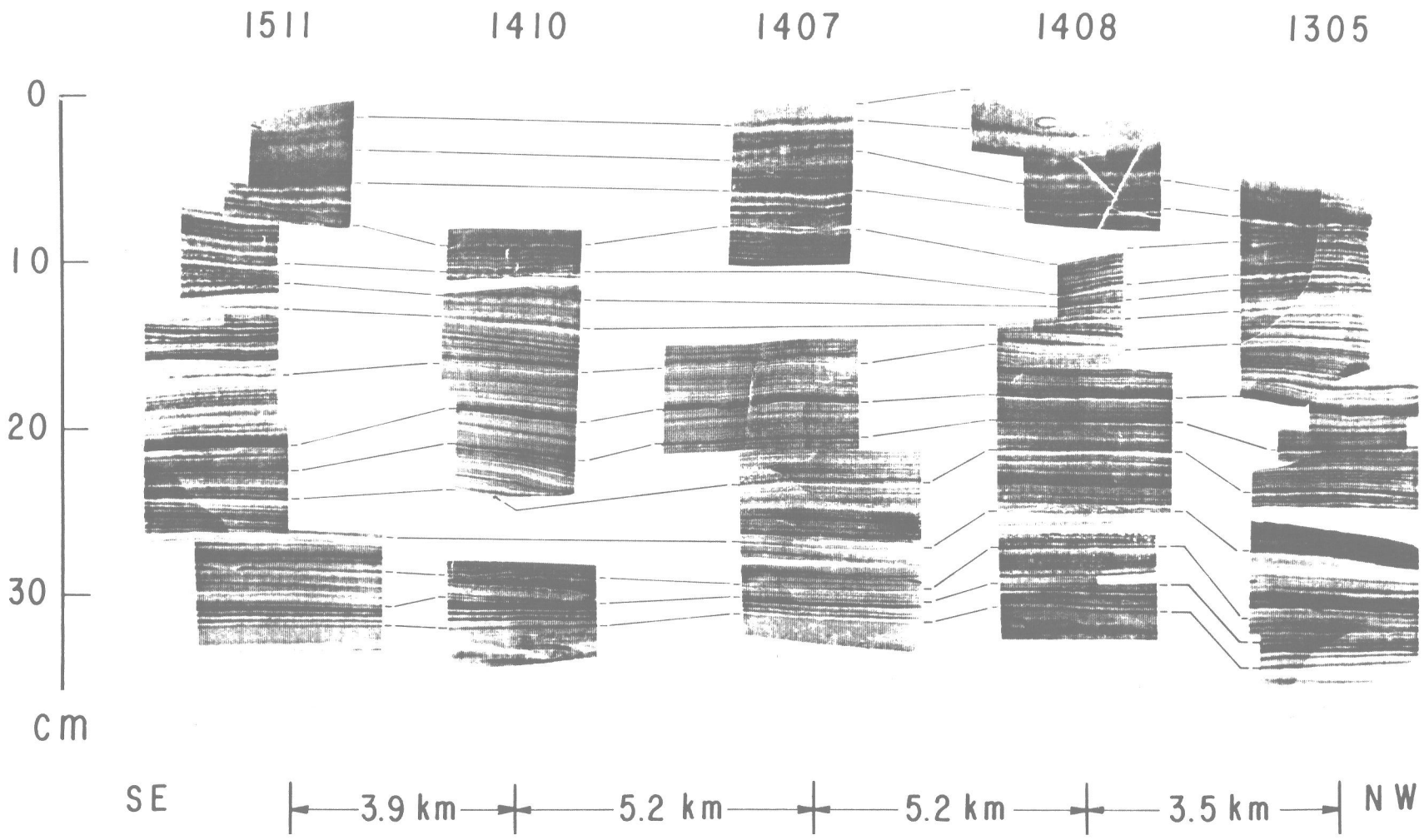

Figure III-7

correlation line corresponds to a distinct marker lamina which can be identified from the radiographs in all of the cores. Between each of these marker laminae is a unique stratigraphic pattern of optical density contrasts reflecting the variability in lamina structure. The only difference evident among core sites is a dilation or compression of these patterns between the marker laminae as they are traced from core to core. Recognition of these non-repetitive sequences in the radiograph densities throughout all cores show that all individual laminae extend through the entire study area.

The area-wide lateral continuity of individual laminae across all five core sites demonstrates that the seasonal deposition of the millimeter-scale layers is relatively uniform along the Guaymas slope over a distance of nearly 20 km. This agrees with Soutar and Crill's (1977) observation that varve sequences can be traced over a distance of at least 14 km on the floor of the Santa Barbara Basin off southern California. The coherent along-slope continuity of laminae within our small sampling area suggests that the processes responsible for varve formation may operate uniformly over a considerably wider region. If the spatial scale of laminae formation is consistent with the scales of motion at the sea surface seen from satellite imagery (Badan-Dangon et al., 1985; their Fig. 4), individual laminae might retain their characteristic structures over distances greater than 100 kilometers along the slope.

DEVELOPMENT OF A TWENTIETH CENTURY VARVE CHRONOLOGY

Reconstruction of Varve Chronostratigraphy

The physical and biological disturbances observed in Figures III-2 through III-6 preclude the use of any single core as the basis to develop a continuous lamina stratigraphy. However, because the laminae are laterally continuous among core sites and discontinuities do not occur within the same stratigraphic intervals among all the cores,

it is possible to patch together a continuous area-wide chronostratigraphy from multiple core sites.

Good zero-age surfaces appear to have been recovered by cores 1407 and 1408 even though Figure III-3 shows that the surface of core 1407 has been partially lost by channelling. The contemporaneous depositional interface in cores 1407 (excluding the channel fill) and 1408 is indicated by a sudden increase in water content in the upper 3 cm and the visual gradation of the sediment into the overlying water on the radiographs. Surfaces of cores 1305, 1410 and 1511 all appear to have been disturbed to some extent, with a substantial loss of material from the surface of core 1410 indicated by Figure III-7.

An area-wide continuous varve stratigraphy can be assembled from short intervals from four of the five available cores. Figure III-8 displays this reconstruction based upon sequences from cores 1407, 1408, 1410 and 1511. The left-hand column of Figure III-8 is a sequence of radiographs; the right-hand column is the equivalent sequence of photographs of the slab surfaces. The sequences used were chosen for their quality of resolution of individual lamina on the radiographs and on the photographs. The cross-hatched regions on Figure III-8 were drawn to indicate stratigraphic continuity between intervals with poor geometric fits taken from different cores. These intervals are spliced together across dark layers. The narrow dot pattern within the 1407 sequence is a splice between two intervals taken from different areas of that core.

Reconstruction of the final chronostratigraphy entails the reduction of the stratigraphic column to a binary sequence of seasonally formed light and dark layers. Laminae couplets are not always clearly recognizable from the radiograph, however. The high resolution sought for in the radiographs often reveals that individual lamina may be composed of several thin submillimeter layers. These "sublaminae" are evident on Figure III-8 within the intervals of varve numbers 30 to 55 and in the light lamina of

Figure III-8

Master chronostratigraphy reconstructed from spliced segments of four of the five available box cores. Left hand column composed of spliced radiograph segments; right hand column composed of identical sequence of surface photographs. The horizontal bars along margins of radiograph and photograph columns mark the positions of individual dark laminae. Correlation lines between radiograph and photograph connect equivalent laminae. Varve dates (on photograph column) and varve numbers (on radiograph column) are marked at base of the dark laminae. Varve years are thus shown as beginning in summer (base of dark laminae) unless otherwise indicated. The box core from which each radiograph/photograph segment was taken is shown to the left. Hatching indicates areas of poor fit between shapes of contiguous stratigraphic segments from different cores. Stippling within radiograph/photograph segment of a single core indicates area of imperfect fit between shapes of lamina sequences taken from different regions in that core.

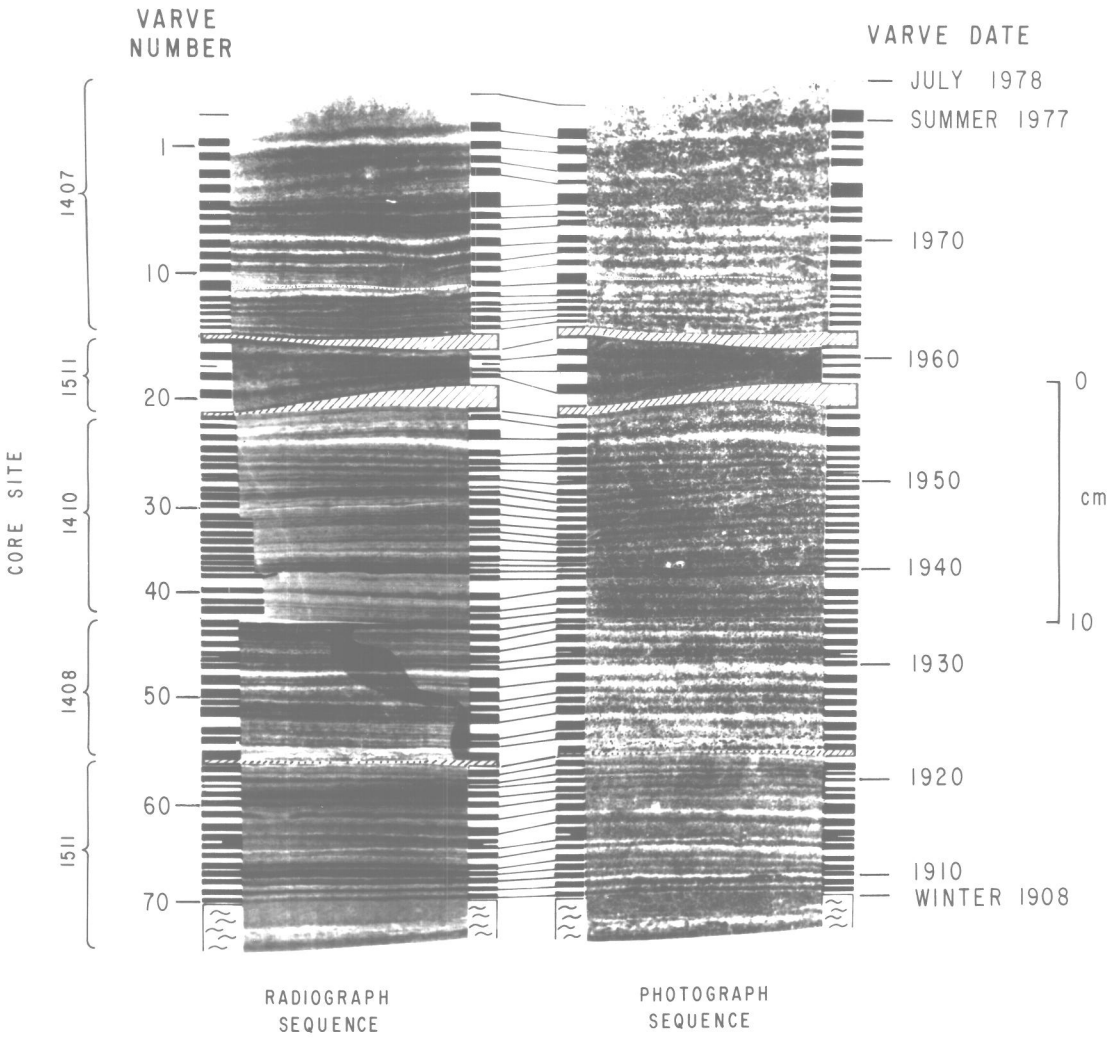
VARVE NUMBER
VARVE DATE
JULY 1978
SUMMER 1977
1970
1960
1950
1940
1930
1920
1910
WINTER 1908
1
10
20
30
40
50
60
70
CORE SITE
1407
1511
1410
1408
1511
0
cm
10
RADIOGRAPH SEQUENCE
PHOTOGRAPH SEQUENCE

Figure III-8

varve number 5. In comparison, the photographs exhibit a much simpler alternating sequence of structurally homogeneous light and dark laminae with greater tonal contrast between the laminae. The sublaminae are only rarely visible as thin separations within the dark layers on the photographs. There is also much more variability in the contrasts between lighter and darker lamina units in the radiographs than in the photographs; that is, adjacent laminae on the radiographs are often marked only by a slight change from a lighter gray to a darker gray.

In order to develop the varve chronostratigraphy, we have assigned seasonal significance only to the structurally homogeneous light and dark laminae defined on the photographs. The thin sublaminae visible on the radiographs are inferred to result from discrete depositional events within a single season. Total seasonal deposition may therefore be represented by a composite of several sublaminae. Interpretation of the laminae stratigraphy within the radiograph sequence is then relatively straightforward. Definition of individual laminae on the radiographs is aided by correlation of short lamina sequences to their equivalent intervals on the photographs where recognition of individual laminae is simplified.

The lower boundary of each dark lamina should reflect the cessation of upwelling and high primary productivity obtained during spring, coinciding with the spring/ summer climatic transition. The lower boundary of a light lamina should likewise correspond to the annual onset of higher productivity which occurs at least as early as January or February.

The horizontal bars to either side of both the radiograph and the photograph columns in Figure III-8 represent our initial interpretation of the seasonal lamina stratigraphy. Where thin light laminae appear in the center of dark laminae on the photograph, as well as in the radiograph, we have drawn a double bar to indicate a more subjective interpretation, where the light internal lamina may or may not represent a season.

Likewise, a dark sublamina is included in the stratigraphy to indicate the possibility that it may represent seasonal deposition (varve number 19). Although it is not visible on the photograph, it shows up clearly on the radiograph.

The chronostratigraphy begins with the bottom-most light lamina immediately overlying the sediment gravity flow, and terminates with the light lamina at the sediment-water interface. There are 68 dark laminae assuming that the three double-dark-laminae noted on Figure III-8 are counted as representing deposition during single seasons. Assuming that the one double-light-lamina noted represents one season, there are 69 light laminae. This interpretation of the varve stratigraphy yields a total count of 68.5 years between the sediment gravity flow and the surface.

The light lamina at the sediment surface corresponds to deposition during the winter and spring prior to collection. The lack of an overlying dark lamina indicates that the summer layer had not yet formed upon the collection date of July 1978. This observation agrees with our concept of varve formation and reinforces our assumption that the date of the sediment-water interface is July 1978, coinciding with the spring/ summer climatic transition. According to our initial interpretation of the varve stratigraphy as representing 68.5 years, the date of the sediment gravity flow would be just prior to the winter-spring season of 1909. Suspecting that the trigger mechanism of the area-wide sediment flow was likely to have been a seismic shock, we examined the historical record of earthquakes located within the region of the Guaymas Basin. Six earthquakes of magnitude six or greater occurred there between 1887 and 1962 (Glover, 1980). The earthquake closest to 1909 occurred during October 1907, and was the largest magnitude (7.5) event recorded, with its epicenter located at 28.0°N, 112.5°W. The next largest magnitude earthquake nearby (7.0) occurred in 1945.

If the date of the sediment flow corresponds to the autumn of 1907, our varve chronology is in error by two years. This suggests that two of the four double-laminae

present in the varve stratigraphy represent two years. Assuming this to be true, we have chosen the two lowermost double-dark-laminae in the section as the most probable source of the presumed chronological error. These are both anomalously thicker than preceeding or following laminae, and the thin interleaved light laminae show up clearly in the photograph as well as in the radiograph. This revision in the varve stratigraphy of Figure III-8 yields an interval of 70.5 years extending from the summer 1978 surface-age, and dates the boundary between the lowermost light lamina and the sediment flow as winter of 1907-1908. The varve numbers and varve dates on Figure III-8 correspond to this interpretation.

^{210}Pb Chronology

The varve chronostratigraphy presented above was developed independently of the ^{210}Pb chronology and is based soley upon the varve counts bracketed by the 1978 surface-age and the 1907 date assumed for the sediment gravity flow. Comparison of the measured excess ^{210}Pb in the subsamples to their stratigraphic position within the varve count, allows us to examine the validity of the chronostratigraphy within the limits of error inherent in ^{210}Pb dating. This is done by first finding the regression equation which gives the best estimate of the ^{210}Pb activity from a level (varve number or position) within the varve sequence. The values for the ^{210}Pb activities obtained from the regression relationship can then be used in the time equation to determine whether the time measured by ^{210}Pb decay corresponds to that measured by the varve count. The range of uncertainty of the ^{210}Pb calculated ages may then also be obtained from the regression of ^{210}Pb against the varve stratigraphy.

Locations of the ^{210}Pb subsamples from all five cores were referenced to the stratigraphy in Figure III-8. Subsamples which could not be referenced to the varve stratigraphy were not included in this comparison. These consist of subsamples taken

from regions in the cores with poor resolution of the lamina structure on the radiographs or those which occur within a discontinuity of the laminae sequences. The remaining 36 ^{210}Pb analyses were distributed throughout the five box cores from above the sediment gravity flow.

Figure III-9 is a plot of the excess ^{210}Pb activities versus their varve positions. The horizontal limits of uncertainty around the points correspond to the stratigraphic thickness of the subsample. The plotted points represent the mid-points between the upper and lower stratigraphic boundaries of each subsample. The vertical limits of uncertainty correspond to the analytical error of the total ^{210}Pb activity plus one standard deviation of the calculated ^{226}Ra equilibrium background value used for the standard correction of the total observed ^{210}Pb activities. The relationship between the log of the excess ^{210}Pb activities and the averaged varve position of the ^{210}Pb subsamples is found by a semi-log linear regression. The regression line is shown on Figure III-9 and corresponds to the equation:

$$\log {}^{210}Pb_{ex(v)} = \log 32.53 - 0.0135\ (v), \qquad (1)$$

where $^{210}Pb_{ex(v)}$ is the predicted value of excess ^{210}Pb at v, and v is a varve number within the sequence 1-70. Relative weights were assigned to the error in observed $^{210}Pb_{ex}$ values so that less significance is given to values with larger error in the regression (Gentleman, 1973). Ninety percent of the variance in the $^{210}Pb_{ex}$ activity is accounted for by its decay relationship to the varve stratigraphy ($R^2 = 0.90$). Deviation of the $^{210}Pb_{ex}$ activities from the regression suggests that the supply of ^{210}Pb to the sediments is not strictly constant. This may occur by normal year-to-year variation in climatic processes which control the amount of ^{210}Pb available for deposition (Krishnaswami and Lal, 1978).

Figure III-9

Excess ^{210}Pb activities measured from all five box cores (note key to symbol patterns) plotted against their position in the master chronostratigraphy of Figure III-8. Horizontal ranges of plotted data points are defined by stratigraphic thickness of subsample. Vertical ranges correspond to one standard deviation of the background value used for correction of the observed ^{210}Pb activities plus the subsample counting error. The line through the data represents the semi-log regression equation (1) given in the text.

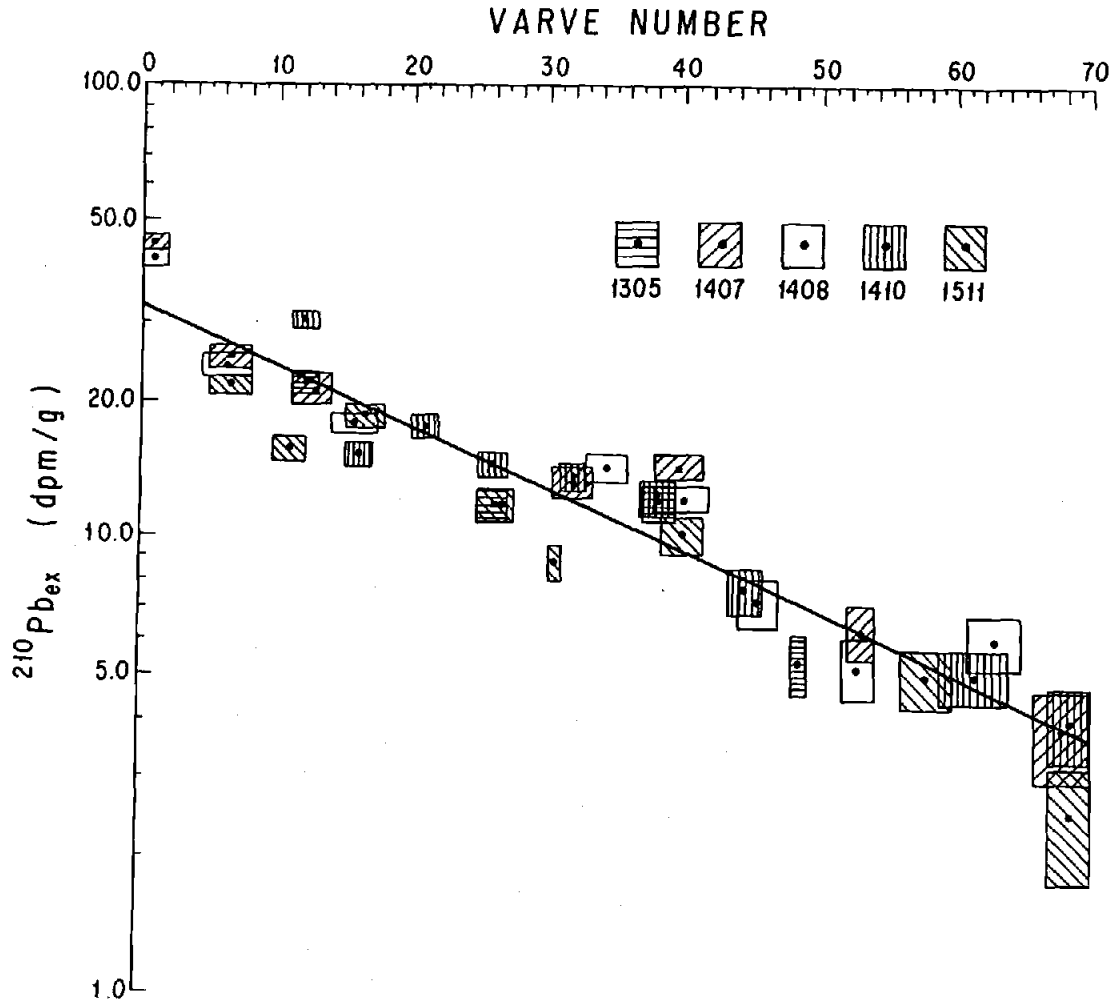
VARVE NUMBER
0
10
20
30
40
50
60
70
100.0
50.0
20.0
10.0
5.0
1.0
$^{210}Pb_{ex}$ (dpm/g)
1305
1407
1408
1410
1511

Figure III-9

Using the parameters from the regression equation (1), we may calculate the predicted age of any varve number in the sequence from the time equation:

$$t_{(v)} = \frac{1}{\lambda} \ln \left[{}^{210}Pb_{ex(v=0)} \Big/ {}^{210}Pb_{ex(v)} \right] , \qquad (2)$$

where $t_{(v)}$ is the age in years of the varve number v, λ is the decay constant of ^{210}Pb, and $^{210}Pb_{ex(v=0)}$ is the zero-age activity at the intercept (32.53 dpm/g). To obtain the ^{210}Pb age of varve number 70, we substitute the $^{210}Pb_{ex(v)}$ activity in the time equation corresponding to varve 70. The predicted $^{210}Pb_{ex}$ activity for varve 70 is found from equation 1 to be 3.68 dpm/g. Using this value in equation 2, the age of varve number 70 is estimated as 70.0 years older than the surface age. The ^{210}Pb age thus agrees to the year with our varve count obtained under the assumption that the sediment gravity flow corresponds to the 1907 earthquake. This perfect concordance should, however, be considered only within the context of the limits of confidence imposed by the uncertainty in the ^{210}Pb dating.

Using the regression statistics, we can estimate the limits of uncertainty associated with the $^{210}Pb_{ex}$ age of the varve number 70. Confidence intervals can be constructed around each predicted $^{210}Pb_{ex}$ value. By finding the maximum error at each end of the regression line (at v = 0 and v = 70), we can estimate the maximum deviation of the relationship from the regression equation for a given probability. The confidence interval (Dixon and Massey, 1969) for a predicted value of $^{210}Pb_{ex}$ is:

$$L_{(v)} = \log {}^{210}Pb_{ex(v)} \pm t_{\alpha/2} \sqrt{S^2_{(v)}} , \qquad (3)$$

where $t_{\alpha/2}$ is the student t statistic for a probability α, and $S^2_{(v)}$ is the variance of the predicted $^{210}Pb_{ex}$ value at varve number v. Variances of the uppermost and lowermost predicted values in the regression (v = 1, v = 69) are both 0.03. Using these values as

estimates of S^2 for v = 70, and assigning a probability of 95% ($\alpha = 0.05$), the confidence intervals for $^{210}Pb_{ex}$ at v = 0 and v = 70 are:

$$L_{(v = 0)} = 32.53 \pm 3.85 ,$$

$$L_{(v = 70)} = 3.68 \pm 0.29 .$$

Substituting the maximum and minimum values for $^{210}Pb_{ex(v=0)}$ and $^{210}Pb_{ex(v=70)}$, respectively, in the time equation (2) yields an age of 76.2 years for varve number 70. Thus the confidence interval for the $^{210}Pb_{ex}$ age of varve number 70 is ± 6 years with an associated probability of $\alpha = .05$ for the occurrence of maximum opposed departures from the regression line at v = 0 and at v = 70.

Our reconstruction of the varve chronostratigraphy from the lamina structure of the five cores is thus strongly supported by the radioisotope chronology presented above. Subsample redundancy over the five core sites provides a large number of degrees of freedom to examine the relationship between the $^{210}Pb_{ex}$ activities and the varve chronostratigraphy. Referencing the $^{210}Pb_{ex}$ analyses to varve position rather than to a depth in the cores enables all subsamples from the five cores to be used collectively for verification of the area-wide chronostratigraphy.

CONTINENTAL DRAINAGE TO THE CENTRAL GULF OF CALIFORNIA

Provenance studies to determine the origin of both sand-sized (van Andel, 1964) and fine-grained sediments (Baba et al., submitted) in the Gulf of California, show that the source for terrigenous material deposited along the eastern margin of the central Gulf is the Sonoran mainland. Sediment dispersion appears to be nearly directly offshore. Mapping of the sediment provinces defined by quartz-feldspar ratios in the silt fraction (Baba et al., submitted) shows that our suite of box cores lies on the border

between material derived from the Yaqui and Mayo drainage basins to the south and material from the Sonora River drainage system to the north.

Figure III-10 shows the extent of the mainland drainage basins with their principal river channels and tributaries which empty into the central Gulf. Our five box core sites along the Guaymas slope are plotted on Figure III-10 to show their positions relative to the river mouths. The locations of all dams built along the stream systems are also shown on Figure III-10. Table III-1 lists the year in which each of the dams began operation as well as the area drained above the dams. All of the major river channels have been dammed. However, the small subsidiary basins of the Bacoachi River and the Cocoraque Arroyo remain undammed. According to the classification used by the Secretaría de Recursos Hidráulicos (1969b), the Bacoachi basin lies within the larger Sonora basin and the Cocoraque basin lies within the Yaqui basin.

Table III-2 compares the mean annual volumes of free discharge available from measurements at key stations within each of the four river basins (stations are shown on Figure III-10). These data were compiled from the Boletin Hidrológico, published by the Secretaría de Recursos Hidráulicos (1969a,b; 1975). The total areas of the drainage basins shown in parenthesis in the Table refer to the areas enclosed by the major drainage divides drawn on Figure III-10.

The Sonora basin is the second largest of the four major basins. Its principal stream system is the Sonora River with an area of 28,880 km^2. The Rodriguez dam, completed in 1947, is located below the gage station which is at El Oregano. The discharge record from 1942 through 1969 shows a mean annual flow of 104 x 10^6 m^3. This value represents free discharge from the 40% of the basin area above El Oregano. The Bacoachi River drains an area 17% the size of the Sonora River system. There is no gage station reported for the Bacoachi River, but its mean annual flow is estimated at

Figure III-10

Map of the four mainland drainage basins showing principal rivers and main tributaries which empty into the central Gulf of California. Borders of the drainage basins are shown by the broken lines. Locations of the gage stations used in this study are labelled and indicated by filled circles. All dams are labelled and indicated by bars across the rivers. The five core sites (see Fig. III-1) are plotted here to show their positions relative to the river mouths. Isobaths show depth in meters.

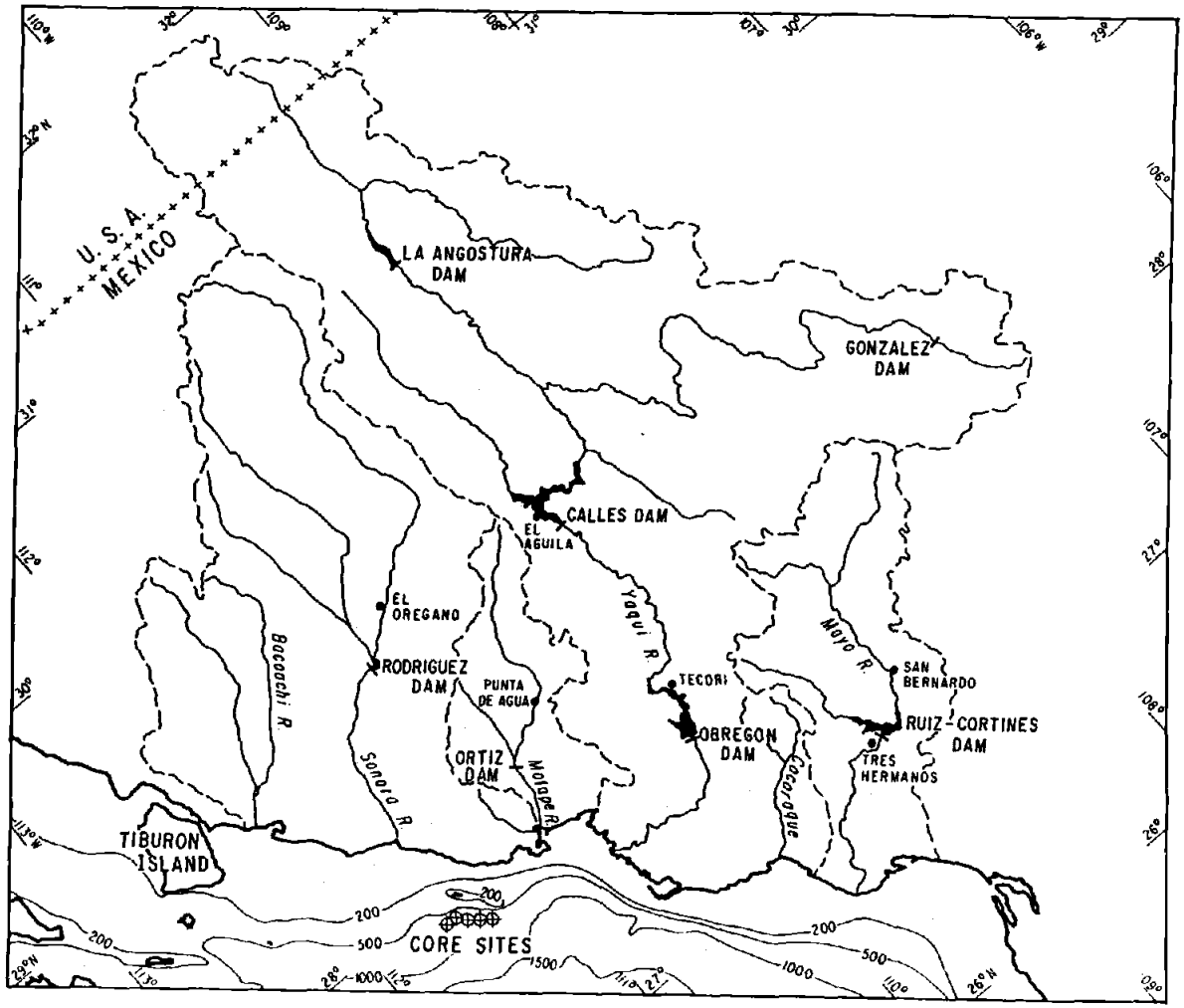

Figure III-10

Table III-1. Years in which dams were completed and began storage of water on the major river systems flowing into the central Gulf of California from the mainland. See Figure III-10 for location of dams.

River System	Name of Dam	Date of Initial Operation	Drainage Area Above Dam (Km^2)
SONORA	Rodriguez	1947	21,035
MATAPE	Ortiz	1956	5,393
	Punta de Agia	1972	3,074
YAQUI	La Angostura	1941	18,305
	Obregon	1952	69,590
	Gonzalez	1961	1,800
	Elias-Calles	1964	57,832
MAYO	Ruiz-Cortines	1955	10,762

38 x 10^6 m^3 (SRH, 1969b). Although there is no major dam on this system, its runoff is diverted for irrigation.

The Matape drainage basin is the smallest of the four shown on Figure III-10. The mean annual value of free discharge from the gage station at Punta de Agua is 35 x 10^6 m^3. This record was taken above the Ortiz dam and represents runoff from approximately 50% of the total drainage area.

The Yaqui basin is the largest of the four drainage systems. Mean annual values of runoff in the main branch of the Yaqui River is shown in Table III-2 from measurements at Tecori and El Aguila for periods prior to and after the construction of upriver dams. Prior to construction of any dams on the Yaqui River, the mean annual flow at Tecori (1929-1940) was 2779 x 10^6 m^3, and represents the runoff from 90% of its drainage area. Construction of the La Angostura dam on one of the tributaries to the main channel had an almost negligible effect on the flow at Tecori. The record at Tecori from 1941 through 1951 shows only a 4% reduction in mean annual flow. The effect of construction of the Gonzalez dam (which controls only 1800 km^2 of drainage) on the El Aguila record appears insignificant from comparison of the 1942-1960 and the 1961-1963 records at El Aguila (less than 1% difference). It is also interesting to note that the flow at Tecori and El Aguila during an equivalent period is virtually the same. The mean annual discharge at Tecori for the period 1942-1951 is 2636 x 10^6 m^3, while that at El Aguila is 2586 x 10^6 m^3, only a 2% difference. Therefore, the runoff at Tecori was derived principally from the precipitation in the mountains above El Aguila. The flow in the undammed Cocoraque arroyo to the south of the main Yaqui channel is insignificant compared to the flow measured at Tecori (a fraction of 1% of the Tecori value).

The Mayo River drainage is the third largest area of the four basins. Before construction of the Ruiz-Cortines dam, the mean annual flow at Tres Hermanos was 853 x

Table III-2. Comparison of the mean annual discharges from the principal streams within the four major drainage basins which empty into the central Gulf of California

Drainage Basin (Total Area in Km^2)	Stream	Station and Period of Observation	Locations and Dates of Upriver Dam Construction	Volume of Mean Annual Discharge (10^6 M^3)	Area Drained Above Station (Km^2)
Sonora (36,989)	Sonora River	El Oregano 1942-1969	No upriver dam	104	11,606
	Bacoachi River	No station on river	No dams on river	38	4,919 (total area of Bac. drainage)
Matape (5,801)	Matape River	Punta de Agua 1958-1969	No upriver dams before 1972	35	3,074
Yaqui (74,562)	Yaqui River	Tecori 1929-1940	No dams on river before 1941	2,779	66,878
		Tecori 1941-1951	La Angostura dam above Tecori since 1941	2,673	48,573 (above Tecori less that above La Angostura dam)
		El Aguila 1942-1960	La Angostura dam above El Aguila since 1941	2,505	39,200 (above El Aguila less that above La Angostura dam)
		El Aguila 1961-1963	Gonzalez dam built above El Aguila in 1961; La Angostura dam above El Aguila since 1941	2,490	37,200 (above El Aguila less that above Gonzalez and La Angostura dams)
	Cocoraque Arroyo	Cocoraque 1975-1978	No dams on arroyo	7	1,208
Mayo (14,534)	Mayo River	Tres Hermanos 1942-1954	No dam on river before 1955	853	11,041
		San Bernardo 1960-1969	No upriver dam	911	7,510

Mean annual discharges were computed for the gage stations and years of record noted in Table. Locations of stations are shown in Figure III-10. Discharge values were taken from stations located above storage dams wherever possible. Mean annual discharge at Tecori on the Yaqui River is given for both pre- and post-damming (La Angostura) period. Likewise, the discharge values at El Aguila on the Yaqui are broken into two periods. Mean annual discharges computed from data in Secretaria de Recursos Hidraulicos (1969a), except for that of Bacoachi River which is taken from estimate given in S.R.H. (1969b).

10^6 m^3. The mean annual runoff at San Bernardo, upriver from the dam (1960-1969), is somewhat higher (911 x 10^6 m^3). The area drained above Tres Hermanos represents 76% of the total basin; the area above San Bernardo, 52% of the basin.

The Yaqui River stands out in Table III-2 by its large volume of runoff reflecting its significantly larger drainage area compared to the other systems. However, differences in mean annual discharge appear related not only to the relative sizes of the drainage areas but also to the increase in aridity to the north. Note that the Mayo River drains only 50% of the area drained by the Sonora River, but the discharge measured at San Bernardo and Tres Hermanos is nearly an order of mangitude greater than that at El Oregano.

The relationships between discharge and quantity of material carried as suspended load is shown in Figure III-11 by plotting the available data for the Sonora, Matape, Yaqui, and Mayo Rivers (SRH, 1969a). Figure III-11 also shows that the relative importance of the rivers, in terms of their characteristic suspended loads, differs from their ranking based on mean annual discharge values. Although the range of discharge of the Sonora River seen in Figure III-11 is an order of magnitude less than that of the Mayo, the quantities of suspended load for both rivers are grouped over nearly an identical range of values. Thus, the Sonora and Mayo Rivers appear to be roughly equivalent when ranked according to their volumes of suspended material. The Yaqui River still stands out by its order of magnitude larger sediment load as a function of the greater volumes of discharge. Of course, these observations were made at stations before or upriver from dam construction which has had a significant effect on the river flow and which also must presently trap most of the sediment load behind the dams.

Figure III-12 shows the effect of damming on the annual cycle of monthly mean discharge values for the Sonora, Yaqui and Mayo Rivers. The Matape River is not

Figure III-11

Plot of the relationships between volume of flow from June through November and the corresponding observed suspended loads on Sonoran rivers. Gage stations (see Fig. III-10 for locations) and years of observations are shown in brackets on the figure. All measurements made either before construction of dams or upstream from the dams so that data reflect conditions of free discharge.

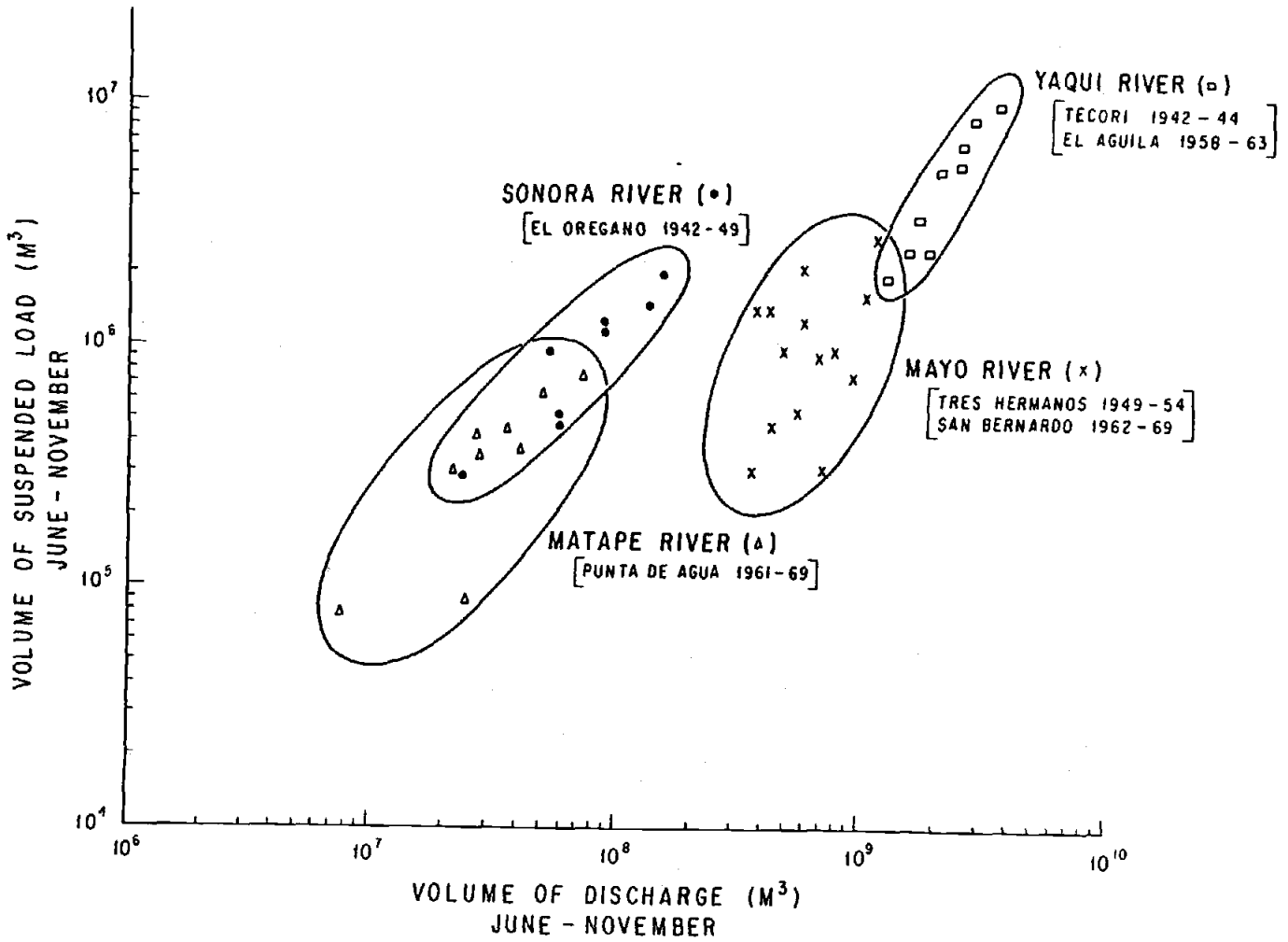

Figure III-11

Figure III-12

Comparison of the annual cycles of mean monthly volumes of flow before, and/or upriver from, dam construction (free flow; left-hand plots) and downriver from dams (controlled release) on the (a) Sonora, (b) Yaqui, and (c) Mayo rivers. Data compiled from years of observation at stations (Fig. III-10) indicated above each plot. The "controlled release" values represent volumes released from the dams to the downstream irrigation channels.

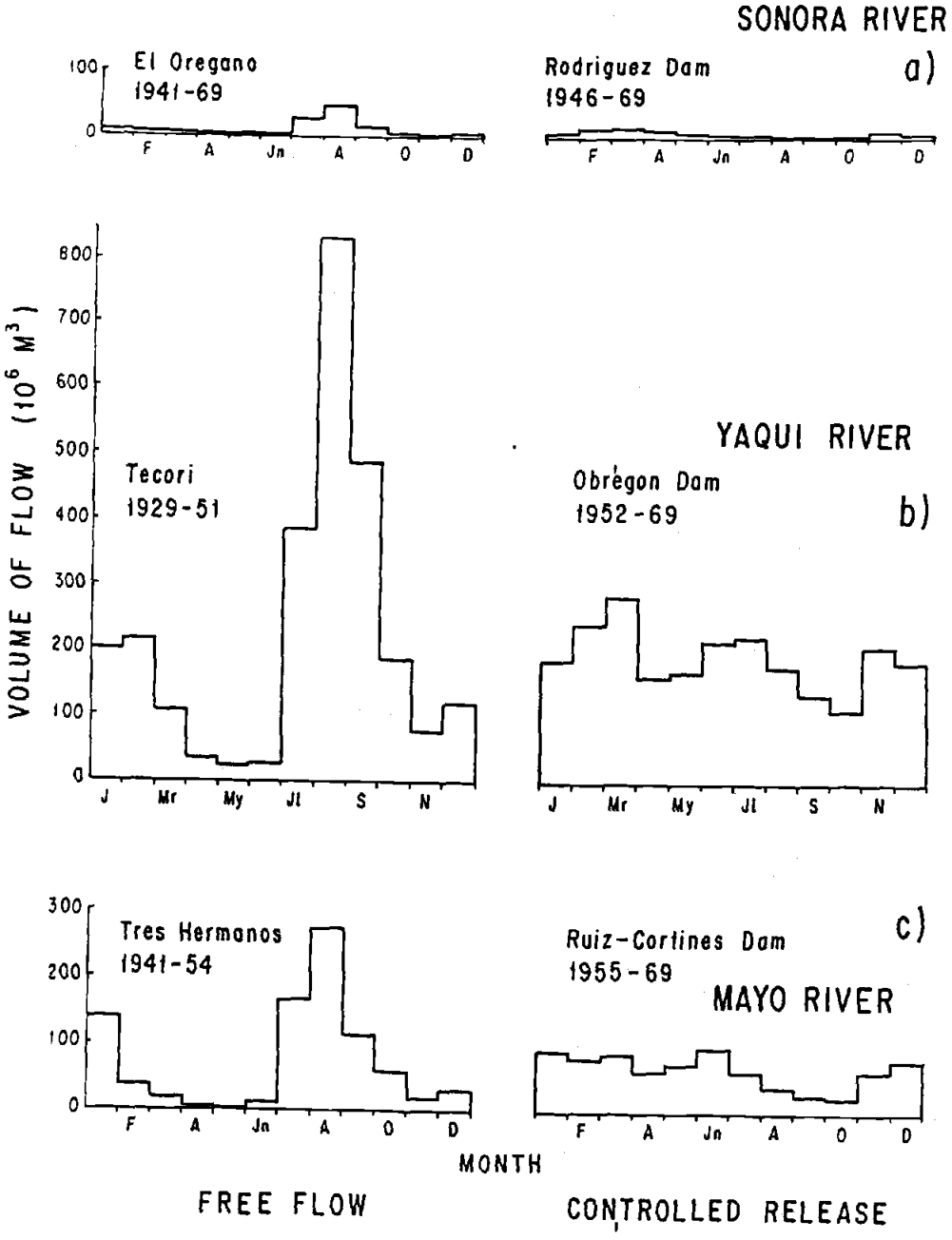

Figure III-12

included here because the data for discharge over the Ortiz dam (operated by a different agency than the SRH) are not included in the Boletin Hydrológico (SRH, 1969a). The annual cycle of free discharge for the Sonora River (Fig. III-12a) was calculated for the 1941-1969) record from El Oregano (above the Rodriguez dam site). The record from Tecori (1929-1951) was used to compile the annual cycle of free discharge on the Yaqui River (Fig. III-12b). Although the upriver dam at La Angostura was built during this period, it did not significantly alter the mean flow at Tecori (Table III-2) or the annual cycle. The free discharge cycle for the Mayo River was compiled from the Tres Hermanos data (1941-1954; Fig. III-12c). The values plotted for the periods after construction of the dams (right side of Fig. III-12a,b,c) represent the mean monthly volumes discharged from the dams to the downstream irrigation channels.

Prior to the completion of the Rodriguez, Obregon and Ruiz-Cortines dams, Figure III-12 shows that each of the three rivers exhibited the marked annual cycle, with peak discharges in August, noted by Calvert (1966b; his Fig. 6). However, the three patterns of monthly mean flow below the dams indicates that the annual runoff cycles have been drastically altered through controlled release of the water stored in the reservoirs behind the dams. This is because, apart from flood control, the major purpose of the dams is to spread the summer discharge peak throughout the year to maximize agricultural benefit from the annual rainfall. The shapes of the annual curves of mean monthly flow have thus been substantially changed while the total volumes of mean annual flow downstream of the dams have not been reduced below 85% of the flow prior to dam construction.

Time series of the annual summer-fall (June through November) runoff data from the Sonora, Yaqui and Mayo Rivers are plotted through 1966 on Figure III-13. This figure shows the differences in pre- and post-damming periods of flow measured from the same stations as shown on Figure III-12, and indicates the substantial reduction of

Figure III-13

Time series of the June through November volumes of flow measured prior to and after dam construction on the (a) Sonora, (b) Yaqui, and (c) Mayo Rivers. Heavy broken lines mark years in which each dam began storage of water. Free flow, prior to dam construction, measured at gage stations which are indicated on the plots. Values of flow during post-damming periods reflects controlled release of water measured at the dams.

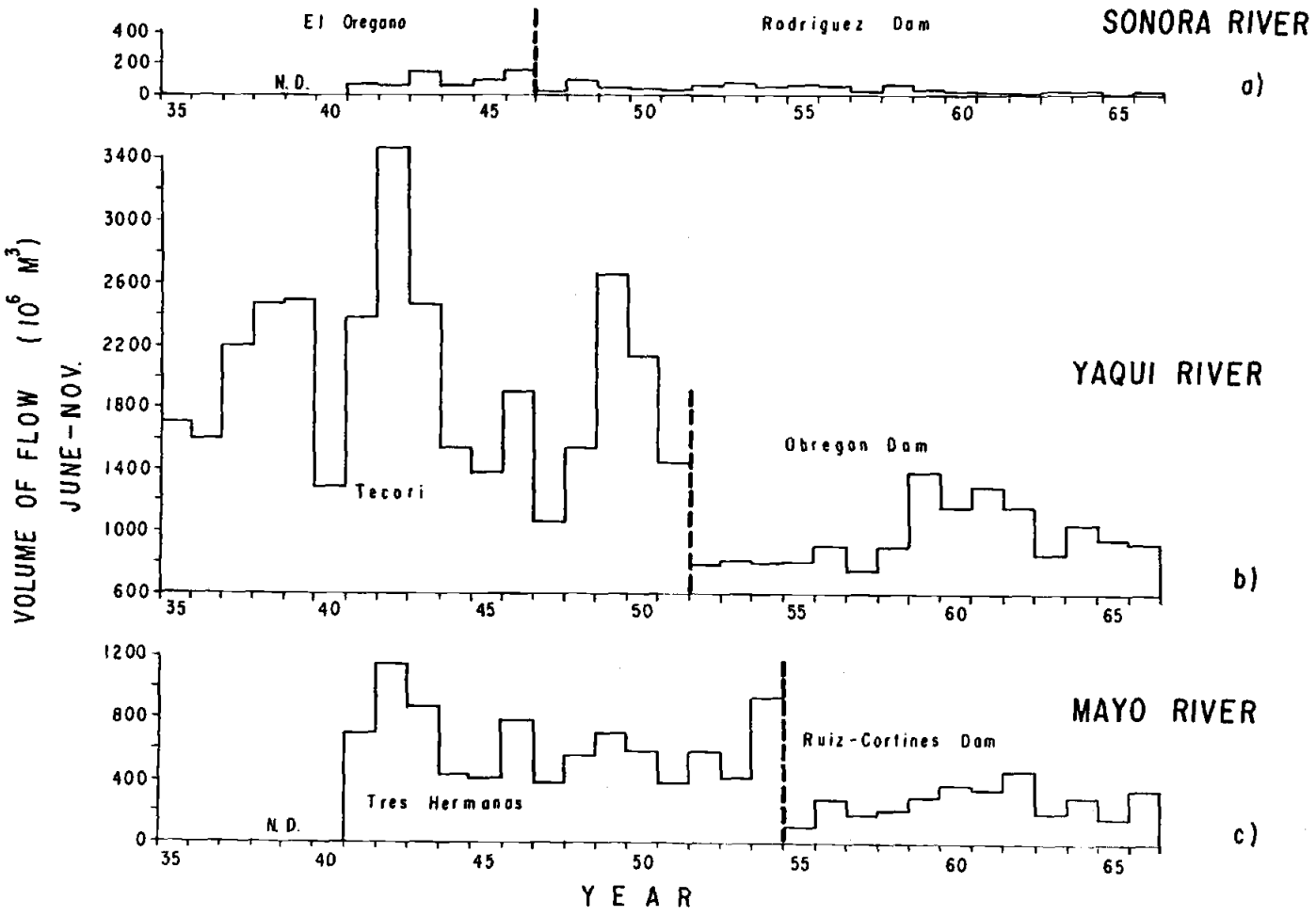

Figure III-13

summer-fall runoff by controlled release of water over the dams. Because much of the water released from the dams is now retained for irrigation, accompanied by substantial loss from infiltration and evapotranspiration, the actual volume of post-damming flow reaching the Gulf must be considerably less than shown on Figure III-13.

Operation of the dams should have therefore changed both the seasonal timing and quantity of sediments delivered to the Gulf by the major river systems. The quantity of suspended material reaching the river mouths must be severely reduced by entrapment behind the dams as well as within the extensive irrigation networks downstream of the dams. Elimination of the summer-fall discharge peak would in turn eliminate the seasonal pulse of terrigenous influx inferred by Calvert (1966b).

DEPOSITION OF DARK LAMINAE AND RIVER DISCHARGE HISTORIES

Despite emplacement of the dams across the major streams flowing to the central Gulf, our reconstruction of the chronostratigraphy (Fig. III-8) shows that varve deposition along the Guaymas slope has continued without interruption. This presents a puzzling contradiction to Calvert's (1966b) hypothesis that fluvial input should control dark laminae formation. In order to examine the relationship between terrigenous deposition along the Guaymas slope and the discharge of Sonoran rivers, we have measured mass accumulation rates from a sequence of dark laminae representing deposition over a period which encompasses both pre- and post-damming conditions of flow in the Sonora, Yaqui and Mayo Rivers.

The mass flux values are compared to the river discharge histories in two ways. First, we neglect the effects of damming and compare the fluxes with available records of continuous free discharge of the rivers during summer and fall, both prior to and after damming. The effects of damming on discharge are eliminated by using station data for periods only in which that station was upriver from a dam or for periods in

which no dam existed. This is done to explore the possibility that even though dam construction has altered the annual runoff cycle, there may exist an association between the offshsore sedimentation and continental drainage that is uninfluenced by impoundment. Secondly, we have compared the mass flux series to the controlled discharge of water over the furthest downstream dams on these three rivers. This allows us to directly evaluate the effects of damming on the varve sedimentation.

The mass accumulation rates were reconstructed from a continuous section of laminae deposition in core 1410 which, according to our chronostratigraphy presented in Figure III-8, corresponds to the years 1934 through 1966. This sequence is the longest continuous section with the most straightforward interpretation of varve stratigraphy found in the five cores from our study area which also brackets the periods of dam construction on the three principal rivers. This section is available from a 3-cm thick interior slab cut perpendicularly to the 1-cm thick outer radiograph slab used for Figure III-7. Although the radiograph slab shows a one-year unconformity near 1960 (Fig. III-7), this discontinuity does not extend into the interior slab.

Figure III-14 compares the year-to-year variation of the total mass flux to the dark laminae in core 1410 with the volumes of free discharge (uncontrolled by damming) for June through November on the three rivers. All values are presented in standard units obtained by subtracting the mean from each series and dividing each observation by the standard deviation of that series. This allows us to visually compare behaviour of the variances among the series without considering the difference in units or the differences in means and standard deviations among the discharge series.

Figure III-14a illustrates the standardized variation of the total "seasonal" mass flux of material obtained from the dark laminae. The mass accumulation values for individual lamina were obtained by gravimetric analysis of the total dry sediment mass, free of salt and oxidizable organic matter, divided by the area of the depositional surface

Figure III-14

Comparison of the time series of standardized values of (a) the total mass flux of material measured from dark laminae of core 1410 with the free (undammed) flow from June through November for the (b) Sonora, (c) Yaqui, and (d) Mayo Rivers. Free flow data obtained from stations upriver from dams and/or prior to dam construction; stations and years of observation shown to the right of plots. Asterisks in (a) mark possible error in chronology of mass flux values; 1940 value may represent "false year". Combining the 1939 and 1940 values into a single value for 1940 yields adjusted chronology for comparison with Yaqui River data (Fig. III-15b, Table III-3). See text for further explanation.

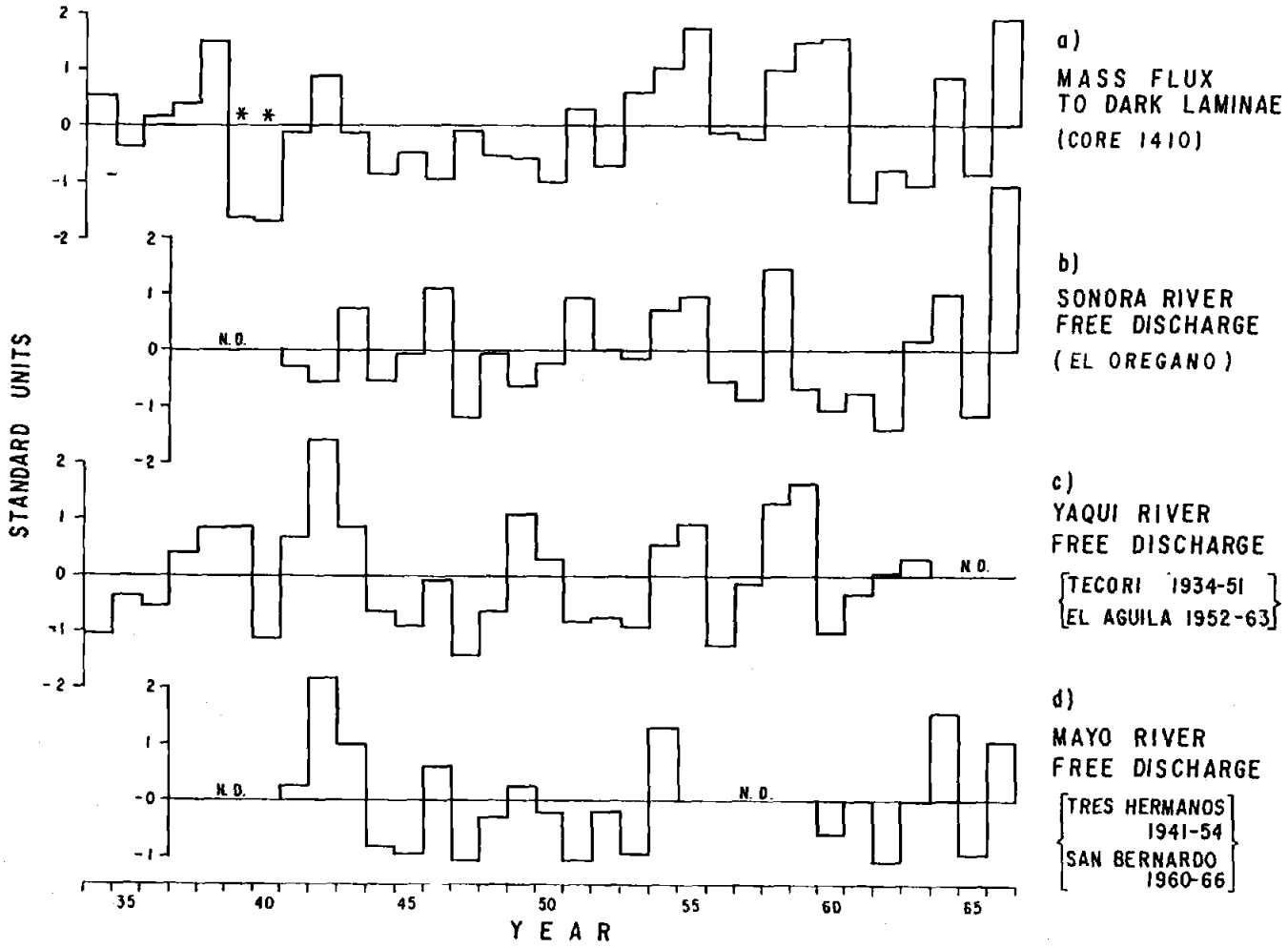

Figure III-14

from which the subsample of dark lamina was taken. Although the total mass reported here includes the biogenic as well as the terrigenous component, separation of the biogenic opal from these samples shows that the proportion of biogenic to terrigenous material does not vary significantly from year to year (Moreno-Hentz, 1982). The mass accumulation over a season of deposition obtained from the dark laminae ranges from 30.4 mg/cm^2 (1966) to 3.5 mg/cm^2 (1940); the mean value of the series is 16.3 mg/cm^2. The mass accumulation values can be converted into flux values by further dividing by the period of accumulation which is considered here to be the six months from June through November. The units of mass accumulation (mg/cm^2) measured for dark laminae can thus be used for rates of accumulation or mass flux if it is understood that the accumulation occurred over a six month time interval.

Measurements of free discharge are continuously available since 1941 for the Sonora River from the station at El Oregano (Table III-1; Fig. III-14b). For the Yaqui River, it is possible to construct a composite series of free discharge from the stations at Tecori and El Aguila (see Table III-2) to obtain a record from 1934 through 1963 (Fig. III-14c). In order to provide a single homogeneous series from these two stations we have standardized each segment independently. The record of free discharge for the Mayo River is taken from the observations at Tres Hermanos made from 1941 through 1954 and at San Bernardo from 1960 through 1966 (Table III-2; Fig. III-14d). Again, data segments from the two different stations were standardized independently.

Figure III-15 shows the standardized mass flux values plotted against standardized values of free discharge of the rivers. Table III-3 summarizes the statistics of the least squares fit obtained by both linear and quadratic regression of mass flux against the discharge values. The coefficients of determination (R^2) given in Table III-3 indicate the proportion of variance in the mass flux series which is associated with that of the corresponding discharge series. The quadratic regressions all yield higher

Figure III-15

Scatter plots of the mass flux of the dark laminae in core 1410 versus the free discharge from June through November for the (a) Sonora, (b) Yaqui, and (c) Mayo Rivers. Note that both mass flux and discharge are plotted as standard units as given on Figure III-14. The curves drawn through the data represent the equations for the quadratic regression fits which are summarized in Table III-3. Relationship shown for Yaqui River based upon adjusted mass flux chronology assuming 1940 value in Figure III-14 to represent "false year".

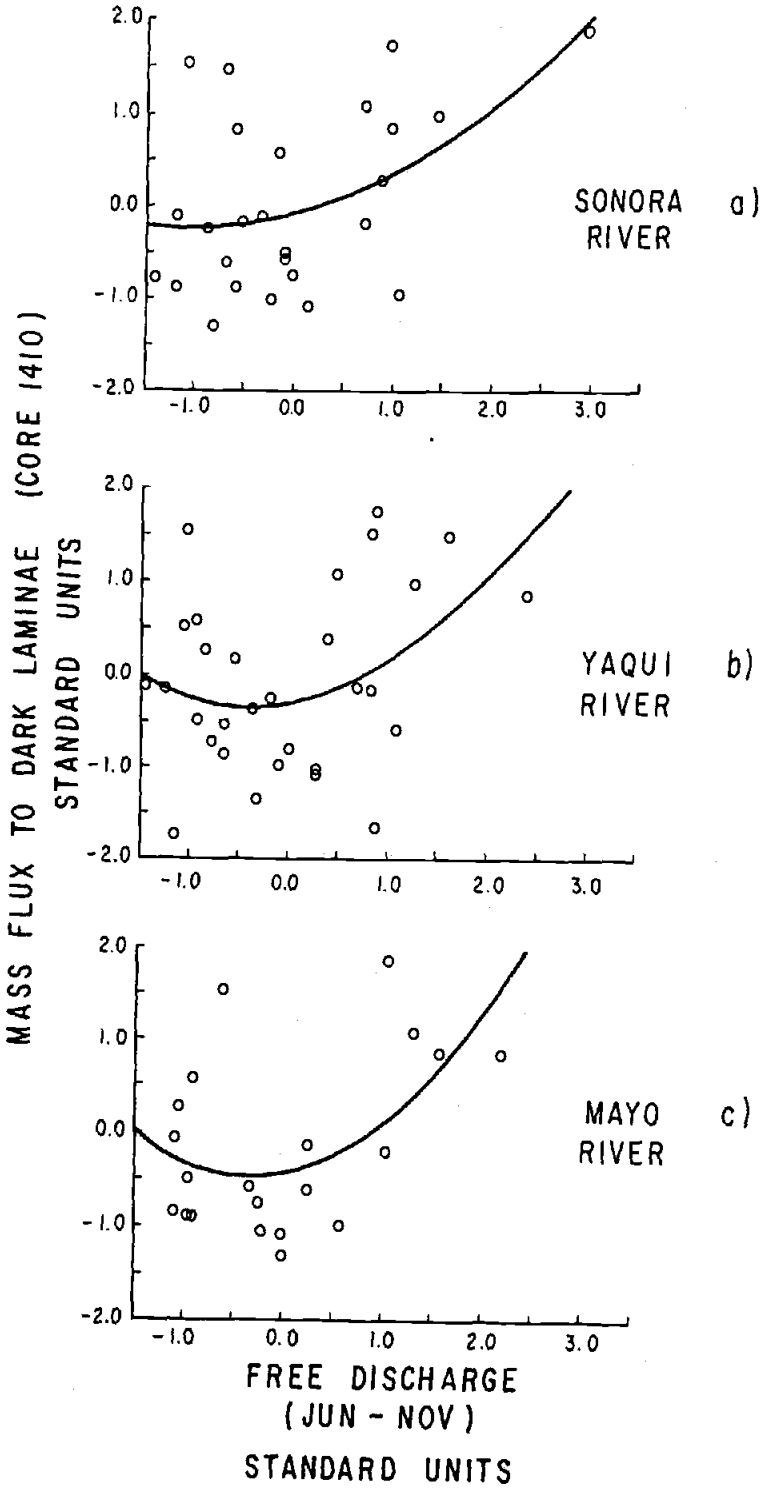

Figure III-15

Table III-3. Results of regression analyses of mass flux measured from dark laminae of core 1410, against the uncontrolled discharges from June-November for the Sonora, Yaqui and Mayo Rivers.

River	Least Squares Fit	
	Linear	Quadratic
SONORA		
El Oregano 1941-1966 N = 26	$R^2 = 0.20$ $\frac{\text{F-test}}{\text{F-tab}} = 1.38$	$R^2 = 0.24$ $\frac{\text{F-test}}{\text{F-tab}} = 1.06$
YAQUI		
Tecori 1934-1951 El Aguila 1952-1963 N = 30	$R^2 = 0.10$ $\frac{\text{F-test}}{\text{F-tab}} = 0.70$	$R^2 = 0.16$ $\frac{\text{F-test}}{\text{F-tab}} = 0.87$
* Tecori 1935-1951 El Aguila 1952-1963 N = 29	$R^2 = 0.14$ $\frac{\text{F-test}}{\text{F-tab}} = 1.08$	$R^2 = 0.21$ $\frac{\text{F-test}}{\text{F-tab}} = 1.06$
MAYO		
Tres Hermanos 1941-1954 San Bernardo 1960-1966 N = 21	$R^2 = 0.18$ $\frac{\text{F-test}}{\text{F-tab}} = 0.92$	$R^2 = 0.28$ $\frac{\text{F-test}}{\text{F-tab}} = 0.98$

Uncontrolled discharge values were obtained from the June-November volumes of flow at stations upriver from dams and/or prior to damming. Significance of the regression fits estimated by the ratio of the F-test statistic to the critical F-value taken from table based upon a 95% level of probability. The F-test assumes that observtions in each of the series are independent from one another. Note that the set of results marked by an asterisk for the Yaqui River refers to analysis made with adjusted mass flux chronology: flux value for 1940 assumed to represent "false year".

coefficients of determination because of the greater flexibility of the curvilinear fits. Although not shown on Table III-3, we also calculated the fit of mass flux to uncontrolled discharges using an exponential model. The levels of variance accounted for by the exponential fits are similar to those of the linear models, yielding lower R^2 values than the quadratic fits. The quadratic curves are drawn through each of the plots on Figure III-15.

The significance of the regression fits is estimated in Table III-3 by comparing the resulting F-test statistic (Davis, 1973; Chap. 3 and 5) with the tabulated critical values of F, presented as the ratio of "F-test" to "F-tab". A value of 1.00 or greater for this ratio indicates a significant regression with an associated probability of 95%. This level of probability assumes the observations within each series to be independent of one another. This is not strictly true for either the mass flux or the discharge series which all exhibit some degree of autocorrelation. Therefore, our F-test does not provide a strict verification of significance with 95% probability, but it still is a useful measure for judging the relative quality of the regression fits. Moreover, a clear lack of significance allows us to conclude that no relationship exists between the two variables compared.

The quadratic fit of mass flux to the free discharge of the Sonora River at El Oregano (Table III-3; Fig. III-15a) accounts for 24% of the variance in the mass flux series. Although Figure III-15a shows a large scatter of the data points, the F-test statistic for the quadratic fit is slightly higher than the critical F-value (F-test/F-tab = 1.06). Thus we cannot disregard the relationship as statistically insignificant. The R^2 value for the linear fit is slightly lower than that of the quadratic fit, but the F-test indicates a somewhat greater significance.

Both the linear and quadratic fits of mass flux to the free discharge of the Yaqui River (the upper set of R^2 values given for the Yaqui River in Table III-3) are consider-

ably lower than those for the Sonora River. The quadratic fit shown on Figure III-15b accounts for 16% of the variance in the mass flux series. In addition, these fits are not significant according to the F-test. It is interesting to note however, that if we consider the thin dark lamina of 1940 (see chronostratigraphy, Fig. III-8) and the dark lamina of 1939 to be two sublaminae of 1940, the fit of the mass flux series to the uncontrolled discharge in the Yaqui River is substantially improved (lower set of R^2 values given for the Yaqui River in Table III-3). The F-test statistics of the linear and quadratic fits using this adjusted chronology in mass flux, are also both greater than their critical values. The unusually low value of the 1939 mass flux followed by the similarly low value for 1940 (marked by asterisks on Fig. III-14a), combined with the resulting improvement in the fit to the Yaqui discharge data argues for a possible revision in the varve chronostratigraphy below 1940. This interpretation suggests that the thin dark laminae representing summer-fall of 1940 and the subjacent light lamina of 1939, as shown on the chronostratigraphy (Fig. III-8), actually represent a "false year" resulting from "non-seasonal" deposition of the intercalated light lamina. Assuming this interpretation to be true, the total mass flux of 1940 would be equivalent to that of the two dark laminae originally assigned to 1939 and 1940 (as shown in Fig. III-14a), plus the interlayered light laminae. The resulting quadratic fit explains 21% (as opposed to 16%) of the variance in the mass flux values, giving the mass flux relationship with the free Yaqui discharge a similar level of significance to that observed for the free discharge on the Sonora River.

The linear fit of mass flux to the free discharge of the Mayo River ($R^2 = 0.18$, Table III-3) is not significant according to the F-test. However, the quadratic fit (see Fig. III-15c, Table III-3) yields a relatively high coefficient of determination ($R^2 = 0.28$) with an associated F-test statistic which is very close to the critical value (F-test/F-tab = 0.98).

The regressions of mass flux against free discharge show consistent results for all three rivers. The three comparisons yield quadratic fits of similar quality each accounting for moderate quantities of variance in the mass flux series (given the adjusted mass flux chronology below 1940 for better alignment to the Yaqui data). The quadratic fits are thus somewhat much better than what we would expect for the lack of any relationship between mass flux and free discharge. Most importantly, the comparisons of mass flux to free discharge do not contradict Calvert's (1966b) hypothesis.

Comparison of the mass flux values from core 1410 to the summer-fall controlled discharges of these three rivers (downriver from the dams) shows markedly different results from those which are obtained by comparison to the free discharges. Figure III-16 displays scatter plots of mass flux against the flow of water released from the Rodríguez (Sonora River), Obregon (Yaqui River), and Ruiz-Cortines (Mayo River) dams. The linear and quadratic regressions of mass flux against controlled flow down the three rivers (Table III-4) all yield coefficients of determination of zero or near zero except for the quadratic fit with the Sonora River series. The R^2 value for this quadratic fit reaches 0.17. However, the value of the F-test statistic is much less than the critical value (F-test/ F-tab = 0.48) and does not approach the level of significance of the fits to the free discharge data seen in Table III-3). The quadratic fit to the Sonora River data is also inverted with respect to the free discharge models on Figure III-15.

Based upon these results, we conclude that the variance in the mass flux series is not significantly related to the controlled release of water during summer and fall for any of the three rivers after damming occurred. These results do contradict Calvert's (1966b) hypothesis which calls for the accumulation of dark laminae to be determined by the summer-fall injection of terrigenous material from these rivers.

Figure III-16

Scatter plots of the mass flux of the dark laminae in core 1410 against controlled discharge (released over dams) for the June through November periods on the (a) Sonora, (b) Yaqui, and (c) Mayo Rivers. Note that data are plotted in standard units. Summaries of regression analyses are given in Table III-4.

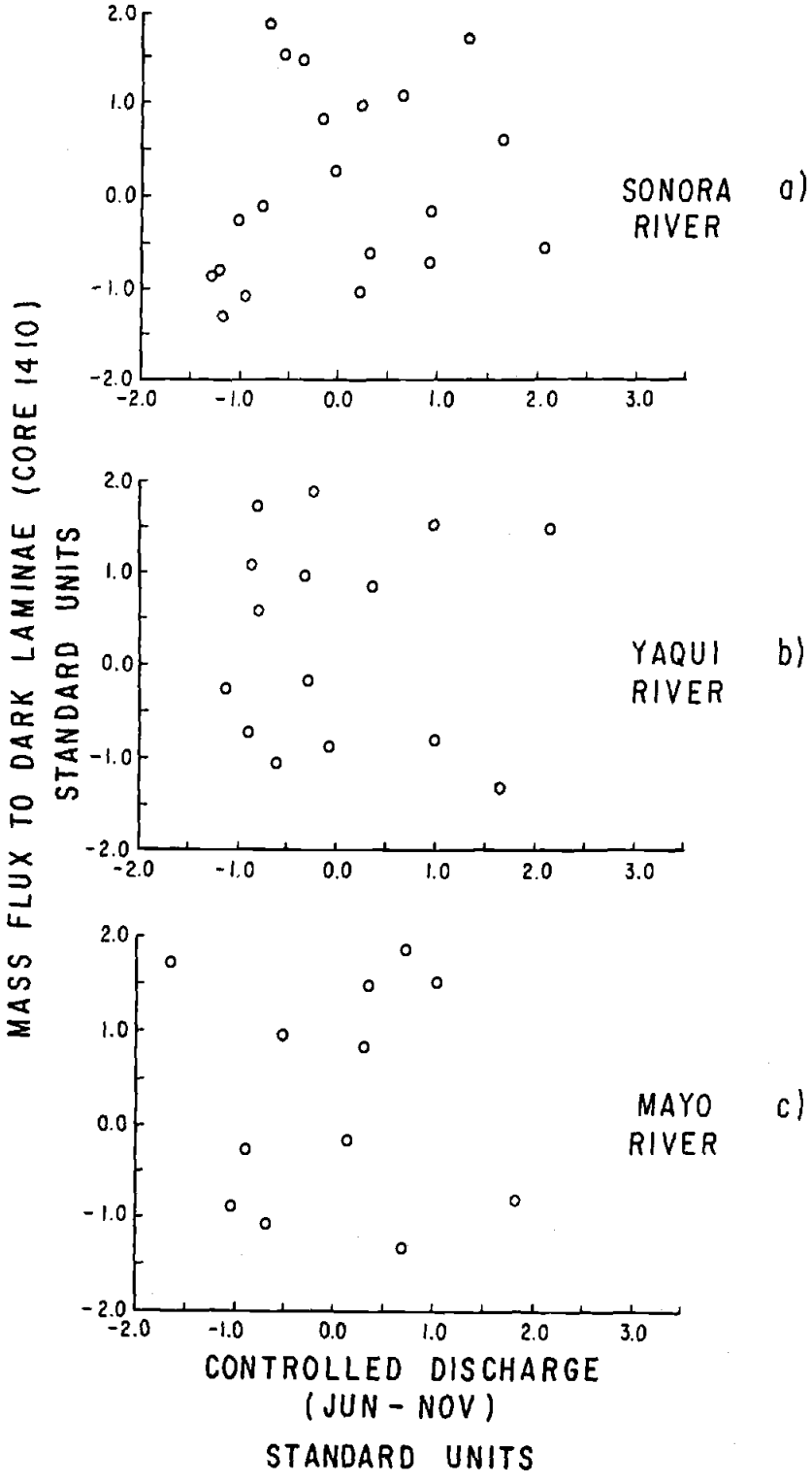

Figure III-16

Table III-4. Results of regression analyses of mass flux, measured from dark laminae of core 1410, against the controlled discharge of water from June-November for the Sonora, Yaqui and Mayo Rivers.

River	Least Squares Fit	
	Linear	Quadratic
SONORA		
Rodríguez Dam 1947-1966 N = 20	$R^2 = 0.04$ $\frac{\text{F-test}}{\text{F-tab}} = 0.16$	$R^2 = 0.17$ $\frac{\text{F-test}}{\text{F-tab}} = 0.48$
YAQUI		
Obregon Dam 1952-1966 N = 15	$R^2 = 0.00$ $\frac{\text{F-test}}{\text{F-tab}} = 0.00$	$R^2 = 0.01$ $\frac{\text{F-test}}{\text{F-tab}} = 0.00$
MAYO		
Ruiz-Cortines Dam 1955-1966 N = 12	$R^2 = 0.00$ $\frac{\text{F-test}}{\text{F-tab}} = 0.00$	$R^2 = 0.02$ $\frac{\text{F-test}}{\text{F-tab}} = 0.00$

Values for controlled discharge of rivers below dams obtained from volumes of water released from dams during June-November periods. Estimation of significance shown by F-test, same as in Table III-3.

The apparent association between deposition of dark laminae and the uncontrolled river discharge, compared to the lack of such an association with the controlled discharge below the dams, gives rise to an interesting paradox. Its resolution calls for a reconsideration of the origin of the dark laminae. The association between the free discharge above the dams and mass flux to the dark laminae must indicate something other than direct control over deposition by river runoff. It is likely that the variance in mass flux and free discharge are therefore associated by their independent responses to a third process or set of controlling variables. In the following section, we examine the possible role of eolian transport for delivery of terrigenous material to the central Gulf. This is used as a basis to formulate what we believe is a reasonable alternative to the control of dark laminae formation by the input of terrigenous material from fluvial sources.

AN ALTERNATIVE PROPOSAL FOR THE ORIGIN OF DARK LAMINAE OF THE CENTRAL GULF

Dust storms which can transport material for hundreds to thousands of kilometers are common in arid and semi-arid regions. Although the Sonoran desert is known to be a source area for eolian dust (Greeley and Iversen, 1985), transport through the atmosphere has not been heretofore considered as an important process for the deposition of terrigenous material in the Gulf of California. This may be, in part, because of the lack of information on dust storms in Sonora. However, the climatology, characteristics and effects of similar dust storms in southern Arizona, lying within the northern reaches of the Sonoran desert, have been documented by Péwé et al. (1981) and Brazel and Hsu (1981).

The major dust storms in central and southern Arizona occur during the summer months of July through September and are closely related to the climatology of the con-

vective storms and summer rainfall over Sonora and Arizona. Hales (1974) has shown that the source for the summer moisture is the eastern tropical Pacific. This moisture is transported up the Gulf of California by low-level southerly winds. Figure III-17 shows the distribution of annual rainfall over Sonora taken from the Climate Diagnostic Charts for Sonora of the Dirección General de Geografía y Meteorología of the Secretaría de Agricultura y Ganadería. This annual pattern closely resembles the summer distribution shown in Hales (1974). A band of high rainfall stretches along the western foothills of the Sierra Madre Occidental mountain range. Note that the 1000 m contour of elevation has been sketched on Figure III-17 to indicate the western margin of the Sierra Madre range. The location of this rainfall axis indicates the orographic control exerted by upslope lifting of air columns producing convective instability along the western slopes of the Sierra Madre. Strong afternoon solar heating along the western slopes produces additional instability resulting in thunderstorm activity if moisture is available.

According to Péwé et al. (1981), the major dust storms in central Arizona are a result of the large thunderstorms which form over the mountains in Sonora and over the Mogollon Rim north of Phoenix. Approximately 35% of the storms recorded in Phoenix appear to originate over Sonora. Low level steering of these storms is controlled by flow of air towards the surface thermal low normally located over southeastern California and western Arizona (Hales, 1972; Brazel and Hsu, 1981) at the head of the Gulf of California. The higher level circulation around 700 mb (approximately 3 km) is dominated by a large high-pressure ridge over the southwestern United States and northern Mexico with flow over Sonora from the east and southeast. The characteristics and intensity of these storms are comparable to the great dust storms over northern Africa which form in the down-drafts at the forward edge of cumulonimbus

Figure III-17

Distribution of mean annual rainfall over Sonora shown by isohyets with 150 mm intervals. Unbroken hachured line is the 1000 m contour of elevation marking the slope along western margin of the Sierra Madre mountain range. The heavy broken lines indicate borders of the continental drainage basins seen in Figure III-10. Bathymetry and box core sites shown as in Figure III-10. Rainfall distribution taken from Climate Diagnostic Charts for Sonora of the Dirección General de Geografía y Meteorología of the Secretaría de Agricultura y Ganadería.

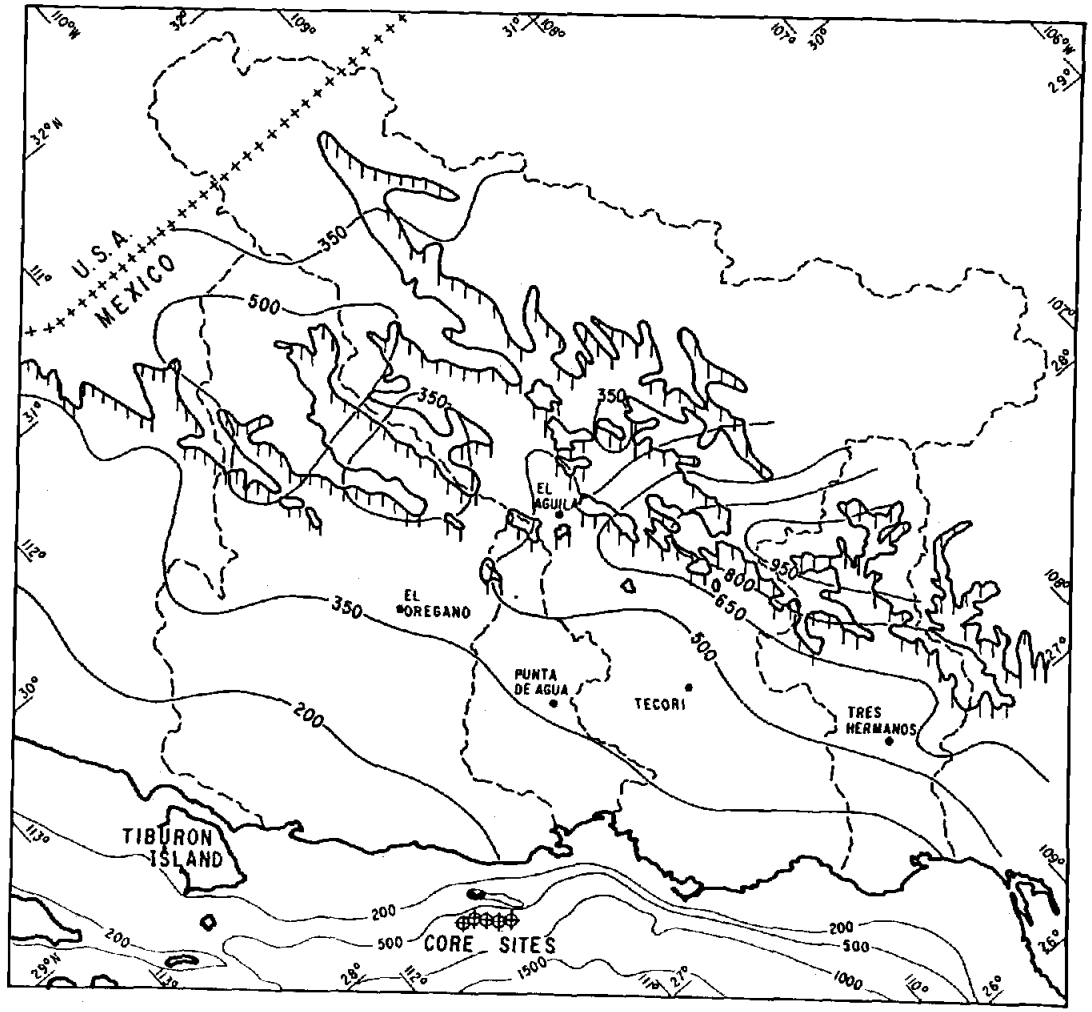

Figure III-17

clouds. Loess-size dust particles in the range of 5-50 μm are commonly lifted to heights of between 1 to 3 km.

Figure III-18 shows the results of measurements of the accumulation of dust near Phoenix, Arizona made by Péwé et al. (1981) from April 1972 through July 1973. The total annual mass flux from the beginning of July 1972 to July 1973, is 5.4 mg/cm^2-yr. Figure III-18 displays a marked annual cycle in the dust deposition with a summer peak similar to those seen in the mean annual river discharge curves prior to damming presented in Figure III-12. Although only one year of observations are available to define the quantity of dust deposition over an annual cycle, the pattern of peak dust fall in summer (seen in Fig. III-18) is inferred to occur over all years. Brazel and Hsu (1981) note that the major dust storms occurring over central Arizona are all confined to the summer months.

The occurrence of increased dust generation during the season of highest rainfall may at first seem counterintuitive because of the expected greater resistance to dust removal from a damp surface. Assuming that precipitation greater than 6.4 mm is necessary to suppress dust removal, Brazel and Hsu (1981) show from precipitation records in central Arizona that there are few days during summer in which the soil would be moist enough to inhibit pick-up of dust. Examination of the daily record for the year 1980 (during which summer precipitation was 25% above the mean) at the site of the Obregon dam (Fig. III-10) shows that the average period, during summer between events with rainfall greater than 6 mm is six days. Brazel and Hsu's (1981) conclusion that rain from one storm does not usually prevent dust generation by the following storm, appears to be valid also for Sonora.

Prospero (1981, his Fig. 10) presents world charts of the frequency of haze at sea by season from data compiled by McDonald (1938). This is cited as indirect

Figure III-18

Time series of the mass flux of airborne dust deposition measured near Phoenix, Arizona during 1972 and 1973 (taken from Péwé et al., 1981). Vertical arrows mark periods of one day accumulation measured after dust storms. All other values correspond to averages over periods from 25 to 56 days.

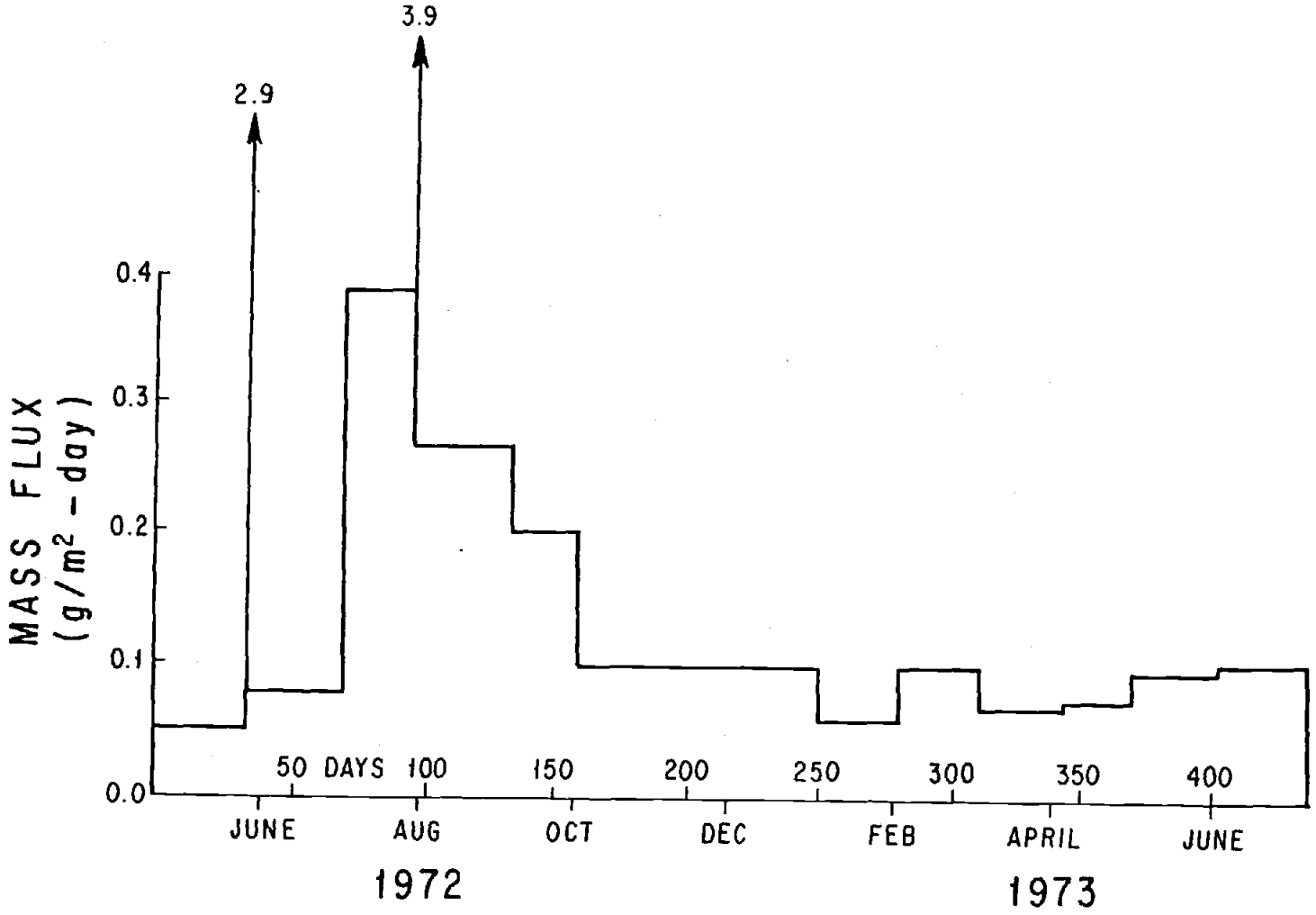

Figure III-18

evidence for the atmospheric transport of dust from continental sources. Off western North America, the highest frequency of haze is shown off Baja California during the months of June through August. The frequency contours bend across the southern portion of the peninsula of Baja California extending across the Gulf of California, and show an increase in haze during the summer over the central Gulf. In addition, a distinct southwest-trending lobe of high quartz concentration in the sediments of the Pacific off Baja California (Moore and Heath, 1978; Leinen et al., 1986) indicates a path of transport of eolian material away from the continent. Although sources in Baja California may contribute to the observed haze and quartz distribution, it seems probable that high level transport of dust aerosol from the Sonoran desert plays a major role in determining these patterns.

In order to compare the dust accumulation at Phoenix with mass flux to the dark laminae measured from core 1410 (Fig. III-14a), we have estimated the mass of dust deposited over Phoenix from the beginning of June through November 1972, from Figure III-18. This value is 3.8 mg/cm^2. We have used the June-November period as representative of the summer-fall season of dark lamina formation in the central gulf. The average of total mass flux measured from the dark laminae deposited between 1935 and 1966 is 17.1 mg/cm^2 per depositional season (using the adjusted mass flux chronology) with a standard deviation of 6.9 mg/cm^2-season. According to estimates by Moreno-Hentz (1982), the average flux of biogenic material to the dark laminae is at least 40% of the total. This means that the average value of terrigenous mass flux to the dark laminae over our period of sampling is approximately 10 mg/cm^2-season. A minimum value represented by one standard deviation below the mean is approximately 3 mg/cm^2-season.

The June-November dust accumulation over Phoenix during 1972 is thus 38% of the estimated average and 127% of the minimum summer-fall mass flux of terrigenous

material observed for the Guaymas slope. Péwé et al. (1981) suggest that the annual value of 5.4 mg/cm^2-yr for the 1972-1973 measurements is probably below average due to higher than normal precipitation at Phoenix and the lower than average number of dust storms. Their comparison to annual values from the Israeli desert (5.0 to 20.0 mg/cm^2-yr; Yaalon and Ganor, 1975) implies that the mean annual accumulation in Arizona may be substantially higher.

Mass flux of terrigenous material to dark laminae along the Guaymas slope thus appears to be comparable to the quantity of dust deposited by eolian processes in central Arizona. Because similar processes are active over the desert in Sonora, originating along the western slopes of the Sierra Madre mountains, we infer that a similar quantity of eolian dust is produced there and lifted to sufficient heights so that it is ultimately reaches the central Gulf of California. Moreover, the marked seasonal peak in dust deposition satisfies the condition of seasonality in the accumulation of terrigenous material in the varves of the central Gulf originally suggested by Calvert (1966b).

The foregoing arguments are presented to support the proposal that a significant, if not principal, pathway for delivery of terrigenous material to the central Gulf is the fallout of airborne dust. Eolian transport provides an alternative mechanism to the seasonal injection of terrigenous clays and silts from river discharge. Transport through the atmosphere may thus "short circuit" the fluvial drainage systems and explain the uninterrupted accumulation of the terrigenous-rich dark laminae despite the damming of the principal river systems which were inferred to be the source of this material by Calvert (1966b). This would also appear to account for the association between mass flux to the dark laminae and the uncontrolled discharge of rivers (Fig. III-15) which reflects the collection of rainfall and hence the storms over the western slopes of the Sierra Madre.

Although we believe that the circumstantial evidence presented above is strong enough to argue for an important role by eolian transport, it does not exclude the possibility that other processes may also contribute significantly to the sediment budget of dark laminae deposition. One of the possible candidates is resuspension of material on the shelf by currents associated with the propagation of coastal trapped waves generated by tropical storms off central and southern Mexico during summer and fall. These are long internal waves with periods of between 10 and 20 days which have recently been found to propagate into the Gulf and dissipate there (Christensen et al., 1983). Enfield and Allen (1983) have modelled the alongshore velocity fluctuations which should be associated with these waves. Their results suggest that current speeds of 15-20 cm/sec, associated with the passage of these waves, may occur at mid-shelf depths near Guaymas. A preliminary data report by Merrifield et al. (1986) clearly indicates the passage of the waves in the temperature field over the Guaymas shelf during summer and fall of 1984. The seasonality of these events and their potential for generating currents which are capable of resuspending recently deposited fine-grained material over the mid-shelf, suggest that they may play a role in summer-fall sedimentation over the slope.

An interesting question which remains concerns the fate of the sediment load carried by the major rivers prior to their damming. If accumulation of terrigenous detritus in the dark layers has not been significantly altered by damming the rivers, we assume that prior to damming, most of the riverborne sediment must have been trapped and stored on the alluvial plains, deltas, in coastal lagoons, and on the continental shelf. Drake et al. (1972) have shown that for record flood discharges from rivers emptying onto the Santa Barbara-Oxnard shelf off southern California, even the finest sediment was rapidly deposited over the inner and middle shelf. Initial distribution as well as resuspension and redistribution of silt and clay-sized particles were controlled by wave

associated currents. Drake et al. (1985) also show that silt and clays are stored at least for one season in the mid-shelf region of the San Pedro margin off southern California. Transfer of this material to deeper water occurs during winter storms. The shelf areas off southern California differ from the Gulf of California by their exposure to open ocean swell produced by the North Pacific storms. Trapping of material on the shelves within the central Gulf of California may be more effective because of the absence of such long-period, high-amplitude winter swell. However, the possible resuspension during summer and fall by currents generated from the coastal trapped internal waves mentioned above, does not allow us to discard the possibility that some of this material escapes over the shelf break.

Finally, it is important to remember that the influx of material to the Gulf by eolian transport should diminish along the gradient of decreasing aridity. South of the Mayo River, the narrowing coastal plain of Sinaloa is increasingly covered with tropical vegetation. Removal of the soil by wind must therefore be increasingly inhibited by vegetation as well as by higher rainfall amounts and frequency of occurrence. Our proposal for a significant contribution to the terrigenous budget of the varved sediments by atmospheric transport is therefore confined to the region of the central Gulf of California.

SUMMARY

Construction of dams across the principal Sonoran Rivers provides a large-scale experiment with which to test the hypothesis proposed by Calvert (1966b) that the formation of dark laminae of the varved sediments in the central Gulf of California is a response to an annual cycle of terrigenous input by fluvial discharge from the mainland. Reconstruction of a 70-year varve chronology beginning in 1908 allows us to compare available records of river runoff, both prior to and after damming, to a series of mass accumulation measurements obtained from the dark laminae.

Although small-scale, downslope mass movement of the sediment has produced repeated short breaks in the varve records at individual core sites, we have succeeded in reassembling a continuous varve chronostratigraphy from five closely spaced box cores collected along the anaerobic continental slope off Guaymas, Sonora. The varve chronostratigraphy is corroborated by ^{210}Pb dating of all five cores. The observed lateral continuity of individual lamina traced among core sites demonstrates that the depositional processes along the slope act uniformly over a distance of nearly 20 km and presumably for a considerably greater distance.

Existence of the coherent, area-wide varve sequence suggests that the presence of the dams, whose construction was begun in the 1940's, has not interfered with the deposition of dark laminae. The annual deposition of light and dark laminae appears to have continued unabated, despite the effects of damming which have effectively eliminated the summer peak of river runoff below the dams. Comparison of mass flux values, measured from the dark laminae, with the controlled discharges of the Sonora, Yaqui and Mayo Rivers after dam construction, shows that there is no relationship between deposition of the dark laminae and river flow below the dams during the summer-fall season of increased rainfall and river runoff.

Although we find no relationship between deposition of the dark laminae and the controlled release of water from the major dams, a weak association does appear to exist between the series of uncontrolled discharge of the rivers during summer-fall and the mass flux to the dark laminae. The uncontrolled river discharge values were taken from stations upriver from the dams and/or for periods prior to dam construction. This apparent contradiction has lead us to propose eolian transport as an alternative mechanism to fluvial discharge as a principal process and pathway for transport of terrigenous material from Sonora to the central Gulf. Our proposal is based upon an inferred annual cycle of eolian transport and deposition of terrigenous silts and clays over the central Gulf of California. This inferrence is made from studies of the deposition of desert dust over south central Arizona.

The annual cycle in the deposition of airborne dust in Arizona exhibits a sharp peak in summer due to the increase in convective thunderstorm activity over Sonora and Arizona. This satisfies the necessary first condition that an annual peak of increased terrigenous input occur during the summer season to produce the dark laminae. The timing of peak terrigenous input must be offset from the annual winter-spring period of increased upwelling and phytoplankton production along the Sonoran coast which is responsible for the formation of the light, diatom-rich laminae. The close link between the climatology of dust deposition and the summer thunderstorm activity and rainfall over Sonora may also explain the weak association found between mass flux to the dark laminae along the Guaymas slope and the free discharge values of the Sonoran rivers.

The second condition which must be met is the agreement between the quantitative mass flux observed from the dark laminae of the varves and the seasonal quantity of dust available for deposition. The summer-fall accumulation of dust over central Arizona is similar to that measured from the dark laminae of the central Gulf. Although there are no data available to estimate the flux of airborne dust over Sonora and into the

central Gulf, we have argued that it should be comparable to that observed over central Arizona. If this is true, then the second necessary condition is fulfilled.

Evidence presented here thus suggests that fluvial injection of terrigenous material has, at best, only a minor role in the annual budget of the varved sediments presently forming in the central Gulf. Although seasonal resuspension of material on the shelf by currents associated with surface and/or internal waves may be important for transfer of material to the slope, we argue strongly for atmospheric transport as a principal means for transfer of sediment from the adjacent mainland. We include a final caveat to limit the validity of the proposed mechanism of eolian transport to the region of the central Gulf. Further south along the mainland, the decreasing aridity and increasingly tropical conditions render this an unlikely mechanism for removal and transport of terrigenous material.

ACKNOWLEDGEMENTS

This investigation was supported by CONACYT Grant PCMABNA-005321 from the Mexican government and by Grant ATM-79-19872 from the U.S. National Science Foundation. Use of the Research Vessel MATAMOROS was provided by the Dirección de Oceanografía of the Secretaría de Marina. We especially thank Cap. Pompeyo Leon and the officers and men of the R/V MATAMOROS for their exceptional cooperation and professionalism shown during collection of the box cores. We thank Ing. Carlos J. Arias, División Hidrométricia de Sonora, for providing daily rainfall records and for discussion of the effects of damming and irrigation on river runoff to the Gulf of California. Ken Bruland supported our efforts by providing laboratory facilities at the University of California, Santa Cruz and advice for the ^{210}Pb dating of the box cores. Finally, we thank José María Domínguez and Sergio Ramos for drafting the figures, and Carmen De Jesús for typing the manuscript.

REFERENCES

Baba, J., K. Scheidegger, H. Schrader and C. Peterson, submitted. Modern terrigenous sediments in the Gulf of California. In: The Gulf and Peninsular Province of the Californias, P. Dauphin and G. Ness (eds), AAPG Memoir.

Badan-Dangon, A., C.J. Koblinsky and T. Baumgartner, 1985. Spring and summer in the Gulf of California: observations of surface thermal patterns. Oceanologica Acta, 8:13-22.

Baumgartner, T.R., V. Ferreira-Bartrina, H. Schrader and A. Soutar, 1985. A 20-year varve record of siliceous phytoplankton variability in the central Gulf of California. Mar. Geol., 64:113-129.

Bischoff, S.W. and J.W. Niemitz, 1980. Bathymetric maps of the Gulf of California. U.S. Geological Survey, Misc. Invest. Ser., Map 1-1244.

Bouma, A.H., 1969. Methods for the Study of Sedimentary Structures. Wiley Interscience, J. Wiley and Sons, New York, 458 pp.

Brazel, A. and S. Hsu, 1981. The climatology of hazardous Arizona dust storms. In: T.L. Péwé (ed), Desert Dust: Origin, Characteristics and Effect on Man. Geol. Soc. Amer. Sp. Paper, 186:293-303.

Bruland, K.W., 1974. ^{210}Pb geochronology in the coastal marine environment. Ph.D. Thesis, University of California, San Diego, 106 pp.

Byrne, J., 1957. The marine geology of the Gulf of California. Ph.D. Thesis, University of Southern California, Los Angeles, 289 pp.

Calvert, S.E., 1964. Factors affecting distribution of laminated diatomaceous sediments in the Gulf of California. In: Tj.H. van Andel and G.G. Shor, Jr. (eds), Marine Geology of the Gulf of California. Amer. Assoc. Petrol. Geol. Mem., 3:311-330.

Calvert, S.E., 1966a. Accumulation of diatomaceous silica in the sediments of the Gulf of California. Geol. Soc. Amer. Bull., 77:569-596.

Calvert, S.E., 1966b. Origin of diatom-rich, varved sediments from the Gulf of California. J. Geol., 76:546-565.

Christensen, N., Jr., R. de la Paz and G. Gutierrez, 1983. A study of subinertial waves off the west coast of Mexico. Deep-Sea Res., 30:835-850.

Davis, J.C., 1973. Statistics and Data Analysis in Geology. John Wiley and Sons, New York, 550 pp.

DeMaster, D.J., 1979. The marine budgets of silica and Si-32. Ph.D. Thesis, Yale University, New Haven, CT, 308 pp.

Dixon, W.J. and F.J. Massey, Jr., 1969. Introduction to Statistical Analysis, 3rd Ed., McGraw-Hill Book Co., New York, 638 pp.

Donegan, D. and H. Schrader, 1981. Modern analogues of the Miocene diatomaceous Monterey Shale of California: evidence from sedimentologic and micropaleontologic study. In: R. Garrison and R. Douglas (eds), Monterey Formation and Related Siliceous Rocks of California. Pacific Section, Soc. Econ. Paleont. Mineral. Sp. Pub., p. 149-157.

Donegan, D. and H. Schrader, 1982. Biogenic and abiogenic components of laminated hemipelagic sediments in the central Gulf of California. Mar. Geol., 48: 215-237.

Drake, D.E., R.L. Kolpack and P.J. Fischer, 1972. Sediment transport on the Santa Barbara-Oxnard shelf, Santa Barbara Channel, California. In: D.J.P. Swift et al. (eds), Shelf Sediment Transport: Process and Pattern. Dowden, Hutchinson and Ross, Stroudsburg, Pa., p. 307-331.

Drake, D.E., D.A. Cacchione and H.A. Karl, 1985. Bottom currents and sediment transport on San Pedro Shelf, California. J. Sed. Petrol., 55:15-28.

Enfield, D.B. and J.S. Allen, 1983. The generation and propagation of sea level variability along the Pacific coast of Mexico. J. Phys. Oceanogr., 13: 1012-1033.

Flynn, W.W., 1968. The determination of low levels of polonium-210 in environmental materials. Analytica Chimica Acta, 43:221-227.

Gentleman, W.M.;, 1973. Least squares computations without square roots. J. Inst. Math. Appl., 12:329-336.

Glover, D.P., 1980. Historical Seismogram Filming Project: Second Progress Report. World Data Center A for Solid Earth Geophysics, Rept. SE-24. NOAA.

Greeley, R. and J.D. Iversen, 1985. Wind as a Geological Process on Earth, Mars, Venus and Titan. Cambridge University Press, Great Britain, 322 pp.

Hales, J.E., Jr., 1972. Surges of maritime tropical air northward over the Gulf of California. Month. Weather Rev., 100:298-306.

Hales, J.E., Jr., 1974. Southwestern United States summer monsoon source—Gulf of Mexico or Pacific Ocean? J. Appl. Meteor., 13:331-342.

Krishnaswami, S. and D. Lal, 1978. Radionuclide Limnochronology. In: M. Storme (ed), Lakes: Chemistry, Geology, Physics. Springer Verlag, p. 153-177.

Leinen, M., D. Cwienk, G.R. Heath, P.E. Biscaye, V. Kolla, J. Thiede and J.P. Dauphin, 1986. Distribution of biogenic silica and quartz in recent deep-sea sediments. Geology, 14:199-203.

McDonald, W.F., 1938. Atlas of climatic charts of the oceans. Washington, DC, Dept. of Agriculture, Weather Bureau, 60 pp.

Merrifield, M.A., C.D. Winant, J.M. Robles, R.T. Guza, N.A. Bray, J. García, A. Badan-Dangon and N.Christensen, Jr., 1986. Observations of currents, temperature, pressure and sea level in the Gulf of California 1982-1986. Data Report—Scripps Institution of Oceanography, Ref. Series 86-11, 153 pp.

Moore, T.C., Jr. and G.R. Heath, 1978. Sea floor sampling techniques. In: J.P. Riley and R. Chester (eds), Chemical Oceanography, Vol. 7. John Wiley, New York, p. 75-126.

Moreno-Hentz, P.E., 1982. Parametros sedimentologicos de varvas marinas en el Golfo de California y su relación con variaciones climaticas recientes. Licenciaturate Thesis, Universidad Autonoma de Baja California, 105 pp.

Péwé, T.L., E.A. Péwé, R.H. Péwé, a. Journaux and R.M. Slatt, 1981. Desert dust: Characteristics and rates of deposition in central Arizona, U.S.A. In: T.L. Péwé (ed), Desert Dust: Origin, Characteristics and Effect on Man. Geol. Soc. Amer. Sp. Paper 186, p. 169-190.

Prospero, J.M., 1981. Arid regions as sources of mineral aerosols in the marine atmosphere. In: T.L. Péwé (ed), Desert Dust: Origin, Characteristics and Effect on Man. Geol. Soc. Amer. Sp. Paper 186, p. 71-86.

Revelle, R.R., 1939. Sediments of the Gulf of California. Geol. Soc. Amer. Bull., 50:1929.

Revelle, R.R., 1950. Sedimentation and oceanography: survey of field observations, Part 5 of 1940 E.W. Scripps cruise to the Gulf of California. Geol. Soc. Amer. Mem., Vol. 43, 6 pp.

Secretaria de Recursos Hidraulicos, 1970a. Datos Hidrometricos de Corrientes de Material de Acarreo en Suspension e Hidrometricos de Vasos hasta Diciembre 1969, Region Hidrologica No. 9, Sonora Sur., Cuencas de los Rios Sonora-Yaqui-Mayo. Boletin Hidrologico No. 40, Tomo I, Jefatura de Irrigación y Control de Rios, Dirección de Hidrologia, Mexico, D.F.

Secretaria de Recursos Hidraulicos, 1970b. Resumenes de Datos Hidrometricos, Crecientes, Gastos Maximos, Areas de Cuenca hasta Diciembre 1969, Region Hidrologica No. 9, Sonora Sur., Cuencas de los Rios Sonora-Yaqui-Mayo. Boletin Hidrologico No. 40, Tomo II, Jefatura de Irrigación y Control de Rios, Dirección de Hidrología, Mexico, D.F.

Secretaria de Recursos Hidraulicos, 1975. Datos Hidrometricos de Corrientes de Acarreo de Azolves en Suspension e Hidrometrico de Vasos, Enero 1970-Diciembre 1973, Region Hidrologica No. 9, Sonora Sur., Cuencas de los Rios Sonora-Yaqui-Mayo. Boletin Hidrologico No. 40, Tomo III, Jefatura de Irrigación y Control de Rios, Dirección de Hidrologia, Mexico, D.F.

Soutar, A., 1978. Collection of benthic sediment samples, Southern California Base-line Study Benthic Year II. Final Rept., Bureau of Land Management, Vol. 2, Pt. 4, No. 2, 54 pp.

Soutar, A. and P.A. Crill, 1977. Sedimentaiton and climatic patterns in the Santa Barbara Basin during the 19th and 20th centuries. Geol. Soc. Amer. Bull., 88:1161-1172.

van Andel, Tj.H., 1964. Recent marine sediments of the Gulf of California. In: Tj.H. van Andel and G.G. Shor (eds), Marine Geology of the Gulf of California. Amer. Assoc. Petrol. Geol. Mem., 3:216-310.

Yaalon, D.H. and E. Gonor, 1975. Rates of aeolian dust accretion in the Mediterranean and desert fringe environments of Israel. 9th Cong. International de Sedimentologie, Nice, p. 169-174.

CHAPTER IV

FACTORS CONTROLLING PRIMARY PRODUCTIVITY IN THE GULF OF CALIFORNIA DURING EL NIÑO CONDITIONS: LESSONS FROM MARCH 1983

ABSTRACT

Analysis of a recent twenty-year period of siliceous phytoplankton deposition preserved in the annually layered sediments of the central Gulf of California, suggests that primary productivity is enhanced during El Niño episodes. The fortuitous occurrence of the very strong 1982-1983 El Niño event provided an opportunity to determine the magnitude and patterns of distribution of primary productivity and phytoplankton biomass associated with this event and to test the inferences made from the sediment record. This paper reports the results from a March 1983 cruise to the Gulf of California designed to provide an integrated picture of the biological and physical processes which occurred as a response to the El Niño phenomenon as well as to other significant scales of forcing. Measured rates of primary productivity during this period reached surprisingly high values along the eastern margin of the central Gulf within the area from which the sediment sample had been recovered.

Results of this study demonstrate that the high primary productivity and phytoplankton biomass observed were consistently associated with upwelling of a locally formed nutrient-rich Gulf Water mass. Distribution of the enhanced fertility was confined to the central Gulf, while low productivity is found associated with the northward penetration of Tropical Surface Water along the western side of the Gulf. The presence of the high productivity and biomass in the northern sector of the central Gulf and within a narrow strip along the eastern margin, reflects a response to direct wind forcing which overrides the effect of remote forcing associated with the El Niño.

This work points to the importance of Gulf Water as a principal source of nutrients to supply the zone of coastal upwelling. A mechanism is proposed here whereby significant interannual variation in nutrient concentration of Gulf Water may explain the variation of phytoplankton production inferred from the sediment record. It is hypothesized that an intensification of poleward advection of Subtropical Subsurface

Water during El Niño episodes results in nutrient enrichment of the Gulf of California by increased flux of nutrients to the source region of the Gulf Water in the northern Gulf.

INTRODUCTION

The Gulf of California is a narrow marginal sea, approximately 1000-km long and 150-km wide, lying between the Mexican mainland and the peninsula of Baja California (Fig. IV-1), open to the Pacific at the southeastern extreme. The Gulf is divided into two major physiographic provinces by a narrow constriction between the opposing shelves and an irregular sill running between Punta San Francisquito and Tiburon Island. Most of the upper Gulf, north of the sill, lies above 200 m depth, except for the region around the pedestal of Angel de la Guarda Island, which lies along a deep and narrow channel off the Baja California margin. The lower Gulf is formed from a sequence of basins which progressively deepen from approximately 1800 m off Guaymas to over 3000 m at the entrance. The lower Gulf has been traditionally sub-divided into a central and southern region with the boundary lying roughly north of Topolobampo (Roden and Groves, 1959).

There are two distinct hydrographic regimes within the upper 150 m of the central and southern regions, corresponding to seasonal differences in the low level wind field over the Gulf and local heating (Robles and Marinone, in press). During winter and spring, near-surface winds blow from the northwest, generally parallel to the axis of the Gulf, while during summer and fall, the winds normally reverse and come from the southeast (Roden, 1964; Candela et al., 1984, 1985; Badan et al., 1985). Winter-spring conditions in the upper ocean are characterized by relatively weak stratification and generally strong upward flexure of the isotherms towards the mainland, indicating divergence at the coast and upwelling from below 50 m. Fully developed summer-fall conditions around August show high surface temperatures, a strongly stratified and stable water column down to 150 m with convergence and downwelling off the main-land, and shallow upwelling (from above 50 m) off Baja California (cf. Figs. 10,11,12 in Roden, 1964). The long length and enclosure of the Gulf, also give rise to an

Figure IV-1

Generalized bathymetry of the Gulf of California based on Bischoff and Niemitz (1980). The 200, 1800 and 3000 m isobaths are shown.

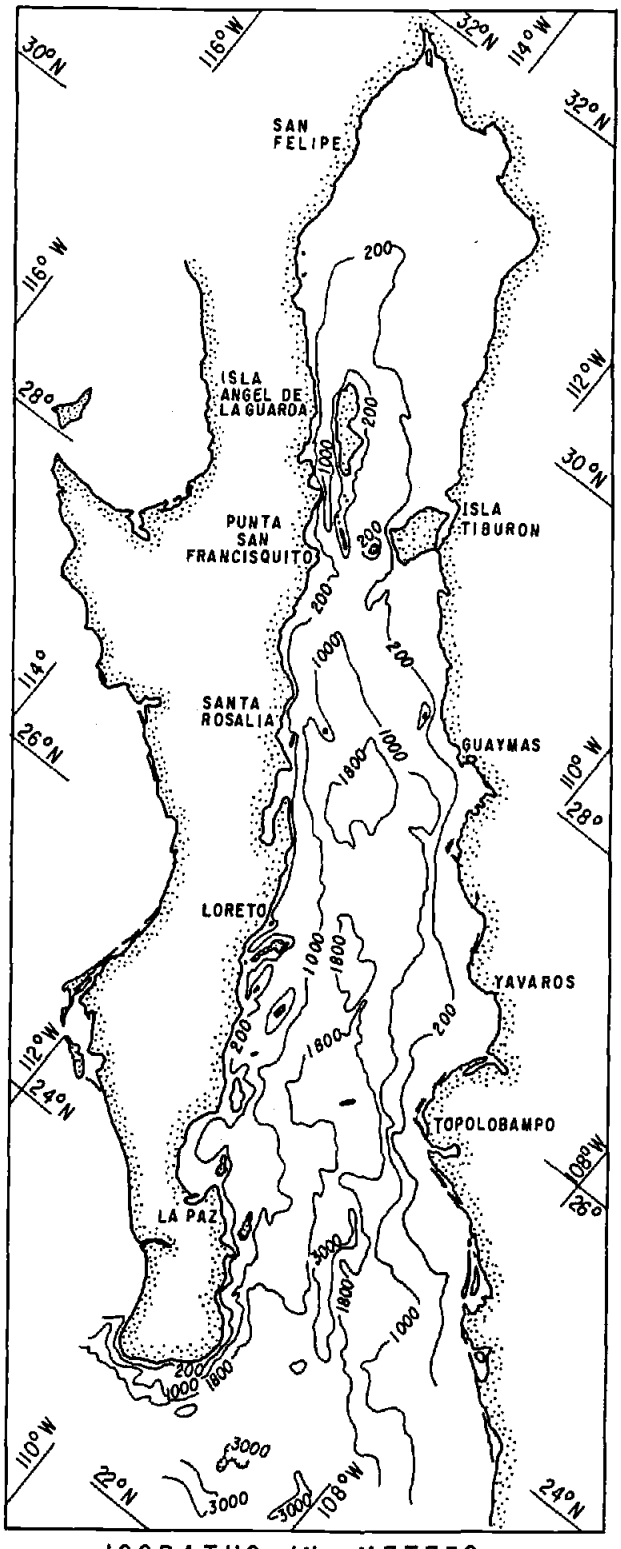
SAN FELIPE
ISLA ANGEL DE LA GUARDA
PUNTA SAN FRANCISQUITO
ISLA TIBURON
SANTA ROSALIA
GUAYMAS
LORETO
YAVAROS
TOPOLOBAMPO
LA PAZ
200
1000
1800
3000
30°N
116°W
32°N
114°W
28°
112°W
26°N
110°W
24°N
108°W
22°N
ISOBATHS IN METERS

Figure IV-1

appreciable climatic gradient. The more tropical, oceanic character of the southern Gulf gives way to an arid, subtropical and continental climate at the shallow, northern extreme where evaporation plays an important role in the formation of a local Gulf Water mass (Roden and Groves, 1959).

The Gulf of California holds particular interest for climatic studies because of the potential long-term record of interannual change preserved in the annually layered or varved sediments deposited there (Calvert, 1964; Schrader and Baumgartner, 1983). Year-to-year variation in the ocean climate observed from sea level, shore temperature and hydrographic data in the Gulf is dominated by oceanographic changes in the equatorial and eastern tropical Pacific linked to the El Niño/Southern Oscillation (ENSO) cycle (Baumgartner and Christensen, 1985; Robles and Marinone, in press). Baumgartner et al. (1985) have shown that the rich assemblages of siliceous phytoplankters (diatoms and silicoflagellates) in the varved sediments of the central Gulf of California record a response of the pelagic ecosystem to the large-scale ENSO phenomenon. An important result from that study is the indication of higher phytoplankton production off Guaymas in the central Gulf during El Niño episodes as compared to anti-El Niño periods. Higher productivity associated with El Niño events is the opposite from that observed in the eastern boundary currents off Peru (Cowles et al., 1977; Barber and Chavez, 1983) and California (Chelton et al., 1982; McGowan, 1984).

The magnitude and wide-spread effect of the 1982-1983 El Niño event presented a unique opportunity to observe the response of the lower trophic levels in the Gulf of California to the physical forcing associated with a very strong El Niño event. This provided the necessary test to determine whether primary productivity in the Gulf is, in fact, enhanced during El Niño as suggested by the diatom record preserved in the varved sediments (Baumgartner et al, 1985); and if true, to determine why. Direct measurements of primary productivity in the central Gulf, made in March, 1983

(Lara-Lara et al., 1984) did show very high values (maximum of nearly 4.5 g C m^{-2} d^{-1}), consistent with the observations obtained from the sediment record. Further measurements indicated high productivity within the central Gulf was sustained during October, 1983 and March, 1984 as the El Niño matured and began to wane. These values are significantly higher than those obtained in November, 1984 and March, 1985 (maximum value of approximately 1.0 g C m^{-2} d^{-1}; Lara-Lara unpublished results) after the decay of the El Niño.

The objective of this paper is to examine the hydrographic framework and distribution of biological parameters observed during March, 1983, in the Gulf in order to determine the physical processes responsible for the unusually high primary productivity measured then. This is part of a continuing effort to determine the ecosystem response to the ENSO cycle in order to better understand and interpret the climatic signal recorded by the siliceous phytoplankton in the varved sediments. This problem is approached by defining the patterns of distribution of phytoplankton biomass and primary productivity and their relationship to the water mass structure and circulation. The focus is on the data collected during March 1983, since they reflect the peak winter-spring conditions combined with the effects imposed by an unusually strong El Niño. Although the annual cycle of primary productivity over the central and southern Gulf has not yet been fully documented, the winter-spring conditions are thought to be normally associated with relatively higher production because of the more intense divergence and upwelling off the mainland coast (associated with the strong northwesterly winds) compared to the summer-fall divergence off Baja California which is driven by the weaker southeasterly winds. The sampling period extended from March 10 through 23 and covered the central and southern regions of the Gulf (Fig. IV-2) which are in open communication with the Pacific.

Figure IV-2

Station plan for cruise 8303. Stations are numbered in sequence from 1 through 79 (stations 13 and 73 are missing because of cancellation during curise). Operations at each station indicated by key at right of figure. Transects of stations across the Gulf are numbered from 1 through 10. Dates of occupation of the transects are also shown on figure.

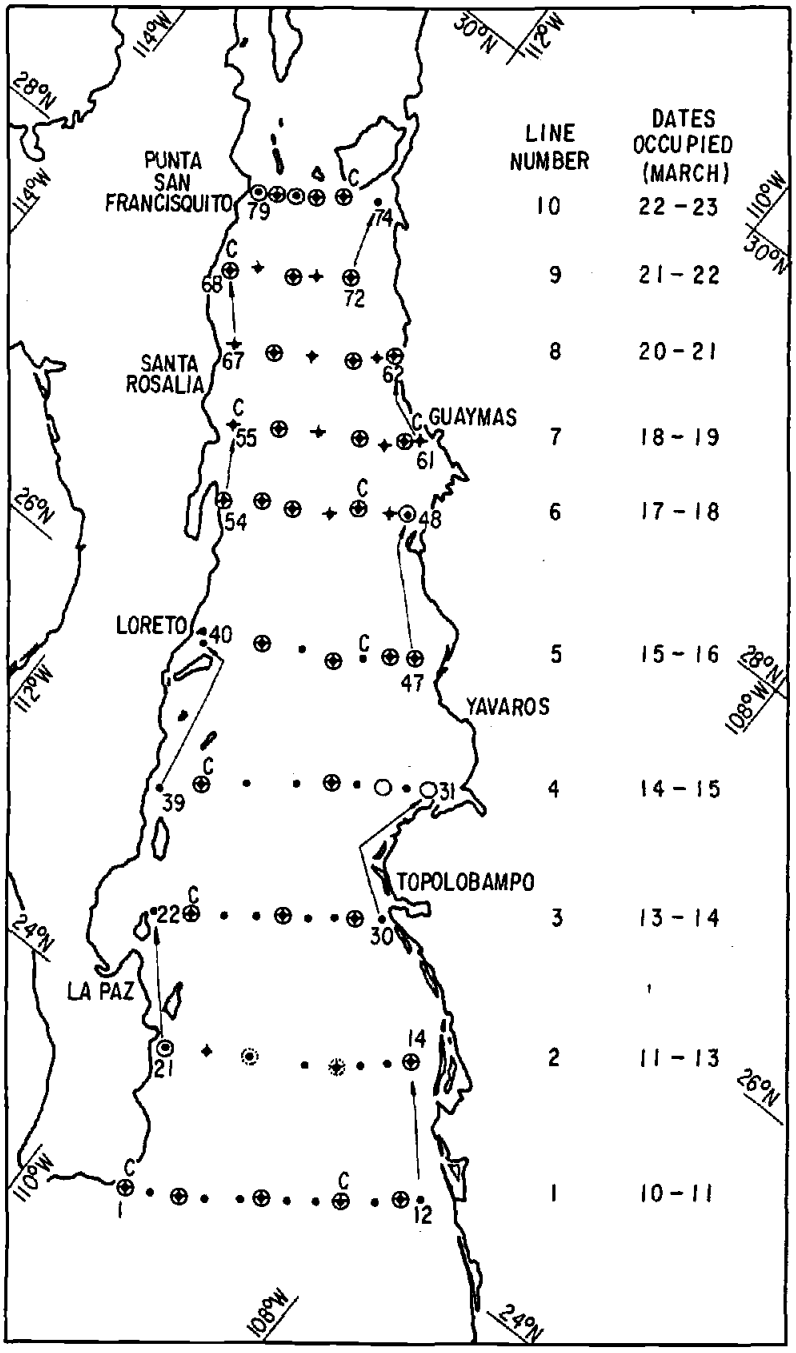

STATION PLAN FOR CRUISE 8303
10-23 MARCH, 1983

Figure IV-2

DATA COLLECTION AND ANALYSIS

A total of 77 stations were occupied from aboard the Research Vessel EL PUMA during March, 1983. The stations were laid out in ten transects across the Gulf with the first line of stations at the mouth of the Gulf and the final line at the northern sill, which marks the boundary between the northern and central Gulf. The station numbers at either end of the sections are shown in Figure IV-2 along with the ship tracks between transects. The station plan in Figure IV-2 uses the pre-cruise station designations running from station 1 through 79. Two stations (13 and 73) were cancelled during the cruise due to unexpected shallow water depths. Work was begun at station 1 at 0900 on March 10 and finished at station 79 at 0100 on March 23. Figure IV-2 shows the dates of occupation of each of the 10 oceanographic sections. Navigation was by satellite and radar.

Seventy-six STD casts were made to a maximum depth of 1200 meters, where possible. The STD was a Plessey Model 9040 Profiling System loaned by the data facility at Scripps Institution of Oceanography. The STD provides a digital record on magnetic tape and an analog record on continuous chart paper. The STD stations are shown on Figure IV-2 by the solid circles. A 1.7-liter Niskin bottle was attached just above the STD to provide a calibration check. At each of the stations, bucket samples were also taken to measure surface temperature by thermometer. Thirty-nine hydrocasts using 1.7-liter Niskin bottles and reversing thermometers were made to a maximum depth of 1000 meters in order to further calibrate and back up the STD data. These stations are shown by the open circles on Figure IV-2. Bottles were placed at nominal depths of 0, 10, 25, 50, 75, 100, 125, 150, 200, 250, 300, 400, 500, 700, and 1000 m. Salinities from the Niskin bottle samples were analyzed onboard with a Kahlsico Model 5165 induction salinometer. Wind speed and direction were taken during the bottle casts by reading the output on the bridge from the ship's anemometer.

Comparisons of the temperature and salinity data from the calibration bottle and the STD as well as differences between the bottle casts and STD casts unfortunately indicate that the STD data are unstable with a significant random deviation from the thermometer and salinometer data. For this reason the temperature and salinity profiles used for this study are principally based on the 39 stations where bottle casts were taken. The one exception is the reconstruction of salinity cross-sections used to trace high salinity Gulf Water. For this purpose salinity data from the STD profiles between the bottle casts were used to fill in the cross-sections. The salinity values from the STD profiles were estimated by running a smooth curve through the analog record.

Forty-four continuous profiles of light attenuation were made to a maximum depth of 600 m in order to estimate the concentrations of total suspended particulate matter. Replicate measurements were made with two identical 25-cm beam transmissometers with 660 nm light source. One was an Oregon State University, Bartz-Zaneveld Sea Tech transmissometer; the other was constructed at the Centro de Investigación Cientifica y Educaión superior de Ensenada and modelled after the Sea Tech instrument with the aid of R. Bartz. Data were recorded with a self-contained film data-logger constructed by Sea-Systems into which were incorporated temperature and depth sensors as well as the power source for the transmissometers. Stations where transmission data were collected are indicated on Figure IV-2 by crosses. In order to calibrate the light transmission data to total suspended mass (TSM), 5- and 7-liter Niskin bottle casts were made at 21 of the 44 transmissometer stations. Five-liter bottles were located at 12 and 30 m while the 7-liter bottles were placed at 75, 150, 300, and 500 m depths. The water samples were vacuum filtered through previously weighed 47 mm Nucleopore filters (0.6 μm pore size) and then frozen to prevent growth of bacteria an mold. The filters were re-weighed on shore with a Mettler HL 52 analytical balance following procedures described in Peterson (1977).

At ten of the stations, water was collected with the 5- and 7-liter Niskin bottles to measure primary productivity by ^{14}C incubation (see Valdez-Holguin, 1986) according to the method described by Steeman-Nielsen (1952). These stations are indicated by the letter "C" on Figure IV-2. Samples were taken from depths corresponding to 100, 50, 25, 10, and 1% of the surface light intensity. Sample depths were determined by measuring the ambient light with a Khalsico 268WA310 photometer. Samples were injected with 2 micro-curies of ^{14}C and incubated on the main deck for approximately two hours at the temperature of the surface sea water using neutral screens to simulate the different light intensities. Locations of the productivity stations were principally determined by the need to sample two hours before noon so that the incubations could all be carried out at roughly mid-day. After incubation, the samples were collected onto 47 mm Nucleopore filters (.45 μm pore size) and frozen. Samples were counted with Chicago Nuclear Unilux III liquid scintillation counter at the Naval Ocean Systems Center at San Diego, CA. Details of the carbon assimilation calculations are given in Valdez-Holguin (1986).

Water was also sampled from the five light depths at the primary productivity stations to measure chlorophyll a concentrations and nutrients (Valdez-Holguin, 1986). The chlorophyll measurements were made to estimate the phytoplankton biomass. Water was collected onto 25 mm GF/C filters with 0.8 μm pore size adding magnesium carbonate to preserve the chlorophyll a and then frozen onboard. Chlorophyll a was then measured on shore with a Turner 111 fluorometer calibrated with pure chlorophyll a following Strickland and Parsons (1972). The phosphate concentrations reported here were measured onshore from water samples frozen aboard ship (Valdez-Holguin, 1986). The analyses were made with a Scientific Instrument autoanalyzer following the procedures in Strickland and Parsons (1972). Continuous fluorescence profiles were also made at 28 stations down to 70 m by pumping water to a shipboard Turner 111

fluorometer modified to measure in vivo fluorescence. Fluorescence profiles from four of these stations are presented here.

WATER MASS STRUCTURE AND CIRCULATION DURING MARCH 1983

Below 400 m, the T-S characteristics within the southern and central Gulf closely resemble that of the eastern tropical Pacific (Roden, 1964; Alvarez-Borrego and Schwartzlose, 1979) with Pacific Intermediate Water found between approximately 400 and 1000 m and Pacific Deep Water extending to the bottom. The water mass structure below 400 m does not vary perceptibly over seasonal and interannual time scales (Robles and Marinone, in press). A persistent subsurface feature in the southern Gulf is also the distinct salinity maximum found between roughly 150 to 400 m (Griffiths, 1968; Roden, 1972b, his Fig. 3; Alvarez-Sanchez, 1974). This salinity maximum corresponds to the Subtropical Subsurface Water defined by Wyrtki (1967).

There are three surface water masses found near the entrance to the Gulf in the hydrographically complex region of transition between waters of the North Pacific gyre and those transported northward along the coast of Central America and southern Mexico by the equatorial circulation (Roden, 1971, his Fig. 2). These are the California Current Water, the Tropical Surface Water and Gulf Water. The California Current Water, flowing equatorward along the west coast of Baja California, between the surface and 100 m depth, consists of two thin layers according to Roden (1971, his Fig. 8). Below 50 m, the water can be characterized as Subarctic Water with low salinities and temperatures (<20° C, <34.4 ppt). Above 50 m, Roden defines a Transition Wate because of its intermediate character between the Subarctic Water in the California Current occurring at the surface off California, and the relatively warm, high-salinity Subtropical Surface Water (20-25°C, >34.4 ppt) to the west of Baja California. The

Subtropical Surface Water is associated with the interior region of the subtropical North Pacific gyre. The warm, low-salinity surface water flowing north-ward off southern and middle Mexico is identified as Tropical Surface Water defined by Wyrtki (1967). South of the entrance to the Gulf, this water is limited to the shallow mixed layer above 50 m. The Gulf Water defined by Roden and Groves (1959) is a high salinity water mass originating in the shallow northern Gulf from the excessive evaporation.

Robles and Marinone (in press) have described seasonal and interannual variation in the thermohaline characteristics of the upper 400 m of the central Gulf. Their analysis shows that California Current Water may reach northward to the central Gulf producing a shallow salinity minimum near 75 m depth in late spring and early summer. When present, this shallow salinity minimum reveals the existence of the Subtropical Subsurface Water from the resulting salinity maximum at approximately 200 m, which is always well defined near the entrance to the Gulf. The salinity maximum of the Subtropical Subsurface Water is often obscured in the central Gulf, however, by the presence of the high salinity Gulf Water which usually lies directly above it. In the central Gulf then, it is normal to find that there is no distinguishable boundary in either temperature or salinity between Gulf Water and Subtropical Subsurface Water, but rather a gradual linear transition.

Figure IV-3 is a T-S diagram with data from the bottle casts made throughout the southern and central Gulf during March 1983. The data are plotted over the fields established by Wyrtki (1967) according to his definitions of the water masses in the subtropical and tropical eastern Pacific above 400 m. The Pacific Intermediate Water is present as the salinity minimum at approximately 6°C.

Griffiths (1968, p. 3) carefully pointed out that the water masses above 150 m, found at the entrance to the Gulf, do not retain their signal characteristics as originally described by Wyrtki (1967), but are "composites", modified by intermixing near the

Figure IV-3

Temperature-salinity plot for the central and southern gulf of California during March, 1983, obtained from bottle casts. Identification of water masses within the Gulf is shown by data fields enclosed by the heavy lines. The lighter lines indicate the water masses defined by Wyrtki (1967) for the eastern tropical and subtropical Pacific.

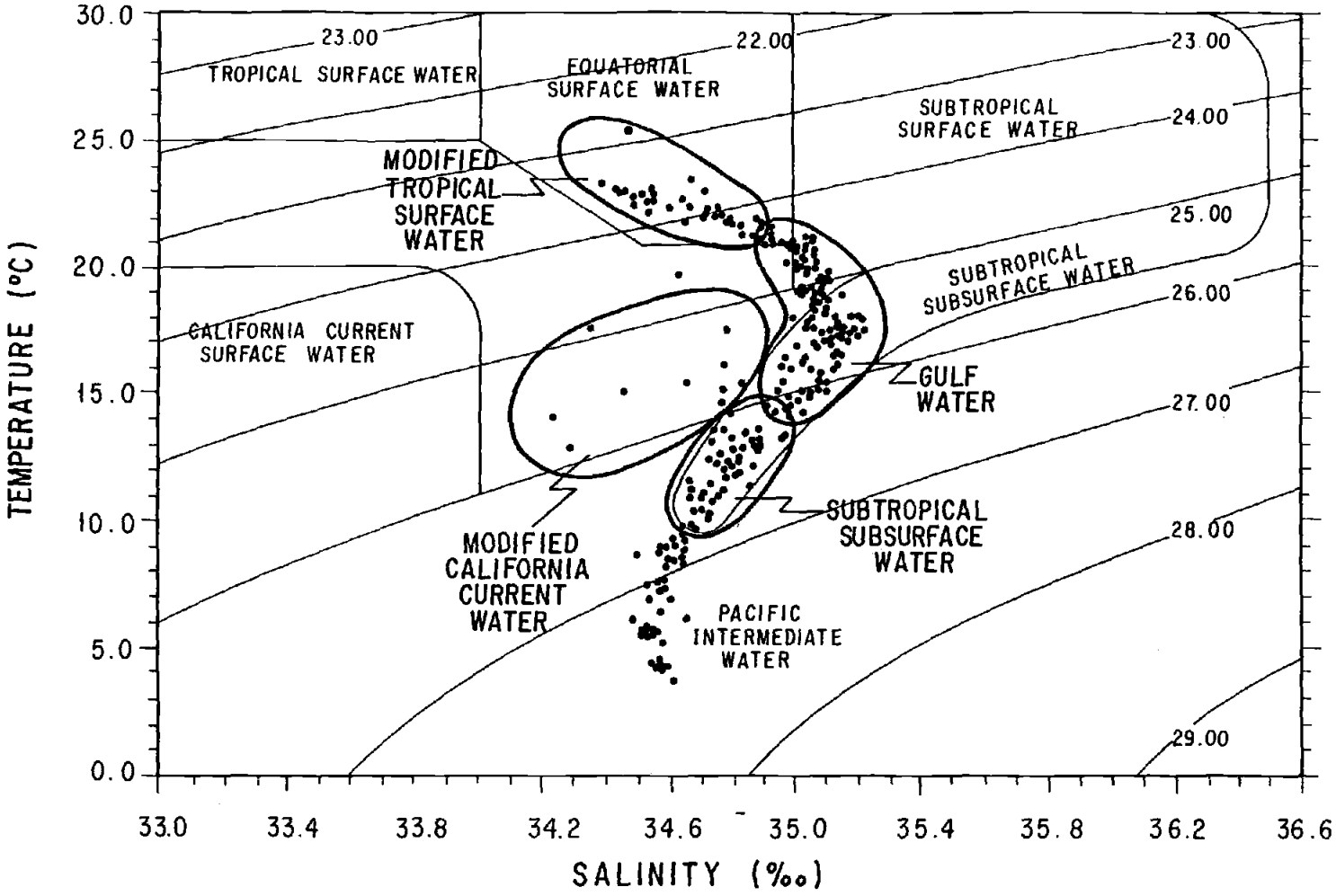
30.0
25.0
20.0
15.0
10.0
5.0
0.0
TEMPERATURE (°C)
33.0
33.4
33.8
34.2
34.6
35.0
35.4
35.8
36.2
36.6
SALINITY (‰)
23.00
TROPICAL SURFACE WATER
22.00
EQUATORIAL SURFACE WATER
23.00
SUBTROPICAL SURFACE WATER
24.00
MODIFIED TROPICAL SURFACE WATER
25.00
SUBTROPICAL SUBSURFACE WATER
26.00
CALIFORNIA CURRENT SURFACE WATER
GULF WATER
27.00
SUBTROPICAL SUBSURFACE WATER
28.00
MODIFIED CALIFORNIA CURRENT WATER
PACIFIC INTERMEDIATE WATER
29.00

Figure IV-3

entrance and within the Gulf. Once this is recognized, it is not too difficult to ascertain the identifying characteristics and origins of the water masses. This is done in Figure IV-3 by superimposing limits through the March, 1983 data to specify the origin of the different kinds of water present then within the central and southern Gulf.

The Subtropical Subsurface Water was clearly present throughout the southern and central Gulf, but the salinity maximum at the temperatures between 12 and 13°C, which occurs over the eastern tropical Pacific is not seen in Figure IV-3 because of the continuous increase in the temperature and salinity along the line of mixing with the Gulf Water. The prominent salinity maximum at 18°C is associated with the "purest" Gulf Water found over the sill between the northern and central Gulf.

The field of high temperatures and low salinities on Figure IV-3 circumscribes water which has been modified from the original Tropical Surface Water. The temperatures and salinities of this water, which is labeled Modified Tropical Surface Water in Figure IV-3, lie along the hypothetical line of mixing between Gulf Water and Wyrtki's (1967) Tropical Surface Water. The boundary placed between Gulf Water and the modified Tropical Surface Water is therefore somewhat arbitrary because of its transitional nature in the mixing region between the two water types. Although the modified Tropical Surface Water falls into the T-S field of Wyrtki's (1967) Equatorial Surface Water, it is clearly unrelated to this water mass which is found only near the equator and limited to the north by its boundary with the Tropical Surface Water (cf. Wyrtki, 1967, his Fig. 3).

A fourth field, which is drawn over the T-S data of Figure IV-3 circumscribes water from the California Current which has been altered by mixing with the Gulf Water and the Subtropical Subsurface Water. This is labeled on Figure IV-3 as Modified California Current Water. This water was present as a subsurface core in the western half of the Gulf, only at the entrance (along section 1).

The interannual variation possible in water mass structure of the Gulf is evident from comparison of Figures IV-3 and IV-4. Figure IV-4 illustrates the T-S characteristics of the southern Gulf during the same month (March) of 1970 which was an anti-El Niño year. This figure is adapted from Alvarez-Sanchez (1974) and demonstrates the complete absence of the Tropical Surface Water. Unlike March, 1983, there was a large volume of water present from the California Current. Note that the linear mixing relationship between Subtropical Subsurface and Gulf Water is maintained. The progressively higher temperatures and salinities in the California Current Water probably indicate a significant contribution of Subtropical Surface Water mixing with the surface water of the California Current before reaching the Gulf (Alvarez-Sanchez, 1974).

The sea surface temperatures and salinities in the southern and central Gulf (Fig. IV-5) show the distribution of the water masses at the surface during March of 1983. A prominent feature in the temperature field is the presence of a high temperature tongue of water extending along the western half of the Gulf and reaching north of Guaymas (Fig. IV-5a). This warm water is associated with lower salinities (Fig. IV-5b) and indicates the presence of the modified Tropical Surface Water (cf. Fig. IV-3). This water becomes increasingly cooler and more saline to the north. Surface water at the northern sill shows the characteristics of Gulf Water. The boundary at the surface between the Gulf Water and the modified Tropical Surface Water in the central Gulf is considered to lie between the 21 and 21.5°C isotherms and between the 34.9 and 35.0 ppt isohalines. The Gulf Water covers the entire surface just south of the main sill. South of Santa Rosalia, the Gulf Water is confined to the eastern half of the Gulf as a distinct tongue of cool, higher salinity water reaching almost as far south as Yavaros. South of Yavaros, this surface expression of Gulf Water is lost.

Figure IV-4

Temperature-salinity plot for the southern Gulf during March, 1970 (adapted from Alvarez-Sanchez, 1974). Broken line represents T-S curve for the central and southern Gulf during March, 1983 from data in Figure IV-3.

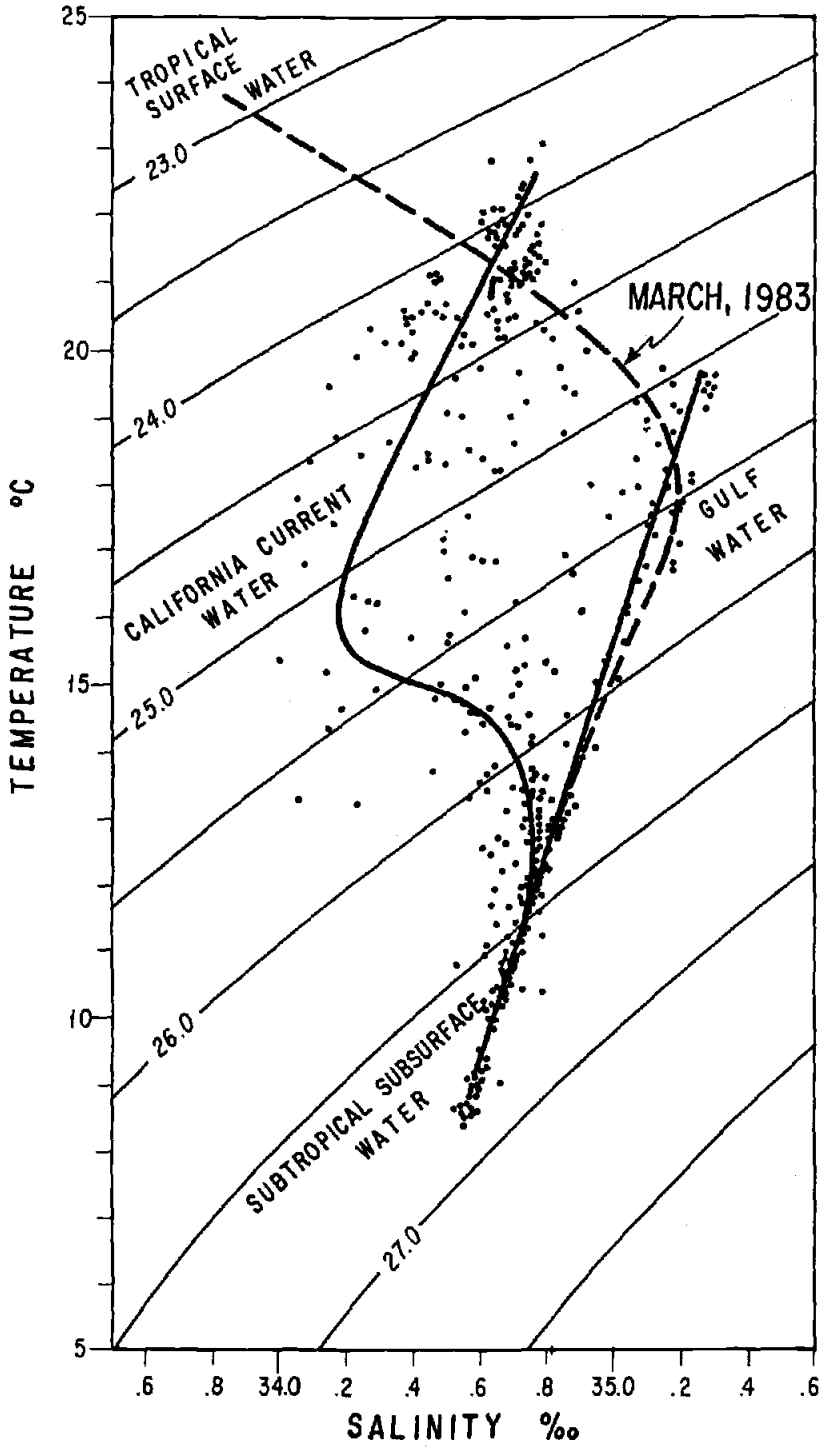
TROPICAL SURFACE WATER
MARCH, 1983
CALIFORNIA CURRENT WATER
GULF WATER
SUBTROPICAL SUBSURFACE WATER
23.0
24.0
25.0
26.0
27.0
TEMPERATURE °C
25
20
15
10
5
.6
.8
34.0
.2
.4
.6
.8
35.0
.2
.4
.6
SALINITY ‰

Figure IV-4

Figure IV-5

(a) Distribution of surface temperatures during March, 1983, based on bucket samples from cruise 8303. Contour interval is 0.5°C. (b) Distribution of surface salinities during March, 1983, taken from surface bottle on hydrocasts of cruise 8303. Contour interval is 0.10 ppt. Missing data points in center of section 2 due to malfunction of salinometer.

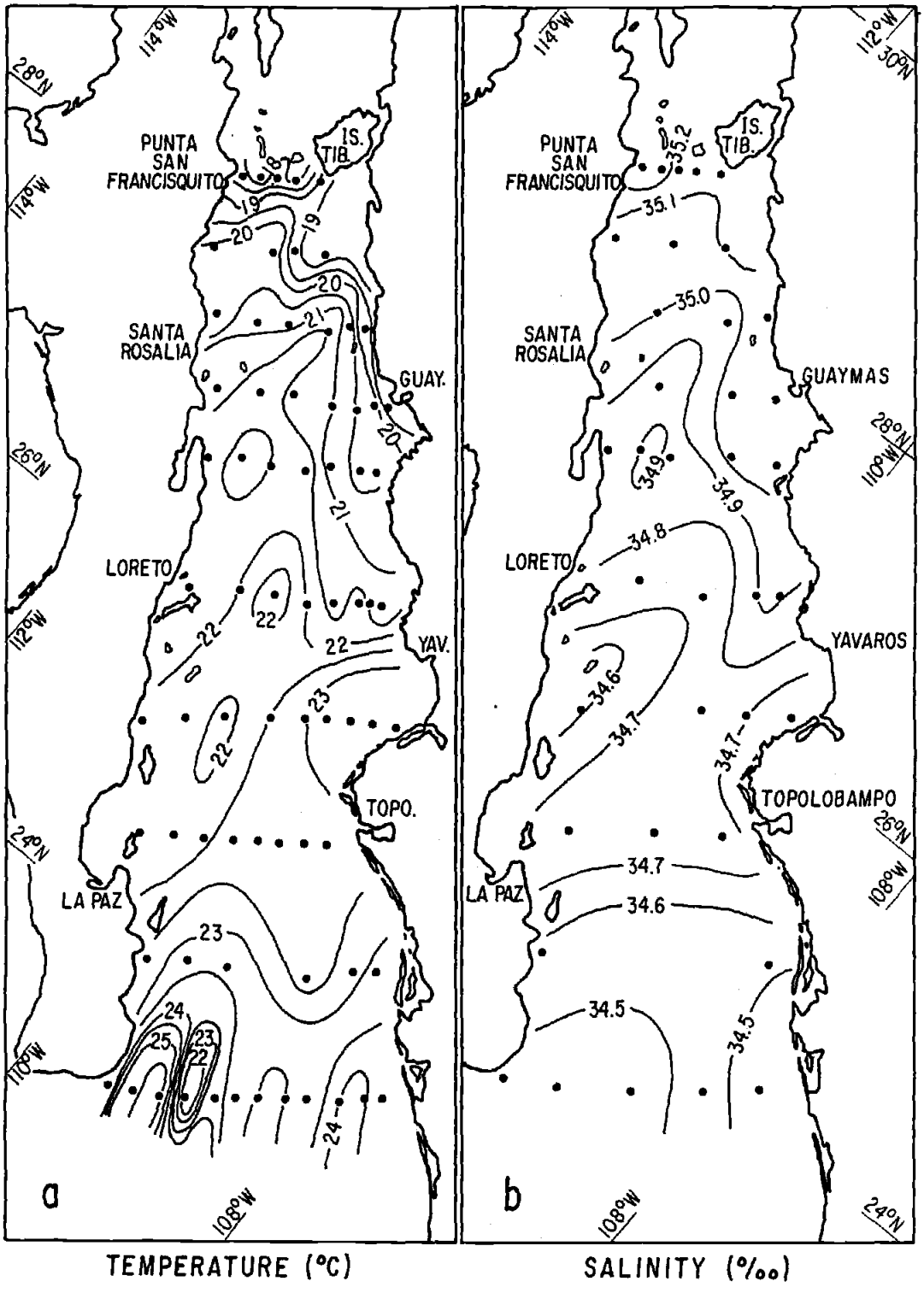
PUNTA SAN FRANCISQUITO
IS. TIB.
SANTA ROSALIA
GUAY.
LORETO
YAV.
TOPO.
LA PAZ
GUAYMAS
YAVAROS
TOPOLOBAMPO
114°W
112°W
110°W
108°W
28°N
26°N
24°N
30°N
a
b
TEMPERATURE (°C)
SALINITY (‰)

Figure IV-5

The surface circulation in the Gulf during March 1983 is estimated by contours of the dynamic heights obtained from the bottle casts. If we assume geostrophic equilibrium, then the contours can be used to represent streamlines of flow at the surface. The relative strength of the flow is determined by the distance between streamlines. The flow intensity is inversely proportional to the streamline separation. The dynamic topography in Figure IV-6 is measured relative to a reference level of 400 db. Although this is shallower than the 500 db level customarily used in coastal regions (see for example, Chelton et al., 1983), use of the shallower level allows us to include more data points near the margins and still provides a reasonable depiction of the surface flow.

Figure IV-6 shows that the flow across the northern sill region is directed southward into the central Gulf. Between the sill and Santa Rosalia, there is a sharp meander with cyclonic flow around a trough in the dynamic topography. The flow then veers abruptly to the south, forming a prominent equatorward coastal jet off Guaymas. Note that comparison of the bathymetry in the sill region and the northern portion of the central Gulf (Fig. IV-1) indicates that the shape of the flow out of the northern Gulf conforms to the bottom topography. The presence of the lighter water mass to the south would also create a local north-south pressure gradient at the water mass boundary in the central Gulf causing the current to veer to the east. (It is also interesting to note that the same general shape of the flow in the northern sector of the central Gulf is observed in the dynamic topography for February, 1957 according to Rosas-Cota, 1977). Strength of the equatorward flow decreases to the south off Topolobampo as the coastal flow begins to broaden. However, the poorer data coverage in the southern Gulf does not permit as good a resolution of the topography as in the central Gulf. Comparison of Figure IV-6 with the temperature and salinity fields in

Figure IV-6

Surface geostrophic flow represented by the geopotential anomaly at the sea-surface relative to the 400 decibar surface. Units are dynamic centimeters. Dynamic heights calculated from the bottle cast data of cruise 8303.

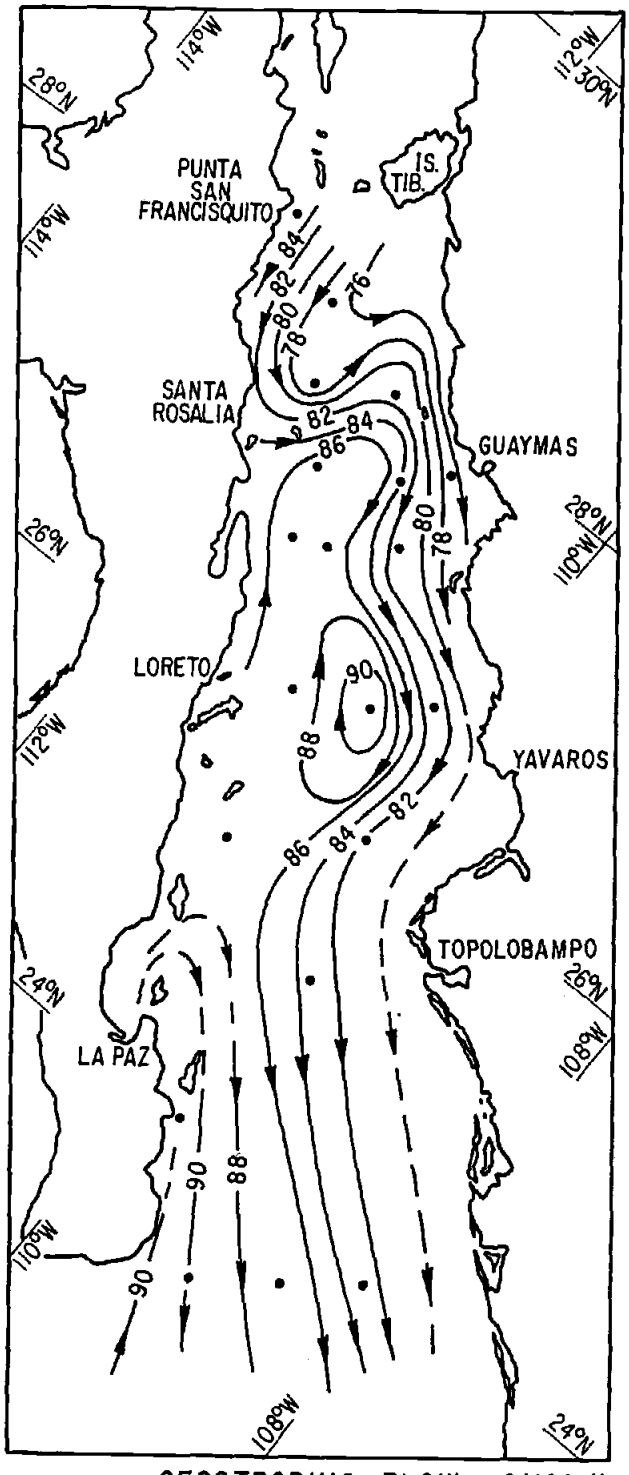

GEOSTROPHIC FLOW 0/400 db
AT SURFACE

Figure IV-6

Figure IV-5 shows that the flow from the northern Gulf and around to the eastern coast is associated with advection of the low temperature, high-salinity Gulf Water.

South of Santa Rosalia, there is a prominent elongated anticyclonic flow around a ridge in the topography located between Loreto and Yavaros. The far northward penetration of the Tropical Surface Water seen in Figure IV-5 must have occurred by the poleward advection seen off Baja California. South of La Paz, poleward flow is indicated only against the western margin. Otherwise, across the mouth of the Gulf, the surface flow is equatorward.

The T-S plot in Figure IV-7 shows data from the northernmost line of stations (section 10) which lies roughly along the main sill which separates the northern and central Gulf. This plot demonstrates that during March, 1983, only Gulf Water and Subtropical Subsurface Water were present along this transect. This is further evidence that the surface flow from the northern Gulf (Fig. IV-6) transported Gulf Water into the central and southern Gulf.

We can trace the southward extension of the Gulf Water by mapping the 25.5 σ_t surface (Fig. IV-8) and by constructing salinity cross-sections down the Gulf (Fig. IV-9). The depth to the 25.5 σ_t surface over the sill is very shallow (10 to 20 m). This represents a shallow, high-salinity core of Gulf Water flowing into the lower Gulf from across the sill. From the sill, the 25.5 σ_t surface descends rapidly indicating sinking of the denser Gulf Water below the warmer, low-salinity Tropical Surface Water present in the central Gulf. The deep trough in the depth contours over the central Gulf reflects the anticyclonic motion apparent in the dynamic topography of Figure IV-6. This pattern of flow is undoubtedly strongly influenced by the overall basin geometry. The upward slope of the 25.5 σ_t surface towards the eastern coast is consistent with equatorward flow of the Gulf Water along Sonora and Sinaloa which becomes increasingly sluggish towards the south. The reversal in slope of the 25.5 σ_t surface in the

Figure IV-7

Temperature-salinity plot from bottle cast data taken along section 10 at the sill between the central and northern Gulf. The fields enclosed by the heavy lines are those shown on Figure IV-4 indicating that only Gulf Water and Subtropical Subsurface Water are present along this line.

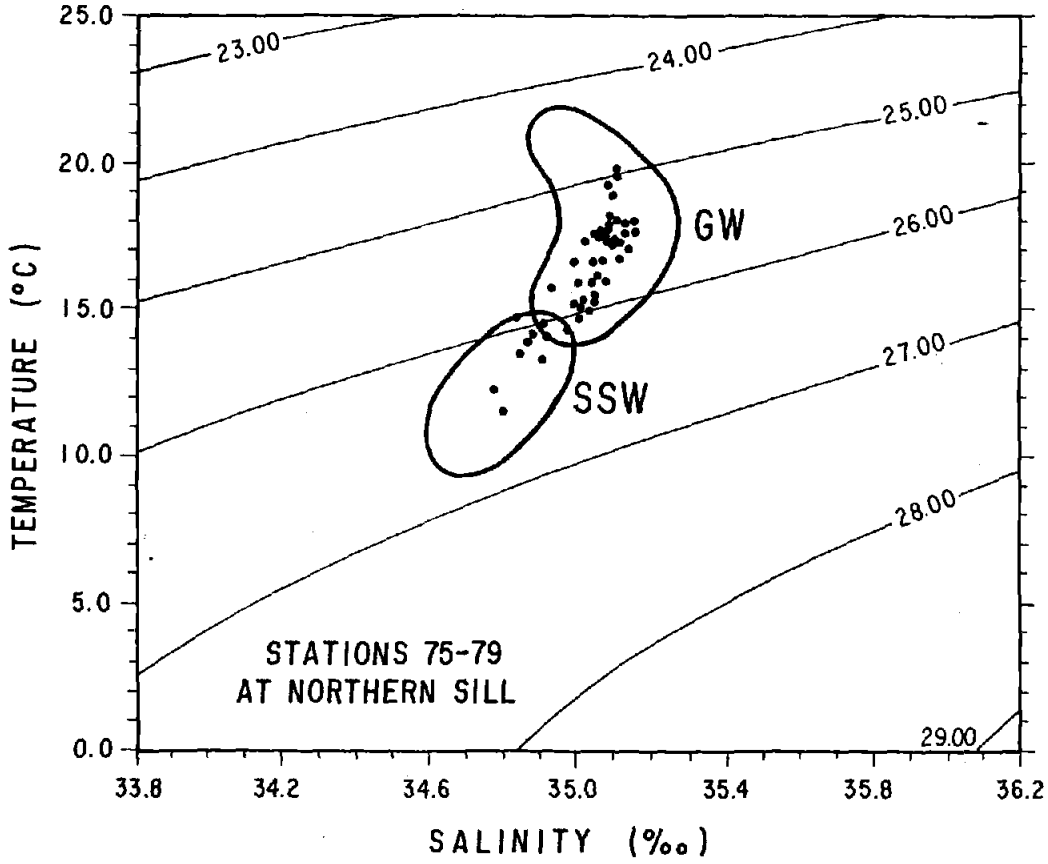
25.0
20.0
15.0
10.0
5.0
0.0
TEMPERATURE (°C)
23.00
24.00
25.00
26.00
27.00
28.00
29.00
GW
SSW
STATIONS 75-79
AT NORTHERN SILL
33.8
34.2
34.6
35.0
35.4
35.8
36.2
SALINITY (‰)

Figure IV-7

Figure IV-8

Depth to the 25.50 σ_t surface during March, 1983, contoured every 10 m from bottle cast data. This density surface approximates the depth of the core of the Gulf Water (see Fig. IV-8) and also represents the deformation of the lower section of the main pycnocline.

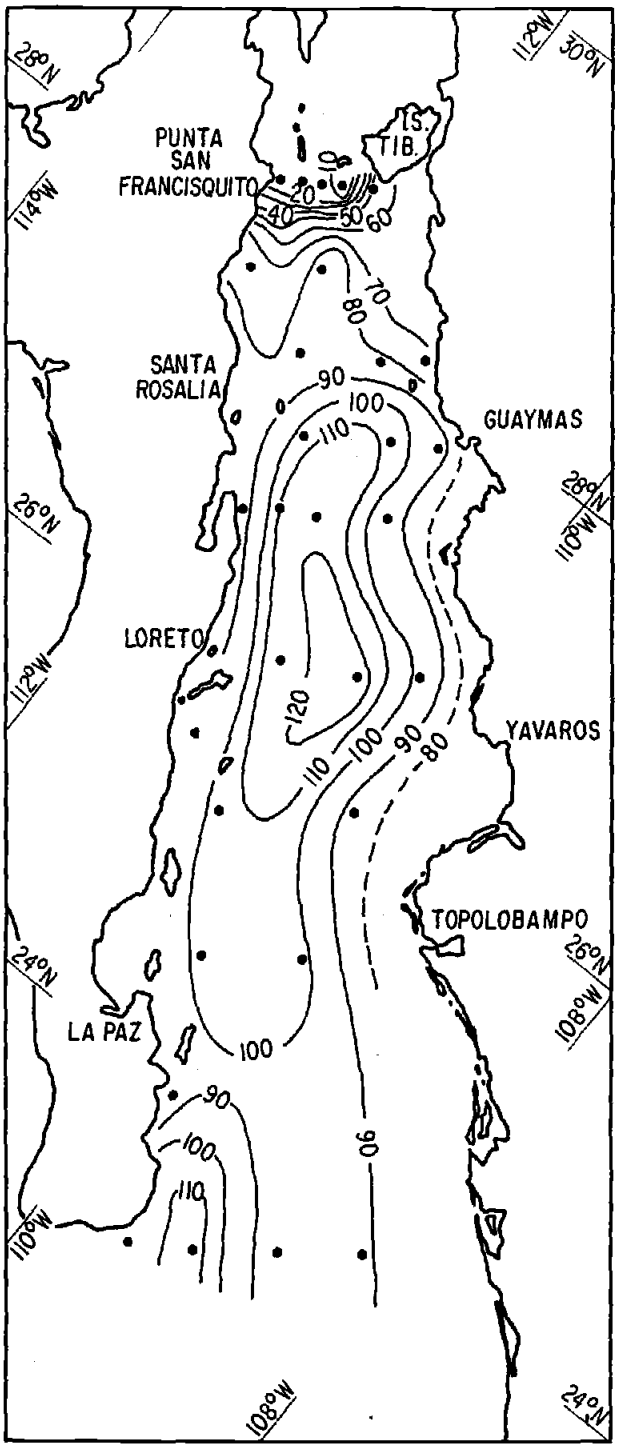

DEPTH TO THE 25.5 σ_t SURFACE
(METERS)

Figure IV-8

central Gulf (upwards towards the western boundary) indicates poleward advection along Baja California from La Paz to Santa Rosalia and again seems to be controlled by the basin geometry (cf. Fig. IV-1).

The salinity cross-sections of Figure IV-9 provide a graphic representation of the gradual erosion of the high-salinity core of Gulf Water by increased mixing towards the south. In this figure, the Gulf Water is shown by the dark pattern indicating salinities greater than 35 ppt. In the two northernmost sections (9 and 10), the Gulf Water occupies the entire water column above roughly 200 m. Off Guaymas (section 7), the Gulf Water is overriden by the lower salinity and warmer water along the western half of the Gulf, but still covers the eastern margin. Further south, but still in the central Gulf (section 5), the Gulf Water is completely blanketed by the warm, low-salinity water of the modified Tropical Surface Water and is detached from the eastern margin. Within the southern Gulf, the high-salinity water has thinned considerably and broken into separate cores (section 3) with water of salinities greater than 35 ppt only found hugging the eastern margin at the entrance (section 1). It is interesting to note that California Current Water is found only along section 1 as a low-salinity subsurface core in the western half of the entrance. Note also that there are two other relatively high-salinity cores (>34.8 ppt) on section 1, indicating remnants of Gulf Water.

The equatorward flow seen in Figure IV-6 indicates a geostrophic balance which would result from northwesterly winds over the Gulf producing an Ekman transport away from the eastern boundary to set up the necessary pressure gradient. Shipboard observation of the winds taken during the bottle casts (Fig. IV-10) indicate considerable temporal variability in the wind speed and direction up the Gulf. The strong wind events are generally northwesterly, but there are significant periods of light winds and backing to the southeast. The variability in the winds is generally consistent with the regional atmospheric pressure gradient from the Pacific to mainland Mexico represented

Figure IV-9

Cross-sections of salinity from selected transects across the Gulf taken from the STD profiles and bottle casts made during March, 1983. Shaded areas show salinities greater than 35 ppt and indicate the area occupied by Gulf Water along each section. See Figure IV-2 for locations of the sections.

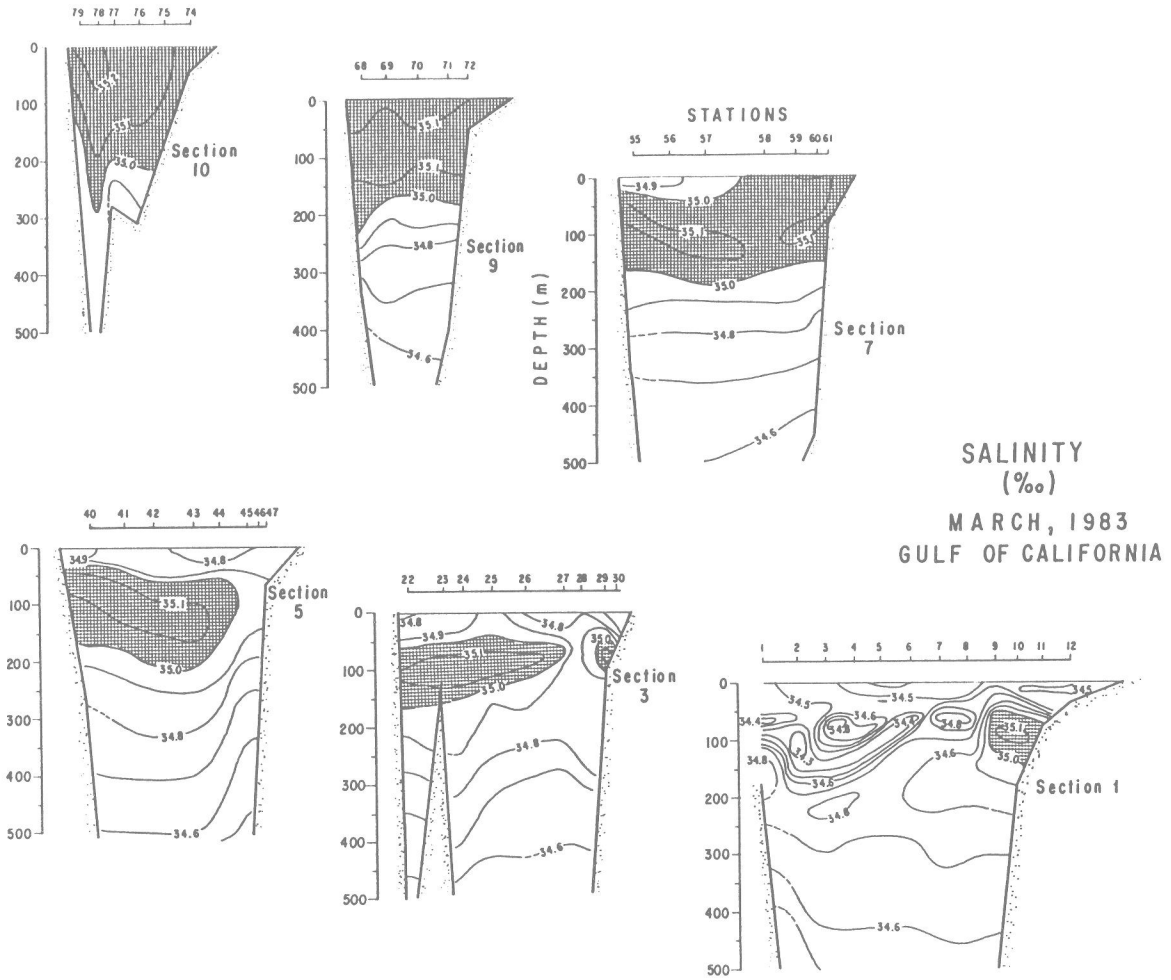
STATIONS
DEPTH (m)
Section 10
Section 9
Section 7
Section 5
Section 3
Section 1
SALINITY
(‰)
MARCH, 1983
GULF OF CALIFORNIA

Figure IV-9

Figure IV-10

Wind vectors taken from shipboard observations at bottle cast stations on cruise 8303. Wind speed scale shown to right of figure in meters per second. Hour and day of observation are shown next to each station position.

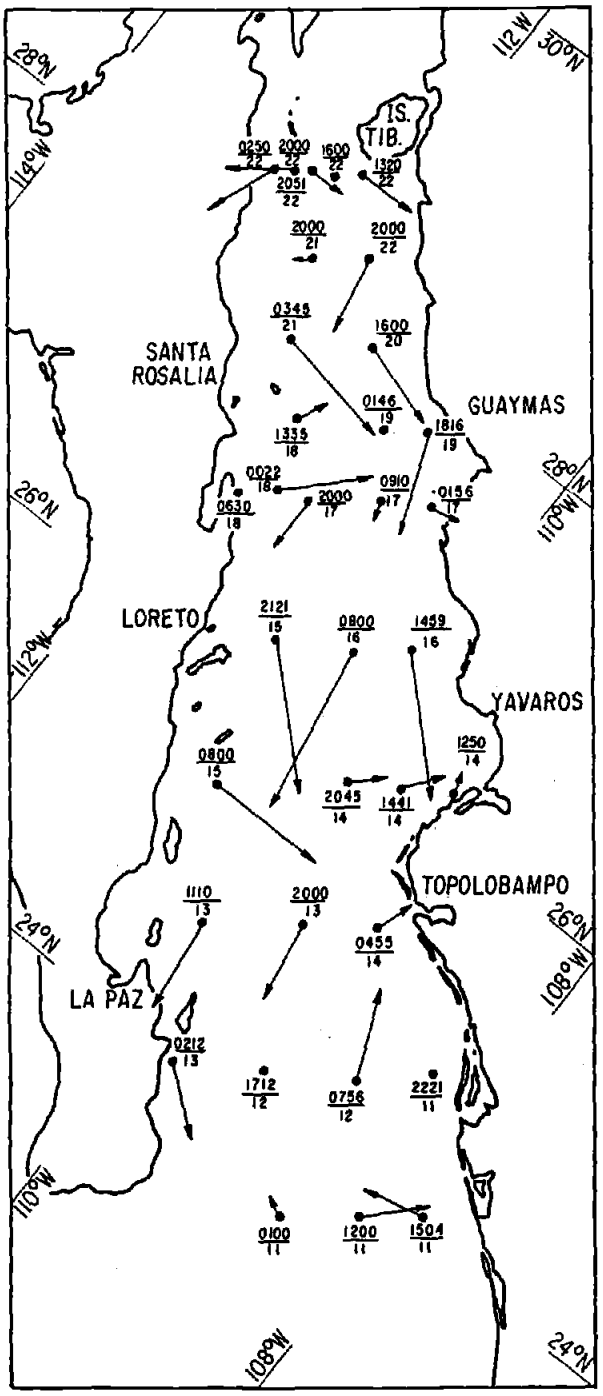

SHIPBOARD WIND OBSERVATIONS
MARCH, 1983

Figure IV-10

by the pressure differences between Guadalupe Island off Baja California and Hermosillo, Sonora (Fig. IV-11). The strongest winds were measured on March 15 and 16 when there should have occurred a maximum in the gradient wind. The pressure series indicates the maintenance of a regional wind field consistent with the observations of northwesterly winds during spring conditions, but with significant departures from northwesterly winds such as occurred prior to the cruise period (March 3 and 4) when a strong low-pressure trough penetrated south over northern Baja California (observed from daily surface analysis charts prepared by NOAA). The smaller scale deviations in Figure IV-11 suggests variability in the strength of northwesterly winds over periods of roughly 7 to 10 days.

PHYTOPLANKTON PRODUCTION, BIOMASS AND PHYSICAL PROCESSES

Rates of primary production averaged over the depth of the euphotic zone (i.e., averages of the individual values at the 100, 75, 50, 25 and 1% light depths) ranged from just above 35 to slightly below 160 mg C m^{-3} d^{-1} throughout the sampling area in the central and southern Gulf during March of 1983. Figure IV-12 is a plot of these averaged primary productivity values against the corresponding concentrations of chlorophyll a measured at each station. The chlorophyll values represent similarly averaged concentrations from the individual samples at each light level and provide an estimate of the phytoplankton biomass in the euphotic zone. Primary production is the product of the agal growth rate and the algal biomass. The relationship between the averaged primary productivity and chlorophyll ($R^2 = 0.97$) thus suggests that the variation in productivity over the Gulf is strongly dependent upon the algal standing stock while the growth rate remains relatively constant.

Figure IV-11

Time series of the difference in atmospheric pressure at sea level between Guadalupe Island and Hermosillo, Sonora. The series begins with March 1 and covers the period of cruise 8303. This is used to estimate the behavior of the large-scale wind field affecting the Gulf of California.

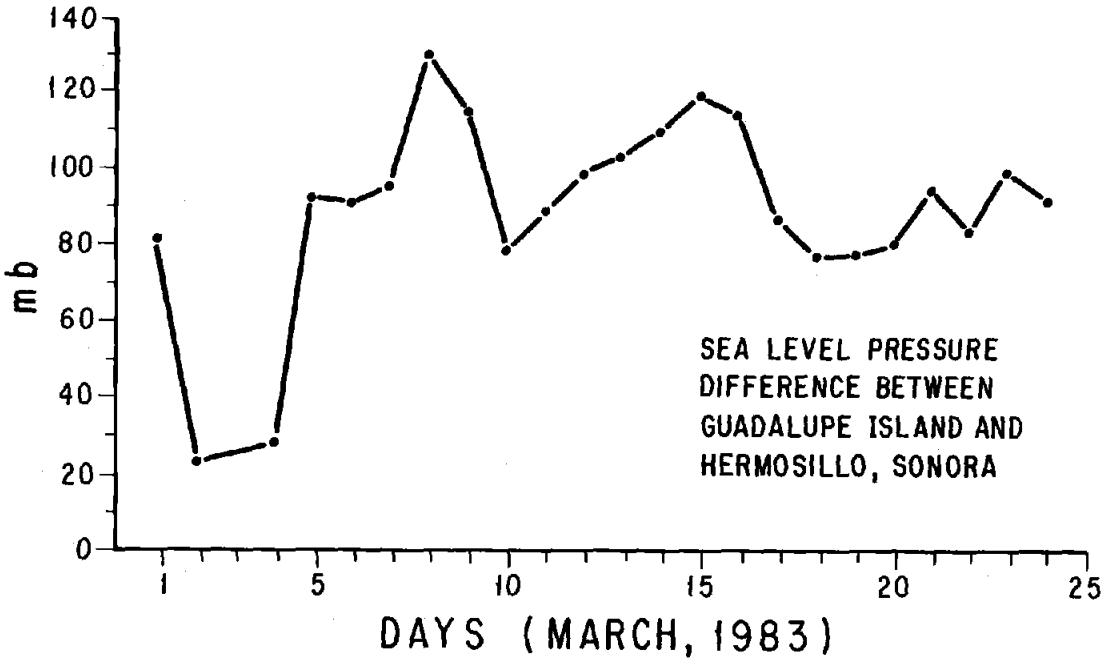
140
120
100
80
60
40
20
0
mb
1
5
10
15
20
25
DAYS (MARCH, 1983)
SEA LEVEL PRESSURE
DIFFERENCE BETWEEN
GUADALUPE ISLAND AND
HERMOSILLO, SONORA

Figure IV-11

Figure IV-12

Primary productivity plotted against chlorophyll a concentrations measured during March, 1983. Productivity and chlorophyll values are averages of the measurements taken at the 100, 75, 50, 25, and 1% light depths. Station numbers (see Fig. IV-2) are shown in parentheses next to each data point. Station 50 not included because of lack of chlorophyll data.

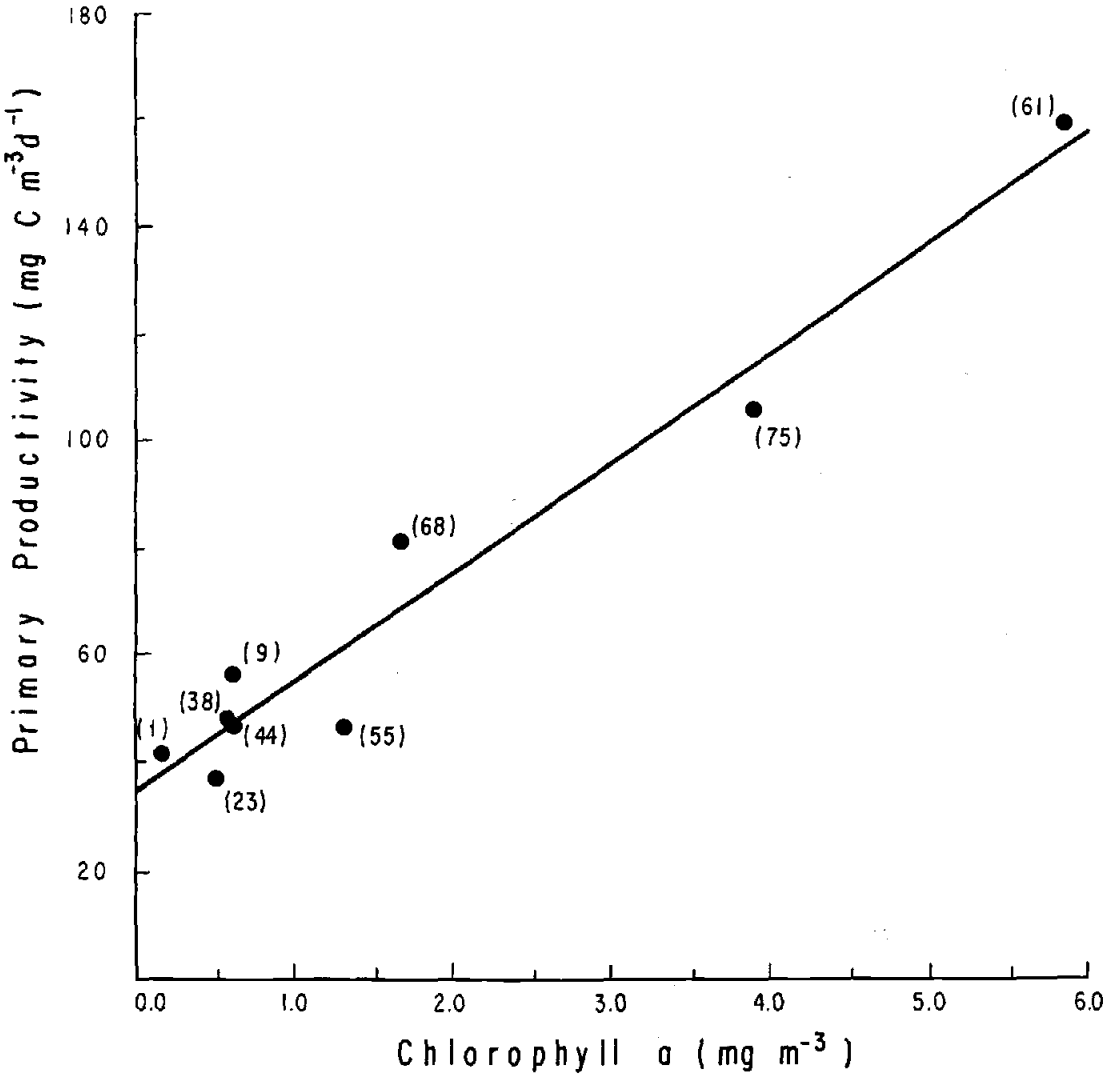
180
140
100
60
20
Primary Productivity (mg C m^{-3}d^{-1})
0.0
1.0
2.0
3.0
4.0
5.0
6.0
Chlorophyll a (mg m^{-3})
(61)
(75)
(68)
(9)
(38)
(1)
(44)
(55)
(23)

Figure IV-12

A similar relationship is reported by King (1986) for a roughly 5-degree square within the eastern tropical Pacific. He points out that only a small portion of the variance in the primary production there is attributed to the algal growth rate. King (1986) further demonstrated that variation in both chlorophyll and primary production is closely related to the flux of nutrients into the mixed layer by comparing productivity and chlorophyll concentrations with the rates of supply of nitrate. His analysis shows that primary production is thus associated with the rates of transport of nutrients (not nutrient concentration) through variation in the phytoplankton biomass. The relationship seen in Figure IV-12 is consistant with a similar control over primary production in the Gulf.

Comparison of major coastal upwelling ecosystems has also demonstrated that differences in the magnitude and distribution of primary productivity is ultimately determined by the nutrient concentrations in the upwelling source waters and the rates of vertical transport of the nutrients (Barber and Smith, 1981; Codispotti et al., 1982; Dugdale, 1985). Eppley et al. (1979) have shown, for the coastal region off southern California, that variation in the vertical flux of nutrients leading to change in primary production is reflected by the variation in depth of the nutrient concentration gradient. The nutrient profiles made at the stations where productivity was measured in the Gulf allows us to examine this association between productivity and the depth of the nutricline.

Nutrient analyses were made for each light depth at which productivity and chlorophyll were measured. Figure IV-13 shows the primary productivity values plotted against the depth at which the phosphate concentrations reach 1.5 μM. This concentration is chosen to represent a value near the center of the gradient between the nutrient-poor surface waters and the enriched waters below the thermocline. The depth of the 1.5 μM concentrations of phosphate is estimated by linear interpolations

Figure IV-13

Primary productivity values plotted against the depth where the concentration of phosphate reaches 1.5 μM during March, 1983. This concentration represents a value near the center of the nutricline. Primary productivities calculated as averages over the euphotic zone as in Figure IV-12.

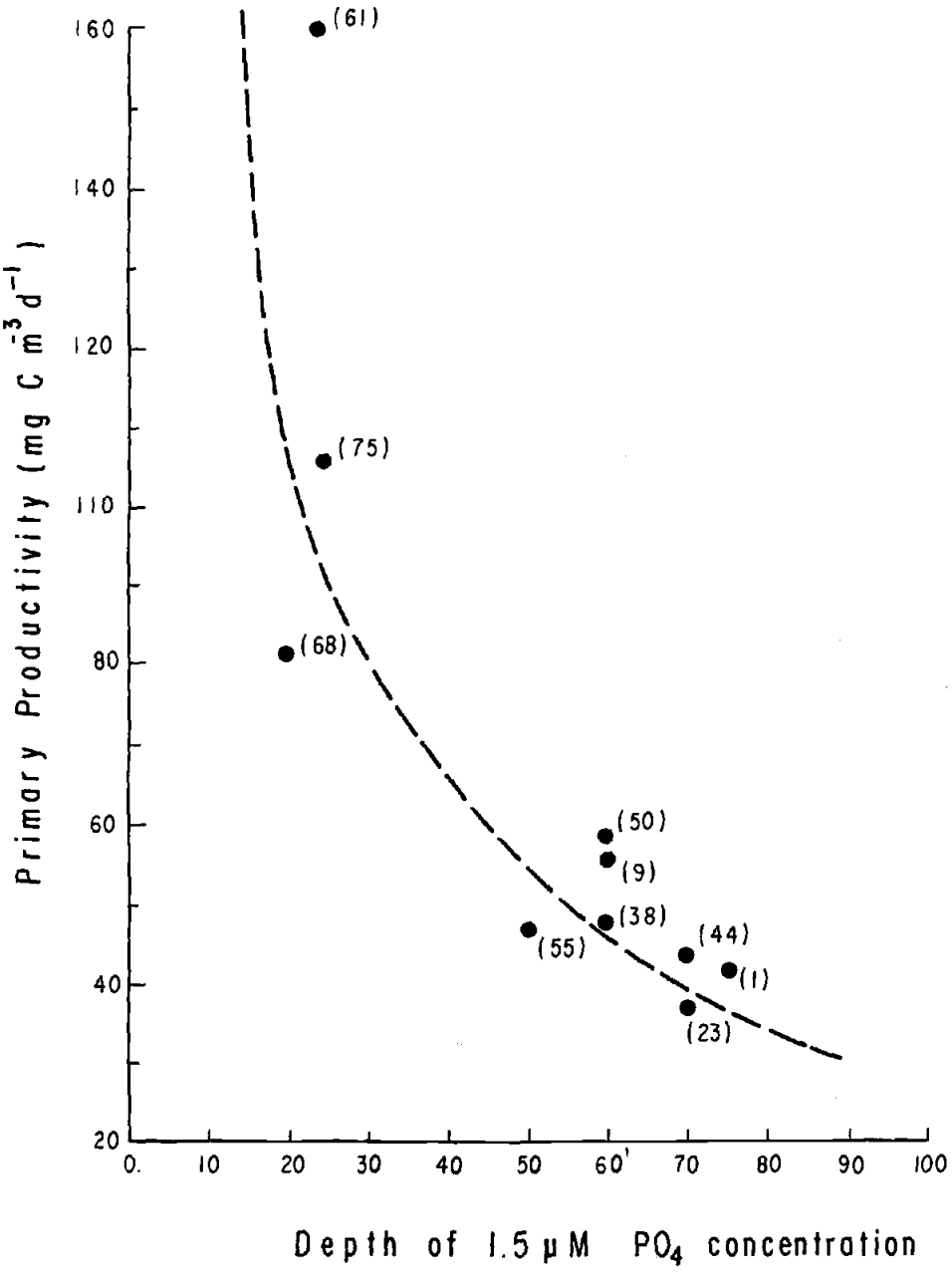
Primary Productivity (mg C m^{-3} d^{-1})
160
140
120
110
80
60
40
20
0.
10
20
30
40
50
60'
70
80
90
100
(61)
(75)
(68)
(50)
(9)
(38)
(55)
(44)
(1)
(23)
Depth of 1.5 µM PO_4 concentration

Figure IV-13

between the phosphate concentrations of the 10% and 1% light depths, or by downward extrapolation of the phosphate profile where the 1.5 μM concentration occurred below the 1% light level. Figure IV-13 suggests an exponential decrease in productivity with a linear increase in the depth of the nutricline. This relationship is consistent with Dugdale's (1985) argument that phytoplankton production varies nonlinearly with the input of nutrients. The higher nutrient concentration at shallower depths indicates an increase in the nutrient flux to the euphotic zone. This may occur by vertical advection causing an upward ridging or flexure of the nutricline in upwelling zones.

Figure IV-14a shows the distribution of total suspended matter (TSM) in mg/m^3 averaged over the upper 60 m of the water column. The TSM values were estimated from measurements of light transmission taken by continuous profiling with a 25-cm beam transmissometer. The linear regression between the mass of TSM and percent light transmission ($R^2 = 0.72$) is given in Figure IV-14b. Microscopic examination of filtered water samples shows that the near-surface suspended particulates are predominantly composed of living and dead phytoplankton cells, cell fragments and aggregates of amorphous organic material. Fluorescence profiles made by continuous pumping down to 70 m indicate the relative concentrations of chlorophyll and phytoplankton biomass. Figure IV-15 compares the shapes of the fluorescence profiles and those of light transmission made on separate casts at the same stations. These four stations were selected to represent the range in the fit between the shapes of the fluorescence and transmission profiles which varies from excellent (St. 62) to only fair (St. 43). Kiefer and Austin (1974) found a very good relationship between light transmission and phytoplankton fluorescence in the Gulf of California. They report a high correlation ($R = 0.96$) between the light attenuation coefficient and fluorescence. Transmission and the derived values for TSM can thus be used as reasonably good estimators of phytoplankton biomass. This is important since light transmission profiles are much simpler

Figure IV-14

(a) Distribution of total suspended mass (TSM) in mg/m^3, averaged over the upper 60 m of the water column for March, 1983. Values of TSM estimated from the calibration of the 25-cm beam transmissometer measurements with TSM measurements from filtered water samples. (b) Regression line through plot of TSM (mg/1) measurements taken from discreet water samples against % transmission observed at the depth of corresponding water sample. This relationship used to estimate distribution of TSM values from transmission profiles.

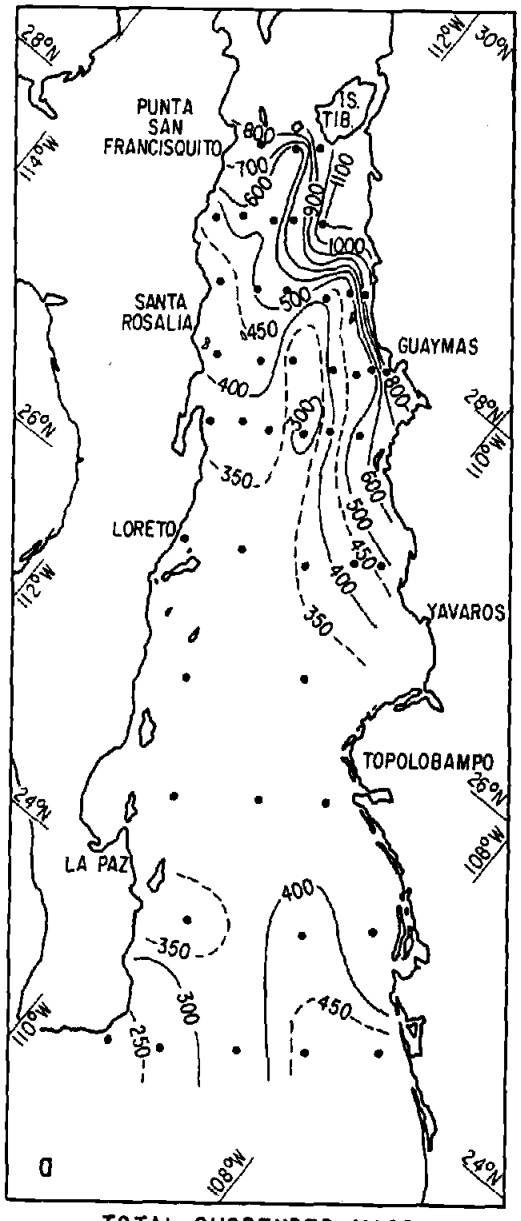

TOTAL SUSPENDED MASS
AVERAGED OVER 0-60 m DEPTH
(mg/m^3)

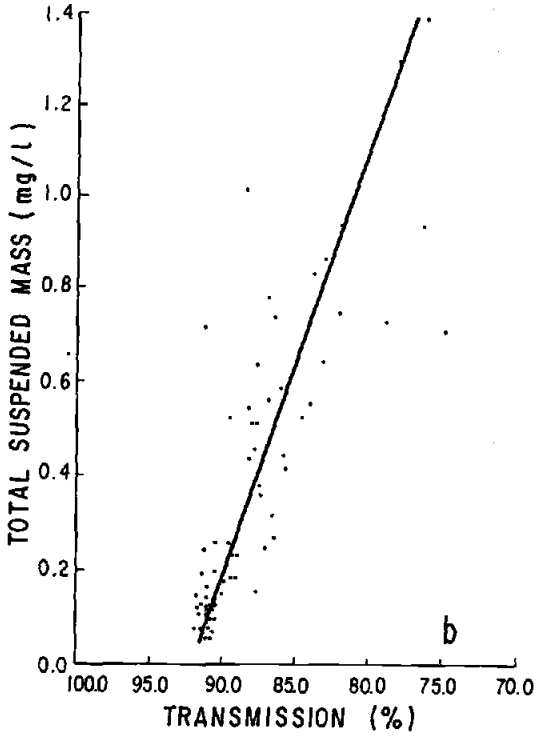

Figure IV-14

Figure IV-15

Comparison of profiles of % light transmission, fluorescence and temperature down to 70 m depth at four selected stations during March, 1983 (see Fig. IV-2 for locations). Fluorescence profiles obtained by pumping of water up to shipboard fluorometer. Temperature profiles obtained by sensor on data logger used to record transmission.

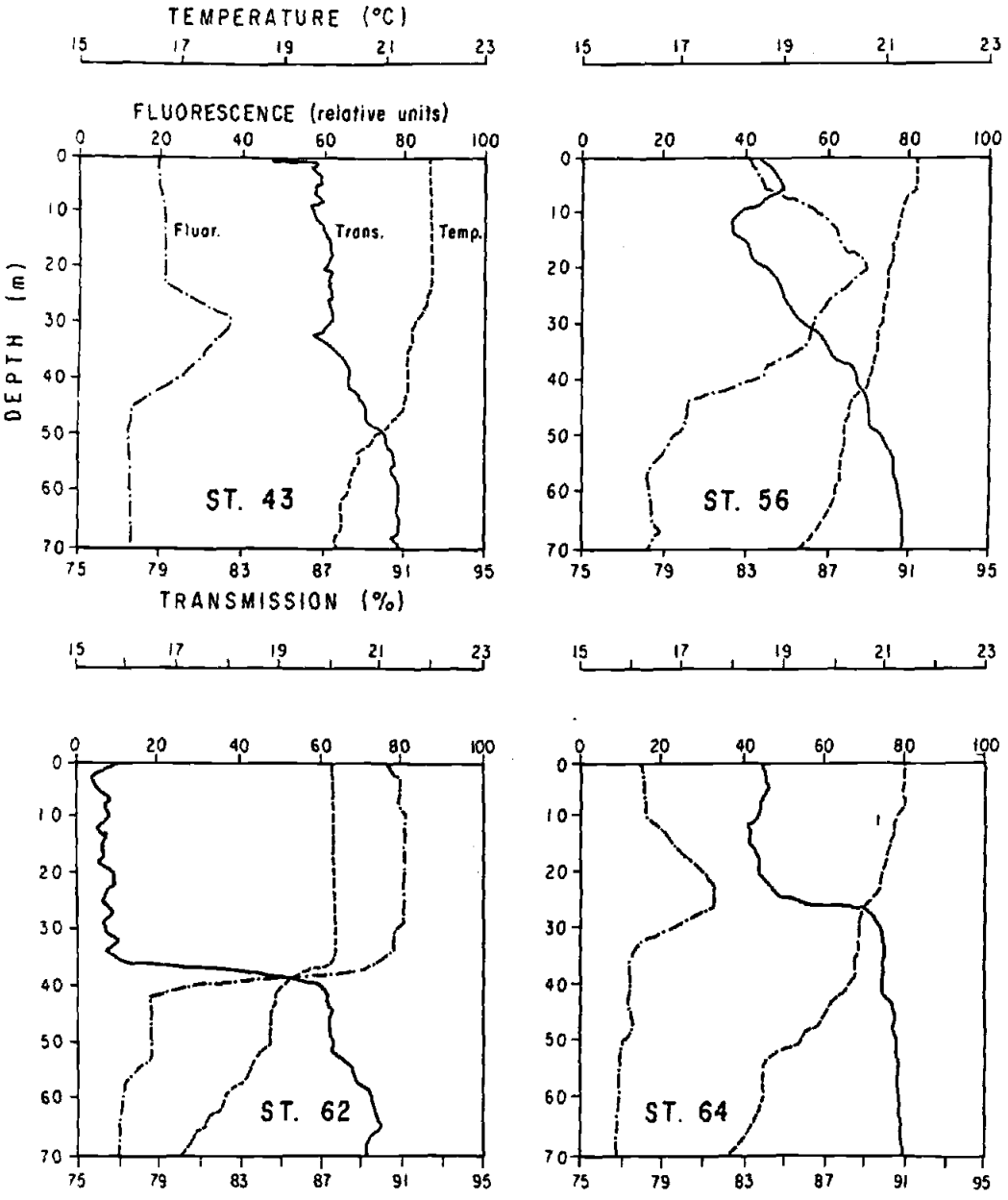
TEMPERATURE (°C)
FLUORESCENCE (relative units)
TRANSMISSION (%)
DEPTH (m)
Fluor.
Trans.
Temp.
ST. 43
ST. 56
ST. 62
ST. 64

Figure IV-15

to obtain than fluorescence profiles and there is much better coverage throughout the euphotic zone with the light transmission data.

Comparison of the pattern of distribution of the near surface TSM in Figure IV-14a, with the distribution of surface temperature and salinity in Figure IV-5 shows that the high concentrations of suspended particulates are associated with cooler, high-salinity water in the central Gulf. The highest particle concentrations (interpreted to be algal biomass) are found over the shelf south of Tiburon Island and along the shelf off Guaymas. The cleanest water is found south of La Paz at the entrance to the Gulf, associated with the highest temperature and lowest salinities. The pattern of lower particle concentrations follows the tongue of high-temperature, low-salinity water into the central Gulf. Comparison of the TSM distribution with the dynamic topography indicates that the ribbon of high particle concentrations is located along the eastern side of the coastal jet off Sonora. The lobe of high TSM extending southward off the shelf south of Tiburon Island appears to be associated with the trough in the dynamic topography which runs north-south between Santa Rosalia and Tiburon Island. This indicates a doming of the thermocline and the nutricline. Likewise, the northward penetration of low TSM values in the central Gulf is located over the northward extension of the ridge in dynamic topography where we expect to find a depression of the thermocline and nutricline (cf. Fig. IV-6, IV-8 and IV-14a). Thus the meander in geostrophic flow in the north central Gulf is mirrored in the near-surface particle field.

The association between the near-surface light transmission values and physical properties (at 10 m depth) are clearly shown on Figure IV-16 from the scatter plots of transmission at 10 m against σ_t, temperature and salinity at 10 m. At this depth, lower transmission and thus higher phytoplankton biomass is confined to water with salinities greater than 35 ppt and temperatures lower than 20.5°C, corresponding to σ_t values greater than approximately 24.5. The relationship between Gulf Water and increased

Figure IV-16

Percent light transmission measured at 10 m depth plotted against σ_t at 10 m, temperature at 10 m, and salinity at 10 m depth. Transmission values read from transmissometer profiles; temperature, salinity and σ_t obtained from bottle casts.

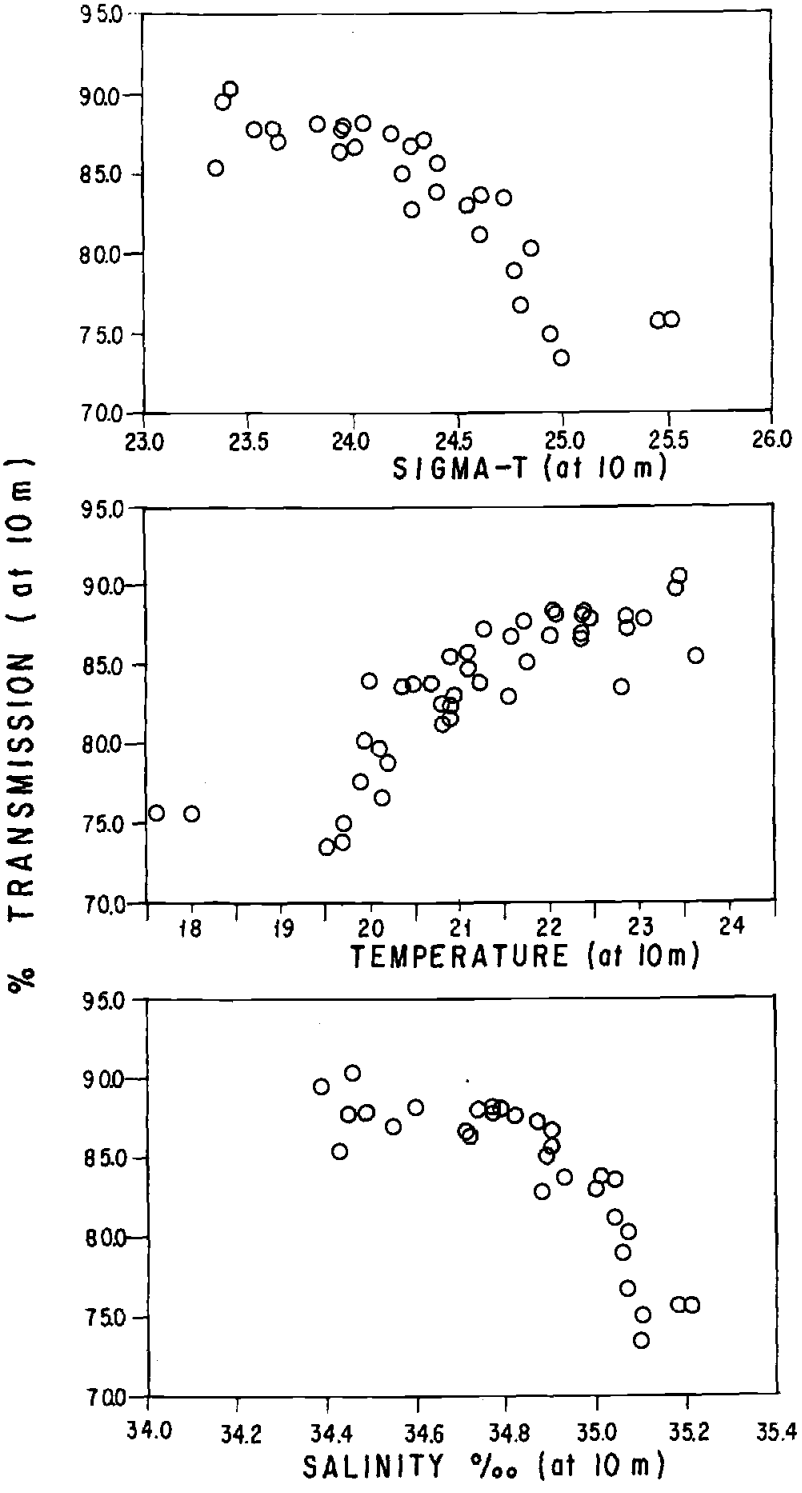
% TRANSMISSION (at 10 m)
95.0
90.0
85.0
80.0
75.0
70.0
23.0
23.5
24.0
24.5
25.0
25.5
26.0
SIGMA-T (at 10 m)
18
19
20
21
22
23
24
TEMPERATURE (at 10m)
34.0
34.2
34.4
34.6
34.8
35.0
35.2
35.4
SALINITY ‰ (at 10 m)

Figure IV-16

primary production, implied by Figure IV-16, is demonstrated by the plot of averaged primary production throughout the euphotic zone, against salinity at 10 m depth in Figure IV-17. The elevated values of primary production are all restricted to salinities above 35 ppt and increase dramatically with higher salinities which coincide with a greater contribution of Gulf Water.

Figure IV-18 shows the vertical distribution of temperature and transmission across the central Gulf along section 7. The temperature section (Fig. IV-18a) shows strong upwelling off Guaymas from a depth near the shelf break of 70 to 80 m. The upwelling depth reaches down close to the core of the Gulf Water (cf. Figs. IV-8 and IV-9). The highest value of primary production reported during March, 1983 was measured at the inshore station (St. 61) on this line. The high nutrient flux rates necessary for this elevated production thus appears to be a function of the high concentration of nutrients available within the Gulf Water.

The vertical distribution of TSM shown by the transmission section (Fig. IV-18b) shows a particle-rich surface layer above roughly 70 m. Very high particle concentrations are found over the shelf on the coastal side of the upwelling zone. The doming of the transmission values in the center of the Gulf represent a diminishing of TSM associated with the intrusion of the Tropical Surface Water (cf. Fig. IV-5) and the depression of the pycnocline in the center of the basin (Fig.IV-8). One of the most interesting features in Figure IV-18b is the bulge of particle-laden water centered near 300 m and extending out from the eastern slope. A smaller bulge occurs at the shelf break. These deeper particle-rich zones appear to be regions where the bottom nepheloid layer has detached from the margin by advection or diffusion. The composition of the particles within these regions are fine amorphous organic material and phytoplankton remains which reflect the "excess" of primary productivity which is exported from the euphotic zone of the coastal upwelling system by sinking over the shelf and

Figure IV-17

Primary productivity plotted against salinity at 10 m observed at corresponding stations during March, 1983. Station numbers are shown in parentheses next to each data point. Primary productivities are average values over the euphotic zone. Salinities taken from STD profiles where bottle data unavailable.

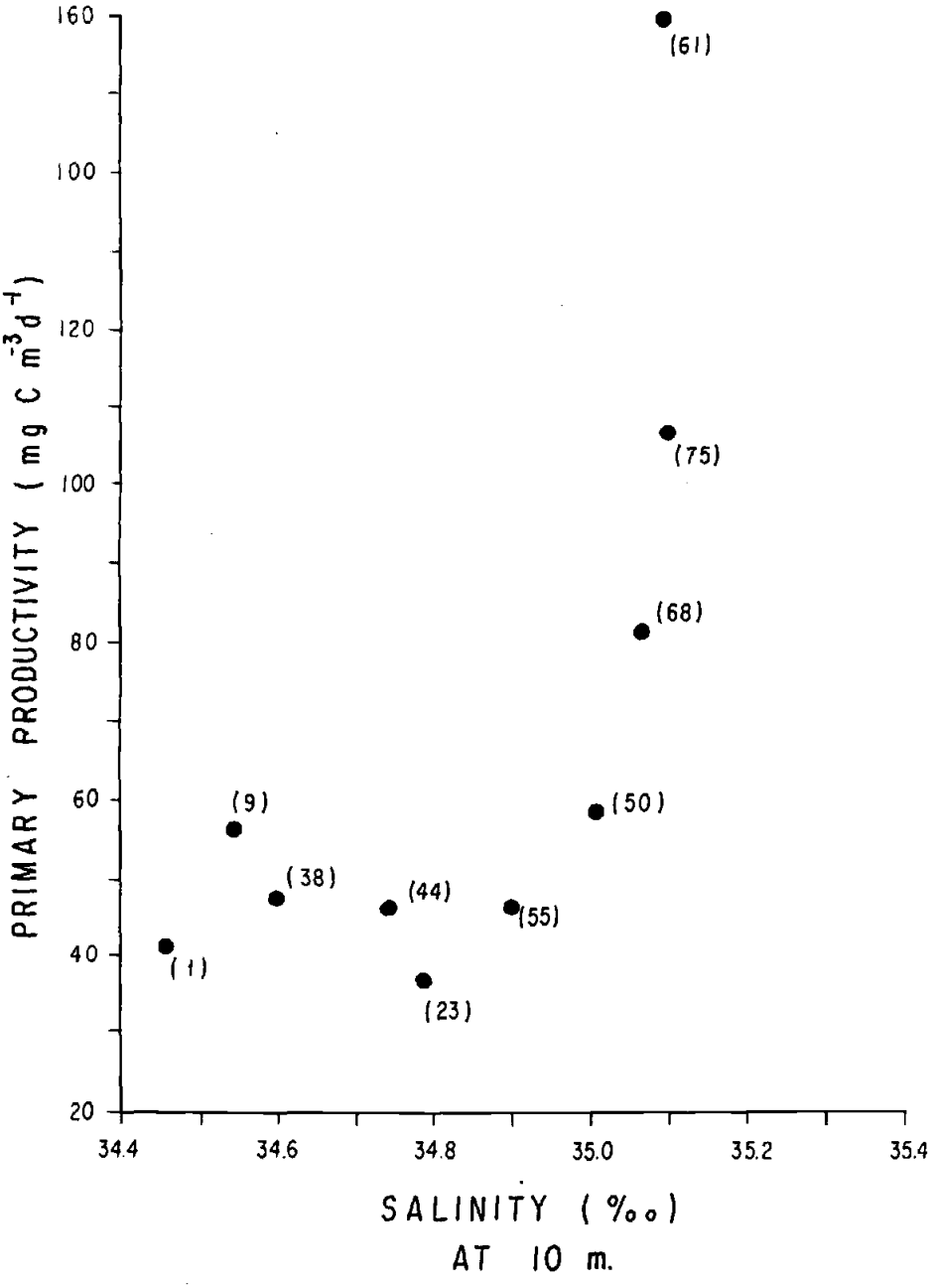
160
100
120
100
80
60
40
20
PRIMARY PRODUCTIVITY (mg C $m^{-3}d^{-1}$)
(61)
(75)
(68)
(9)
(50)
(38)
(44)
(55)
(1)
(23)
34.4
34.6
34.8
35.0
35.2
35.4
SALINITY (‰)
AT 10 m.

Figure IV-17

Figure IV-18

(a) Cross section of temperatures made along section number 7 during March, 1983. This section is located off Guaymas. Temperatures measured with sensor on transmissometer data logger providing simultaneous record of transmission and temperature. (b) Corresponding cross-section of % transmission made along line 7 during March 1983.

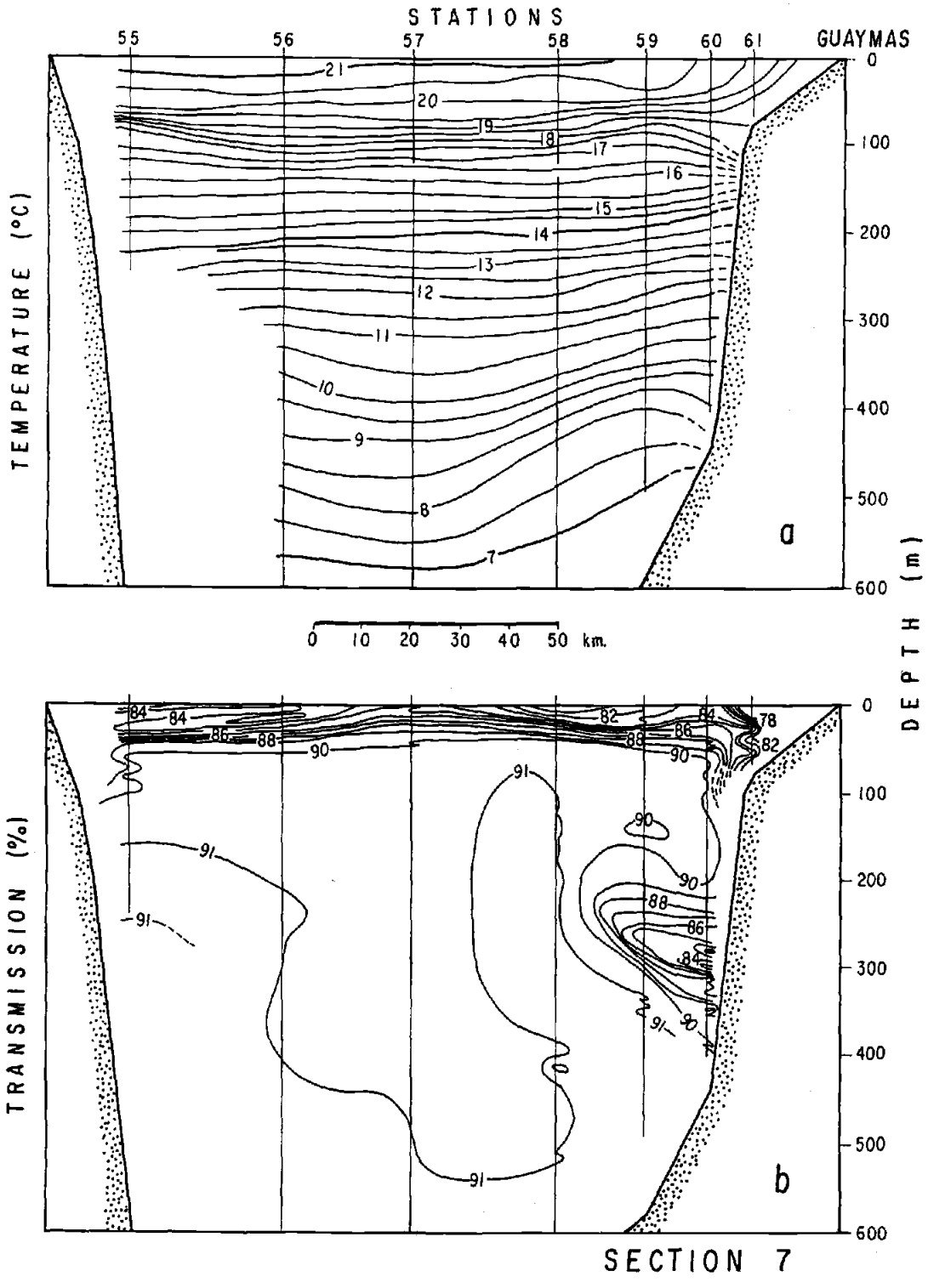
STATIONS
55
56
57
58
59
60
61
GUAYMAS
TEMPERATURE (°C)
21
20
19
18
17
16
15
14
13
12
11
10
9
8
7
a
0
100
200
300
400
500
600
DEPTH (m)
0 10 20 30 40 50 km.
TRANSMISSION (%)
84
86
88
90
91
82
78
b
SECTION 7

Figure IV-18

upper slope (Baumgartner and Ferreira, in preparation). These intermediate layers at the shelf break, and at 300 m, are well developed along the Sonoran margin. The 300 m layer can be traced from south of Tiburon Island (section 9) to north of Topolobampo (section 4).

The intermediate depth particle-rich layers appear to represent the fraction of "new" production of the coastal upwelling system. Phytoplankton production has been partitioned into "new" and "regenerated" production by Dugdale and Goering (1967). New production is defined by the portion which results from the injection of preformed nutrients into the euphotic zone, while regenerated production is that which is sustained by nutrient recycling from grazing and excretion of organic compounds by zooplankton and other heterotrophs of the food web in the upper ocean. Eppley et al. (1979) have pointed out that for steady state conditions, new production is that fraction which is exported from the euphotic zone by sinking. They note that a high ratio of new to total production would mean that only a small part is cycled through heterotrophs and a correspondingly high proportion is due to nutrient input. The high flux of material out of the euphotic zone, suggested by the strong development of the particle-rich layers extending off the shelf and upper slope, is thus consistent with the relationship between nutrient input and productivity inferred from Figures IV-13 and IV-17.

COMPARISONS WITH EASTERN BOUNDARY SYSTEMS

The biological response of the Gulf of California to El Niño can probably be best understood by first considering the effect of El Niño upon the eastern boundary systems of the Pacific. The biological richness of these regions stems from the interaction of mesoscale and basin-wide physical processes which feed primary nutrients into the near-surface, light-rich layer. The underlying reason for the enhanced productivity of the eastern boundary systems is the basin-wide tilt of the thermal structure

of the ocean maintained by the large-scale, wind-driven gyral flow (Reid et al., 1978; Barber and Chavez, 1983). This tilt is most strongly marked along the equator where the thermocline progressively deepens westward from the accumulation of warm water in the western Pacific as a response to the easterly tradewind field (Meyers, 1979; Wyrtki, 1985). Therefore, the large-scale zonal easterlies and meridional equatorward winds, paralleling the continental borders, set-up the basin-wide tilt which brings nutrient-rich water below the thermocline near enough to the surface along the eastern boundaries so that it can be entrained by local processes responsible for vertical transport. One of the more important of these is coastal upwelling which is a mesoscale response to the local equatorward alongshore winds embedded within the large-scale subtropical anticyclones. The coastal upwelling off Peru, for example, typically occurs within a 50 km band offshore and lifts water from depths of 40 to 80 m (Barber and Smith, 1981).

El Niño decreases the primary productivity off Peru by depressing the thermocline below the depths from which nutrient-rich water is normally available for entrainment by upwelling processes (Barber and Chavez, 1983) even though the coastal winds remain upwelling favorable over most of the Peru coast (Enfield, 1981; Wyrtki, 1975). Deepening of the thermocline and nutricline off California during 1983 also resulted in a drastic reduction of productivity offshore (McGowan, 1984). A principal cause for deepening of the thermocline along the coast of western North and South America is the poleward propagation of downwelling Kelvin wave fronts trapped along the coast (McCreary, 1976; Enfield and Allen, 1980). The coastally-trapped Kelvin waves are generated at the equator by the arrival of equatorial Kelvin waves excited by weakening and reversal of the equatorial tradewinds over the central Pacific during the onset and development of El Niño. The deepening of the thermocline is spread offshore from the eastern boundary by slower, westward travelling Rossby waves (O'Brien et al., 1981).

The increase in sea level height throughout the eastern Pacific is a reflection of the widespread thickening of the surface layer associated with depression of the thermocline towards the coastal boundary (Wyrtki, 1985). The rapid poleward propagation of positive sea level anomalies during the development of El Niño shown by Enfield and Allen (1980) and Chelton and Davis (1982) is consistent with the speed of a Kelvin wave.

It has also been observed that the depression of the thermal structure (and the nutricline) within the California Current may occur by anomalous onshore Ekman transport (Chelton, 1981; McLain and Thomas, 1983) occurring with El Niño and, occasionally, in anti-El Niño years. Simpson (1984a,b) argues that the 1982-1983 El Niño in the California Current resulted from direct wind forcing rather than by remote forcing from Kelvin wave propagation. The subsequent onshore Ekman transport, decreased upwelling and increased flow in the California Countercurrent would then be responsible for the thermal anomalies.

Whatever the reason responsible for deepening of the thermocline along the coastal boundary during El Niño years, it has important consequences for the geostrophic balance within the coastal current systems. Initiation of a downward tilt of the thermocline towards the coast requires a dynamic adjustment which results in the poleward advection of water along the eastern boundary (McCreary, 1976). This is consistent with McLain and Thomas' (1983) observation of the increased flow of the California Countercurrent during El Niño years.

Robles and Marinone (in press) demonstrate that the main pycnocline within the central Gulf was much deeper than normal by March 1983. However, primary productivity in the central Gulf during this period reached historically high values (Valdez-Holguin, 1986). This appears to be the opposite response expected from comparison to the Peru and California Current systems. It is then reasonable to ask, why should we

observe high productivity when the thermal structure is depressed as off Peru and California?

First, it is important to remember that the breadth of the eastern boundary currents is significantly greater than the width of the Gulf of California. Nutrient enrichment and enhanced productivity may extend 400 km offshore off Peru during normal conditions (Barber and Chavez, 1983), while the high-productivity axis in the California Current is between 100 and 200 km offshore (Bernal, 1981). Chelton (1982) has also pointed out that the offshore productivity in the California Current north of about 31°N arises from Ekman pumping driven by the wind stress curl and is not a coastal upwelling phenomenon. McGowan (1984) indicated that although the near-surface waters were devoid of nutrients between 50-300 km offshore during April 1983, the onshore region exhibited near-normal plankton distributions. Barber and Chavez (1983) show that during much of the 1982-1983 El Niño, a narrow band of nutrient enrichment and normal concentrations of phytoplankton biomass was also present against the coast, coinciding with a 30-50 km strip of coastal upwelling. This narrow strip of production was gradually reduced and disappeared, however, by May 1983, during the maximum thermocline depression.

SCALES OF FORCING AFFECTING THE GULF OF CALIFORNIA

To explain the differences noted between the Gulf and the eastern boundary systems, we should consider the nature and scales of the dominant oceanic processes affecting the Gulf. The results of this study, combined with earlier work of Baumgartner and Christensen (1985) and Robles and Marinone (in press), suggest that three scales of physical forcing interact to control the patterns and levels of primary production in the Gulf during El Niño episodes. These are (1) the basin-wide scale of remote forcing associated with the El Niño/Southern Oscillation phenomenon, (2) an

intermediate scale of ocean response, still large compared to the size of the Gulf of California, which is associated with the regional wind field, and (3) a local or meso-scale forcing manifested by the narrow band of coastal upwelling.

The basin-wide ENSO forcing results in the deepening of the thermal structure by at least 100 m in the Gulf (Robles and Marinone, in press). The dynamic adjustment required by the deepening of the thermal structure from this large-scale, remote forcing also produces anomalous or intensified poleward advection of Tropical Surface and Subtropical Subsurface Water along the coast of Central America and southern Mexico within the Costa Rica Current as suggested by Baumgartner and Christensen (1985). The penetration of Tropical Surface Water into the central Gulf during March 1983 is now well documented by this work and in Robles and Marinone (in press). This contrasts with the absence of the Tropical Surface Water mass in the Gulf under similar seasonal conditions but within an anti-El Niño period as shown from Figure IV-4. Note that the upward tilt of the pycnocline (Fig. IV-8) toward Baja California is consistent with poleward advection. This tilt is not produced by wind forcing but rather indicates the impingement of the poleward flow against the western boundary of the Gulf. If this western boundary were removed the reversal in slope of the pycnocline (now observed in the sections across the Gulf) would not exist.

The deepening of the thermal structure along the eastern boundary is mirrored by the anomalous rise in coastal sea level during El Niño episodes (Wyrtki, 1985). Figure IV-19 shows the behaviour of monthly sea level at Guaymas over the five-year period from 1980 through 1984. The variability in the upper curve contains both the component of the annual cycle as well as the component due to the ENSO forcing. The lower curve is the sea level anomaly which remains after removing the annual cycle. This has been done by subtracting the long-term mean for each month (calculated for 1952-1984) from the corresponding monthly sea level value in the upper curve. The rapid rise in

Figure IV-19

Variation in sea level measured at Guaymas from 1980 through 1984. The upper curve shows the deviation of monthly averages of sea level height from the long-term mean calculated between 1952 and 1984. Note the component of the annual cycle of sea level in the upper curve. The lower curve shows the sea level anomaly after subtracting the long-term (1952-1984) averages for each individual month. This is done to remove the effect of the annual cycle. The sea level anomalies are given in units of standard deviation from the long-term mean anomaly calculated over the 1952-1984 period.

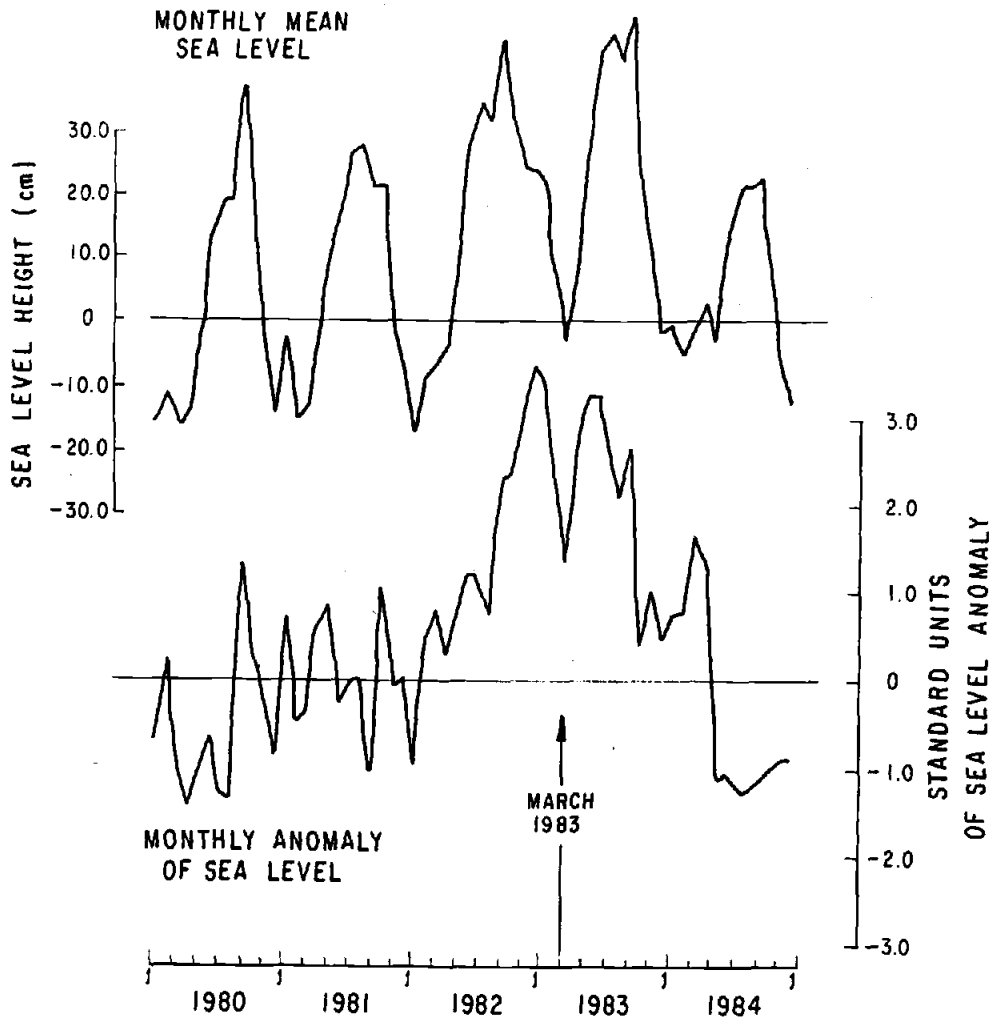
MONTHLY MEAN
SEA LEVEL
SEA LEVEL HEIGHT (cm)
30.0
20.0
10.0
0
-10.0
-20.0
-30.0
MONTHLY ANOMALY
OF SEA LEVEL
MARCH
1983
3.0
2.0
1.0
0
-1.0
-2.0
-3.0
STANDARD UNITS
OF SEA LEVEL ANOMALY
1980
1981
1982
1983
1984

Figure IV-19

the sea level anomaly between September and December 1982 indicates a correspondingly abrupt deepening of the thermocline along the eastern boundary which would lead to an anomalous increase in the poleward advection along the coast. The large positive sea level anomaly persisted through the autumn of 1983, but was interrupted by a sharp dip centered over March, 1983. However, even the minimum sea level anomaly observed during spring, 1983 was still of a large positive amplitude and comparable to the sea level anomalies at Guaymas during past El Niño's. For example, the monthly anomalies during the 1957-1958 episode ranged from approximately 0.8 to 2.6 standard units on the scale of the anomaly curve in Figure IV-19.

The biological response to the ENSO related forcing is apparent in the distribution of primary productivity and phytoplankton biomass during March, 1983. The region of the Gulf covered by the least altered Tropical Surface Water during this period exhibited uniformly low values of primary productivity (Fig. IV-17) and low biomass (Fig. IV-14). The lower values of primary productivity in the Tropical Surface Water were associated with a considerably deeper nutricline (Fig. IV-13) than the areas of high productivity. It should also be pointed out that although there exists a considerable upward tilt of the pycnocline towards Baja California in the central Gulf, the productivity and biomass along the peninsula are still low to moderate within that zone. This can be explained by the lack of local wind driven coastal upwelling along the western margin which would feed nutrient-rich subsurface Gulf Water (Fig. IV-9) from the depth of the pycnocline into the surface layer. The slightly increasing biomass along the western margin north of Loreto (Fig. IV-14a) probably reflects the steepening of the slope of the pycnocline and increasing rate of vertical nutrient flux, although it is still much lower than along the Sonoran shelf which is under the influrnce of wind-driven coastal upwelling.

In addition to the significant interannual variability in the ocean climate, apparent from the sea level anomalies in Figure IV-19, the mean sea level (upper curve) exhibits a strong annual cycle associated with the seasonal change in hydrographic regime from winter-spring to summer-fall. This variability is due principally to the intermediate or "regional" scale forcing related to changes in the wind field over the subtropical eastern Pacific and the Gulf of California. Strengthening and expansion of the Aleutian Low during winter produces a southeastward displacement of the subtropical anticyclone (Namias, 1974). During this period, the coastal northwesterly winds increase over northwestern Mexico and the Gulf of California. The winds continue to increase in the spring (Roden, 1972a) with the intensification of the North Pacific high pressure before its northward summer migration. The southeasterly winds which occur during summer and early autumn over the Gulf of California appear to be a response to the northward migration of the North Pacific high pressure and regional thermal patterns developed over the southwestern United States and northwestern Mexico (Hales, 1974).

Comparison of the surface geostrophic flow between winter-spring and summer-fall seasons presented by Rosas-Cota (1977) shows a clear reversal, with flow to the north during summer-fall (1957, 1965) and to the south during winter-spring periods (1956, 1957, 1963). This seasonal reversal in geostrophic flow can be inferred from the annual cycle of sea level height at Guaymas (Fig. IV-19, upper curve). The seasonal variation in coastal sea level itself reflects a change in the slope of the sea surface away from the coast, produced by the change from offshore to onshore Ekman transport between winter-spring and summer-fall. Roden (1972a) has shown, for example, that the offshore transport during late spring of 1970 was coherent for several hundred kilometers offshore from central California to 20°S. This included both inside the Gulf of California as well as off the Pacific coast of Baja California. The pattern of divergence and convergence off Baja California and within the Gulf would produce a

regional scale tilt in the pycnocline which is much greater than the radius of deformation (less than 30 km off Guaymas) associated with local mesoscale coastal upwelling.

The maps of dynamic heights (Fig. IV-6) and the depth of the 25.5 σ_t surface (Fig. IV-8) indicate that the equatorward geostrophic flow of the Gulf Water was associated with a tilt in the density structure toward the eastern coast which is also significantly greater than the radius of deformation. The scale of the offshore tilt to the pycnocline seen on Figure IV-8 extends to over 70 Km between Yavaros and Loreto. The seasonal minimum in the monthly mean sea level centered over March 1983 (Fig. IV-19, upper curve) is consistent with the southward flow and the regional scale upward slope of the pycnocline towards the mainland observed during cruise 8303. In effect, there appears to have been a seasonal override of the El Niño scale forcing. The basin-wide forcing associated with El Niño does not appear to have disrupted the normal pattern of northwesterly wind flow over the central Gulf (Figs. IV-10 and IV-11). This intermediate seasonal scale had important biological consequences in producing a large-scale tilt to the pycnocline to bring the nutricline within reach of entrainment by the more local scale coastal upwelling processes along the Sonoran coast.

It is clear from the sharp upward flexure of the isotherms within 30 km of the coast off Guaymas (Fig. IV-18a) that the mesoscale process of coastal upwelling also played an important role in the maintenance of the elevated productivity and high biomass observed along the coastal strip off Sonora in the central Gulf. The high primary productivity within this area (station 61) is associated with strong shoaling of the nutricline (Fig. IV-13). From this we may infer enhanced vertical transport of nutrients over the shelf from depths of 70 to 80 m (Fig. IV-18a) leading to expansion of the biomass and productivity within areas of the cool water stretching from Isla Tiburon to south of Cabo Lobos (Fig. IV-14a). The localized coastal upwelling apparently occurred as a response to local alongshore northwesterly wind events occurring over periods of 7 to

10 days (Figs. IV-10 and IV-11). The widening of the band of high phytoplankton biomass north of Guaymas and south of Tiburon Island occurs as the shelf broadens abruptly to the north. The most intense coastal upwelling probably remains localized along a band following the shelf break as suggested by Fig. IV-18a, while the high productivity over the shallower inner shelf may reflect a significant contribution by stirring processes as well as shallow upwelling.

THE ROLE OF GULF WATER IN REGULATION OF PRIMARY PRODUCTIVITY

The formation of a local Gulf Water mass to the north of the principal area of winter-spring productivity in the Gulf of California points to a significant difference between the eastern boundary systems and the Gulf of California. It has been shown here that during March 1983, the high primary productivity and biomass concentrations were limited to regions in the central Gulf covered by Gulf Water, either from upwelling or from the direct flow over the sill. This association is sufficiently compelling to warrant a closer examination of the origin and possible role of Gulf Water as a factor in determining year-to-year variability in the biological productivity of the Gulf.

Roden and Groves' (1959) original definition of Gulf Water does not specify its source other than to say it is "equatorial water which has been transformed at the surface by evaporation". Alvarez-Borrego and Schwartzlose (1979) presented a plausible mechanism for the formation of Gulf Water by the apparent convective overturn of water observed during March 1973 in the upper Gulf. They showed cool and highly saline surface water sinking from the northern extreme of the upper Gulf forming a high-salinity, near-bottom tongue, extending towards the sill to the south. At the same time, a plume of subsurface water just north of the sill is seen rising from a depth of approximately 200 m (Alvarez-Borrego and Schwartzlose, 1979, their Fig. 1). The

mechanism of convective overturn is also suggested by satellite infrared images in Badan-Dangon et al. (1985, their Fig. 8) which show a complex textured surface thermal pattern in the northern Gulf during April 1980, resembling the surface network of cells produced by Benard convection (Triton, 1977, Chap. 4 and 17).

The absence of water masses other than Gulf Water and Subtropical Subsurface Water at the sill during March of 1983 (Fig. IV-7), suggests that Gulf Water is an immediate derivative of Subtropical Subsurface Water which would be produced from the high evaporation and deep convective motion in the upper Gulf described above. This interpretation is supported from the mixing relationship between the two extreme Gulf and Subtropical Subsurface Water types on the T-S diagrams of Figures IV-3 and IV-7. The inferred derivative relationship of Gulf Water to Subtropical Subsurface Water is of particular interest because of the high nutrient concentrations in the Subtropical Subsurface Water shown below.

We may examine the association between nutrient content and water masses in the Gulf using earlier published data. Figure IV-20 is a phosphate-salinity diagram from the southern Gulf adapted from Warsh et al. (1973, their Fig. 8) to show the relationship between nutrient concentration and mixing of water masses during July 1967. Based upon the thermohaline characteristics given by Warsh et al. (1973), it is possible to identify the water masses on their Figure 8 in terms of the water masses defined on Figure IV-3. The lines are drawn through the data points in Figure IV-20 to show reasonable paths of mixing among the different water masses indicated. Figure IV-20 illustrates the high concentrations associated with the Subtropical Subsurface Water which is found between roughly 200 and 400 m; the highest concentrations are located in the Pacific Intermediate Water below 400 m. The diagram suggests that the higher nutrient concentrations in subsurface California Current Water were obtained by mixing with the Subtropical Subsurface Water. Moreover, the high nutrient content in

the subsurface Gulf Water appears to be derived from the Subtropical Subsurface Water which is believed to have been the source for the Gulf Water in March 1983. The low nutrient concentrations associated with the highest salinity Gulf Water are found at the surface and reflect depletion by phytoplankton comsumption.

The relationship between Gulf water and Subtropical Subsurface Water is strong enough to suggest an hypothesis to explain the high productivity measured in the central Gulf during the 1982-1983 El Niño. This hypothesis is also seen as a step towards explaining the increase in diatom flux associated with El Niño episodes observed from the microfossil analysis of the varved sediment record off Guaymas (Baumgartner et al., 1985). The hypothesis can be stated in the following way. If we assume that Gulf Water is derived principally from the Subtropical Subsurface Water then the year-to-year variation in the advective strength and extent of northward penetration of the Subtropical Subsurface Water, associated with the ENSO cycle, should be an important factor in regulating the richness of the subsurface nutrient source for the Gulf Water.

The extent of northward penetration of nutrient-rich subsurface water along the Pacific side of Baja California can vary significantly over a relatively short period. This variation is illustrated from a set of five CalCOFI cruises made during 1969, covering the region from central California to 25°N. Figure IV-21 presents two of the maps taken from the CalCOFI Atlas No. 20 (Thomas and Seibert, 1974) to show the maximum and minimum northward penetration of the nutrient-rich water observed on these five cruises. These maps display the phosphate concentrations at 100 m depth.

Wooster and Jones (1970) note that the water transported northward along Baja California in the California Undercurrent is subsurface water from the tropics. Their description of this water shows that it has the same thermohaline characteristics as that of the Subtropical Subsurface Water in the eastern tropical Pacific and in the Gulf of California. This water is probably transported from the tropics as subsurface water in

Figure IV-20

Phosphate-salinity relationship for the southern Gulf of California during July, 1967 (modified from Warsh et al., 1973). Water masses noted on plot are Pacific Intermediate Water (PIW); Subtropical Subsurface Water (SSW); Gulf Water (GW); and California Current Water (CCW). Water mass labels are placed next to the data regions according to interpretation of characteristics given in Warsh et al., 1973 (see text for explanation). Continuous lines through data indicate inferred mixing relationships among water masses. The vertical broken line connects the offset between values in the subsurface and surface Gulf Water.

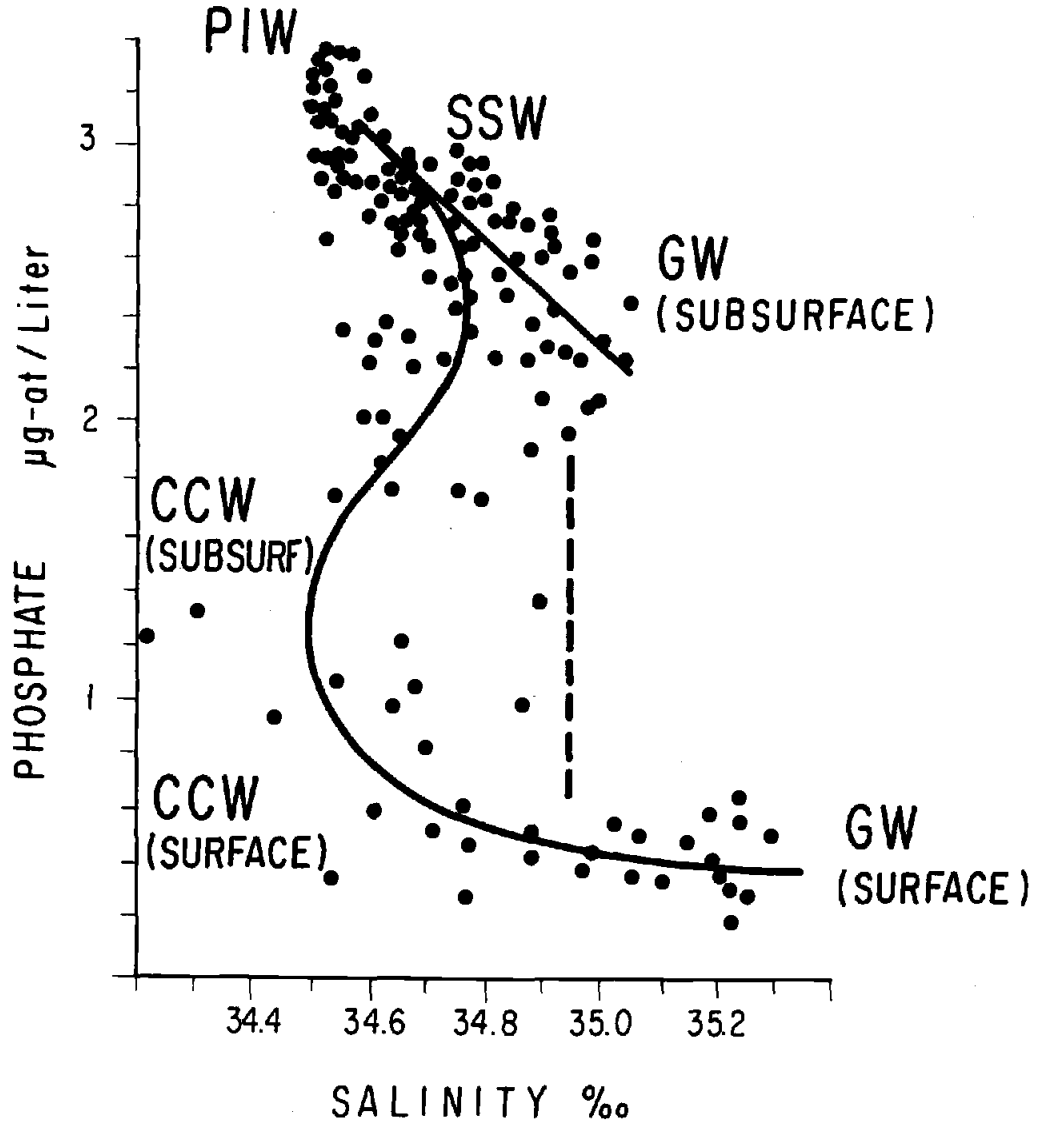
PIW
SSW
GW
(SUBSURFACE)
CCW
(SUBSURF)
CCW
(SURFACE)
GW
(SURFACE)
PHOSPHATE µg-at / Liter
3
2
1
34.4
34.6
34.8
35.0
35.2
SALINITY ‰

Figure IV-20

the Costa Rica Current into the region of the mouth of the Gulf (Baumgartner and Christensen, 1985) and off the tip of Baja California where it is entrained into the California Undercurrent. The higher phosphate concentrations at 100 m along Baja California during July, relative to October and November, indicates shoaling of the Subtropical Subsurface Water probably associated with stronger poleward advection and an increase in the volume of water transported. These processes should also enhance vertical mixing of nutrients into the upper layers.

It is fortunate for this study that an El Niño event developed during summer 1968 and persisted through early fall of 1969. Quinn et al. (1978) classify this as a weak event. The effect of the El Niño on sea level in the Gulf of California is shown by the Guaymas sea level record in Figure IV-22. The Guaymas record begins in September 1968 due to a gap in the data beginning in 1966. However, the period displayed still shows the development of the anomaly and its decay which had begun by October and November indicating a transition to anti-El Niño conditions of 1970.

The maps of phosphate concentration in Thomas and Seibert (1974) for the April and June cruises (not shown here) indicate that the northward penetration had begun by April and that by June had reached the maximum seen here in July (Fig. IV-21). Comparison of the Guaymas sea level anomaly with the mean sea level shows that the anomaly development occurred roughly in phase with the seasonal rise in sea level indicating that the anomalous northward advection due to El Niño was added to that normally occurring during summer (Fig. IV-22). Thus, the relatively low value of the June and July anomalies still represent considerable and increasing northward advection. It is also interesting that as the nutrient-rich water withdrew to the south off southern Baja California during October and November, a nutrient-rich tongue appeared off California, indicating increased southward advection of the subarctic water in the California Current.

Figure IV-21

Concentration of phosphate at 100 m depth in CalCOFI region during July and October-November of 1969. Maps are redrawn from the CalCOFI Atlas No. 20 (Thomas and Seibert, 1974). Shaded areas indicate values greater than 2.0 ug-at/1.

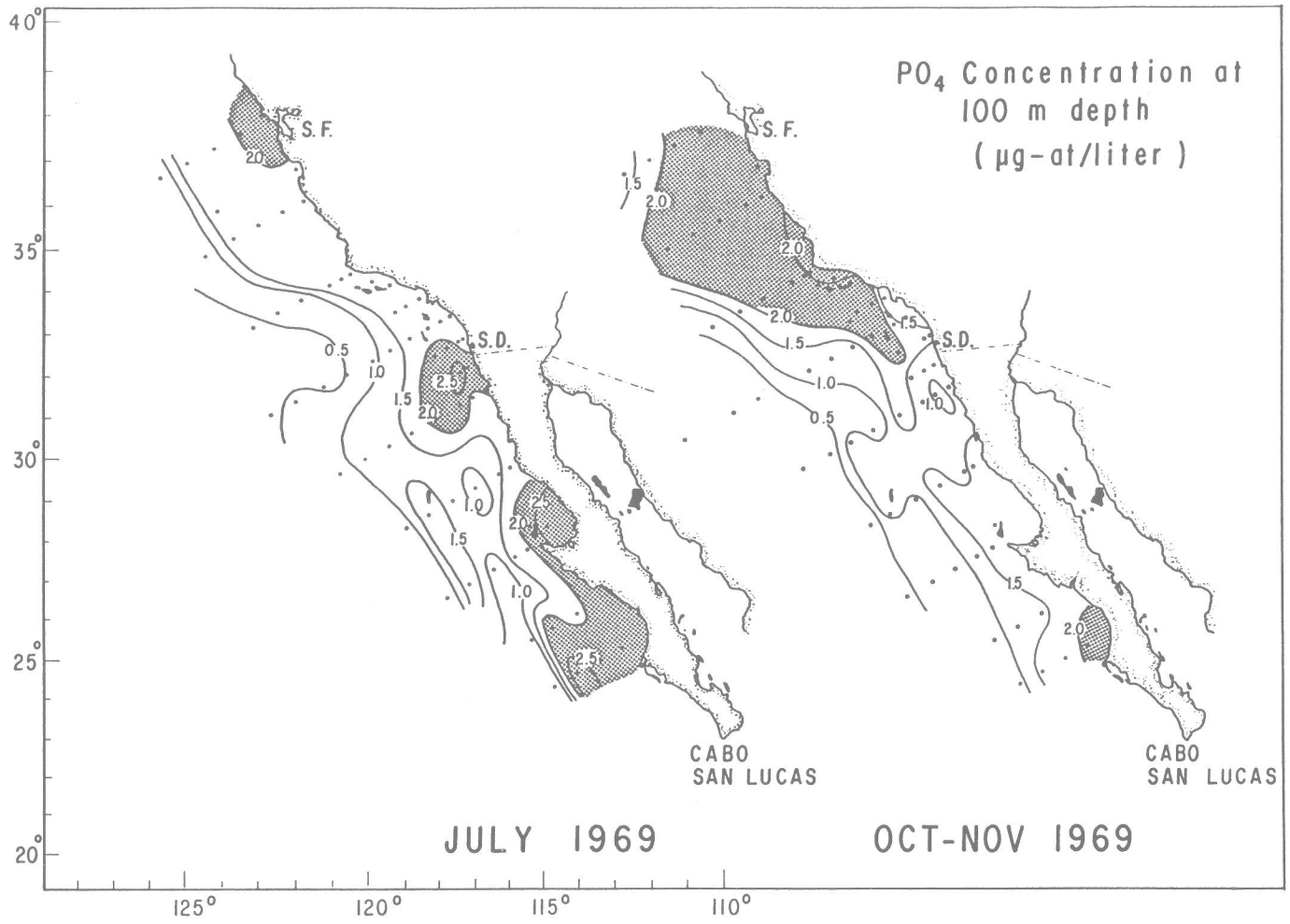
PO4 Concentration at
100 m depth
(µg-at/liter)
S. F.
S. D.
CABO
SAN LUCAS
JULY 1969
OCT-NOV 1969
40°
35°
30°
25°
20°
125°
120°
115°
110°

Figure IV-21

Figure IV-22

Variation in sea level measured at Guaymas from October, 1968, through January, 1972. Monthly mean sea level height shown in upper curve and monthly anomaly in lower curve as in Figure IV-19.

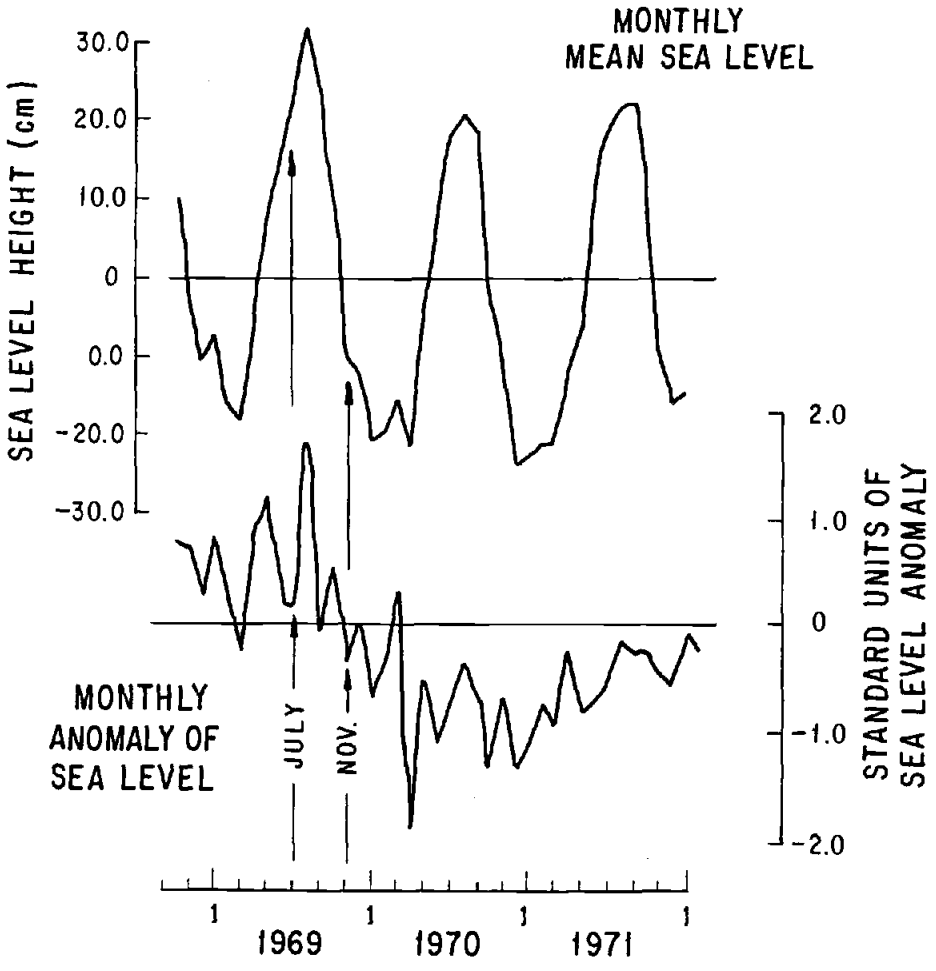
MONTHLY
MEAN SEA LEVEL
SEA LEVEL HEIGHT (cm)
30.0
20.0
10.0
0
0.0
-20.0
-30.0
MONTHLY
ANOMALY OF
SEA LEVEL
JULY
NOV.
2.0
1.0
0
-1.0
-2.0
STANDARD UNITS OF
SEA LEVEL ANOMALY
1
1
1
1
1969
1970
1971

Figure IV-22

The hypothesis of enhanced nutrient supply to Gulf Water suggests that increasingly nutrient-rich Subtropical Subsurface Water was pumped into the Gulf of California beginning in September 1982. The northward penetration of high nutrient subsurface water observed for July 1969 (Fig. IV-21) further suggests that this water would have reached into the northern Gulf since it reaches a comparable latitude along Baja California. The sea level anomaly of Figure IV-19 indicates that during the 1982-1983 event, the anomalous poleward advection reached a maximum during December and January, the season for which the formation of Gulf Water has been previously inferred (Alvarez-Borrego and Schwartzlose, 1979). Thus, the presumed source for Gulf Water should have been anomalously enriched in nutrients from late fall through winter.

The proposed mechanism can be likened to a large-scale chemostat in which an increased rate of flow of nutrients to the Gulf of California occurs by anomalous intensification of poleward advection of the Subtropical Subsurface Water. The anomalous enrichment of the Gulf Water at its site of origin would in turn increase productivity in the central Gulf by an increased rate of nutrient flux resulting from the higher nutrient concentrations in the Gulf Water which is ultimately entrained towards the surface by coastal upwelling. The interannual variability resulting from this proposed model would explain the variation of siliceous phytoplankton deposition inferred from the sediment record in the central Gulf (Baumgartner et al., 1985) as well as the high values of primary production and phytoplankton biomass observed off Sonora in the central Gulf during the El Niño conditions in March 1983.

CONCLUSIONS

Three distinct scales of physical forcing can be inferred from the hydrographic data collected in the central and southern Gulf during March, 1983. These scales of forcing drive the physical processes which in turn control the magnitude of primary productivity in the Gulf. Coupling of the biological activity to the physical processes is inferred by the close association between the physical structure of the ocean and the distribution of phytoplankton biomass and productivity.

The remote forcing associated with the El Niño phenomenon is reflected by the presence of Tropical Surface Water in the central Gulf. This northward penetration is produced by poleward advection along the western margin evident in the dynamic topography and the upward tilt of the pycnocline which occurs in the western half of the Gulf. Primary productivity within the Tropical Surface Water is uniformly low. The lack of local wind-driven coastal upwelling along the western margin also prevents the pumping of the subsurface Gulf Water from below the Tropical Surface Water into the light-rich surface layer so that productivity remains depressed there.

The tilt of the pycnocline from the axis of the Gulf towards the eastern coast is thought to be a response to the regional wind field over the subtropical eastern Pacific and the Gulf of California. This would reflect a second scale of forcing which is related to the annual cycle in the strength and direction of the winds. The observed equatorward flow is consistent with raising of the pycnocline along the eastern margin by the northwesterly winds which predominate during spring. Thus, the seasonal wind field appears to override the ENSO effects along the eastern boundary by lifting the pycnocline to depths of 70 to 90 meters along the coast and reversing the tilt towards the western margin which is produced by propagation of energy from the tropics.

The third scale of physical forcing is recognized by the presence of localized coastal upwelling occurring over the eastern shelf within the central Gulf. The band of upwelling is less than 30 km wide off Guaymas but widens to the north as the shelf broadens. The intense coastal upwelling observed is thought to represent the mesoscale response to the 7 to 10 day wind events and entrains nutrient-rich water from a depth of approximately 70-80 m.

The magnitude of primary productivity is closely associated with the depth of the nutricline suggesting that the rate of vertical transport of nutrients is the principal control over productivity. The strong link between production and the variation in algal biomass is also consistent with the concept of mediating primary productivity by regulation of the rate of nutrient transfer to the biomass through vertical advection.

The nutrient-rich source water entrained by coastal upwelling along the Sonoran margin is identified as the locally formed Gulf Water. The similar thermohaline characteristics and transitional nature between the Subtropical Subsurface Water and Gulf Water indicates that Gulf Water is derived principally from the Subtropical Subsurface Water by evaporation in the northern Gulf. The elevated nutrient concentration of the Subtropical Subsurface Water is proposed here as the indirect source of the enhanced fertility associated with the Gulf water during El Niño conditions observed in the spring of 1983. It is further proposed here that interannual variability in primary productivity may be governed by the extent and rate of poleward advection of the Subtropical Subsurface Water. This mechanism is analogous to a large-scale chemostat where anomalous poleward advection, occurring during El Niño events, represents an increased horizontal subsurface flux of nutrients to the site of Gulf Water formation. The year-to-year variation in the enrichment of Gulf Water implied by this model is consistent with the long-term record of siliceous phytoplankton deposition in the varved sediments off

Guaymas as well as the historically high values of primary productivity measured in the central Gulf during spring of 1983.

ACKNOWLEDGEMENTS

This investigation was supported by the Mexican government through CONACYT grant PCECBNA-021265 to the Centro de Investigación Cientifica y de Educación Superior de Ensenada. CONACYT also supplied separate funding for use of the Research Vessel EL PUMA. Preparation of the manuscript was carried out with help from NSF grant ATM83-19371-03. We are especially indebted to Ron Zaneveld and Bob Bartz for advice and assistance in construction of the Sea Tech transmissometer and to Terry Hendricks for the construction of the Sea Systems data logger. George Hemingway and Andy Soutar kindly facilitated necessary loans of oceanographic equipment from the Scripps Institution of Oceanography. Al Zirino provided laboratory facilities at the Naval Ocean Systems Center at San Diego for counting the ^{14}C samples. Nick Pisias, Dave Enfield and Dave Nelson all provided valuable comments for improvement of the manuscript. We also thank Jackie Poppleton for her word-processing skills with the Apple Macintosh and José María Domínguez and Sergio Ramos who drafted the figures.

REFERENCES

Alvarez-Borrego, S. and R.A. Schwartzlose, 1979. Water masses of the Gulf of California. Ciencias Marinas, 6:43-63.

Alvarez-Sanchez, L.G., 1974. Currents and water masses at the entrance to the Gulf of California, Spring 1979. M.S. Thesis, Oregon State University, 75 pp.

Badan-Dangon, A., C.J. Koblinsky and T. Baumgartner, 1985. Spring and summer in the Gulf of California: observations of surface thermal patterns. Oceanologica Acta, 8:13-22.

Barber, R.T. and R.L. Smith, 1981. Coastal upwelling ecosystems. In: A.R. Longhurst (ed), Analysis of Marine Ecosystems. Academic Press, London, p. 31-68.

Barber, R.T. and F.P. Chavez, 1983. Biological consequences of El Niño. Science, 222:1203-1210.

Baumgartner, T. and N. Christensen, 1985. Coupling of the Gulf of California to large-scale interannual climatic variability. J. Mar. Res., 43:825-848.

Baumgartner, T., V. Ferreira-Bartrina, H. Schrader and A. Soutar, 1985. A 20-year varve record of siliceous phytoplankton variability in the central Gulf of California. Mar. Geol., 64:113-129.

Bernal, P., 1981. A review of the low-frequency response of the pelagic ecosystem in the California Current. CalCOFI Rept., 22:49-62.

Bischoff, J.L. and J.W. Niemitz, 1980. Bathymetric maps of the Gulf of California, U.S. Geological Survey, Misc. Invest. Series, Map 1-1244.

Calvert, S.E., 1964. Factors affecting the distribution of laminated diatomaceous sediments in the Gulf of California. In: Tj.H. van Andel and G.G. Shor (eds), Marine Geology of the Gulf of California. Amer. Assoc. Petrol. Geol. Mem., 3:311-330.

Candela, J., A. Badan-Dangon and C.D. Winant, 1984. Spatial distribution of lower atmospheric physical variables over the Gulf of California. A Data Report, Vol. 1, Summer 1983. SIO Reference Series #84-33.

Candela, J., A. Badan-Dangon and C.D. Winant, 1985. Spatial distribution of lower atmospheric physical variables over the Gulf of California. A Data Report, Vol. 2, Winter 1984. SIO Reference Series #85-11.

Chelton, D.B., 1981. Interannual variability of the California Current—physical factors. CalCOFI Rept., 22:34-48.

Chelton, D.B., 1982. Large-scale response of the California Current to forcing by the wind-stress curl. CalCOFI Rept., 23:130-148.

Chelton, D.B., P.A. Bernal and J.A. McGowan, 1982. Large-scale interannual physical and biological interaction in the California Current. J. Mar. Res., 40: 1095-1125.

Chelton, D.B. and R.E. Davis, 1982. Monthly mean sea-level variability along the west coast of North America. J. Phys. Oceanogr., 12:757-783.

Codispoti, L.A., R.C. Dugdale and H.J. Minas, 1982. A comparison of the nutrient regimes off northwest Africa, Peru and Baja California. Rapp. P-v. Reun. Cons. Int. Explor. Mer., 180:177-194.

Cowles, T.J., R.T. Barber and O. Guillen, 1977. Biological consequences of the 1975 El Niño. Science, 195:546-565.

Dugdale, R.C., 1985. The effects of varying nutrient concentration on biological production in upwelling regions. CalCOFI Rept., 26:93-96.

Dugdale, R.C. and J. Goering, 1967. Uptake of new and regenerated forms of nitrogen in primary productivity. Limnol. Oceanogr., 12:196-206.

Enfield, D.B., 1981. Thermally driven wind variability in the planetary boundary layer above Lima, Peru. J. Geophys. Res., 83:2005-2016.

Enfield, D.B. and J.S. Allen, 1980. On the structure and dynamics of monthly mean sea level anomalies along the Pacific Coast of North and South America. J. Phys. Oceanogr., 10:557-578.

Enfield, D.B. and J.S. Allen, 1983. The generation and propagation of sea level variability along the Pacific Coast of Mexico. J. Phys. Oceanogr., 13:1012-1033.

Eppley, R.W., E.H. Renger and W.G. Harrison, 1979. Nitrate and phytoplankton production in southern California coastal waters. Limnol. Oceanogr., 24: 483-494.

Griffiths, R.C., 1968. Physical, chemical and biological oceanography of the entrance to the Gulf of California, Spring 1960. Sp. Sci. Rept., U.S. Fish and Wildlife Service. Fisheries, 573, 47 pp.

Hales, J.E., Jr., 1974. Southwestern United States summer monsoon source—Gulf of Mexico or Pacific Ocean? J. Appl. Meteor., 13:331-342.

Kiefer, D.A. and R.W. Austin, 1974. The effect of phytoplankton concentration on submarine light transmission in the Gulf of California. Limnol. Oceanogr., 19: 55-64.

King, F.D., 1986. The dependence of primary production in the mixed layer of the eastern tropical Pacific on the vertical transport of nitrate. Deep-Sea Res., 33: 733-754.

Lara-Lara, J.R., J.E. Valdez-Holguin and L.C. Jimenez-Perez, 1984. Plankton studies in the Gulf of California during the 1982-1983 El Niño. Tropical Ocean-Atmosphere Newsletter, 28:16-17.

McCreary, J., 1976. Eastern tropical ocean response to changing wind systems with application to El Niño. J. Phys. Oceanogr., 6:632-645.

McGowan, J.A., 1984. The California El Niño 1983. Oceanus, 27:48-51.

McLain, D.R. and D. Thomas, 1983. Year-to-year fluctuations of the California Counter-current and effects on marine organisms. CalCOFI Rept., 24:165-181.

Meyers, G., 1979. Annual variation in the slope of the 14°C isotherm along the equato in the Pacific Ocean. J. Phys. Oceanogr., 9:885-891.

Namias, J., 1975. Northern hemisphere seasonal sea level pressure and anomaly charts, 1974-1974. CalCOFI Atlas, No. 22.

O'Brien, J., A. Busalacchi and J. Kindle, 1981. Ocean models of El Niño. In: M.H. Glantz (ed), Resource Management and Environmental Uncertainty. John Wiley and Sons, New York, p. 159-212.

Peterson, R.E., 1977. A study of suspended perticulate matter: Arctic ocean and northern Oregon continental shelf. Ph.D. Thesis, Oregon State University, 122 pp.

Quinn, W.H., D.O. Zoph, K.S. Short and R.T.W. Kuo Yang, 1978. Historical trends and statistics of the Southern Oscillation, El Niño and Indonesian droughts. Fish. Bull., 76:663-678.

Reid, J.L., E. Brinton, J. Fleminger, E.L. Venrick and A. McGowan, 1978. Ocean circulation and marine life. In: H. Charnock and G. Deacon (eds), Advances in Oceanography. Plenum Press, New York, p. 65-130.

Robles, J.M. and S.G. Marinone, in press. Seasonal and interannual thermohaline variability in the Guaymas Basin in the Gulf of California. Cont. Shelf. Res.

Roden, G.I., 1964. Oceanographic aspects of the Gulf of California. In: Tj.H. van Andel and G.G. Shor (eds), Marine Geology of the Gulf of California. Amer. Assoc. Petrol. Geol. Mem., 3:30-50.

Roden, G.I., 1971. Aspects of the transition zone in the northeastern Pacific. J. Geophys. Res., 76:3462-3475.

Roden, G.I., 1972a. Thermohaline structure and baroclinic flow across the Gulf of California entrance and the Revilla Gigedo Islands region. J. Phys. Oceanogr., 2:177-183.

Roden, G.I., 1972b. Large-scale upwelling off northwestern Mexico. J. Phys. Oceanogr., 2:184-189.

Roden, G.I. and G.W. Groves, 1959. Recent oceanographic investigations in the Gulf of California. J. Mar. Res., 18:10-35.

Rosas-Cota, A., 1977. Corrientes geostroficas en el Golfo de California en la superficie y a 200 metros durante las estaciones de Invierno y Verano. CalCOFI Rept., 19: 89-106.

Schrader, H. and T. Baumgartner, 1983. Decadal variation of upwelling in the central Gulf of California. In: J. Thiede and E.Suess (eds), Coastal Upwelling: Its Sediment Record, Part B. Plenum Press, New York, p. 247-273.

Simpson, J.J., 1984a. El Niño-induced onshore transport in the California Current during 1982-1983. Geophys. Res. Lett., 11:241-242.

Simpson, J.J., 1984b. A simple model of the 1982-83 Californian El Niño. Geophys. Res. Lett., 11:243-246.

Steemann-Nielsen, E., 1952. The use of radioactive carbon (^{14}C) for measuring organic production in the sea. J. Cons. Explor. Mer., 18:117-140.

Strickland, J.D.H. and T.R. Parson, 1972. A practical handbook of seawater analysis. Bull. Fish. Res. Bd. Canada, 167, 2nd Ed., 311 pp.

Thomas, W.H. and D.L.R. Seibert, 1974. Distribution of nitrate, nitrite, phosphate and silicate in the California Current region, 1969. CalCOFI Atlas No. 20, 97 pp.

Triton, D.J., 1977. Physical Fluid Dynamics. Van Nostrand Reinhold Co. Ltd., United Kingdom, 362 pp.

Valdez-Holguin, E., 1986. Distribucion de la Biomasa y Productividad del Fitoplancton en el Golfo de California durante el Evento del Niño 1982-1983. M.S. Thesis, Centro de Investigacion Cientifica y Educacion Superior de Ensenada, B.C., Mexico, 92 pp.

Warsh, C.E., K.L. Warsh and R.C. Staley, 1973. Nutrients and water masses at the mouth of the Gulf of California. Deep-Sea Res., 20:561-570.

Wooster, W.S. and J.H. Jones, 1970. California Undercurrent off northern Baja California. J. Mar. Res., 28:235-250.

Wyrtki, K., 1967. Circulation and water masses in the eastern equatorial Pacific Ocean. J. Oceanol. Limnol., 1:117-147.

Wyrtki, K., 1975. El Niño—The dynamic response of the equatorial Pacific Ocean to atmosphere forcing. J. Phys. Oceanogr., 5:572-584.

Wyrtki, K., 1985. Water displacements in the Pacific and the genesis of El Niño cycles. J. Geophys. Res., 90:7129-7132.

BIBLIOGRAPHY

Alvarez-Borrego, S. and R.A. Schwartzlose, 1979. Water masses of the Gulf of California. Ciencias Marinas, 6:43-63.

Alvarez-Sanchez, L.G., 1974. Currents and water masses at the entrance to the Gulf of California, Spring 1979. M.S. Thesis, Oregon State University, 75 pp.

Baba, J., K. Scheidegger, H. Schrader and C. Peterson, submitted. Modern terrigenous sediments in the Gulf of California. In: The Gulf and Peninsular Province of the Californias, P. Dauphin and G. Ness (eds), AAPG Memoir.

Badan-Dangon, A., C.J. Koblinsky and T. Baumgartner, 1985. Spring and summer in the Gulf of California: observations of surface thermal patterns. Oceanologica Acta, 8:13-22.

Barber, R.T. and R.L. Smith, 1981. Coastal upwelling ecosystems. In: A.R. Longhurst (ed), Analysis of Marine Ecosystems. Academic Press, London, p. 31-68.

Barber, R.T. and F.P. Chavez, 1983. Biological consequences of El Niño. Science, 222:1203-1210.

Baumgartner, T. and N. Christensen, 1985. Coupling of the Gulf of California to large-scale interannual climatic variability. J. Mar. Res., 43:825-848.

Baumgartner, T.R., V. Ferreira-Bartrina, H. Schrader and A. Soutar, 1985. A 20-year varve record of siliceous phytoplankton variability in the central Gulf of California. Mar. Geol., 64:113-129.

Berlage, H.P., 1957. Fluctuations of the general atmospheric circulation of more than one year, their nature and prognostic value. Mededel. Verhandel., Koninkl. Nederlands Meteor. Inst., No. 69, 152 pp.

Bernal, P.A., 1981. A review of the low frequency response of the pelagic ecosystem in the California Current. Calif. Coop. Oceanic Fish. Invest. Rpts., 22:49-62.

Bischoff, J.L. and J.W. Niemitz, 1980. Bathymetric maps of the Gulf of California. U.S. Geological Survey, Miscellaneous Investigation Series, Map 1-1244.

Bjerknes, J., 1969. Atmospheric teleconnections from the equatorial Pacific. Month. Weather Rev., 97:163-172.

Blackman, R.B. and J.W. Tukey, 1959. The Measurement of Power Spectra. Dover Publishing Inc., New York, 190 pp.

Bouma, A.H., 1969. Methods for the Study of Sedimentary Structures. Wiley Interscience, J. Wiley and Sons, New York, 458 pp.

Brazel, A. and S. Hsu, 1981. The climatology of hazardous Arizona dust storms. In: T.L. Péwé (ed), Desert Dust: Origin, Characteristics and Effect on Man. Geol. Soc. Amer. Sp. Paper, 186:293-303.

Bruland, K.W., 1974. ^{210}Pb geochronology in the coastal marine environment. Ph.D. Dissertation, University of California, San Diego, 106 pp.

Byrne, J., 1957. The marine geology of the Gulf of California. Ph.D. Thesis, University of Southern California, Los Angeles, 289 pp.

Candela, J., A. Badan-Dangon and C.D. Winant, 1984. Spatial distribution of lower atmospheric physical variables over the Gulf of California. A Data Report, Vol. 1, Summer 1983. SIO Reference Series #84-33.

Candela, J., A. Badan-Dangon and C.D. Winant, 1985. Spatial distribution of lower atmospheric physical variables over the Gulf of California. A Data Report, Vol. 2, Winter 1984. SIO Reference Series #85-11.

Calvert, S.E., 1964. Factors affecting distribution of laminated diatomaceous sediments in the Gulf of California. In: Tj.H. van Andel and G.G. Shor, Jr. (eds), Marine Geology of the Gulf of California. Amer. Assoc. Petrol. Geol. Mem., 3:311-330.

Calvert, S.E., 1966a. Accumulation of diatomaceous silica in the sediments of the Gulf of California. Geol. Soc. Amer. Bull., 77:569-596.

Calvert, S.E., 1966b. Origin of diatom-rich, varved sediments from the Gulf of California. J. Geol., 76:546-565.

Chelton, D.B., 1980. Low frequency sea level variability along the west coast of North America. Ph.D. Dissertation, Scripps Institution of Oceanography, University of California, San Diego, 212 pp.

Chelton, D.B., 1981. Interannual variability of the California Current—physical factors. Calif. Coop. Fish. Investig. Rept., 22:34-48.

Chelton, D.B., 1982. Large-scale response of the California Current to forcing by the wind-stress curl. CalCOFI Rept., 23:130-148.

Chelton, D.B. and R.E. Davis, 1982. Monthly mean sea level variability along the west coast of North America. J. Phys. Oceanogr., 9:757-784.

Chelton, D.B., P.A. Bernal and J.A. McGowan, 1982. Large-scale interannual physical and biological interaction in the California Current. J. Mar. Res., 40: 1095-1125.

Christensen, N. Jr., and N. Rodriguez S., 1979. A study of sea level variations and currents off Baja California. J. Phys. Oceanogr., 9:631-638.

Christensen, N., Jr., R. de la Paz and G. Gutierrez, 1983. A study of subinertial waves off the west coast of Mexico. Deep-Sea Res., 30:835-850.

Codispoti, L.A., R.C. Dugdale and H.J. Minas, 1982. A comparison of the nutrient regimes off northwest Africa, Peru and Baja California. Rapp. P-v. Reun. Cons. Int. Explor. Mer., 180:177-194.

Cowles, T.J., R.T. Barber and O. Guillen, 1977. Biological consequences of the 1975 El Niño. Science, 195:285-287.

Cupp, E.E., 1943. Marine plankton diatoms of the west coast of North America. Bull. Scripps Instit. Ocean., 5:1-238.

Cushing, D.H., 1981. The effect of El Niño upon the Peruvian anchoveta stock. In: F.A. Richards (ed), Coastal Upwelling. Amer. Geophys. Union, pp. 449-457.

Davis, J.C., 1973. Statistics and Data Analysis in Geology. John Wiley and Sons, New York, 550 pp.

Davis, R.E., 1976. Predictability of the sea surface temperature and sea level pressure anomalies over the North Pacific Ocean. J. Phys. Oceanogr., 6:249-266.

De Geer, G., 1912. A geochronology of the last 12,000 years. Cong. Geol., Internat. 11th, Stockholm, 1910, Comptes Rendus., pp. 241-253.

DeMaster, D.J., 1979. The marine budgets of silica and ^{32}Si. Ph.D. Dissertation, Yale Univ., 308 pp.

Dixon, W.J. and F.J. Massey, Jr., 1969. Introduction to Statistical Analysis, 3rd Ed., McGraw-Hill Book Co., New York, 638 pp.

Donegan, D. and H. Schrader, 1981. Modern analogues of the Miocene diatomaceous Monterey Shale of California: evidence from sedimentologic and micropaleontologic study. In: R. Garrison and R. Douglas (eds), Monterey Formation and Related Siliceous Rocks of California. Pacific Section, Soc. Econ. Paleont. Mineral. Sp. Pub., p. 149-157.

Donegan D. and H. Schrader, 1982. Biogenic and abiogenic components of laminated hemipelagic sediments in the central Gulf of California. Mar. Geol., 48:215-237.

Drake, D.E., D.A. Cacchione and H.A. Karl, 1985. Bottom currents and sediment transport on San Pedro Shelf, California. J. Sed. Petrol., 55:15-28.

Drake, D.E., R.L. Kolpack and P.J. Fischer, 1972. Sediment transport on the Santa Barbara-Oxnard shelf, Santa Barbara Channel, California. In: D.J.P. Swift et al. (eds), Shelf Sediment Transport: Process and Pattern. Dowden, Hutchinson and Ross, Stroudsburg, Pa., p. 307-331.

Dugdale, R.C., 1985. The effects of varying nutrient concentration on biological production in upwelling regions. CalCOFI Rept., 26:93-96.

Dugdale, R.C. and J. Goering, 1967. Uptake of new and regenerated forms of nitrogen in primary productivity. Limnol. Oceanogr., 12:196-206.

Egger, J., G. Meyers and P.B. Wright, 1981. Pressure, wind and cloudiness in the tropical Pacific related to the Southern Oscillation. Month. Weather. Rev., 109:1139-1149.

Enfield, D.B., 1981. Thermally driven wind variability in the planetary boundary layer above Lima, Peru. J. Geophys. Res., 86:2005-2016.

Enfield, D.B. and J.S. Allen, 1980. On the structure and dynamics of monthly mean sea level anomalies along the Pacific Coast of North and South America. J. Phys. Oceanogr., 10:557-578.

Enfield, D.B. and J.S. Allen, 1983. The generation and propagation of sea level variability along the Pacific coast of Mexico. J. Phys. Oceanogr., 13: 1012-1033.

Eppley, R.W., E.H. Renger and W.G. Harrison, 1979. Nitrate and phytoplankton production in southern California coastal waters. Limnol. Oceanogr., 24: 483-494.

Fenner, J., H.J. Schrader and H. Wienigk, 1976. Diatom phytoplankton studies in the southern Pacific Ocean, composition and correlation to the Antarctic convergence and its paleoecological significance. In: C.D. Hollister, C. Craddock et al. (eds), Initial Reports of the Deep Sea Drilling Project, Vol. 35, U.S. Government Printing Office, Washington, DC, pp. 757-813.

Flynn, W.W., 1968. The determination of low levels of polonium-210 in environmental materials. Analytica Chimica Acta, 43:221-227.

Fryxell, G.A. and G.R. Hasle, 1972. Thalassiosira eccentrica (Ehrenb.) Cleve, T. symmetrica sp. nov., and some related centric diatoms. J. Phycol., 8:297-317.

Gentleman, W.M.;, 1973. Least squares computations without square roots. J. Inst. Math. Appl., 12:329-336.

Glover, D.P., 1980. Historical Seismogram Filming Project: Second Progress Report. World Data Center A for Solid Earth Geophysics, Rept. SE-24. NOAA.

Greeley, R. and J.D. Iversen, 1985. Wind as a Geological Process on Earth, Mars, Venus and Titan. Cambridge University Press, Great Britain, 322 pp.

Griffiths, R.C., 1968. Physical, chemical and biological oceanography of the entrance to the Gulf of California, Spring 1960. Sp. Sci. Rept., U.S. Fish and Wildlife Service. Fisheries, 573, 47 pp.

Grivel-Piña, F., 1977. Datos Geofísicos, Serie A, Oceanografía 3. Instituto Geofísica. Univ. Nac. Auton. de México, 197 pp.

Hales, J.E., Jr., 1972. Surges of maritime tropical air northward over the Gulf of California. Month. Weather Rev., 100:298-306.

Hales, J.E., Jr., 1974. Southwestern United States summer monsoon source—Gulf of Mexico or Pacific Ocean? J. Appl. Meteor., 13:331-342.

Hasle, G.R., 1960. Phytoplankton and ciliate species from the tropical Pacific. Skr. Norske Vidensk., Akad. Oslo, Mat. Nat. Kl., 2:1-50.

Hasle, G.R., 1976. The biogeography of some marine planktonic diatoms. Deep-Sea Res., 23:319-338.

Hendey, N.I., 1964. An introductory account of the smaller algae of British coastal waters. Part V. Bacillariophyceae (Diatoms). Her majesty's Stationary Office, London, 317 pp.

Horel, J.D. and J. M. Wallace, 1981. Planetary-scale atmospheric phenomena associated with the Southern Oscillation. Month. Weather Rev., 109:813-829.

Hustedt, F., 1930. Die Kieselalgen Deutschlands, Österreichs und der Schweiz mit Berücksichtigung der übrigen Länder Europas sowie der agrenzenden Meeresgebiete. In: L. Rabenhorst (ed), Kryptogamenflora von Deutschland, Österreich und der Schweiz, 7: Part 1. Akad. Verlag., Leipzig, 920 pp.

Hustedt, F., 1959. Die Kieselalgen Deutschlands, Österreichs und der Schweiz mit Berücksichtigung der übrigen Länder Europas sowie der agrenzenden Meeresgebiete. In: L. Rabenhorst (ed), Kryptogamenflora von Deutschland, Österreich und der Schweiz, 7: Part 2. Acad. Verlag., Leipzig, 845 pp.

Jousé, A.P., O.G. Kozlova and V.V. Mukhina, 1971. Distribution of diatoms in the surface layer of sediment from the Pacific Ocean. In: B.M. Funnel and W.R. Riedel (eds), Micropaleontology of the Oceans. Cambridge University Press, pp. 263-269.

Kanaya, T. and I. Koizumi, 1966. Interpretation of diatom thanatocoenoses from the North Pacific applied to a study of core V20-130. The Science Report of the Tohoku University, Sendai, Japan, 2nd Series (Geology), 37:89-130.

Karohji, K., 1972. Regional distribution of phytoplankton in the Bering Sea and eastern and northern subarctic regins of the North Pacific Ocean in summer. In: A.Y. Takenonti (ed), Biological Oceanography of the northern North Pacific. Idemitsu Shoten, Japan, pp. 99-115.

Kiefer, D.A. and R.W. Austin, 1974. The effect of phytoplankton concentration on submarine light transmission in the Gulf of California. Limnol. Oceanogr., 19: 55-64.

King, F.D., 1986. The dependence of primary production in the mixed layer of the eastern tropical Pacific on the vertical transport of nitrate. Deep-Sea Res., 33: 733-754.

Kozlova, O.G. and V.V. Mukhina, 1967. Diatoms and silicoflagellates in suspension and floor sediments of the Pacific Ocean. Int. Geol. Rev., 9:1322-1342.

Krishnamurti, T.N., 1971. Tropical east-west circulation during the northern summer. J. Atmos. Sci., 28:1342-1347.

Krishnamurti, T.N., M. Kanamitsu, W.J. Koss and J.D. Lee, 1973. Tropical east-west circulations during the northern winter. J. Atmos. Sci., 30:780-787.

Krishnaswami, S. and D. Lal, 1978. Radionuclide Limnochronology. In: M. Storme (ed), Lakes: Chemistry, Geology, Physics. Springer Verlag, p. 153-177.

Kundu, P.K., J.S. Allen and R.L. Smith, 1975. Modal decomposition of the velocity field near the Oregon coast. J. Phys. Oceanogr., 5:683-704.

Lara-Lara, J.R., J.E. Valdez-Holguin and L.C. Jimenez-Perez, 1984. Plankton studies in the Gulf of California during the 1982-1983 El Niño. Tropical Ocean-Atmosphere Newsletter, 28:16-17.

Leinen, M., D. Cwienk, G.R. Heath, P.E. Biscaye, V. Kolla, J. Thiede and J.P. Dauphin, 1986. Distribution of biogenic silica and quartz in recent deep-sea sediments. Geology, 14:199-203.

McCreary, J., 1976. Eastern tropical ocean response to changing wind systems with application to El Niño. J. Phys. Oceanogr., 6:632-645.

McCreary, J.P., 1978. Eastern tropical ocean response to changing wind systems. In: Review Papers of Equatorial Oceanography—Proc. FINE Workshop. Nova University Press, Ft. Lauderdale, FL., Chap. 7.

McDonald, W.F., 1938. Atlas of climatic charts of the oceans. Washington, DC, Dept. of Agriculture, Weather Bureau, 60 pp.

McGowan, J.A., 1974. The nature of oceanic ecosystems. In: C.B. Miller (ed), The Biology of the Oceanic Pacific. Oregon State University Press, pp. 9-28.

McGowan, J.A., 1984. The California El Niño 1983. Oceanus, 27:48-51.

McLain, D.R. and D. Thomas, 1983. Year-to-year fluctuations of the California Countercurrent and effects on marine organisms. Calif. Coop. Oceanic Fish. Invest. Rpts., 24:165-181.

Merrifield, M.A., C.D. Winant, J.M. Robles, R.T. Guza, N.A. Bray, J. García, A. Badan-Dangon and N.Christensen, Jr., 1986. Observations of currents, temperature, pressure and sea level in the Gulf of California 1982-1986. Data Report—Scripps Institution of Oceanography, Ref. Series 86-11, 153 pp.

Meyers, G., 1975. Seasonal variations in transport of the Pacific North Equatorial Current relative to the wind field. J. Phys. Oceanogr., 5:442-449.

Meyers, G., 1979. Annual variation in the slope of the 14°C isotherm along the equato in the Pacific Ocean. J. Phys. Oceanogr., 9:885-891.

Moore, T.C., Jr. and G.R. Heath, 1978. Sea floor sampling techniques. In: J.P. Riley and R. Chester (eds), Chemical Oceanography, Vol. 7. John Wiley, New York, p. 75-126.

Moreno-Hentz, P.E., 1982. Parametros sedimentologicos de varvas marinas en el Golfo de California y su relación con variaciones climaticas recientes. Licenciaturate Thesis, Universidad Autonoma de Baja California, 105 pp.

Murray, D. and H. Schrader, 1983. Distribution of silicoflagellates in plankton and core top samples from the Gulf of California. Mar. Micropaleo., 7:517-539.

Namias, J., 1975. Northern hemisphere seasonal sea level pressure and anomaly charts, 1974-1974. CalCOFI Atlas, No. 22.

O'Brien, J., A. Busalacchi and J. Kindle, 1981. Ocean models of El Niño. In: M.H. Glantz (ed), Resource Management and Environmental Uncertainty. John Wiley and Sons, New York, p. 159-212.

Pazen, S.E. and G. Meyers, 1982. Interannual fluctuations of the tropical Pacific wind field and the Southern Oscillation. Month. Weather Rev., 110:587-600.

Peterson, R.E., 1977. A study of suspended perticulate matter: Arctic ocean and northern Oregon continental shelf. Ph.D. Thesis, Oregon State University, 122 pp.

Péwé, T.L., E.A. Péwé, R.H. Péwé, A. Journaux and R.M. Slatt, 1981. Desert dust: Characteristics and rates of deposition in central Arizona, U.S.A. In: T.L. Péwé (ed), Desert Dust: Origin, Characteristics and Effect on Man. Geol. Soc. Amer. Sp. Paper 186, p. 169-190.

Philander, S.G.H., 1983. El Niño Southern Oscillation phenomena. Nature, 302:295-301.

Poelchau, H.S., 1976. Distribution of Holocene silicoflagellates in North Pacific sediments. Micropaleo., 22:164-193.

Price, J.M., 1981. Monthly mean sea level fluctuations at Honolulu and San Francisco and the intervening geostrophic currents. J. Phys. Oceanogr., 11:1375-1382.

Prospero, J.M., 1981. Arid regions as sources of mineral aerosols in the marine atmosphere. In: T.L. Péwé (ed), Desert Dust: Origin, Characteristics and Effect on Man. Geol. Soc. Amer. Sp. Paper 186, p. 71-86.

Quinn, W.H., D.O. Zoph, K.S. Short and R.T.W. Kuo Yang, 1978. Historical trends and statistics of the Southern Oscillation, El Niño, and Indonesian droughts. Fish. Bull., 76:663-678.

Rasmusson, E.M. and T.H. Carpenter, 1982. Variations in tropical sea surface temperature and surface wind fields associated with the Southern Oscillation/El Niño. Month. Weather Rev., 110:354-384.

Reid, R.O., 1948. The equatorial currents of the eastern pacific as maintained by the stress of the wind. J. Mar. Res., 7, 74-99.

Reid, J.L., E. Brinton, J. Fleminger, E.L. Venrick and A. McGowan, 1978. Ocean circulation and marine life. In: H. Charnock and G. Deacon (eds), Advances in Oceanography. Plenum Press, New York, p. 65-130.

Reiter, E.R., 1978. Long-term wind variability in the tropical Pacific, its possible causes and effects. Month. Weather Rev., 106:324-330.

Revelle, R.R., 1939. Sediments of the Gulf of California. Geol. Soc. Amer. Bull., 50:1929.

Revelle, R.R., 1950. Sedimentation and oceanography: survey of field observations, Part 5 of 1940 E.W. Scripps cruise to the Gulf of California. Geol. Soc. Amer. Mem., Vol. 43, 6 pp.

Robles, J.M. and S.G. Marinone, in press. Seasonal and interannual thermohaline variability in the Guaymas Basin in the Gulf of California. Cont. Shelf. Res.

Roden, G.I., 1964. Oceanographic aspects of the Gulf of California. In: Tj.H. van Andel and G.G. Shor (eds), Marine Geology of the Gulf of California. Amer. Assoc. Petrol. Geol. Mem., 3:30-50.

Roden, G.I., 1971. Aspects of the transition zone in the northeastern Pacific. J. Geophys. Res., 76:3462-3475.

Roden, G.I., 1972a. Thermohaline structure and baroclinic flow across the Gulf of California entrance and the Revilla Gigedo Islands region. J. Phys. Oceanogr., 2:177-183.

Roden, G.I., 1972b. Large-scale upwelling off northwestern Mexico. J. Phys. Oceanogr., 2:184-189.

Roden, G.I. and G.W. Groves, 1959. Recent oceanographic investigations in the Gulf of California. J. Mar. Res., 18:10-35.

Rosas-Cota, A., 1977. Corrientes geostroficas en el Golfo de California en la superficie y a 200 metros durante las estaciones de Invierno y Verano. CalCOFI Rept., 19: 89-106.

Rusnak, G.A., R.L. Fisher and F.P. Shepard, 1964. Bathymetry and faults of the Gulf of California. In: Tj.H. van Andel and G.G. Shor, Jr. (eds), Marine Geology of the Gulf of California. Amer. Assoc. Petrol. Geol. Mem. 3, Tulsa, OK, p. 59-75.

Saur, J.F.T., 1972. Monthly sea level differences between the Hawaiian Islands and the California coast. Fish. Bull., 70:619-636.

Schrader, H. and T. Baumgartner, 1983. Decadal variation of upwelling in the central Gulf of California. In: J. Thiede and E.Suess (eds), Coastal Upwelling: Its Sediment Record, Part B. Plenum Press, New York, p. 247-273.

Schrader, H-J. and R. Gersonde, 1978. Diatoms and silicoflagellates. Utrecht Micropaleont. Bull., 17:129-176.

Secretaria de Recursos Hidraulicos, 1970a. Datos Hidrometricos de Corrientes de Material de Acarreo en Suspension e Hidrometricos de Vasos hasta Diciembre 1969, Region Hidrologica No. 9, Sonora Sur., Cuencas de los Rios Sonora-Yaqui-Mayo. Boletin Hidrologico No. 40, Tomo I, Jefatura de Irrigación y Control de Rios, Dirección de Hidrologia, Mexico, D.F.

Secretaria de Recursos Hidraulicos, 1970b. Resumenes de Datos Hidrometricos, Crecientes, Gastos Maximos, Areas de Cuenca hasta Diciembre 1969, Region Hidrologica No. 9, Sonora Sur., Cuencas de los Rios Sonora-Yaqui-Mayo. Boletin Hidrologico No. 40, Tomo II, Jefatura de Irrigación y Control de Rios, Dirección de Hidrología, Mexico, D.F.

Secretaria de Recursos Hidraulicos, 1975. Datos Hidrometricos de Corrientes de Acarreo de Azolves en Suspension e Hidrometrico de Vasos, Enero 1970-Diciembre 1973, Region Hidrologica No. 9, Sonora Sur., Cuencas de los Rios Sonora-Yaqui- Mayo. Boletin Hidrologico No. 40, Tomo III, Jefatura de Irrigación y Control de Rios, Dirección de Hidrologia, Mexico, D.F.

Simonsen, R., 1974. The diatom plankton of the Indian Ocean Expedition of RV "Meteor" 1964-1965. In: "Meteor" Forschung., Deutschen Forschungsgem., Reihe D., No. 19. Biologie, pp. 1-65.

Simpson, J.J., 1984a. El Niño-induced onshore transport in the California Current during 1982-1983. Geophys. Res. Lett., 11:241-242.

Simpson, J.J., 1984b. A simple model of the 1982-83 Californian El Niño. Geophys. Res. Lett., 11:243-246.

Smayda, T.J., 1958. Biogeographical studies of marine phytoplankton. Oikos, 9:158-191.

Soutar, A., 1978. Collection of benthic sediment samples, Southern California Baseline Study Benthic Year II. Final Rept., Bureau of Land Management, Vol. 2, Pt. 4, No. 2, 54 pp.

Soutar, A. and P.A. Crill, 1977. Sedimentation and climatic patterns in the Santa Barbara Basin during the 19th and 20th centuries. Geol. Soc. Amer. Bull., 88:1161-1172.

Soutar, A., S.R. Johnson and T.R. Baumgartner, 1981. In search of modern depositional analogs to the Monterey Formation. In: R.E. Garrison and K. Pisciotto (eds), The Monterey Formation and Related Siliceous Rocks of California. Spec. Publ., soc. Econ. Paleontol. and Mineral. Pac. Sect., pp. 123-147.

Steemann-Nielsen, E., 1952. The use of radioactive carbon (^{14}C) for measuring organic production in the sea. J. Cons. Explor. Mer., 18:117-140.

Strickland, J.D.H. and T.R. Parson, 1972. A practical handbook of seawater analysis. Bull. Fish. Res. Bd. Canada, 167, 2nd Ed., 311 pp.

Thomas, W.H. and D.L.R. Seibert, 1974. Distribution of nitrate, nitrite, phosphate and silicate in the California Current region, 1969. CalCOFI Atlas No. 20, 97 pp.

Triton, D.J., 1977. Physical Fluid Dynamics. Van Nostrand Reinhold Co. Ltd., United Kingdom, 362 pp.

van Andel, Tj.H., 1964. Recent marine sediments of the Gulf of California. In: Tj.H. van Andel and G.G. Shor (eds), Marine Geology of the Gulf of California. Amer. Assoc. Petrol. Geol. Mem., 3:216-310.

Valdez-Holguin, E., 1986. Distribucion de la Biomasa y Productividad del Fitoplancton en el Golfo de California durante el Evento del Niño 1982-1983. M.S. Thesis, Centro de Investigacion Cientifica y Educacion Superior de Ensenada, B.C., Mexico, 92 pp.

Venrick, E.L., 1971. Recurrent groups of diatom species in the North Pacific. Ecology, 52:614-625.

Walker, G.T. and E.W. Bliss, 1932. World Weather V, Mem. Roy. Met. Soc., London, 4:53-84.

Warsh, C.E., K.L. Warsh and R.C. Staley, 1973. Nutrients and water masses at the mouth of the Gulf of California. Deep-Sea Res., 20:561-570.

White, W.B., 1975. Secular variability in the large-scale baroclinic transport of the North Pacific from 1950-1970. J. Mar. Res., 33:144-155.

White, W.B., 1977. Secular variability in the baroclinic structure of the interior North Pacific from 1950-1970. J. Mar. Res., 35:587-607.

White, W.B. and T.P. Barnett, 1972. A servomechansm in the ocean/atmosphere system of the mid-latitude North Pacific. J. Phys. Oceanogr., 2:372-381.

Wooster, W.S. and J.H. Jones, 1970. California Undercurrent off northern Baja California. J. Mar. Res., 28:235-250.

Wright, P.B., 1977. The Southern Oscillation —patterns and mechanisms of the teleconnections and their persistence. Hawaii Institute of Geophysics Rept. HIG-77-13.

Wright, P.B.;, 1983. Sea surface temperature fluctuations in the Pacific, 0-50°N. Tropical Ocean-Atmospheric Newsletter, No. 19, pp. 14-15.

Wyrtki, K., 1962. The oxygen minimum in relation to ocean circulation. Deep-Sea Res., 9:11-23.

Wyrtki, K., 1965a. Summary of the physical oceanography of the eastern Pacific Ocean. University of California, IMR Ref. 65-10, 78 pp.

Wyrtki, K., 1965b. Surface currents of the Eastern Tropical Pacific. Inter. Amer. Trop. Tuna Comm. Bull., 9:271-304.

Wyrtki, K., 1966. Oceanography of the eastern equatorial Pacific Ocean. Oceanogr. Mar. Biol. Ann. Rev., 4:33-68.

Wyrtki, K., 1967. Circulation and water masses in the eastern equatorial Pacific Ocean. J. Oceanol. Limnol., 1:117-147.

Wyrtki, K., 1974a. Equatorial currents in the Pacific 1950 to 1970 and their relations to the trade winds. J. Phys. Oceanogr., 4:372-380.

Wyrtki, K., 1974b. Sea level and the seasonal fluctuations of the equatorial currents in the western Pacific Ocean. J. Phys. Oceanogr., 4:91-103.

Wyrtki, K., 1975. El Niño—The dynamic response of the equatorial Pacific Ocean to atmospheric forcing. J. Phys. Oceanogr., 5:572-584.

Wyrtki, K., 1977. Sea level during the 1972 El Niño. J. Phys. Oceanogr., 7:779-787.

Wyrtki, K., 1979a. Sea level variations: monitoring the breath of the Pacific. EOS, 60:25-27.

Wyrtki, K., 1979b. The response of sea surface topography to the 1976 El Niño. J. Phys. Oceanogr., 9:1223-1231.

Wyrtki, K., 1985. Water displacements in the Pacific and the genesis of El Niño cycles. J. Geophys. Res., 90:7129-7132.

Yaalon, D.H. and E. Gonor, 1975. Rates of aeolian dust accretion in the Mediterranean and desert fringe environments of Israel. 9th Cong. International de Sedimentologie, Nice, p. 169-174.